

MOLECULAR AND CELLULAR REGULATION OF
MAMMARY EPITHELIAL DISSEMINATION

by

Elijah Shamir

A dissertation submitted to Johns Hopkins University in conformity with the
requirements for the degree of Doctor of Philosophy.

Baltimore, Maryland

August 2014

© 2014 Elijah Shamir
All Rights Reserved

Abstract

Dissemination of epithelial cancer cells represents the first step in metastatic spread. One postulated mechanism for dissemination is activation of an epithelial to mesenchymal transition (EMT), in which repression of the cell adhesion gene *E-cadherin* (*E-cad*) is considered the driving molecular event. We sought to test the sufficiency of single gene perturbations to induce dissemination out of primary mouse mammary epithelium. Deletion of *E-cad* disrupted simple architecture and morphogenesis but, contrary to expectation, rarely resulted in dissemination. In contrast, expression of the EMT transcription factor *Twist1* induced rapid dissemination of cytokeratin⁺ epithelial cells. A core concept in EMT is that cells lose epithelial characteristics, such as tight cell-cell adhesion, and acquire mesenchymal characteristics to escape. However, we found that *Twist1* did not significantly regulate epithelial-specific genes, such as *E-cad*. Rather, *Twist1* induced dramatic transcriptional changes in extracellular compartment and cell-matrix adhesion genes. Surprisingly, *Twist1*⁺ cells disseminated with membrane-localized *E-cad*, and *E-cad* knockdown strongly inhibited *Twist1*-induced single cell dissemination. Dissemination can therefore occur through an innately epithelial migratory program.

The integrity of the myoepithelium, the outer mammary epithelial layer, is the major diagnostic criterion used to distinguish in situ from invasive breast tumors. Interestingly, we found that constitutive *Twist1* expression induced dissemination of both inner luminal and outer myoepithelial cells and abnormal myoepithelial ingression, resulting in gaps in myoepithelial coverage at the basal surface. We next developed mouse models to restrict *Twist1* to distinct mammary lineages. *Twist1* expression in the myoepithelial compartment induced cell autonomous myoepithelial dissemination. In contrast, *Twist1*

expression in the luminal compartment rarely resulted in dissemination. Using cell type-specific fluorescent reporters, we observed that normal myoepithelial cells appear to contain Twist1⁺ luminal cells protruding into the extracellular matrix. Myoepithelial cells display a similar response to invasive E-cad⁻ luminal cell behavior. Taken together, our data supports the hypothesis that normal myoepithelial cells dynamically block luminal cell escape. We now seek to test the molecular basis of myoepithelial barrier function through knockdown of myoepithelial-specific genes important for contractility, cell-cell adhesion, and the intermediate filament network. We expect that perturbation of myoepithelial function will enable E-cad⁻ and Twist1⁺ luminal cell dissemination.

Dr. Andrew J. Ewald, Advisor

Dr. Phuoc T. Tran, Reader

Acknowledgements

I have many people to thank for helping me achieve this major career step, some for scientific or academic support and others for the emotional and moral support that helped me get through this demanding training program.

My scientific collaborators were instrumental in enabling me to expand the scope of my research and increase the significance of our work: Phuoc Tran, Joel Bader, Elisa Pappalardo, Kester Coutinho, Danielle Jorgens, and Manfred Auer. I owe special thanks to Phuoc for designing the incredible Twist1 mouse model that provided the basis for most of my graduate work.

Various members of the Hopkins community have provided crucial academic support during my training: the BCMB Program, particularly Carolyn Machamer; the Cell Biology Department and funding by the Hay Fellowship Award; my thesis committee (Jeremy Nathans, Debbie Andrew, and Phuoc Tran); and the SKCCC Breast Cancer Program. I want to especially acknowledge Bob Siliciano, Andrea Cox, and Sharon Welling, formidable pillars of the MD/PhD Program, who have served as my family here. Their encouragement and guidance have made the length of the training and the often-difficult transitions more bearable and tractable.

I have been extremely fortunate to conduct my PhD research among outstanding colleagues who not only challenge me intellectually on a daily basis but also are a pleasure to work with. Vy Nguyen-Ngoc, Robert Huebner, and Kevin Cheung joined the lab with me as the first cohort, and it was a truly unique and rewarding experience to build a lab with them from the ground up. I feel very lucky to have matured with such a

talented group – we struggled, failed, learned, and grew together. It is exciting to see how the lab has since expanded to welcome a new and diverse group of individuals, each remarkably talented, passionate, loyal, and caring: Neil Neumann, Dan Georgess, Katarina Sirka, Vanesa Silvestre, Amanda Fairchild, and Veena Padmanaban. I will certainly miss working with all of them and look forward to following their trajectories in the lab and beyond. I also want to thank Jen Beck, a former lab member, for her significant help early on in my research and for teaching me the invaluable lesson of how to properly run a mouse colony.

I could not have asked for a better PhD training experience or for a better mentor than Andy Ewald. From the time I was just considering a rotation, Andy has gone above and beyond my expectations, serving as a true exemplar for what an extraordinary PI looks like. He has enormously invested in my career development, coaching me on how to ask and investigate important questions, how to write and present my work, how to perform research at the highest level of academic integrity and precision, and how to mentor others. His firm belief in my ability to make important contributions to scientific research has paved my career path and fueled my passion to pursue a future in science. I particularly appreciate how early and regularly he sent me to meetings, as with each one, I have increasingly gained confidence, honed my presentation skills, and benefited from the opportunity to network with and learn from other scientists. I know that Andy will continue to serve as a role model, sponsor, and colleague throughout my career, and I can only hope to find other equally exceptional and dedicated mentors as I progress.

Finally, I would like to thank my family and all of my friends who have cheered me on and been there for me through the highs and lows. Thank you for your unwavering

confidence in me. To my parents, my biggest fans, I could not have done this without you.

Table of Contents

Title Page	i
Abstract	ii
Acknowledgements	iv
Table of Contents	vii
List of Tables	viii
List of Figures	ix
CHAPTER 1: 3D organotypic culture: experimental models of mammalian biology and disease	1
CHAPTER 2: The ECM microenvironment regulates collective migration and local dissemination in normal and malignant mammary epithelium	54
CHAPTER 3: 3D culture assays of murine mammary branching morphogenesis and epithelial invasion	95
CHAPTER 4: Twist1-induced dissemination preserves epithelial identity and requires E-cadherin	135
CHAPTER 5: Dissemination of Twist1⁺ epithelial cells involves directional amoeboid migration and is regulated by heterotypic cell-cell dynamics	201
CHAPTER 6: Myoepithelial and luminal cell-cell interactions appear to regulate epithelial invasion and dissemination	234
CHAPTER 7: Conclusion: Rethinking the concept of an “epithelial” cell	255
APPENDIX A: A collagen I ECM induces dissemination of E-cadherin⁻ luminal cells	266
Curriculum Vitae	274

List of Tables

Table 1-1. Cellular and molecular techniques for 3D culture.....	52
---	----

List of Figures

Figure 1-1. Cellular inputs to organotypic cultures.....	38
Figure 1-2. The major categories of cell culture.....	40
Figure 1-3. The cellular basis of epithelial tube elongation.....	42
Figure 1-4. Genetic regulation of cell behaviours in mammalian tissues.....	45
Figure 1-5. The role of the microenvironment in regulating epithelial function.....	47
Figure 1-6. Therapeutic applications of 3D culture.....	49
Figure 2-1. ECM microenvironments modulate the pattern of collective migration and local dissemination in human mammary carcinomas.....	78
Figure 2-2. Normal human mammary epithelium undergoes branching morphogenesis in Matrigel.....	80
Figure 2-3. Despite intra- and inter-tumor heterogeneity, the ECM microenvironment regulates collective migration and dissemination in human breast tumors.....	81
Figure 2-4. The ECM governs the migratory pattern and disseminative behavior of both tumor and normal murine mammary epithelium.....	82
Figure 2-5. The current, local ECM microenvironment determines the collective migration pattern of murine mammary epithelium.....	84
Figure 2-6. Cell dissemination into collagen I is persistent in tumor and transient in normal epithelium.....	86
Figure 2-7. Normal epithelium transiently protrudes and disseminates into collagen I but reestablishes a complete basement membrane.....	87
Figure 2-8. Tumor and normal epithelium remain transcriptionally distinct despite morphological similarities induced by the ECM.....	89
Figure 2-9. Cell-cell adhesion and extracellular genes are downregulated in tumor epithelium.....	90

Figure 2-10. Extracellular matrix genes and metalloproteinases are differentially expressed by normal and tumor epithelium.....	92
Figure 2-11. Loss of P-cadherin causes precocious branching morphogenesis in Matrigel and enhanced, sustained dissemination into collagen I.....	93
Figure 3-1. Collection of mouse mammary glands for organoid isolation and 3D culture.....	123
Figure 3-2. Mammary organoid isolation.....	125
Figure 3-3. Precoating tubes and pipette tips with BSA.....	127
Figure 3-4. Setting up the tissue culture hood for plating.....	128
Figure 3-5. Plating organoids in 3D Matrigel and collagen I.....	129
Figure 3-6. 3D organotypic culture assays.....	131
Figure 3-7. Phenotypic variability in assay outcomes.....	132
Figure 3-8. Correlation between epithelial morphologies in 3D organotypic assays and in vivo.....	134
Figure 4-1. <i>E-cad</i> deletion induced loss of simple epithelial architecture.....	171
Figure 4-2. <i>E-cad</i> deletion induced loss of adherens junction proteins in 3D culture and in vivo.....	173
Figure 4-3. <i>E-cad</i> ⁻ cells displayed reductions in multiple classes of intercellular junctions.....	175
Figure 4-4. Loss of <i>E-cad</i> inhibited branching morphogenesis and induced epithelial disorganization in 3D culture.....	177
Figure 4-5. <i>E-cad</i> ⁻ cells were excluded from polarized ducts and the body cell compartment of the terminal end bud in vivo.....	179
Figure 4-6. Twist1 induced robust dissemination of normal epithelial cells.....	181
Figure 4-7. Organoids recovered epithelial behaviors when Twist1 was turned off.....	183

Figure 4-8. Twist1-induced dissemination was cell autonomous, and Twist1 was sufficient for dissemination in vivo.....	185
Figure 4-9. Twist1 induced single cell dissemination despite membrane-localized adherens junction proteins.....	187
Figure 4-10. Adherens junction protein levels were partially reduced in Twist1-expressing tissue.....	189
Figure 4-11. Twist1 induced changes in genes regulating cell-ECM interactions and the extracellular space.....	191
Figure 4-12. Heat maps of DE genes within relevant GO Slim biological process and cellular component categories.....	193
Figure 4-13. Enzymatic activities upregulated by Twist1 offer candidate targets for blocking dissemination.....	195
Figure 4-14. Significantly enriched pathways relate to cell-matrix adhesion.....	197
Figure 4-15. E-cad is required for Twist1-induced single cell dissemination.....	199
Figure 5-1. Twist1+ cells disseminated by successive basal extrusion and epithelial detachment.....	222
Figure 5-2. Basal, protrusive Twist1+ cells were connected to the epithelium by multiple classes of intercellular junctions.....	223
Figure 5-3. The status of the myoepithelium could influence luminal cell dissemination.....	225
Figure 5-4. Twist1 induced myoepithelial ingression into the epithelium.....	226
Figure 5-5. Twist1-expressing epithelium frequently contained electron-dense tunnels.....	228
Figure 5-6. Twist1– cells reattached to disseminated Twist1+ cells.....	230
Figure 5-7. Disseminated Twist1+ cells migrate by filopodal, amoeboid motility.....	231

Figure 5-8. Twist1+ cells disseminate from the epithelium with high directional persistence.....	233
Figure 6-1. Distinct mammary epithelial lineages express cell type-specific markers..	248
Figure 6-2. Myoepithelial-specific Twist1 expression induces cell autonomous dissemination that is regulated by FGF2.....	249
Figure 6-3. Luminal-specific Twist1 expression induces rare to no dissemination.....	251
Figure 6-4. The myoepithelium appears to contain protruding Twist1+ luminal cells...	253
Figure 6-5. Myoepithelial cells appear to restrain E-cad- cell dissemination.....	254
Figure 7-1. Normal transitions in adhesion during epithelial branching morphogenesis.....	264
Figure 7-2. Is there are conserved epithelial migratory program?.....	265
Figure A-1. A collagen I-rich ECM induces E-cad- cell dissemination in 3D culture and in vivo.....	271
Figure A-2. A stromal ECM induces E-cad- cell dissemination in vivo.....	273

CHAPTER 1

3D organotypic culture: experimental models of
mammalian biology and disease

(Modified from Shamir and Ewald, *Nat Rev Mol Cell Biol* 2014)

Abstract

Mammalian organs are challenging to study as they are relatively inaccessible to experimental manipulation and optical observation. Recent advances in three-dimensional (3D) culture techniques, coupled with the ability to independently manipulate genetic and microenvironmental factors, enable the real-time study of mammalian tissues. These systems have been used to visualize the cellular basis of epithelial morphogenesis, to test the role of specific genes in regulating cell behaviours within epithelial tissues, and to elucidate the contribution of microenvironmental factors to normal and disease processes. Collectively, these novel models can answer fundamental biological questions, generate replacement human tissues and enable testing of novel therapeutic approaches, often using patient-derived cells.

Introduction

Natural historians identified and named diverse organs across species, and a crucial simplification came when Bichat recognized that organs represented combinations of a few fundamental tissues¹. Compound microscopes enabled Virchow to define epithelium, connective tissue, nerve, muscle and blood as the universal tissues², and by 1900, the microscopic anatomy of humans was well known³. However, it remains difficult at a cellular and molecular level to understand how mammalian organs form during development and change during disease.

Compared to the transparent embryos of externally developing species, mammalian tissues and organs are relatively inaccessible to experimental manipulation and optical observation. Furthermore, mammalian development occurs over days to years. These limitations led Harrison et al. to develop two dimensional (2D) culture techniques in 1907⁴. 2D culture enabled biologists to observe and manipulate mammalian cells and laid the foundation for cell and molecular biology. However, 2D cultures do not completely recapitulate the 3D organization of cells and extracellular matrix (ECM) within tissues and organs. Consequently, there is a large gap between our detailed knowledge of subcellular processes and our incomplete understanding of mammalian biology at the tissue level. Dynamic analyses of organogenesis have instead relied on model systems such as *C. elegans*, *Drosophila melanogaster*, *Xenopus laevis* and zebrafish.

The goal of reconstituting organ function *ex vivo* is broadly shared, and successful examples exist for most tissues and organs (Table 1). In pursuit of this goal, a wide range of techniques has been developed that are referred to as 3D culture or organotypic or organoid culture. Various subfields use these terms interchangeably or

distinctly. For example, in the field of mammary gland biology, organoids refer to primary explants of epithelial ducts into 3D ECM gels⁵. Conversely, in studies of intestinal biology, organoids can refer to clonal derivatives of primary epithelial stem cells grown without mesenchyme⁶ or to epithelial-mesenchymal co-cultures derived from embryonic stem cells (ES cells) or induced pluripotent stem cells (iPS cells)⁷.

In this Review, we first provide an overview of the commonly used cellular inputs and culture formats. We then discuss how these experimental systems have been used to visualize the cellular mechanisms that drive epithelial tissue development, to study the genetic regulation of cell behaviors in epithelial tissues and to evaluate the role of microenvironmental factors in normal development and disease. Finally, we provide examples of how 3D culture techniques can be used to build complex organs and advance therapeutic approaches.

Cellular inputs into 3D culture

To understand how mammalian organs can be cultured *ex vivo*, it is useful to consider their constituent parts. The external surfaces of the body and the linings of organs are built from epithelial tissues⁸. Epithelial cells are connected to each other by intercellular junctions and are located within a specialized ECM, termed the basement membrane. These cell-cell and cell-ECM interactions are not completely modeled in 2D culture. Epithelial tissues are avascular and exist in close proximity to vascularized connective tissue⁸. In contrast to epithelium, connective tissue contains an abundance of ECM and a diverse population of stromal cells, including fibroblasts, immune cells, and adipocytes⁸. Epithelium and connective tissue are functionally interdependent units

within the organs and are integrated with nerves and muscle to varying degrees depending on organ-specific function.

The first crucial design choice in 3D culture is the extent to which the full *in vivo* complexity of the organ is recapitulated. Organ function arises from the cooperation among different tissues, but it can be difficult to isolate the role of specific genes or cell behaviours *in vivo*. One approach is to deconstruct organs into their parts (for example, epithelium, stromal cells, vasculature or ECM) and then selectively recombine these parts in 3D culture. Embedding epithelial cells within an ECM gel enables the cells to self-assemble into tissues and to both interpret and remodel the ECM⁹. Similarly, endothelial cells and perivascular cells can be patterned into functional, perfused networks within ECM gels to model vascular development within connective tissue^{10,11,12}. Alternatively, multiple tissue components can be combined into the same culture.

Whole organ and organ slice cultures.

The conceptually simplest unit to explant into 3D culture is the whole organ (Fig. 1-1A). This approach was used successfully to study skeletal development as early as 1929¹³ and was expanded to kidney, lung, salivary gland, liver, pancreas and mammary gland by the mid-20th century^{14,15,16}. However, the limited diffusion of extracellular molecules into thick tissues restricts these studies to embryonic or thin organs. Alternatively, organs such as lung¹⁷, small intestine^{18,19}, colon^{19,20}, brain^{21,22} and aorta²³ can be sectioned into tissue 'slices' and mounted onto siliconized filter paper²⁴ or porous culture membranes²⁵ for mechanical support. Slices from the same organ can be subjected to different experimental conditions, which enables the evaluation of both matrix-bound and soluble paracrine signals. For example, the lactogenic hormones were defined by their ability to induce milk production in whole mammary gland cultures derived from virgin

mice²⁶. Although these culture formats permit optical access to the tissue and experimental interventions within native stromal tissues, it can be challenging to maintain tissue viability, and the interpretation of experimental manipulations is more difficult within complex organs.

Tissue organoids.

A fundamental developmental question is whether epithelial cells determine organ pattern or whether the pattern emerges through a dialogue between the epithelium and the connective tissue or mesenchyme. To answer this question, epithelial tissues are isolated and cultured without their corresponding stromal cells; this approach is termed mesenchyme-free or organoid culture (Fig. 1-1B). Tissue organoids are freshly isolated from primary mammalian organs for every experiment. Each tissue organoid contains several hundred cells, which are accessible to signalling molecules and can be genetically modified using robust lentivirus- and adenovirus-based techniques^{27,28,29,30,31}. Organoid protocols have been developed for mammary gland^{5,32}, salivary gland³³, kidney³⁴, lung³⁵, small intestine^{6,36}, colon^{36,37}, liver³⁸, stomach³⁹, pancreas⁴⁰ and prostate⁴¹. Tissue organoids are typically explanted into commercial matrices, such as Matrigel⁴² or collagen I⁴³, which enable optical imaging. As pieces of tissue are explanted intact into culture, the resulting organoids contain a diversity of cell types organized in their normal spatial configurations as observed *in vivo*. This culture format has been used to study the cell movements driving organogenesis and to model the cell and tissue consequences of genetic changes.

Stem cell organoids.

Organoids can also be expanded from primary stem cells purified from organs, ES cells, or iPS cells (Fig. 1-1C). For example, primary tissue-derived, Lgr5⁺ intestinal stem cells

clonally generate crypt-villus architecture in 3D culture⁶. This approach was extended to stomach³⁹, colon³⁷, pancreas⁴⁰, and liver³⁸. Investigators have also developed robust techniques to generate stem cell organoids from ES cells and iPS cells (Table 1-1). An advantage of iPS cell-derived organoids is that they can be generated from a patient's cells. ES cell- or iPS cell-derived organoids have also been used to demonstrate the self-organization of the retina^{44,45}, cerebral cortex^{46,47} and pituitary⁴⁸. However, *in vivo* organs do not expand from single isolated stem cells, and therefore the mechanisms driving the formation of stem cell organoids may be distinct from organogenesis *in vivo*. For example, cortical organoids formed from ES cells generate stratified structures with layer-specific neuronal differentiation⁴⁶. However, the inside-out pattern of layer formation observed *in vivo* is reversed in 3D culture⁴⁶. Nonetheless, the extent to which brain anatomy can be recapitulated from defined cellular and molecular starting materials is remarkable^{46,47}. An additional issue is the timing of molecular interventions in tissues compared to single cells, as differences in timing could easily change phenotypes.

Reaggregated single cell suspensions.

Clonal expansion from a single ES cell or iPS cell requires many rounds of cell division to generate organoids. Accordingly, many 3D culture assays start from suspensions of single cells, either cell lines, stem cells or freshly isolated primary cells (Fig. 1-1D). Classic amphibian embryology experiments revealed that disaggregated single cells would spontaneously reaggregate and recapitulate their normal tissue architecture⁴⁹. Similarly, mammalian kidney⁵⁰ or mammary⁵¹ cell lines readily form acini from single cells when cultured on top of Matrigel. These epithelial models were used to dissect the molecular basis of epithelial adhesion and polarity^{50,51}. A single-cell suspension can also generate more complex tissues. For example, isolated epidermal or esophageal

keratinocytes organize into a stratified epithelium with highly realistic tissue architecture^{52,53,54}. Similarly, dissociated cells from mouse embryonic kidneys reaggregate to form renal structures that contain epithelial-derived ureteric buds and mesenchyme-derived nephrons^{55,56}. These approaches facilitate the formation of chimeric tissues that consist of different cell types or cells with distinct genetic modifications.

Culture formats for 3D culture

In addition to the cellular inputs, culture formats can be varied independently to answer specific biological questions (Table 1-1).

2.5D cultures.

The addition of basement membrane proteins to the medium in 2D cultures is sufficient to induce tissue-specific differentiation of diverse epithelial cells, including mammary⁵⁷, kidney⁵⁸ and lung⁵⁹ (Fig. 1-2A). Most experiments rely on a commercial basement membrane protein source, such as Matrigel⁴². Conversely, epithelial tissues often lose their differentiated state and migrate individually when cultured in a stromal matrix such as collagen I⁶⁰. These observations led to the development of diverse assays in which single cells are plated on top of Matrigel, with additional Matrigel in the medium^{50,51,61}. This technique is frequently referred to as 2.5D culture or ‘drip’ culture, in reference to the ECM in the medium (Fig. 1-2B). This format does not perfectly model the *in vivo* environment, as the cells contact a large fluid reservoir that they would not encounter *in vivo*. As a result, fluid-facing surfaces of the cell lack ECM contact, and cell-generated paracrine factors are diluted. Despite these limitations, 2.5D assays are experimentally

convenient, they induce cells to adopt a more physiological tissue architecture than 2D assays, and the cells remain accessible for molecular analysis⁵¹.

3D-embedded cultures.

To better model *in vivo* tissue organization, cells can be fully embedded within 3D ECM gels (Fig. 1-2C). Tissue organoids embedded in 3D ECM have been used to study branching morphogenesis of the mammary^{5,32,62}, salivary^{33,63}, kidney⁶⁴, lung³⁵ and pancreatic ductal⁶⁵ epithelium. In this format, both the composition and mechanics of the ECM environment can be varied^{66,67,68,69,70,71}. Collagen I models connective tissue ECM, basement membrane extracts, such as Matrigel, recapitulate the tissue context of epithelial ducts, and fibroblast-conditioned matrix, which is rich in fibronectin, models the microenvironment during wound healing. Embedded cultures also support a broader and more complex range of tissue architectures than is typically observed in 2.5D formats. However, due to the location of the cells within a thick ECM gel, both optical imaging⁷² and recovery of cells is more complex than in 2.5D.

Mechanically supported cultures.

Both whole organ explant cultures and stratified epithelial cultures reconstituted from single cells are typically cultured on top of mechanical supports. Historically, these cultures were grown on top of siliconized paper^{14,16,24} and, more recently, cell culture inserts with semi-permeable membranes (Fig. 1-2D; Table 1-1). For organ explants, these membranes provide flexible support and enable delivery of nutrients and signalling molecules to the bottom surface of the tissue, or optionally to the top surface. Epidermal keratinocytes seeded on ECM-coated culture inserts form a monolayer when submerged, and they stratify and differentiate into epidermis when exposed to an air-liquid interface^{52,53}. The addition of fibroblasts to a floating collagen lattice enables the

formation of an underlying dermis and self-organization of full-thickness human skin⁵³. Similar approaches generate histologically realistic normal and neoplastic models of oral, esophageal and cervical epithelium^{54,73} (Table 1-1). These reconstituted tissues are used to study normal development and disease processes, and they can also be utilized for toxicity assays.

Bioengineering inspired culture systems.

Though we cannot review them in detail here, a diverse range of engineered culture assays has also been developed, both to answer fundamental biological questions and to serve as platforms for constructing replacement tissues. Important examples include synthetic polymer systems for 2.5D and 3D cultures^{74,75,76}, integration of microfluidics in complex cultures^{77,78,79}, cell surface modification techniques to pattern the assembly of epithelial tissues⁸⁰, microfabricated 3D environments to control tissue geometry and mechanics⁸¹ and 3D patterning of perfused vascular networks^{10,11}.

Imaging in 3D cultures.

Imaging in 3D cultures enables a continuous cellular and molecular description of tissue-level development over days to weeks⁷². Imaging is typically performed using an inverted microscope and requires the robust control of temperature, humidity, CO₂ and evaporation. A major obstacle is the scattering of light in thick 3D cultures. One strategy to minimize scattering is to simplify the culture to its core components, such as tissue organoids instead of whole organs^{62,82}. A second approach is to match the index of refraction of the immersion medium to that of the culture medium. Finally, the working distance of the lens must be sufficient to image structures throughout the culture.

Different microscope systems can be used in a complementary way. Differential

interference contrast enables optical sectioning in thick ECM gels and label-free visualization of collagen I fibers. Confocal imaging enables multicolor 3D time-lapse imaging up to 70-100 microns deep within the tissue^{82,83,84,85}, and two-photon microscopy facilitates deeper imaging and visualization of fibrillar ECM through second harmonic signals^{43,86}. However, limitations of two-photon microscopy include increased cost and high levels of energy deposition at the plane of focus. Finally, 3D culture samples can be prepared for transmission and scanning electron microscopy^{27,59,87,88}.

Tailoring the culture format.

Ideally, 3D culture assays would be perfectly representative of the *in vivo* situation, easy to manipulate and inexpensive. In practice, however, tradeoffs typically must be made, especially with primary human tissues. It is useful to identify the main experimental goal and then tailor the 3D culture to achieve that goal. For example, replacement human tissues need to be large in size and incorporate into the host vasculature, and the host response to the graft needs to be minimized. By contrast, 3D cultures designed for drug screening should ideally fit within 384-well plates, have a low cost per well and predict the results of testing in preclinical animal models and in human clinical trials. Important factors to consider include the throughput required in the assay, the ease of molecular manipulations and molecular readouts, the necessary recapitulation of the *in vivo* histology, and the availability of primary cells and tissues for that specific organ. For a close match to *in vivo* histology, the more complex embedded culture or culture insert models are most suitable. For genome-scale molecular interference approaches, the least complex culture system enables the most rapid analysis. Efficient use of limited starting materials is required if the cultures involve primary human tissues. If optical imaging is crucial, the 3D culture needs to be relatively thin and transparent. Finally, the goals of the experiment will determine which cell types need to be incorporated. Many

published assays are essentially monocultures of epithelial cells, endothelial cells or neurons. However, each assay format can incorporate additional cell types. For example, cancer cells or stromal cells can be incorporated to study the interactions between normal and neoplastic cells or between epithelial and stromal cells, respectively^{54,89}.

The great variety in 3D culture techniques reflects both the various requirements of the different organs and the distinct goals of the investigators. A large body of work has been published on 3D, organotypic or organoid culture, the results of which cannot be comprehensively reviewed here. However, a few common themes emerge that both capture the challenges that motivated the development of 3D culture techniques and illustrate the various biological questions that can be uniquely answered using these approaches.

Organ morphogenesis

It is of fundamental interest to understand how cells build tissues and organs. However, the slow timescale of mammalian development and its location deep within an opaque animal limit most organogenesis studies to comparisons of fixed sections from different animals. Due to the large number of cells and the morphological heterogeneity of developing organs, these studies often cannot distinguish among several mechanistic possibilities of organ formation. Furthermore, an imprecise understanding of the normal developmental trajectory necessarily limits our ability to identify the molecular and cellular differences that define the mutant phenotype. Accordingly, many 3D culture techniques were initially developed to enable direct observation of developmental processes. In the examples below, we focus mainly on epithelial tissues, due to the

extensive literature describing their formation, and highlight common mechanistic themes as well as species- and organ-specific differences.

Cellular mechanisms driving epithelial tube elongation.

A good example of the application of 3D cultures in developmental biology is the study of epithelial tubulogenesis. This process involves an increase in epithelial surface area and changes in tissue shape (Fig. 1-3A). Tube elongation can, in principle, be accomplished through various combinations of changes in cell number, cell shape and cell size. Terminal branching of the *D. melanogaster* trachea occurs without proliferation by subcellular branching of the leading cell⁹⁰, whereas mammalian tubulogenesis in the mammary gland, salivary gland, kidney and lungs involves a large increase in epithelial tissue size (Fig. 1-3B-E). The iterative branched structure of these tubular networks and the simple epithelial organization of the resulting ducts led to the concept of a conserved process of branching morphogenesis⁹¹.

However, it remained an open question whether conceptually related processes of ductal elongation and bifurcation occurred through a common sequence of cellular events across these organs. Answering this question was challenging because it was difficult to be certain that a duct was elongating at the moment it was fixed. 3D confocal imaging of 3D cultures of mammary gland, salivary gland, kidney and lung has in fact revealed distinct cellular mechanisms of branching morphogenesis. Mammary ducts first undergo a simple to stratified transition, elongate as a stratified epithelium, and then polarize to reestablish simple ductal architecture^{62,82,88} (Fig. 1-3B). Salivary glands start as a stratified epithelium that first clefs and then progressively polarizes to form a network of simple ducts^{29,92} (Fig. 1-3C). The kidney ureteric bud transitions from simple to pseudostratified, elongates as a pseudostratified epithelium and then polarizes to a

simple epithelium^{93,94} (Fig. 1-3D). By contrast, epithelial buds initiate and elongate as a polarized simple epithelium during monopodial branching in the chick lung⁸⁵ (Fig. 1-3E). Therefore, these tubes exhibit distinct tissue architectures and utilize different cellular mechanisms during elongation.

Cell proliferation in tubulogenesis.

The imaging analyses discussed above generated a general framework for branching morphogenesis that enabled researchers to identify the underlying cellular mechanisms. In turn, cell division was shown to have distinct roles in different epithelial organs. For example, asymmetric divisions within mammary luminal epithelial cells initiate stratification and lead to a loss of polarity during both development and ErbB2-induced oncogenic stratification⁸². Salivary epithelial cell proliferation is increased at ductal tips and involves heparan sulphate-mediated regulation of FGF10-FGFR2 signalling; disruption of heparin signalling results in an expanded zone of proliferation and abnormal branching⁹⁵ (Fig. 1-3F). In the ureteric bud, proliferating cells delaminate into the luminal space, and daughter cells reintegrate at nonadjacent locations, which leads to mixing of different cellular populations⁹⁶ (Fig. 1-3G). The requirement for proliferation in organ development also varies across species. In the chick lung, monopodial branching occurs even in the absence of proliferation⁸⁵ (Fig. 1-3H), whereas in the mouse lung, both domain branching and bud bifurcation involve polarized cell divisions⁹⁷ (Fig. 1-3I). These species-specific and tissue-specific differences in cell proliferation during tubulogenesis highlight the importance of real-time analysis as a framework for interpreting molecular interventions. Understanding the role of cell proliferation in development is also relevant in cancer, as oncogenic activation of proliferation might have different consequences in different organs.

Gene regulation of cell behaviour

3D culture techniques have also been developed to elucidate the molecular mechanisms regulating tissue organization and function in developmental and disease states. Although *in vivo* studies can test whether a gene is required for organ development, they cannot always determine how the gene regulates cell behaviours to change tissue architecture and function. Conversely, the roles of individual proteins in biochemical pathways have largely been elucidated in 2D culture studies; yet these molecular interactions can differ in a 3D tissue context. For example, the molecular composition and phosphorylation status of focal adhesions within fibroblasts are different on 2D surfaces compared with 3D ECM gels⁹⁸. Recently, RNAi, Cre-lox-based recombination and lentiviral shRNA approaches have all been adapted to 3D culture, which enables the evaluation of single genes and genome-scale screening in tissues, including mammary²⁷, intestinal²⁸ and salivary^{99,100} epithelium. The application of CRISPR-Cas9-based genome editing¹⁰¹ further offers the potential for the rapid introduction and functional correction of disease mutations¹⁰².

Tissue-specific genetics.

MDCK kidney acinar formation in 2.5D culture served as an early model of a generic epithelium that was readily accessible to genetic manipulation^{50,58}. The molecular machinery guiding polarity initiation, specification of an apical membrane and lumen formation were identified in this system and provided a conceptual foundation for our current understanding of polarity in more complex tissues^{58,103,104,105,106}. Analogous studies in 2.5D cultures of MCF-10A cells enabled the detailed dissection of the role of growth factor receptors and polarity proteins in normal development and cancer^{107,108,109,110}. Both systems have facilitated high-resolution, real-time studies of the

role of oncogenes in disrupting normal epithelial cell behaviours^{111,112}. Nevertheless, these cell lines lack important features of epithelial tissues, such as tight junctions in MCF-10A cells⁸⁷.

Ultimately, the molecular pathways defined in cell line-based assays need to be validated in more physiologic contexts. However, many genes are required during early mammalian embryonic development, preventing the study of their role in later developmental processes. This challenge has been overcome through the use of tissue-specific promoters to induce gene deletion or overexpression at later stages. However, many promoters are mosaically expressed within organs, leading to complex mixtures of wild-type and genetically modified cells. Depending on the phenotype, this heterogeneity can greatly complicate the interpretation of gene function. This challenge can be overcome by combining *ex vivo* gene manipulation and 3D culture of primary tissues. siRNA-mediated knockdown of p63 showed that this transcription factor (which is essential for neonatal survival) is required for both proliferation and differentiation in regenerating organotypic epidermis, with distinct contributions from different p63 isoforms¹¹³ (Fig. 1-4A). p63 depletion leads to tissue hypoplasia, defects in epidermal stratification and induction of simple epithelial markers¹¹³. In genetic mosaic epidermis, retrovirally delivered LacZ and HA-epitope-tagged keratin 14 labels were used to distinguish between wild-type and *p63*^{-/-} populations and to demonstrate that control of differentiation by p63 is cell-autonomous¹¹³. Additional regulators of epidermal differentiation, such as the long non-coding RNA TINCR, have been identified by further combining human organotypic skin cultures with transcriptome sequencing, RNAi, protein microarrays and RIA-Seq¹¹⁴.

Incorporation of fluorescent reporters simplifies the interpretation of mosaic tissues, as it

allows real-time comparisons between genetically modified cells and wild-type cells. For example, deletion of *E-cadherin* in a large fraction (>80%) of mammary epithelial cells in tissue organoids does not prevent initiation of new epithelial ducts²⁷. This result suggests that E-cadherin is dispensable for mammary morphogenesis. However, real-time imaging with Cre biosensors revealed that these new ducts are elongated by E-cadherin positive cells²⁷. E-cadherin is in fact required for the maintenance of epithelial architecture and branching morphogenesis²⁷. Importantly, this is consistent with *in vivo* findings, and therefore, the combination of *ex vivo* gene manipulation and fluorescent biosensors enables the rapid evaluation of gene requirement in primary tissues.

Real-time genetic analysis.

Real-time tracking can be used to determine the effects of genetic modifications on specific cell behaviours. For example, studies using fluorescent labeling, siRNA knockdown and time-lapse imaging identified the signals that are required for salivary gland clefting^{29,92,115}. Gene expression analysis revealed increased levels of *Btbd7* in epithelial cells located within clefts²⁹ (Fig. 1-4B). Moreover, it was shown that *Btbd7* promotes cleft progression by inducing *Snail2* expression and reducing E-cadherin levels²⁹. Live-cell imaging has also been used in embryonic whole lung explants to demonstrate the requirement for the polarity protein Scribble in lumen morphogenesis in the mammalian lung but not in bud bifurcation¹¹⁶; the depletion of *Scribble* in lungs leads to the mislocalization of junction proteins and misalignment of distal epithelial cells. Importantly, the finding that Scribble is required for epithelial cell-cell contacts and lumen morphogenesis is consistent with the *in vivo Scribble* loss-of-function phenotype (that is, small, misshapen lungs, reduced airway number and defects in epithelial architecture)¹¹⁶. Thus, genetic manipulation, together with live-cell imaging in 3D culture, identified the specific genes that have a key role in salivary gland clefting and lung

morphogenesis. In the future, this approach will aid in the identification the genes involved in other cellular processes in additional organs.

A major advantage of 3D culture is the ability to observe and follow the same cells over time. This approach was used in the murine kidney to isolate which cells required the receptor tyrosine kinase (RTK) Ret during branching morphogenesis⁹⁴. Imaging in embryonic whole organ chimeras demonstrated the dynamic exclusion of epithelial cells lacking Ret (*Ret*^{-/-} cells) from the tips of elongating ureteric buds⁹⁴ (Fig. 1-4C). The authors then increased Ret signaling by deletion of *Sprouty1*. In chimeras with wild-type cells, *Spry1*^{-/-} cells are enriched in the ureteric bud tip domain. Importantly, normal Wolffian duct cells *in vivo* display heterogeneous Ret signalling and therefore likely compete on this basis for contribution to the ureteric bud⁹⁴. Taken together, these results reveal a critical role for Ret signaling, specifically in the cells most involved in tube elongation.

Inducible gene expression.

Recent advances also enable inducible gene expression and precisely timed molecular analyses in 3D cultures²⁷. For example, expression of the transcription factor *Twist1* in mammary epithelial cells induces rapid dissemination of cells into the ECM. Surprisingly, *Twist1*-positive disseminated cells retain epithelial gene expression, and dissemination requires E-cadherin²⁷ (Fig. 1-4D). The fraction of cells within a tissue that expresses a gene can also regulate tissue architecture. Mosaic, but not ubiquitous, expression of an activated form of the GTPase *H-Ras* induces multicellular protrusions in MCF-10A aggregates¹¹⁷. In a separate study, activated *H-Ras* was sufficient to drive tissue overgrowth when expressed in myoepithelial or luminal mammary epithelial cells¹¹⁸. However, inhibitor studies demonstrated the involvement of different Ras effectors,

revealing that different pathways were utilized in the two cell types to induce proliferation downstream of the same oncogene¹¹⁸. Taken together, 3D culture enables the elucidation of the cellular and molecular effects of gene activity in distinct cell populations within a tissue.

The microenvironment and cell behaviour

The examples above highlight biological insights from the study of isolated epithelial tissues *ex vivo*. However, *in vivo* epithelial cells are surrounded by connective tissue, which contains immune cells, blood vessels, fibroblasts and ECM-bound signalling molecules (Fig. 1-5A). These components can regulate adjacent epithelial and neuronal tissues and contribute to disease progression, particularly in cancer^{119,120}. However, it is difficult to specifically alter either stromal cell or ECM composition *in vivo*. By contrast, 3D culture systems enable the precise manipulation of components of the microenvironment and the analysis of how they affect the structure and function of a cell or tissue^{69,121,122}.

Epithelial-stromal interactions.

The ability to add or remove stromal cells in 3D co-cultures has been particularly exploited in cancer invasion studies. It was known that macrophages regulate breast cancer cell invasion and metastasis *in vivo*¹²³. To study the underlying molecular mechanisms various immune cells and immune cell-derived soluble factors have been added to 3D cultures of breast tumour organoids¹²⁴. Macrophages, T cells that express IL-4 or exogenous IL-4 each promote tumour invasion¹²⁴. Similarly, squamous cell carcinoma invasion into collagen I is strongly promoted by co-culture with fibroblasts¹²⁵, which interact with both cancer cells and the ECM¹²⁵. Importantly, if the fibroblasts are

allowed to remodel the ECM and are then removed, their tracks within the matrix are sufficient to promote invasion¹²⁵. Fibroblasts can therefore create lasting, pro-invasive changes in the tumour microenvironment¹²⁵. In breast cancer, fibroblasts use Hippo signalling to promote matrix stiffening and invasion¹²⁶. In esophageal cancer, fibroblasts promote invasion through HGF signalling⁸⁹ and alter the differentiation state of cancer cells¹²⁷.

The vasculature represents another potent source of regulatory signals. Recent studies have implicated thrombospondin 1 (TSP1), an angiogenesis inhibitor, in normal epithelial differentiation and tumour growth. A clonal 3D co-culture model was used to show that lung but not liver endothelial cells can direct lineage specification in distal lung stem cells¹²⁸, and TSP1 promotes differentiation into an alveolar fate following injury¹²⁸. In a different co-culture model, 3D niches composed of lung or bone marrow stroma mixed with endothelial cells were used to demonstrate that TSP1 regulates tumour dormancy¹²⁹ (Fig. 1-5B). This study revealed that TSP1 induces breast tumour cell dormancy in mature endothelium, whereas TGF- β 1 and periostin promote tumour cell growth in neovascular tips, which lack TSP1¹²⁹. Neovascularization therefore promotes disseminated tumour cells to develop into macrometastases.

3D models of the perivascular niche have also been used to study interactions between brain endothelial cells and cancer stem cells (CSCs) in glioblastoma¹³⁰. Vascular networks within 3D-engineered scaffolds enhance CSC maintenance, growth and migration via paracrine IL-8 signalling, and co-implantation of endothelial cells and CSCs *in vivo* enhances tumour formation through IL-8 receptor signalling in CSCs¹³⁰. Importantly, conditioned medium collected from 3D cultures of endothelial cells promotes the maintenance of stem cell markers in CSCs, whereas conditioned medium from 2D

cultures does not¹³⁰. Taken together, the tumour stroma emerges as a potent regulator of primary tumour growth and metastasis.

Mesenchymal components can also regulate an organ's regenerative capacity. In the salivary gland, removal of the parasympathetic ganglion decreases branching morphogenesis and depletes the pool of keratin 5-positive progenitor cells¹³¹. Morphogenesis and proliferation of these progenitors can be rescued by activation of muscarinic receptors with an acetylcholine analogue¹³¹. Parasympathetic innervation therefore maintains progenitors in an undifferentiated state, and this signalling axis may enable therapeutic intervention to promote organ repair¹³².

Epithelial-epithelial interactions.

Tumours are increasingly recognized to contain cancer cells with different genetic and phenotypic characteristics¹³³. 3D cultures of cancer cells revealed subtype-specific differences in invasive behaviour and in the capacity of fibroblasts to promote invasion^{134,135}. Interestingly, cell lines with greater migratory capacity are observed to lead collective invasion of less migratory cell lines through direct contact between cancer cells¹³⁴. A recent study developed an assay to prospectively identify the most invasive cells within primary mouse and human tumours by embedding tumour-derived organoids into 3D collagen I gels³⁰. Cancer cells expressing basal epithelial markers were found to lead collective invasion in mouse breast cancer models and in patient samples, in 3D culture and *in vivo* across breast cancer subtypes³⁰. Cancer cells expressing basal markers directly adhere to, and lead the collective invasion of, cancer cells expressing luminal markers³⁰. Thus, interactions between epithelial cancer cells in different differentiation states are crucial for collective invasion. These techniques can be readily generalized to any epithelial malignancy and enable unbiased identification of the cells

most responsible for invasion and systemic spread. Interestingly, interactions between normal basal and luminal epithelial cells have also been shown to regulate tissue architecture and polarity in the mammary gland^{136,137}.

ECM composition.

In both 2.5D and 3D culture, cells from the same source can be explanted into microenvironments with varied ECM composition or mechanics. In the MDCK kidney acini model, ECM composition regulates the efficiency and mechanism of lumen formation¹⁰⁴. In collagen I gels, cell polarization is slow, and lumen formation requires apoptosis¹⁰⁴. By contrast, in Matrigel, cell polarization is rapid, and apoptosis is dispensable for lumen formation¹⁰⁴. Direct comparisons of the mammary epithelium in different microenvironments revealed that the composition of the ECM regulates invasive and disseminative behaviours of both normal and malignant tissues⁶⁶ (Fig. 1-5C). Importantly, the consequences of gene deletion at the tissue level also depend on the ECM, as *P-cadherin* deletion results in mammary epithelial hyperplasia in Matrigel and dissemination in collagen I⁶⁶. Finally, the organization of the ECM can modulate tissue architecture. Radially aligned collagen I fibers promote breast cancer invasion⁷⁰ and correlate with poor patient outcomes¹³⁸. Interestingly, aligned collagen I fibers also promote directional growth of normal epithelial cells^{67,68}, which suggests that structural cues can pattern normal morphogenesis.

Mechanical cues.

The mechanical properties of the microenvironment also change during development and disease. For example, epithelial tumours increase in rigidity due to both ECM stiffening and increased cytoskeletal tension¹³⁹. 3D culture experiments revealed that stiff matrices induce integrin clustering, cytoskeletal tension, and focal adhesion

assembly¹³⁹. Increased cytoskeletal tension, whether induced by matrix stiffness or by ERK signalling, promotes malignant progression¹³⁹. Matrix stiffness can also contribute to cell fate specification, as mesenchymal stem cells commit to distinct lineages when cultured on gels with varied rigidity¹²². Soft matrices promote neurogenic differentiation, intermediate matrices promote myogenic differentiation and rigid matrices promote osteogenic differentiation¹²².

Recent studies have focused on identifying the signals that cells are responding to within these microenvironments. For example, lysyl oxidase-mediated collagen I crosslinking increases ECM rigidity and promotes metastatic progression through stimulation of PI3K signalling⁶⁹. A recent study reported the effect of rigidity on cell behaviour by crosslinking poly(ethylene) glycol (PEG) networks within Matrigel scaffolds¹²¹; high rigidity alone suppresses growth of both normal and neoplastic tissue but does not induce invasion or dissemination¹²¹ (Fig. 1-5D). However, the addition of adhesive peptides to the PEG network promotes dissemination of both normal and tumour cells¹²¹. These studies collectively show that stromal cells, ECM composition and microenvironmental mechanics can independently regulate cell and tissue function¹⁴⁰.

Stem cell-derived organs and therapeutics

3D culture can be used to define the necessary and sufficient components to replicate the structure and function of an organ. This approach, sometimes termed synthetic tissue biology¹⁴¹, can guide our understanding of normal development and generate replacement tissues¹⁴². For example, single Lgr5+ epithelial cells isolated from the small intestine are sufficient to generate organoids with crypt-villus architecture, without mesenchymal cells⁶. However, the efficiency of generating intestinal organoids from

Lgr5+ cells is greatly enhanced by co-culture with Paneth cells¹⁴³. Organoid cultures can also be passaged indefinitely to produce sufficient cells for transplantation^{37,38,144}. In principle, stem cells from a patient's own injured organ could be used to generate organoids to repair the damage. Supporting this concept, a recent study induced experimental colitis in mice and introduced Lgr5+ organoids into the colon¹⁴⁴. The organoids engrafted and formed crypts with barrier function¹⁴⁴. In cases in which the disease state is caused by a known mutation, combinations of patient-derived iPS cells with genome editing techniques, such as Crispr-Cas9, could enable the generation of replacement cells and tissues in which the mutation has been corrected¹⁰². This strategy has been validated in cystic fibrosis patient-derived organoids in which correction of the disease-inducing mutation in the cystic fibrosis transmembrane conductor receptor (CFTR) restored channel function in 3D culture¹⁰².

3D cultures of ES cells or iPS cells can also assemble into specific tissues and organs. A striking example is the formation of the optic cup from ES cell aggregates, with the stratified neural tissue containing all six cell types in their appropriate spatial arrangement⁴⁴. Improved culture conditions have enabled routine production of both rod and cone photoreceptors, and cryogenic storage of sheets of stratified human neural retina⁴⁵. Adaptation of these techniques for mouse retina enabled transplantation and functional engraftment into retinal degenerative mice¹⁴⁵. This therapeutic approach has also been used for endocrine glands: mouse iPS cells were first differentiated into immature pancreatic cells and then differentiated in 3D culture into islets¹⁴⁶. Upon transplantation into mice, these islets incorporate into the pancreas and improve blood glucose levels in hyperglycemic mice¹⁴⁶. A recent study further revealed that co-culture with mesenchyme increases the efficiency of expansion of human endodermal progenitors more than one million fold, while preserving the capacity of the progenitors

to give rise to glucose-sensing, insulin-secreting cells following transplantation *in vivo*¹⁴⁷. In the thyroid, transient expression of two transcription factors enables the generation of thyroid follicular cells from ES cells in 3D culture, and following transplantation into athymic mice, these cells rescue plasma levels of thyroid hormones¹⁴⁸. Taken together, these studies reveal 3D culture as a crucial method to generate replacement tissues for therapeutic purposes¹⁴⁹.

An additional strength of these approaches emerges when studying organs that considerably diverge between mice and humans. ES cell- and iPS cell-based methods enable the real-time analysis of anatomically complex human organs such as the brain. A recent study developed cerebral organoids from human iPS cells in 3D culture and replicated the anatomical organization of multiple human brain regions, including cerebral cortex⁴⁷. In turn, organoids derived from iPS cells isolated from a patient with severe microcephaly displayed premature neuronal differentiation and reduced amounts of neuroepithelium, demonstrating that even complex disorders of the central nervous system can be modeled using 3D culture⁴⁷.

Future directions

A major goal of biomedical science is translating our understanding of the fundamental principles governing biological systems to improve patient outcomes. 3D culture can function as an integration point for the modeling of human disease in experimental systems that also yields precise answers to biological questions. Achieving the full potential of these methods will involve the expertise of both scientists and clinicians and may require new funding mechanisms to sustain the interdisciplinary work required.

We anticipate that recent advances in 3D culture will accelerate our understanding of the cellular and molecular basis of mammalian organogenesis, both through the study of primary mouse tissues and in artificially generated human organs. Equally important, real-time analysis promises to yield insights into the dynamic cellular basis of disease processes, especially when robust mouse models have been developed. This combined knowledge of normal development and pathobiology should enable the identification of molecular signals that promote tissue regeneration, restore tissue function and resist disease progression.

A particularly exciting new direction is the ability to explant the living tissue of a patient into 3D culture to obtain individualized predictive or prognostic information, which is the ultimate goal of personalized medicine (Fig. 1-6A-C). It is now possible to culture primary human cells or tissues using excess material from surgery^{30,37,73,102}. These human cell cultures could be used to test novel therapeutic strategies, to guide the selection of therapies for a specific patient or to grow replacement cells or tissues from the cells of a patient. The success of this therapeutic approach will require a high degree of standardization and reproducibility across experiments. Additionally, patient tissue in 3D culture could be analyzed for its dynamic molecular responses to standardized cellular and molecular cues, such as targeted therapies¹⁵⁰.

The development of robust vascular networks in 3D culture^{10,11} should enable the generation of larger and more complex tissue constructs¹⁵¹, improve transplant efficiency¹⁰ and catalyze a transition in 3D culture from self-organization of simple tissues to the synthetic assembly of multicomponent organs. This transition in complexity should enable an expanded focus on the recapitulation of organ function^{152,153}. Recent efforts in this direction suggest that functional properties of an organ can be replicated in

microfluidic assays that don't closely model the normal in vivo tissue architecture⁷⁸. Finally, the successful functional incorporation of transplanted organoids into murine colon¹⁴⁴, retina¹⁴⁵, thyroid¹⁴⁸, liver^{38,152} and pancreas^{146,147} suggest that organ function can be restored in human patients through transfer of functional units of tissue rather than through whole organ transplantation.

References

- 1 Bichat, X. General anatomy, applied to physiology and medicine. (Richardson and Lord, 1822).
- 2 Virchow, R. Cellular pathology, as based upon physiological and pathological histology. Twenty lectures delivered in the Pathological institute of Berlin during the months of February, March and April, 1858. (R. M. De Witt, 1860).
- 3 Sobotta, J., Huber, G. C. & De Witt, L. M. b. Atlas and epitome of human histology and microscopic anatomy. (W. B. Saunders & company, 1903).
- 4 Harrison, R. G., Greenman, M. J., Mall, F. P. & Jackson, C. M. Observations on the living developing nerve fiber. *The Anatomical Record* 1, 116-128, (1907).
- 5 Simian, M. *et al.* The interplay of matrix metalloproteinases, morphogens and growth factors is necessary for branching of mammary epithelial cells. *Development* 128, 3117-3131, (2001).
- 6 Sato, T. *et al.* Single Lgr5 stem cells build crypt-villus structures in vitro without a mesenchymal niche. *Nature* 459, 262-265, (2009).
- 7 Finkbeiner, S. R. & Spence, J. R. A gutsy task: generating intestinal tissue from human pluripotent stem cells. *Dig Dis Sci* 58, 1176-1184, (2013).
- 8 Alberts, B. *Molecular biology of the cell*. 4th edn, (Garland Science, 2002).
- 9 Nelson, C. M. & Bissell, M. J. Of extracellular matrix, scaffolds, and signaling: tissue architecture regulates development, homeostasis, and cancer. *Annu Rev Cell Dev Biol* 22, 287-309, (2006).
- 10 Baranski, J. D. *et al.* Geometric control of vascular networks to enhance engineered tissue integration and function. *Proceedings of the National Academy of Sciences of the United States of America* 110, 7586-7591, (2013).
- 11 Zheng, Y. *et al.* In vitro microvessels for the study of angiogenesis and thrombosis. *Proc Natl Acad Sci U S A* 109, 9342-9347, (2012).
- 12 Nguyen, D.-H. T. *et al.* Biomimetic model to reconstitute angiogenic sprouting morphogenesis in vitro. *Proceedings of the National Academy of Sciences of the United States of America* 110, 6712-6717, (2013).
- 13 Fell, H. B. & Robison, R. The growth, development and phosphatase activity of embryonic avian femora and limb-buds cultivated in vitro. *Biochem J* 23, 767-784 765, (1929).
- 14 Chen, J. M. The cultivation in fluid medium of organised liver, pancreas and other tissues of foetal rats. *Exp Cell Res* 7, 518-529, (1954).
- 15 Ichinose, R. R. & Nandi, S. Lobuloalveolar Differentiation in Mouse Mammary Tissues in Vitro. *Science* 145, 496-497, (1964).
- 16 Waymouth, C. in *Biology of the Laboratory Mouse* (ed Earl L. Green) (Dover Publications, Inc., 1966).
- 17 Guerrero, R. R., Rounds, D. E. & Booher, J. An improved organ culture method for adult mammalian lung. *In Vitro* 13, 517-524, (1977).
- 18 Browning, T. H. & Trier, J. S. Organ culture of mucosal biopsies of human small intestine. *J. Clin. Invest.* 48, 1423-1432, (1969).
- 19 Randall, K. J., Turton, J. & Foster, J. R. Explant culture of gastrointestinal tissue: a review of methods and applications. *Cell Biol. Toxicol.* 27, 267-284, (2011).
- 20 Autrup, H. *et al.* Explant culture of rat colon: a model system for studying metabolism of chemical carcinogens. *In vitro* 14, 868-877, (1978).
- 21 Stoppini, L., Buchs, P. A. & Muller, D. A simple method for organotypic cultures of nervous tissue. *J. Neurosci. Methods* 37, 173-182, (1991).

22 Gähwiler, B. H., Capogna, M., Debanne, D., McKinney, R. A. & Thompson, S. M. Organotypic slice cultures: a technique has come of age. *Trends Neurosci.* 20, 471-477, (1997).

23 Aplin, A. C., Fogel, E., Zorzi, P. & Nicosia, R. F. Vol. 443 119-136 (Elsevier, 2008).

24 Topper, R. J., Oka, T. & Vonderhaar, B. K. Techniques for studying development of normal mammary epithelial cells in organ culture. *Methods Enzymol* 39, 443-454, (1975).

25 Hardman, P., Klement, B. J. & Spooner, B. S. Growth and morphogenesis of embryonic mouse organs on non-coated and extracellular matrix-coated Biopore membrane. *Dev Growth Differ* 35, 683-690, (1993).

26 Trott, J. F., Vonderhaar, B. K. & Hovey, R. C. Historical perspectives of prolactin and growth hormone as mammogens, lactogens and galactagogues--agog for the future! *J Mammary Gland Biol Neoplasia* 13, 3-11, (2008).

27 Shamir, E. R. *et al.* Twist1-induced dissemination preserves epithelial identity and requires E-cadherin. *J Cell Biol* 204, 839-856, (2014).

28 Koo, B. K. *et al.* Controlled gene expression in primary Lgr5 organoid cultures. *Nat Methods* 9, 81-83, (2011).

29 Onodera, T. *et al.* Btdb7 regulates epithelial cell dynamics and branching morphogenesis. *Science* 329, 562-565, (2010).

30 Cheung, K. J., Gabrielson, E., Werb, Z. & Ewald, A. J. Collective invasion in breast cancer requires a conserved basal epithelial program. *Cell* 155, 1639-1651, (2013).

31 Daley, W. P., Gulfo, K. M., Sequeira, S. J. & Larsen, M. Identification of a mechanochemical checkpoint and negative feedback loop regulating branching morphogenesis. *Dev Biol* 336, 169-182, (2009).

32 Fata, J. E. *et al.* The MAPKERK-1,2 pathway integrates distinct and antagonistic signals from TGF α and FGF7 in morphogenesis of mouse mammary epithelium. *Dev. Biol.* 306, 193-207, (2007).

33 Steinberg, Z. *et al.* FGFR2b signaling regulates ex vivo submandibular gland epithelial cell proliferation and branching morphogenesis. *Development* 132, 1223-1234, (2005).

34 Zhang, X., Bush, K. T. & Nigam, S. K. Vol. 886 13-21 (Humana Press, 2012).

35 Liu, Y. *et al.* Novel role for Netrins in regulating epithelial behavior during lung branching morphogenesis. *Curr Biol* 14, 897-905, (2004).

36 Ootani, A. *et al.* Sustained in vitro intestinal epithelial culture within a Wnt-dependent stem cell niche. *Nat Med* 15, 701-706, (2009).

37 Sato, T. *et al.* Long-term expansion of epithelial organoids from human colon, adenoma, adenocarcinoma, and Barrett's epithelium. *Gastroenterology* 141, 1762-1772, (2011).

38 Huch, M. *et al.* In vitro expansion of single Lgr5+ liver stem cells induced by Wnt-driven regeneration. *Nature* 494, 247-250, (2013).

39 Barker, N. *et al.* Lgr5(+ve) stem cells drive self-renewal in the stomach and build long-lived gastric units in vitro. *Cell Stem Cell* 6, 25-36, (2010).

40 Huch, M. *et al.* Unlimited in vitro expansion of adult bi-potent pancreas progenitors through the Lgr5/R-spondin axis. *The EMBO journal* 32, 2708-2721, (2013).

41 Ghosh, S. *et al.* PI3K/mTOR signaling regulates prostatic branching morphogenesis. *Dev Biol* 360, 329-342, (2011).

42 Kleinman, H. K. & Martin, G. R. Matrigel: basement membrane matrix with biological activity. *Semin Cancer Biol* 15, 378-386, (2005).

43 Wolf, K. *et al.* Collagen-based cell migration models in vitro and in vivo. *Semin*
44 *Cell Dev Biol* 20, 931-941, (2009).

45 Eiraku, M. *et al.* Self-organizing optic-cup morphogenesis in three-dimensional
46 culture. *Nature* 472, 51-56, (2011).

47 Nakano, T. *et al.* Self-formation of optic cups and storable stratified neural retina
48 from human ESCs. *Cell Stem Cell* 10, 771-785, (2012).

49 Eiraku, M. *et al.* Self-Organized Formation of Polarized Cortical Tissues from
50 ESCs and Its Active Manipulation by Extrinsic Signals. *STEM* 3, 519-532, (2008).

51 Lancaster, M. A. *et al.* Cerebral organoids model human brain development and
52 microcephaly. *Nature* 501, 373-379, (2013).

53 Suga, H. *et al.* Self-formation of functional adenohypophysis in three-dimensional
54 culture. *Nature* 480, 57-62, (2011).

55 Townes, P. L. & Holtfreter, J. Directed movements and selective adhesion of
56 embryonic amphibian cells. *Journal of Experimental Zoology* 128, 53-120,
57 (1955).

58 O'Brien, L. E., Zegers, M. M. & Mostov, K. E. Opinion: Building epithelial
59 architecture: insights from three-dimensional culture models. *Nat Rev Mol Cell*
60 *Biol* 3, 531-537, (2002).

61 Debnath, J., Muthuswamy, S. K. & Brugge, J. S. Morphogenesis and
62 oncogenesis of MCF-10A mammary epithelial acini grown in three-dimensional
basement membrane cultures. *Methods* 30, 256-268, (2003).

Green, H., Kehinde, O. & Thomas, J. Growth of cultured human epidermal cells
into multiple epithelia suitable for grafting. *Proc Natl Acad Sci U S A* 76, 5665-
5668, (1979).

Fuchs, E. Epidermal differentiation: the bare essentials. *J Cell Biol* 111, 2807-
2814, (1990).

Kalabis, J. *et al.* Isolation and characterization of mouse and human esophageal
epithelial cells in 3D organotypic culture. *Nat Protoc* 7, 235-246, (2012).

Unbekandt, M. & Davies, J. A. Dissociation of embryonic kidneys followed by
reaggregation allows the formation of renal tissues. *Kidney Int* 77, 407-416,
(2009).

Ganeva, V., Unbekandt, M. & Davies, J. A. An improved kidney dissociation and
reaggregation culture system results in nephrons arranged organotypically
around a single collecting duct system. *Organogenesis* 7, 83-87, (2011).

Streuli, C. H., Bailey, N. & Bissell, M. J. Control of mammary epithelial
differentiation: basement membrane induces tissue-specific gene expression in
the absence of cell-cell interaction and morphological polarity. *J Cell Biol* 115,
1383-1395, (1991).

O'Brien, L. E. *et al.* Rac1 orientates epithelial apical polarity through effects on
basolateral laminin assembly. *Nat Cell Biol* 3, 831-838, (2001).

Yu, W. *et al.* Formation of cysts by alveolar type II cells in three-dimensional
culture reveals a novel mechanism for epithelial morphogenesis. *Mol Biol Cell* 18,
1693-1700, (2007).

Greenburg, G. & Hay, E. D. Epithelia suspended in collagen gels can lose
polarity and express characteristics of migrating mesenchymal cells. *J Cell Biol*
95, 333-339, (1982).

Debnath, J. & Brugge, J. S. Modelling glandular epithelial cancers in three-
dimensional cultures. *Nat Rev Cancer* 5, 675-688, (2005).

Ewald, A. J., Brenot, A., Duong, M., Chan, B. S. & Werb, Z. Collective epithelial
migration and cell rearrangements drive mammary branching morphogenesis.
Dev Cell 14, 570-581, (2008).

63 Morita, K. & Nogawa, H. EGF-dependent lobule formation and FGF7-dependent
stalk elongation in branching morphogenesis of mouse salivary epithelium in
64 vitro. *Dev Dyn* 215, 148-154, (1999).

65 Qiao, J., Sakurai, H. & Nigam, S. K. Branching morphogenesis independent of
mesenchymal-epithelial contact in the developing kidney. *Proc Natl Acad Sci U S*
A 96, 7330-7335, (1999).

66 Wescott, M. P. *et al.* Pancreatic ductal morphogenesis and the Pdx1
homeodomain transcription factor. *Molecular biology of the cell* 20, 4838-4844,
(2009).

67 Nguyen-Ngoc, K.-V. *et al.* ECM microenvironment regulates collective migration
and local dissemination in normal and malignant mammary epithelium.
Proceedings of the National Academy of Sciences of the United States of
America 109, E2595-2604, (2012).

68 Nguyen-Ngoc, K. V. & Ewald, A. J. Mammary ductal elongation and myoepithelial
migration are regulated by the composition of the extracellular matrix. *J Microsc*
251, 212-223, (2013).

69 Brownfield, D. G. *et al.* Patterned collagen fibers orient branching mammary
epithelium through distinct signaling modules. *Curr Biol* 23, 703-709, (2013).

70 Levental, K. R. *et al.* Matrix crosslinking forces tumor progression by enhancing
integrin signaling. *Cell* 139, 891-906, (2009).

71 Provenzano, P. P. *et al.* Collagen reorganization at the tumor-stromal interface
facilitates local invasion. *BMC Med* 4, 38, (2006).

72 Provenzano, P. P. *et al.* Collagen density promotes mammary tumor initiation
and progression. *BMC Med* 6, 11, (2008).

73 Ewald, A. J. Practical considerations for long-term time-lapse imaging of
epithelial morphogenesis in three-dimensional organotypic cultures. *Cold Spring*
Harb Protoc 2013, (2013).

74 Ridky, T. W., Chow, J. M., Wong, D. J. & Khavari, P. A. Invasive three-
dimensional organotypic neoplasia from multiple normal human epithelia. *Nat.*
Med. 16, 1450-1455, (2010).

75 Baker, B. M. & Chen, C. S. Deconstructing the third dimension: how 3D culture
microenvironments alter cellular cues. *J Cell Sci* 125, 3015-3024, (2012).

76 Dvir, T., Timko, B. P., Kohane, D. S. & Langer, R. Nanotechnological strategies
for engineering complex tissues. *Nat Nanotechnol* 6, 13-22, (2010).

77 Singh, A. & Elisseeff, J. Biomaterials for stem cell differentiation. *Journal of*
Materials Chemistry 20, 8832-8847, (2010).

78 Young, E. W. & Beebe, D. J. Fundamentals of microfluidic cell culture in
controlled microenvironments. *Chem Soc Rev* 39, 1036-1048, (2010).

79 Huh, D. *et al.* Reconstituting Organ-Level Lung Functions on a Chip. *Science*
328, 1662-1668, (2010).

80 Stroock, A. D. & Fischbach, C. Microfluidic culture models of tumor angiogenesis.
Tissue Engineering Part A 16, 2143-2146, (2010).

81 Gartner, Z. J. & Bertozzi, C. R. Programmed assembly of 3-dimensional
microtissues with defined cellular connectivity. Proceedings of the National
Academy of Sciences of the United States of America 106, 4606-4610, (2009).

82 Varner, V. D. & Nelson, C. M. Let's push things forward: disruptive technologies
and the mechanics of tissue assembly. *Integr Biol (Camb)* 5, 1162-1173, (2013).

Huebner, R. J., Lechler, T. & Ewald, A. J. Developmental stratification of the
mammary epithelium occurs through symmetry-breaking vertical divisions of
apically positioned luminal cells. *Development* 141, 1085-1094, (2014).

83 Larsen, M. *et al.* Role of PI 3-kinase and PIP3 in submandibular gland branching
morphogenesis. *Dev Biol* 255, 178-191, (2003).

84 Puri, S. & Hebrok, M. Dynamics of embryonic pancreas development using real-
time imaging. *Dev Biol* 306, 82-93, (2007).

85 Kim, H. Y., Varner, V. D. & Nelson, C. M. Apical constriction initiates new bud
formation during monopodial branching of the embryonic chicken lung.
Development 140, 3146-3155, (2013).

86 Provenzano, P. P. *et al.* Nonlinear optical imaging of cellular processes in breast
cancer. *Microsc Microanal* 14, 532-548, (2008).

87 Underwood, J. M. *et al.* The ultrastructure of MCF-10A acini. *J Cell Physiol* 208,
141-148, (2006).

88 Ewald, A. J. *et al.* Mammary collective cell migration involves transient loss of
epithelial features and individual cell migration within the epithelium. *J Cell Sci*
125, 2638-2654, (2012).

89 Grugan, K. D. *et al.* Fibroblast-secreted hepatocyte growth factor plays a
functional role in esophageal squamous cell carcinoma invasion. *Proceedings of
the National Academy of Sciences of the United States of America* 107, 11026-
11031, (2010).

90 Ghabrial, A. S. & Krasnow, M. A. Social interactions among epithelial cells during
tracheal branching morphogenesis. *Nature* 441, 746-749, (2006).

91 Lu, P. & Werb, Z. Patterning mechanisms of branched organs. *Science* 322,
1506-1509, (2008).

92 Larsen, M., Wei, C. & Yamada, K. M. Cell and fibronectin dynamics during
branching morphogenesis. *J Cell Sci* 119, 3376-3384, (2006).

93 Shakya, R., Watanabe, T. & Costantini, F. The role of GDNF/Ret signaling in
ureteric bud cell fate and branching morphogenesis. *Dev Cell* 8, 65-74, (2005).

94 Chi, X. *et al.* Ret-dependent cell rearrangements in the Wolffian duct epithelium
initiate ureteric bud morphogenesis. *Dev Cell* 17, 199-209, (2009).

95 Patel, V. N. *et al.* Specific Heparan Sulfate Structures Modulate FGF10-mediated
Submandibular Gland Epithelial Morphogenesis and Differentiation. *J. Biol.
Chem.* 283, 9308-9317, (2008).

96 Packard, A. *et al.* Luminal Mitosis Drives Epithelial Cell Dispersal within the
Branching Ureteric Bud. *Dev. Cell* 27, 319-330, (2013).

97 Schnatwinkel, C. & Niswander, L. Multiparametric image analysis of lung-
branching morphogenesis. *Dev. Dyn.* 242, 622-637, (2013).

98 Cukierman, E., Pankov, R., Stevens, D. R. & Yamada, K. M. Taking cell-matrix
adhesions to the third dimension. *Science* 294, 1708-1712, (2001).

99 Hsu, J. C. *et al.* Viral Gene Transfer to Developing Mouse Salivary Glands. *J.
Dent. Res.* 91, 197-202, (2012).

100 Sequeira, S. J., Gervais, E. M., Ray, S. & Larsen, M. Genetic Modification and
Recombination of Salivary Gland Organ Cultures. *Journal of Visualized
Experiments*, (2013).

101 Mali, P. *et al.* RNA-guided human genome engineering via Cas9. *Science* 339,
823-826, (2013).

102 Schwank, G. *et al.* Functional Repair of CFTR by CRISPR/Cas9 in Intestinal
Stem Cell Organoids of Cystic Fibrosis Patients. *STEM* 13, 653-658, (2013).

103 Yu, W. *et al.* Beta1-integrin orients epithelial polarity via Rac1 and laminin. *Mol
Biol Cell* 16, 433-445, (2005).

104 Martin-Belmonte, F. *et al.* Cell-polarity dynamics controls the mechanism of
lumen formation in epithelial morphogenesis. *Curr Biol* 18, 507-513, (2008).

105 Bryant, D. M. *et al.* A molecular network for de novo generation of the apical
surface and lumen. *Nat. Cell Biol.* 12, 1035-1045, (2010).

106 Gálvez-Santisteban, M. *et al.* Synaptotagmin-like proteins control the formation of
a single apical membrane domain in epithelial cells. *Nat. Cell Biol.* 14, 838-849,
(2012).

107 Muthuswamy, S. K., Li, D., Lelievre, S., Bissell, M. J. & Brugge, J. S. ErbB2, but
not ErbB1, reinitiates proliferation and induces luminal repopulation in epithelial
acini. *Nat Cell Biol* 3, 785-792, (2001).

108 Aranda, V. *et al.* Par6–aPKC uncouples ErbB2 induced disruption of polarized
epithelial organization from proliferation control. *Nat. Cell Biol.* 8, 1235-1245,
(2006).

109 Zhan, L. *et al.* Deregulation of scribble promotes mammary tumorigenesis and
reveals a role for cell polarity in carcinoma. *Cell* 135, 865-878, (2008).

110 Xue, B., Krishnamurthy, K., Allred, D. C. & Muthuswamy, S. K. Loss of Par3
promotes breast cancer metastasis by compromising cell–cell cohesion. 1-14,
(2013).

111 Leung, C. T. & Brugge, J. S. Outgrowth of single oncogene-expressing cells from
suppressive epithelial environments. *Nature* 482, 410-413, (2012).

112 Sakurai, A., Matsuda, M. & Kiyokawa, E. Activated Ras protein accelerates cell
cycle progression to perturb Madin-Darby canine kidney cystogenesis. *J Biol
Chem* 287, 31703-31711, (2012).

113 Truong, A. B., Kretz, M., Ridky, T. W., Kimmel, R. & Khavari, P. A. p63 regulates
proliferation and differentiation of developmentally mature keratinocytes. *Genes
Dev.* 20, 3185-3197, (2006).

114 Kretz, M. *et al.* Control of somatic tissue differentiation by the long non-coding
RNA TINCR. *Nature* 493, 231-235, (2013).

115 Sakai, T., Larsen, M. & Yamada, K. M. Fibronectin requirement in branching
morphogenesis. *Nature* 423, 876-881, (2003).

116 Yates, L. L. *et al.* Scribble is required for normal epithelial cell–cell contacts and
lumen morphogenesis in the mammalian lung. *Dev. Biol.* 373, 267-280, (2013).

117 Liu, J. S., Farlow, J. T., Paulson, A. K., Labarge, M. A. & Gartner, Z. J.
Programmed cell-to-cell variability in Ras activity triggers emergent behaviors
during mammary epithelial morphogenesis. *Cell Rep* 2, 1461-1470, (2012).

118 Plichta, K. A., Mathers, J. L., Gestl, S. A., Glick, A. B. & Gunther, E. J. Basal but
not luminal mammary epithelial cells require PI3K/mTOR signaling for Ras-driven
overgrowth. *Cancer Res.* 72, 5856-5866, (2012).

119 Egeblad, M., Nakasone, E. S. & Werb, Z. Tumors as organs: complex tissues
that interface with the entire organism. *Dev Cell* 18, 884-901, (2010).

120 Egeblad, M., Rasch, M. G. & Weaver, V. M. Dynamic interplay between the
collagen scaffold and tumor evolution. *Curr Opin Cell Biol* 22, 697-706, (2010).

121 Beck, J. N., Singh, A., Rothenberg, A. R., Elisseeff, J. H. & Ewald, A. J. The
independent roles of mechanical, structural and adhesion characteristics of 3D
hydrogels on the regulation of cancer invasion and dissemination. *Biomaterials*
34, 9486-9495, (2013).

122 Engler, A. J., Sen, S., Sweeney, H. L. & Discher, D. E. Matrix elasticity directs
stem cell lineage specification. *Cell* 126, 677-689, (2006).

123 Condeelis, J. & Pollard, J. W. Macrophages: obligate partners for tumor cell
migration, invasion, and metastasis. *Cell* 124, 263-266, (2006).

124 DeNardo, D. G. *et al.* CD4(+) T cells regulate pulmonary metastasis of mammary
carcinomas by enhancing protumor properties of macrophages. *Cancer Cell* 16,
91-102, (2009).

125 Gaggioli, C. *et al.* Fibroblast-led collective invasion of carcinoma cells with
differing roles for RhoGTPases in leading and following cells. *Nat Cell Biol* 9,
1392-1400, (2007).

126 Calvo, F. *et al.* Mechanotransduction and YAP-dependent matrix remodelling is
required for the generation and maintenance of cancer-associated fibroblasts.
Nat Cell Biol 15, 637-646, (2013).

127 Okawa, T. *et al.* The functional interplay between EGFR overexpression, hTERT
activation, and p53 mutation in esophageal epithelial cells with activation of
stromal fibroblasts induces tumor development, invasion, and differentiation.
Genes & Development 21, 2788-2803, (2007).

128 Lee, J.-H. *et al.* Lung Stem Cell Differentiation in Mice Directed by Endothelial
Cells via a BMP4-NFATc1-Thrombospondin-1 Axis. *Cell* 156, 440-455, (2014).

129 Ghajar, C. M. *et al.* The perivascular niche regulates breast tumour dormancy.
Nat. Cell Biol. 15, 807-817, (2013).

130 Infanger, D. W. *et al.* Glioblastoma Stem Cells Are Regulated by Interleukin-8
Signaling in a Tumoral Perivascular Niche. *Cancer Res.*, (2013).

131 Knox, S. M. *et al.* Parasympathetic Innervation Maintains Epithelial Progenitor
Cells During Salivary Organogenesis. *Science* 329, 1645-1647, (2010).

132 Knox, S. M. *et al.* Parasympathetic stimulation improves epithelial organ
regeneration. *Nature communications* 4, 1494, (2013).

133 Marusyk, A., Almendro, V. & Polyak, K. Intra-tumour heterogeneity: a looking
glass for cancer? *Nat Rev Cancer* 12, 323-334, (2012).

134 Carey, S. P., Starchenko, A., McGregor, A. L. & Reinhart-King, C. A. Leading
malignant cells initiate collective epithelial cell invasion in a three-dimensional
heterotypic tumor spheroid model. *Clin Exp Metastasis* 30, 615-630, (2013).

135 Dang, T. T., Prectl, A. M. & Pearson, G. W. Breast cancer subtype-specific
interactions with the microenvironment dictate mechanisms of invasion. *Cancer
Res* 71, 6857-6866, (2011).

136 Gudjonsson, T. *et al.* Normal and tumor-derived myoepithelial cells differ in their
ability to interact with luminal breast epithelial cells for polarity and basement
membrane deposition. *J Cell Sci* 115, 39-50, (2002).

137 Chanson, L. *et al.* Self-organization is a dynamic and lineage-intrinsic property of
mammary epithelial cells. *Proceedings of the National Academy of Sciences of
the United States of America* 108, 3264-3269, (2011).

138 Conklin, M. W. *et al.* Aligned collagen is a prognostic signature for survival in
human breast carcinoma. *Am J Pathol* 178, 1221-1232, (2011).

139 Paszek, M. J. *et al.* Tensional homeostasis and the malignant phenotype. *Cancer
Cell* 8, 241-254, (2005).

140 Friedl, P. & Alexander, S. Cancer invasion and the microenvironment: plasticity
and reciprocity. *Cell* 147, 992-1009, (2011).

141 Sia, S. K., Gillette, B. M. & Yang, G. J. Synthetic tissue biology: tissue
engineering meets synthetic biology. *Birth Defects Res C Embryo Today* 81, 354-
361, (2007).

142 Elliott, M. J. *et al.* Stem-cell-based, tissue engineered tracheal replacement in a
child: a 2-year follow-up study. *Lancet* 380, 994-1000, (2012).

143 Sato, T. *et al.* Paneth cells constitute the niche for Lgr5 stem cells in intestinal
crypts. *Nature* 469, 415-418, (2011).

144 Yui, S. *et al.* Functional engraftment of colon epithelium expanded in vitro from a
single adult Lgr5+ stem cell. *Nat. Med.* 18, 618-623, (2012).

145 Assawachananont, J. *et al.* Transplantation of Embryonic and Induced
Pluripotent Stem Cell-Derived 3D Retinal Sheets into Retinal Degenerative Mice.
Stem Cell Reports 2, 662-674, (2014).

146 Saito, H., Takeuchi, M., Chida, K. & Miyajima, A. Generation of glucose-
responsive functional islets with a three-dimensional structure from mouse fetal
pancreatic cells and iPS cells in vitro. PLoS One 6, e28209, (2011).

147 Sneddon, J. B., Borowiak, M. & Melton, D. A. Self-renewal of embryonic-stem-
cell-derived progenitors by organ-matched mesenchyme. Nature 491, 765-768,
(2012).

148 Antonica, F. *et al.* Generation of functional thyroid from embryonic stem cells.
Nature 491, 66-71, (2012).

149 Sasai, Y. Next-generation regenerative medicine: organogenesis from stem cells
in 3D culture. Cell Stem Cell 12, 520-530, (2013).

150 Schayowitz, A. *et al.* Functional profiling of live melanoma samples using a novel
automated platform. PLoS One 7, e52760, (2013).

151 Miller, J. S. *et al.* Rapid casting of patterned vascular networks for perfusable
engineered three-dimensional tissues. Nature materials 11, 768-774, (2012).

152 Takebe, T. *et al.* Vascularized and functional human liver from an iPSC-derived
organ bud transplant. Nature 499, 481-484, (2013).

153 Sudo, R. Multiscale tissue engineering for liver reconstruction. Organogenesis
10, (2014).

154 Schrag, D. *et al.* American Society of Clinical Oncology Technology Assessment:
chemotherapy sensitivity and resistance assays. J Clin Oncol 22, 3631-3638,
(2004).

155 Burstein, H. J. *et al.* American Society of Clinical Oncology Clinical Practice
Guideline Update on the Use of Chemotherapy Sensitivity and Resistance
Assays. Journal of Clinical Oncology 29, 3328-3330, (2011).

156 Vaira, V. *et al.* Preclinical model of organotypic culture for pharmacodynamic
profiling of human tumors. Proceedings of the National Academy of Sciences of
the United States of America 107, 8352-8356, (2010).

157 Merz, F. *et al.* Organotypic slice cultures of human glioblastoma reveal different
susceptibilities to treatments. Neuro-Oncology 15, 670-681, (2013).

158 Dekkers, J. F. *et al.* A functional CFTR assay using primary cystic fibrosis
intestinal organoids. Nat. Med. 19, 939-945, (2013).

159 Muranen, T. *et al.* Inhibition of PI3K/mTOR Leads to Adaptive Resistance in
Matrix-Attached Cancer Cells. CCELL 21, 227-239, (2012).

160 Walker, J. L. *et al.* Diverse roles of E-cadherin in the morphogenesis of the
submandibular gland: Insights into the formation of acinar and ductal structures.
Dev. Dyn. 237, 3128-3141, (2008).

161 Weaver, V. M. *et al.* Reversion of the malignant phenotype of human breast cells
in three-dimensional culture and in vivo by integrin blocking antibodies. J Cell
Biol 137, 231-245, (1997).

162 Ginsburg, E. & Vonderhaar, B. K. in Methods in Mammary Gland Biology and ...
147-154 (Springer US, 2000).

163 Nguyen-Ngoc, K. V. *et al.* in Tissue Morphogenesis: Methods and Protocols Vol.
1189 Methods in Molecular Biology (ed C.M. Nelson) (Springer
Science+Business Media, 2014).

164 Akhtar, N. & Streuli, C. H. An integrin--ILK--microtubule network orients cell
polarity and lumen formation in glandular epithelium. Nat. Cell Biol. 15, 17-27,
(2012).

165 Daley, W. P. *et al.* ROCK1-directed basement membrane positioning coordinates
epithelial tissue polarity. *Development* 139, 411-422, (2011).

166 Pradhan-Bhatt, S. *et al.* Implantable Three-Dimensional Salivary Spheroid
Assemblies Demonstrate Fluid and Protein Secretory Responses to
167 Neurotransmitters. *Tissue Engineering Part A* 19, 1610-1620, (2013).

168 Wei, C., Larsen, M., Hoffman, M. P. & Yamada, K. M. Self-Organization and
Branching Morphogenesis of Primary Salivary Epithelial Cells. *Tissue Eng.* 13,
721-735, (2007).

169 O'Brien, L. E. *et al.* Morphological and biochemical analysis of Rac1 in three-
dimensional epithelial cell cultures. *Methods Enzymol* 406, 676-691, (2006).

170 Yagi, S., Matsuda, M. & Kiyokawa, E. Suppression of Rac1 activity at the apical
membrane of MDCK cells is essential for cyst structure maintenance. *EMBO Rep*
13, 237-243, (2012).

171 Srinivas, S. *et al.* Expression of green fluorescent protein in the ureteric bud of
transgenic mice: a new tool for the analysis of ureteric bud morphogenesis. *Dev*
Genet 24, 241-251, (1999).

172 Costantini, F., Watanabe, T., Lu, B., Chi, X. & Srinivas, S. Dissection of
Embryonic Mouse Kidney, Culture In Vitro, and Imaging of the Developing
Organ. *Cold Spring Harbor Protocols* 2011, pdb.prot5613-pdb.prot5613, (2011).

173 Rosines, E. *et al.* Constructing kidney-like tissues from cells based on programs
for organ development: toward a method of in vitro tissue engineering of the
kidney. *Tissue Engineering Part A* 16, 2441-2455, (2010).

174 Steer, D. L., Bush, K. T., Meyer, T. N., Schwesinger, C. & Nigam, S. K. A
strategy for in vitro propagation of rat nephrons. *Kidney international* 62, 1958-
1965, (2002).

175 Taub, M., Wang, Y., Szczesny, T. M. & Kleinman, H. K. Epidermal growth factor
or transforming growth factor alpha is required for kidney tubulogenesis in
matrigel cultures in serum-free medium. *Proceedings of the National Academy of*
Sciences of the United States of America 87, 4002-4006, (1990).

176 Morizane, R. *et al.* Kidney Specific Protein-Positive Cells Derived from
Embryonic Stem Cells Reproduce Tubular Structures In Vitro and Differentiate
into Renal Tubular Cells. *PLoS ONE* 8, e64843, (2013).

177 Taguchi, A. *et al.* Redefining the in vivo origin of metanephric nephron
progenitors enables generation of complex kidney structures from pluripotent
stem cells. *Cell Stem Cell* 14, 53-67, (2014).

178 Takasato, M., Little, M. H. & Elefanty, A. G. Directing human embryonic stem cell
differentiation towards a renal lineage generates a self-organizing kidney. *Nat.*
Cell Biol. 16, 118-126, (2013).

179 Parrish, A. R., Gandolfi, A. J. & Brendel, K. Precision-cut tissue slices:
applications in pharmacology and toxicology. *Life Sci* 57, 1887-1901, (1995).

180 del Moral, P.-M. & Warburton, D. Vol. 633 71-79 (Humana Press, 2010).

181 Rock, J. R. *et al.* Basal cells as stem cells of the mouse trachea and human
airway epithelium. *Proceedings of the National Academy of Sciences* 106,
12771-12775, (2009).

182 Mondrinos, M. J. *et al.* Engineering three-dimensional pulmonary tissue
constructs. *Tissue Eng.* 12, 717-728, (2006).

Jaffe, A. B., Kaji, N., Durgan, J. & Hall, A. Cdc42 controls spindle orientation to
position the apical surface during epithelial morphogenesis. *J Cell Biol* 183, 625-
633, (2008).

- 183 Magudia, K., Lahoz, A. & Hall, A. K-Ras and B-Raf oncogenes inhibit colon
epithelial polarity establishment through up-regulation of c-myc. *The Journal of*
cell biology 198, 185-194, (2012).
- 184 Kovbasnjuk, O. *et al.* Human enteroids: preclinical models of non-inflammatory
diarrhea. *Stem Cell Res Ther* 4 Suppl 1, S3, (2014).
- 185 Spence, J. R. *et al.* Directed differentiation of human pluripotent stem cells into
intestinal tissue in vitro. *Nature* 470, 105-109, (2011).
- 186 Li, X. *et al.* Oncogenic transformation of diverse gastrointestinal tissues in
primary organoid culture. *Nat Med* 20, 769-777, (2014).
- 187 Stange, D. E. *et al.* Differentiated Troy+ Chief Cells Act as Reserve Stem Cells to
Generate All Lineages of the Stomach Epithelium. *Cell* 155, 357-368, (2013).
- 188 Reichert, M. *et al.* Isolation, culture and genetic manipulation of mouse
pancreatic ductal cells. *Nat Protoc* 8, 1354-1365, (2013).
- 189 Okugawa, Y. A Novel Three-Dimensional Cell Culture Method to Analyze
Epidermal Cell Differentiation In Vitro. *Methods in molecular biology* (Clifton,
N.J.), (2013).
- 190 Lang, S. H. *et al.* Experimental prostate epithelial morphogenesis in response to
stroma and three-dimensional matrigel culture. *Cell growth & differentiation :
the molecular biology journal of the American Association for Cancer Research*
12, 631-640, (2001).
- 191 Kubota, Y., Kleinman, H. K., Martin, G. R. & Lawley, T. J. Role of laminin and
basement membrane in the morphological differentiation of human endothelial
cells into capillary-like structures. *The Journal of cell biology* 107, 1589-1598,
(1988).
- 192 Arnaoutova, I. & Kleinman, H. K. In vitro angiogenesis: endothelial cell tube
formation on gelled basement membrane extract. *Nature Protocols* 5, 628-635,
(2010).
- 193 Davis, G. E. *et al.* Vol. 1066 17-28 (Humana Press, 2013).
- 194 Morgan, J. P. *et al.* Formation of microvascular networks in vitro. *Nature*
Protocols 8, 1820-1836, (2013).

Figure 1-1. Cellular inputs to organotypic cultures. (A) **Whole organ and organ slice.** Tissues that develop during embryogenesis, such as salivary gland, kidney and lung, are commonly explanted as whole organs. For example, explants of metanephric kidney isolated from the embryonic urogenital ridge will undergo vigorous branching morphogenesis in 3D culture. Tissues that develop postnatally, such as mammary gland, intestine, brain and aorta, can be sectioned into tissue 'slices' due to their large size. (B) **Tissue organoid.** Primary organs can be harvested and processed through mechanical disruption and enzymatic digestion into tissue fragments (known as 'tissue organoids'). The native stromal cells and extracellular matrix are typically removed, enabling isolated culture of the epithelial tissues. The resulting organoids contain a diversity of epithelial cell types organized in their normal spatial configuration and are typically explanted into commercial extracellular matrices, such as Matrigel or collagen I. For example, mammary epithelial organoids will undergo branching morphogenesis in 3D Matrigel. (C) **Stem cell organoid.** Stem cells can be used to generate organoids that model the architecture and cellular composition of a larger organ. Both embryonic and adult induced pluripotent stem cells (iPS cells) have been used to generate organoids of kidney, lung, intestine, liver, the optic cup and brain. For example, ES cells cultured in the presence of Matrigel and differentiation factors will aggregate and self-organize into optic cup-like structures. Alternatively, single tissue stem cells isolated from an adult organ can be used; for example, $Lgr5^+$ tissue stem cells embedded within Matrigel will generate many tissues of the digestive tract. (D) **Primary cells.** Primary keratinocytes from the skin and esophagus have been cultured on cell culture inserts to organize into stratified epithelium. In addition, primary epithelial cells from the salivary gland, lung, kidney and pancreas, as well as endothelial cells, have been used in 2.5D or 3D culture.

Figure 1-1

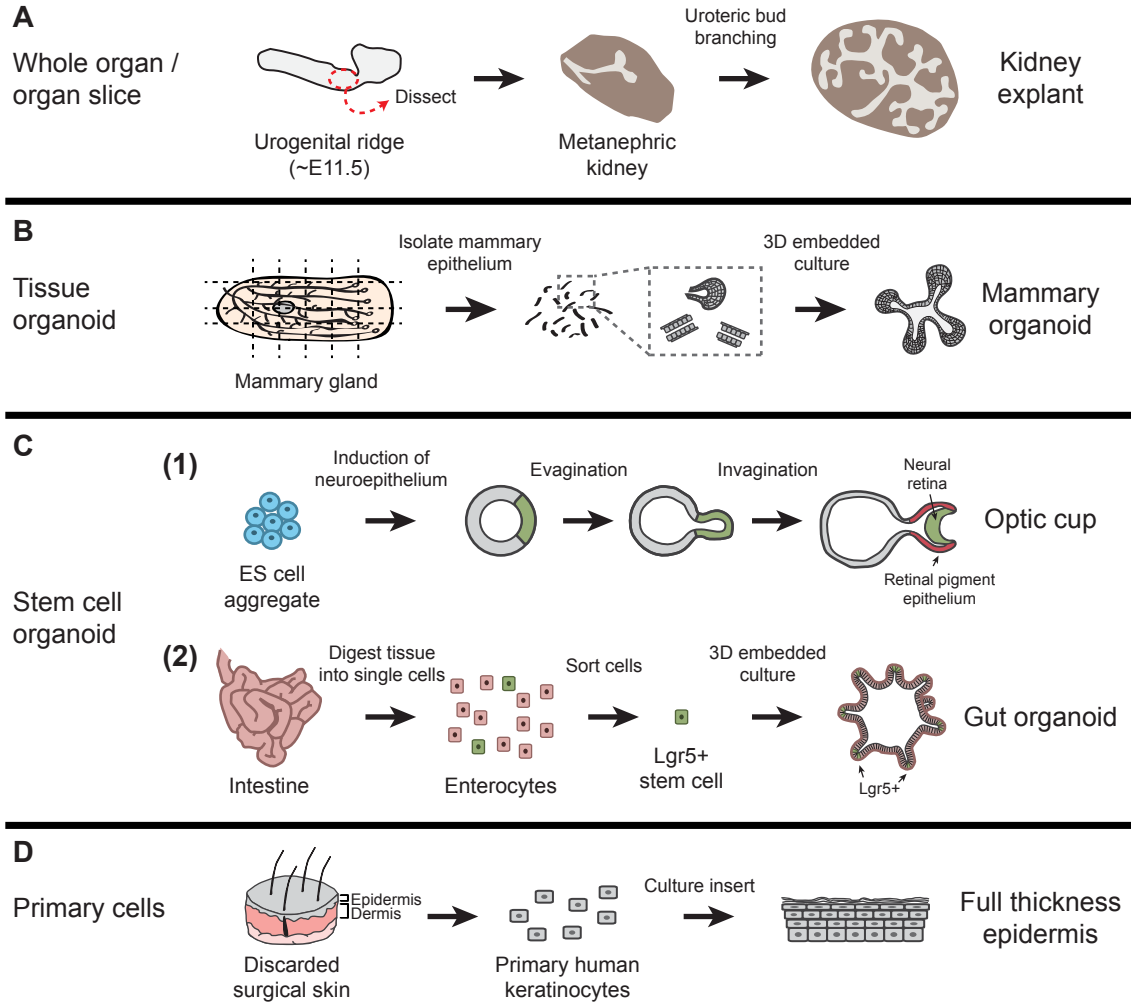
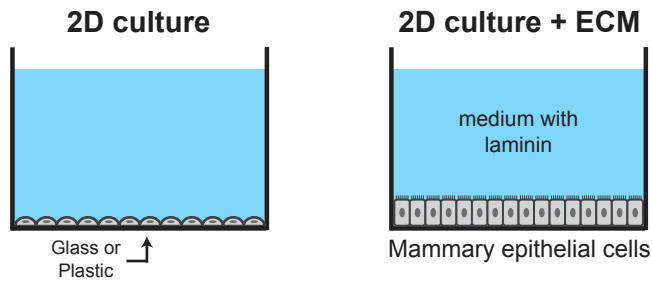


Figure 1-2. The major categories of cell culture. (A) **2D cell culture.** Cells are typically cultured directly on a highly rigid substrate such as glass or plastic. The medium can be supplemented with extracellular matrix (ECM) proteins to induce a more differentiated cell state. For example, addition of laminin I will induce differentiation of mammary epithelial cells. (B) **2.5D or drip culture.** Cells are cultured on top of a thin, organized layer of ECM, and diluted ECM proteins (such as laminins) are present in the medium. This format is ideal for imaging and antibody staining and is sufficient for epithelial acinar formation (for example, in MCF10A and MDCK cell lines). Drip cultures have also been used to generate endothelial networks. The mechanical or structural properties of the ECM layer can be varied, and microfluidics can be used to generate flow-over gradients. (C) **3D-embedded culture.** Cells are cultured within a gel of ECM proteins. Cells are uniformly exposed to an organized ECM and can further remodel and restructure the ECM over time. For example, mammary tissue organoids will undergo branching morphogenesis in 3D Matrigel. This format requires that the ECM solution is cell-compatible both in liquid and in gelled form, and it enables the incorporation of different ECM components, multicellular tissues and stromal cells. If constructed within microfluidic devices, these cultures can be subjected to in- or through-gel gradients. ECMs can also be precisely patterned in 3D. (D) **Mechanically supported culture.** Cells, organ slices or whole organs are cultured on a tissue culture insert that is either submerged in medium or maintained at an air-liquid interface. Histologically realistic epithelial tissues can be constructed in stages, with initial assembly of keratinocytes into an epithelial cell layer on a submerged culture insert followed by exposure of these cells to an air-liquid interface to induce formation of stratified epidermis. Stromal cells can be co-cultured with the epithelial cells or added to a separate compartment, within the culture dish, to study paracrine effects without direct physical contact between cell types. Slices of large organs, such as the brain, can be cultured on these inserts.

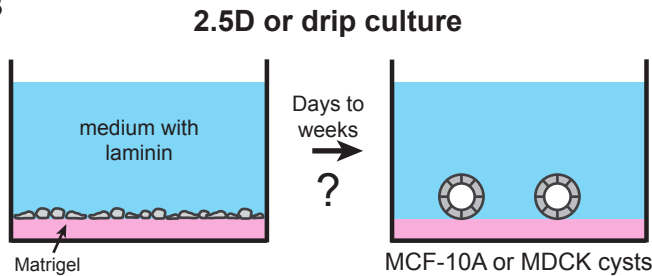
Figure 1-2

A



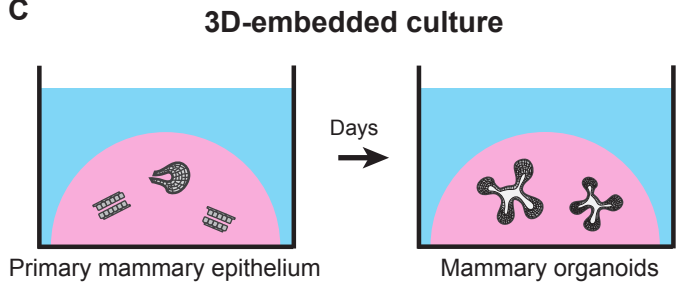
Variables:
a) Supplemental ECM (optional)

B



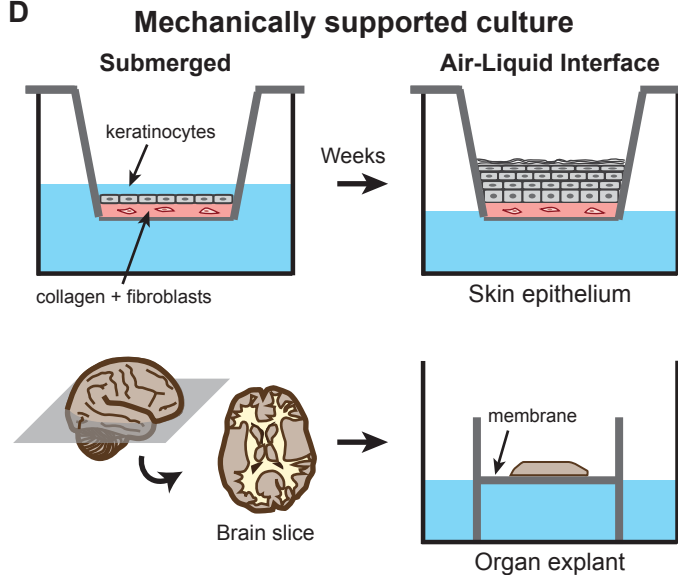
Variables:
a) ECM composition
b) ECM mechanics / rigidity
c) Flow-over gradients

C



Variables:
a) Cellular input: primary tissue, primary single cells, or stem cells
b) ECM composition
c) ECM organization / rigidity
d) Stromal cells
e) In-gel gradients
f) Precise patterning

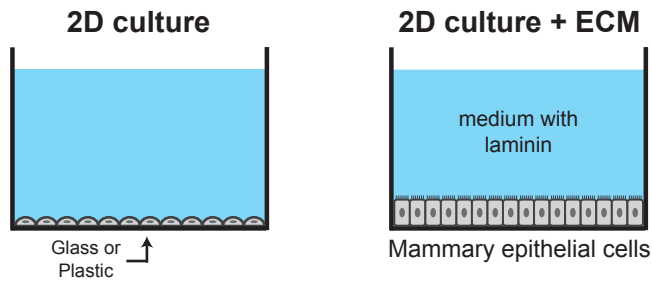
D



Variables:
a) Stratified tissue organization
b) ECM composition
c) Stromal cells (in same or separate compartment)
d) Air-liquid interface, O₂ perfusion
e) Immersion or rocker culture

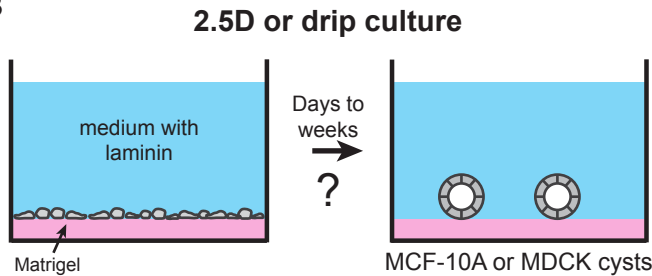
Figure 1-2

A



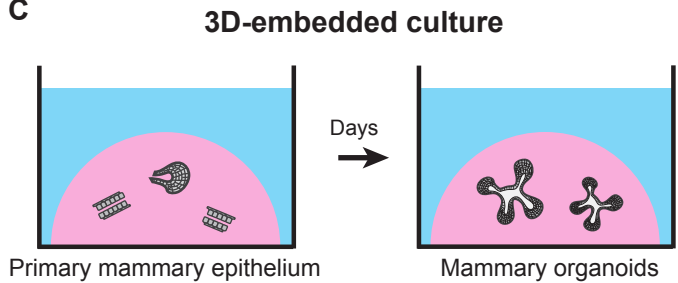
Variables:
a) Supplemental ECM (optional)

B



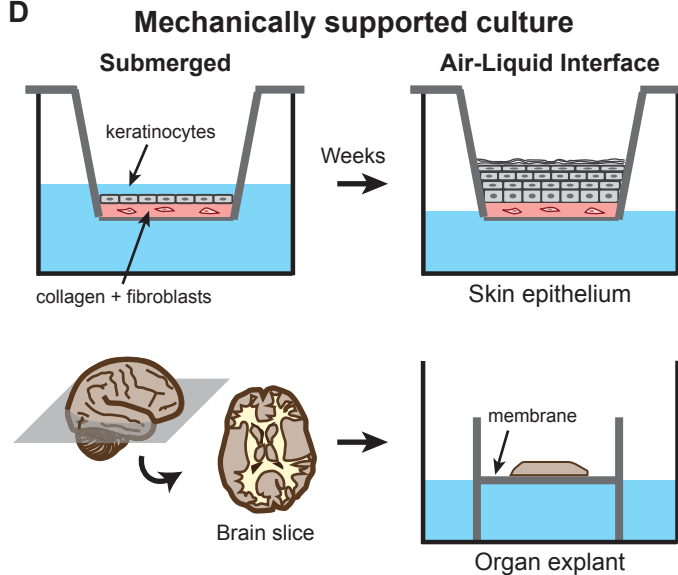
Variables:
a) ECM composition
b) ECM mechanics / rigidity
c) Flow-over gradients

C



Variables:
a) Cellular input: primary tissue, primary single cells, or stem cells
b) ECM composition
c) ECM organization / rigidity
d) Stromal cells
e) In-gel gradients
f) Precise patterning

D

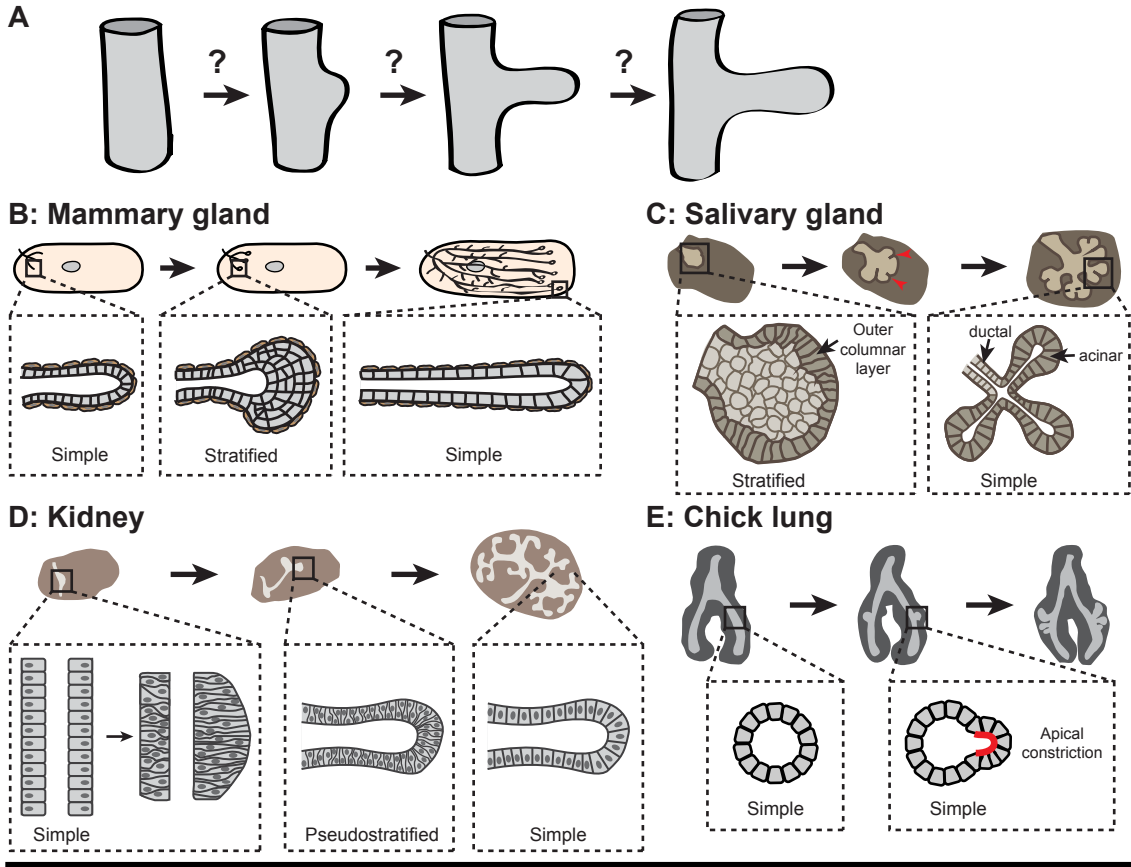


Variables:
a) Stratified tissue organization
b) ECM composition
c) Stromal cells (in same or separate compartment)
d) Air-liquid interface, O₂ perfusion
e) Immersion or rocker culture

Figure 1-3. The cellular basis of epithelial tube elongation. (A) Schematic diagram showing epithelial bud initiation and tube elongation. While conceptually a similar process across the various organs, it was unclear whether tube elongation was accomplished by conserved cellular mechanisms. (B) Mammary epithelium elongates from a mammary placode into a surrounding fat pad starting at 3 weeks after birth. Branching morphogenesis involves transitions from simple to stratified to simple epithelium. The terminal end bud, at the growing front, initiates and elongates as a multilayered structure and eventually repolarizes into a simple bi-layer⁶² (inset). (C) Salivary epithelium develops embryonically from a single stratified bud that undergoes successive clefting and ECM remodeling to form a branched network with simple architecture. At the single bud stage (E13.5), the epithelium already contains a morphologically distinct outer layer of columnar cells, which form the acinar epithelium of the gland, and many inner rounded cells, which form the ductal epithelium¹⁶⁰ (inset). (D) Kidney branching morphogenesis initiates embryonically when the Wolffian duct evaginates into the surrounding metanephric mesenchyme as the ureteric bud. The epithelial bud transitions from simple to pseudostratified to simple architecture⁹⁴ (inset). (E) Lung development occurs embryonically. Avian lung maintains simple organization throughout branching morphogenesis and initiates new buds through apical constriction⁸⁵ (inset). (F) Salivary epithelium requires FGF10 for branching morphogenesis, and heparan sulphate increases the affinity of FGF10 for its receptor. Specific sulphation patterns of heparan sulphate regulate FGF10-mediated morphogenetic events, such as proliferation, end bud expansion and duct elongation⁹⁵. (G) In branching ureteric bud tips, pre-mitotic epithelial cells delaminate into the lumen to undergo cell division while maintaining a thin basal process at the site of origin. One daughter cell reinserts (blue) at the original site and the second daughter cell (green) inserts at a position one to three cell diameters away⁹⁶. (H) In the avian lung, treatment

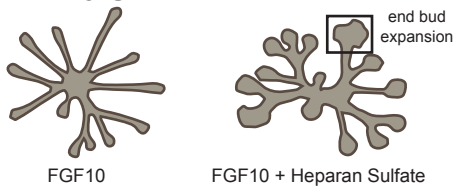
with the proliferation inhibitor aphidicolin does not block bud formation, demonstrating that cell proliferation is dispensable for bud initiation⁸⁵. (I) During mouse lung development, domain branching is characterized by a localized increase in cell division within the incipient bud relative to adjacent trunk cells. Within the bifurcating bud at the end of the tube there is both an enrichment of proliferation relative to the trunk and a polarization of the plane of cell division within the future cleft region⁹⁷. Arrows indicate the orientation of cell division.

Figure 1-3

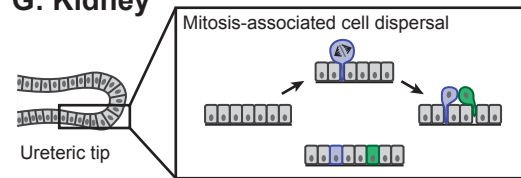


What is the role of proliferation in branching morphogenesis?

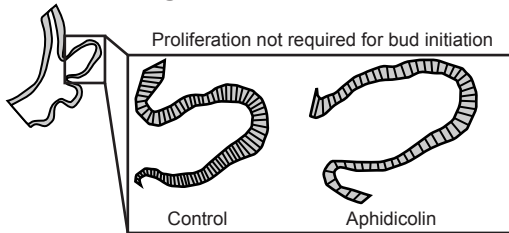
F: Salivary gland



G: Kidney



H: Chick lung



I: Mouse lung

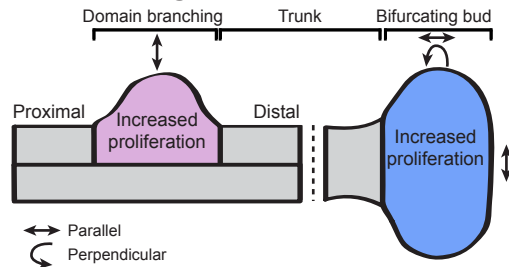


Figure 1-4. Genetic regulation of cell behaviours in mammalian tissues. (A) siRNA-mediated knockdown of p63 demonstrated that this transcription factor is required for both proliferation and differentiation in regenerating organotypic postnatal epidermis. p63 depletion in all cells leads to tissue hypoplasia, defects in epidermal stratification and differentiation and loss of simple epithelial markers¹¹³. Mosaic mixtures of control cells and p63 siRNA-treated cells leads to a cell autonomous failure of differentiation in the p63 knockdown cells¹¹³. (B) Fibronectin was known to accumulate within the forming clefts in the salivary gland¹¹⁵. Gene expression analysis revealed that fibronectin binding induces expression of *Btbd7* in epithelial cells within the clefts²⁹. *Btbd7* regulates cleft progression by reducing cell-cell adhesion and promoting formation of transient intercellular gaps²⁹. (C) Labeled cells within chimeric embryonic kidneys compete for contribution to the ureteric bud depending on their individual level of Ret signalling⁹⁴. In a chimeric Wolffian duct, labelled epithelial cells lacking the receptor tyrosine kinase (RTK) Ret (*Ret*^{-/-} cells) are excluded from the tips of elongating ureteric buds in favor of wild-type cells⁹⁴. By contrast, cells depleted of Sprouty1 (*Spry1*^{-/-}), which is a repressor of RTK signalling, have increased Ret levels and accumulate at the ureteric bud tip domain at the expense of wild-type cells. (D) Tet-inducible *Twist1* expression leads to loss of tissue polarity and the rapid dissemination of otherwise normal mammary epithelial cells²⁷. Disseminated cells retain epithelial gene expression (for example, cytokeratin-8), localize E-cadherin and b-catenin to the membrane, and require E-cadherin protein to disseminate as single cells²⁷.

Figure 1-4

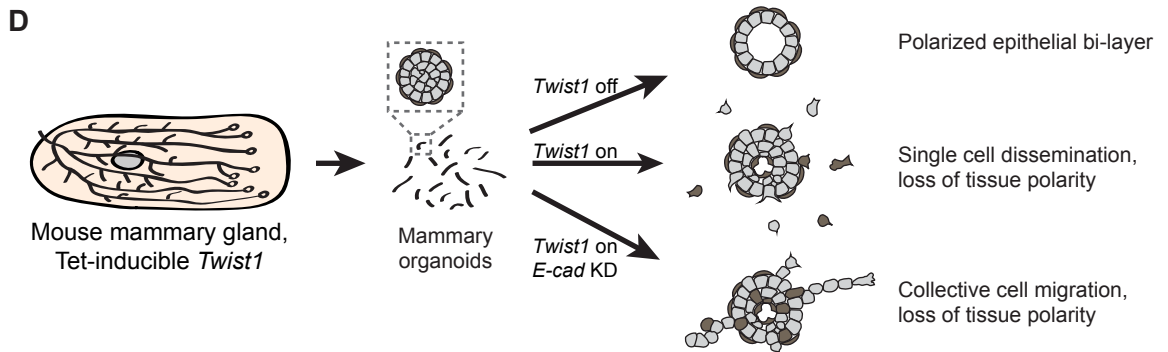
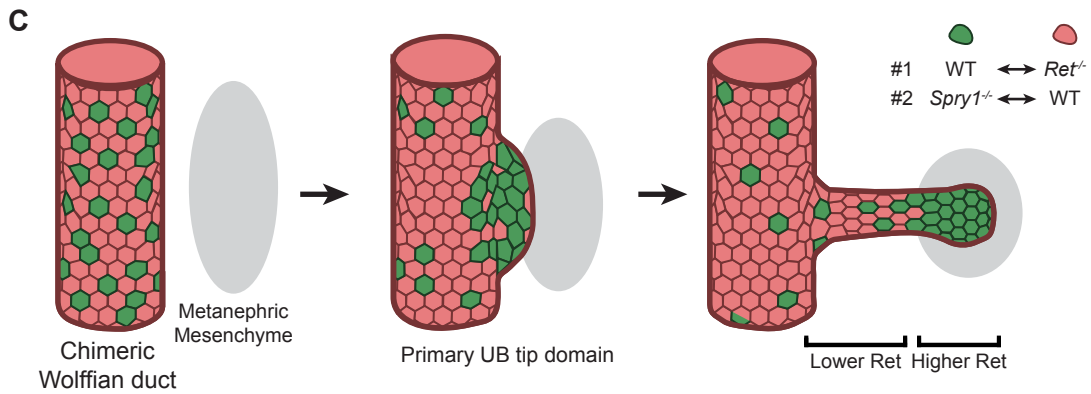
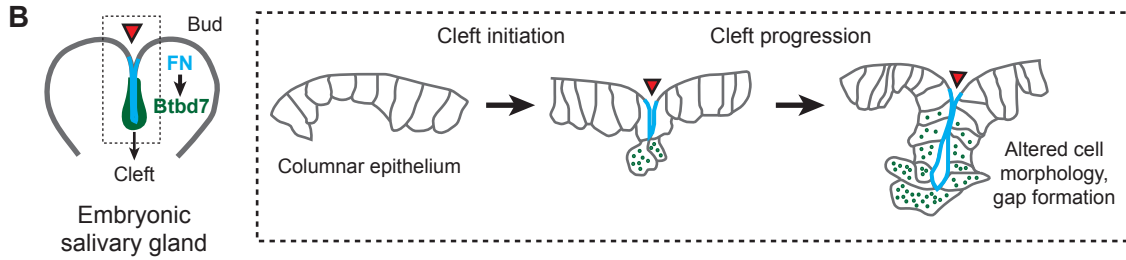


Figure 1-5. The role of the microenvironment in regulating epithelial function. (A)

Schematic overview of different components of the tissue microenvironment, including immune cells (for example, macrophages), blood vessels, fibroblasts and extracellular matrix (for example, collagen I). The components and properties of the microenvironment can be readily modified in 3D culture. (B) Co-cultures of lung or bone marrow stroma mixed with endothelial cells were used to generate a 3D organotypic microvascular niche. The angiogenesis inhibitor thrombospondin 1 (TSP1) induces breast tumour cell dormancy in the mature endothelium, whereas TGF- β 1 and periostin promote tumour cell growth in neovascular tips, which lack TSP1¹²⁹. (C) Direct comparisons of the same tissue in different microenvironments (that is, Matrigel or collagen I) shows that the composition of the ECM regulates invasive and disseminative behaviours of both normal and malignant mammary epithelium⁶⁶. (D) The mechanical properties of the microenvironment can affect cell and tissue function. High rigidity (through crosslinking poly(ethylene) glycol (PEG) networks within Matrigel scaffolds) suppresses growth of both normal and neoplastic tissue but does not induce invasion or dissemination¹²¹. The addition of adhesive peptides promotes dissemination of both normal and tumour cells¹²¹.

Figure 1-5

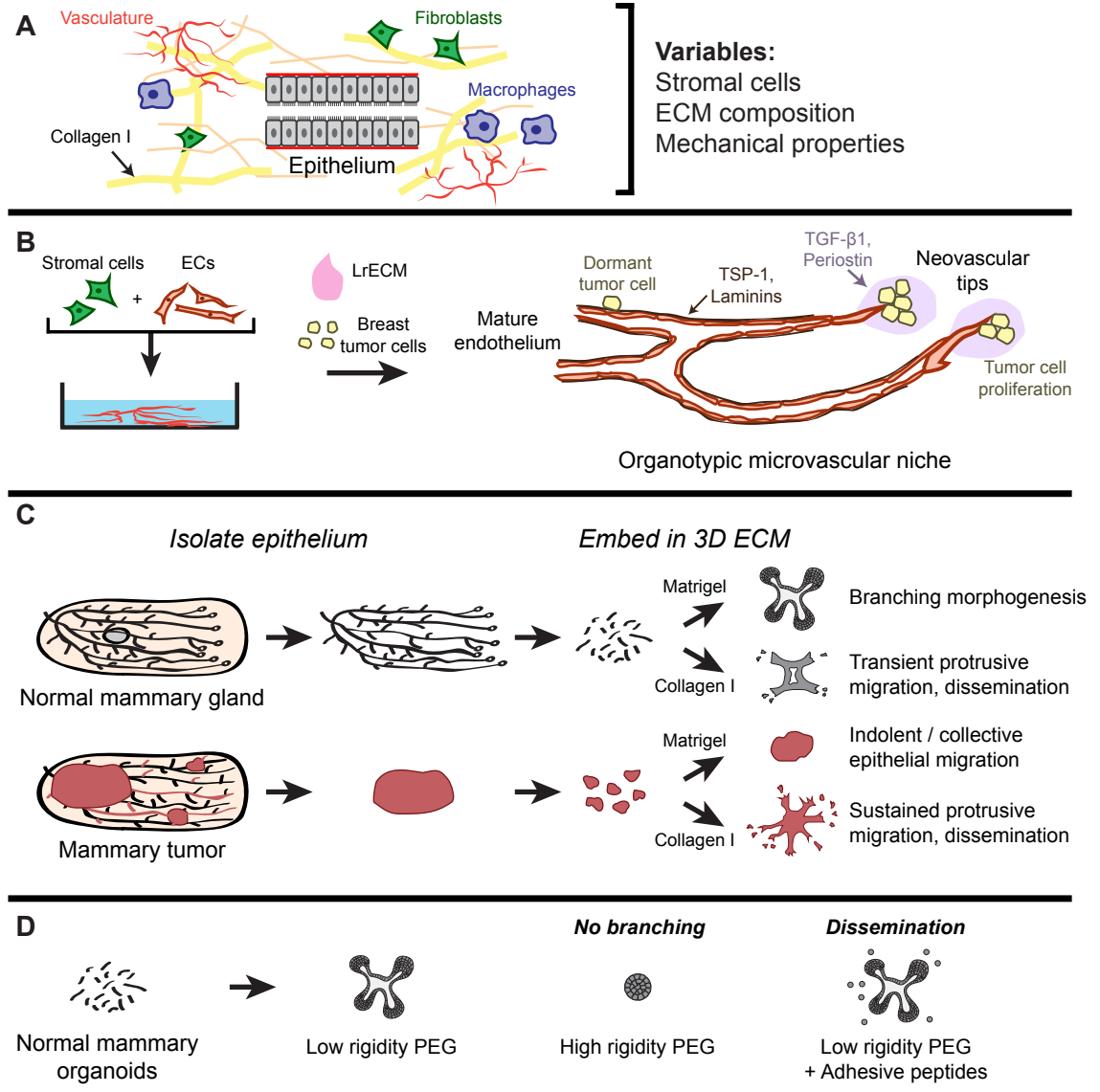


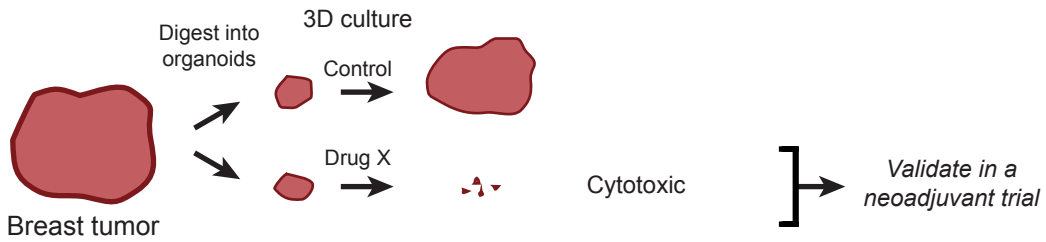
Figure 1-6. Therapeutic applications of 3D culture. (A) **Predictive assays:** The vast number of potential cancer drugs and drug combinations cannot be serially evaluated in individual patients. This challenge has motivated efforts to develop chemotherapy sensitivity and resistance assays in which the therapeutic response of a patient's own tumour could be directly assessed^{154,155}. Although no current assays are ready for routine clinical practice^{154,155}, emerging techniques based on 3D culture and microfluidic systems can potentially provide personalized information on response to therapy. For example, *ex vivo* slice cultures of tumours have been used to identify heterogeneous responses to small molecule compounds such as PI3K inhibitors¹⁵⁶. Similarly, primary glioblastoma specimens show variable cell death rates and DNA damage responses upon treatment with the chemotherapeutic drug temozolomide following irradiation¹⁵⁷. Primary samples can also be challenged with molecular therapeutics and assayed for downstream signalling responses¹⁵⁰. Validation of the predictive value of such assays will require clinical trials that test whether assay-guided clinical management results in better patient outcomes than standard of care^{154,155}. (B) **Prognostic assays:** Prognostic assays could be developed to measure functionally based outputs, such as morphological criteria (for example, extent of invasion into a defined microenvironment³⁰) or molecular criteria (for example, expression of components of the MAPK pathway¹⁵⁰). These assays can potentially provide information that is independent of that derived from static phenotypic analyses conducted on formalin-fixed paraffin-embedded (FFPE) sections. If such assays correlate with patient outcomes, they could provide a means to generate individualized prognoses based on a patient's own tissue. (C) **Pre-clinical therapeutic testing:** Organotypic models of disease can provide efficient proof-of-principle tests of novel molecular approaches to disease management. *Genome editing.* Primary intestinal organoids derived from patients with cystic fibrosis carry mutations in the gene encoding the cystic fibrosis transmembrane conductance regulator (for

example, CFTR Δ F508)¹⁰². Forskolin induces rapid swelling in organoids from healthy subjects but not in organoids from patients with cystic fibrosis. Correction of the CFTR Δ F508 mutation by CRISPR-Cas9 in patient-derived Lgr5⁺ stem cells results in restoration of CFTR function and forskolin-induced swelling in the organoids¹⁰². Notably, CFTR function improves more with gene editing than with small-molecule drugs¹⁵⁸.

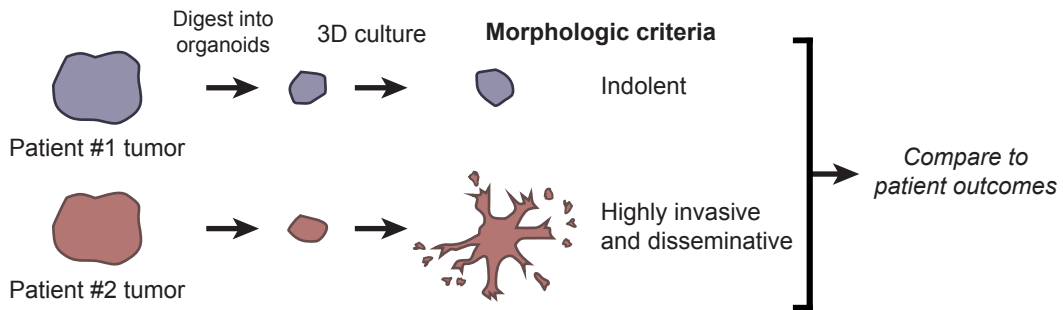
Rational therapeutic design. The survival of a cancer cell in the presence of a therapeutic agent can depend on its 3D localization within a tissue. Dual inhibition of PI3K and mTOR in ovarian cancer spheroids leads to the death of inner matrix-deprived cells but the upregulation of pro-survival programmes in matrix-attached cells¹⁵⁹. Combined inhibition of PI3K, mTOR and Bcl-2 eliminates both matrix-deprived and matrix-attached cells by apoptosis in tumour xenografts and in primary ovarian and breast cancer samples from patients.

Figure 1-6

A: Predictive Assay

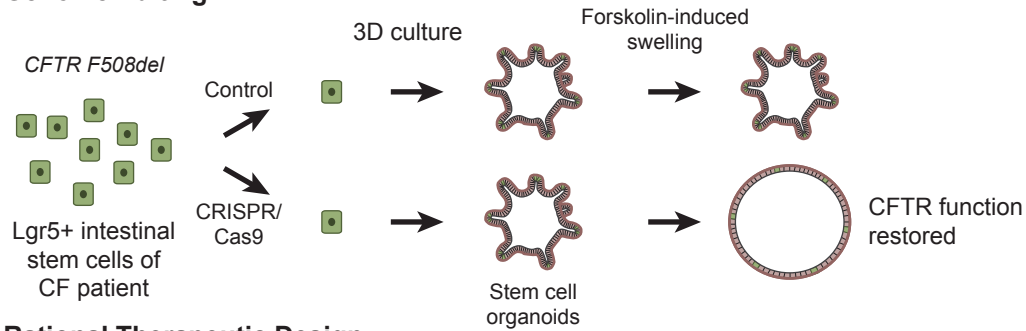


B: Prognostic Assay



C: Pre-Clinical Therapeutics

Genome Editing



Rational Therapeutic Design

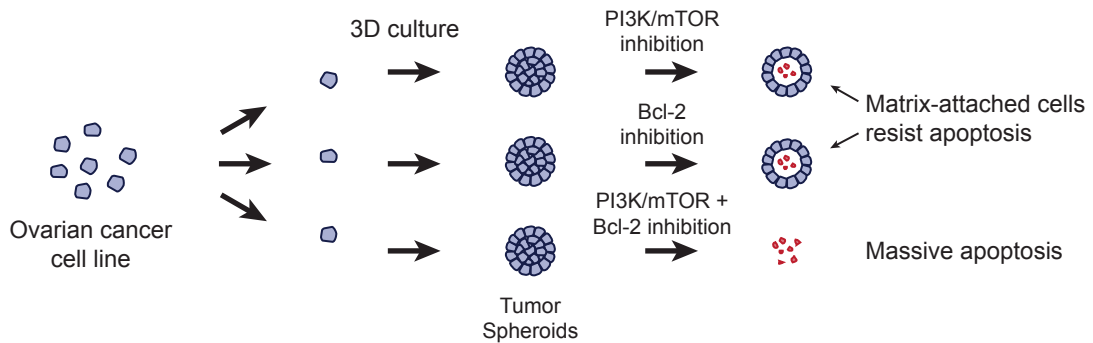


Table 1-1

Organ	Cellular input	Culture format	Refs
Mammary gland	Cell line (for example, MCF-10A)	2.5D culture	51,111,161
	Whole organ	Mechanically supported	15,162
	Tissue organoid	3D embedded culture	5,27,66,72,163
	Primary cells	2.5D culture	57,164
Salivary gland	Embryonic whole organ	Mechanically supported	92,99,115
	Ex vivo epithelial-mesenchymal recombination	Mechanically supported	100,165
	Tissue organoid	3D embedded culture	33,63,95
	Primary cells	3D embedded culture	166,167
Kidney	Cell line (MDCK)	2.5D culture	58,105,168,169
	Embryonic whole organ	Mechanically supported	96,170,171
	Ex vivo epithelial-mesenchymal recombination	Mechanically supported or 3D embedded	172,173
	Tissue organoid	3D embedded culture	34,64,174
	Stem cell organoid (ES cells)	2.5D culture	175
	Stem cell organoid (ES cells and iPS cells)	Mechanically supported	176,177
	Primary embryonic cells	Mechanically supported	55,56
Lung	Normal or neoplastic lung slice	Mechanically supported	17,156,178
	Embryonic whole organ	Mechanically supported	14,116,179
	Tissue organoid	3D embedded culture	35,179
	Stem cell organoid (tissue stem cells)	3D embedded culture	128,180
	Primary cells (human alveolar cells)	2.5D culture	59
	Primary cells (fetal pulmonary cells)	3D embedded culture	181
Small intestine	Cell line (Caco-2)	2.5D culture	182,183
	Organ slice	Mechanically supported	18,19
	Tissue organoid	3D embedded culture	6,28,36,102,184
	Stem cell organoid (Lgr5 ⁺)	3D embedded culture	6,143
	Stem cell organoid (iPS cells)	3D embedded culture	185
Colon	Organ slice	Mechanically supported	19,20
	Tissue organoid	3D embedded culture	36,37,144,184,186
	Stem cell organoid (Lgr5 ⁺)	3D embedded culture	37,144

Organ	Cellular input	Culture format	Refs
Liver	Whole organ and organ slice	Mechanically supported	14,153,178
	Tissue organoid	3D embedded culture	38
	Stem cell organoid (Lgr5 ⁺)	3D embedded culture	38
	Stem cell organoid (iPS cells)	2.5D culture	152
Stomach	Tissue organoid	3D embedded culture	39
	Stem cell organoid (Lgr5 ⁺ and Troy ⁺)	3D embedded culture	39,187
Pancreas	Embryonic whole organ	Mechanically supported	14,84
	Tissue organoid	3D embedded culture	40
	Stem cell organoid (Lgr5 ⁺)	3D embedded culture	40
	Primary pancreatic ductal cells	3D culture	65,188
Esophagus	Primary cells (esophageal keratinocytes)	Mechanically supported	54,89,127
Skin	Cell line (HaCaT)	3D embedded culture	189
	Primary cells (epidermal keratinocytes)	Mechanically supported	52,53,73,114
Prostate	Tissue organoid	3D embedded culture	41
	Primary cells (human prostatic epithelium)	3D embedded culture	190
Optic cup	Stem cell organoid (ES cells)	3D suspension or embedded culture	44,45
Brain	Organ slice	Mechanically supported	21,22
	Stem cell organoid (ES cells)	3D suspension culture	46
	Stem cell organoid (iPS cells)	3D embedded culture, spinning bioreactor	47
Blood vessels	Primary cells (HUVEC)	2.5D culture	191,192
	Primary cells (HUVEC)	3D embedded culture	193
	Organ slice (aorta)	3D embedded culture	23
	Primary cells (HUVEC)	3D bioengineered platform	11,12,151,194

Table 1-1. Cellular and molecular techniques for 3D culture. Where possible, the original reference for the approach is included, supplemented with additional recent references highlighting major technical advances.

CHAPTER 2

The ECM microenvironment regulates collective migration and local dissemination in normal and malignant mammary epithelium

(Modified from Nguyen-Ngoc et al., *Proc Natl Acad Sci USA* 2012)

Abstract

Breast cancer progression involves genetic changes and changes in the extracellular matrix (ECM). To test the importance of the ECM to tumor cell dissemination, we cultured epithelium from primary human breast carcinomas in different ECM gels. We utilized basement membrane gels to model the normal microenvironment and collagen I to model the stromal ECM. In basement membrane gels, malignant epithelium was either indolent or grew collectively, without protrusions. In collagen I, epithelium from the same tumor invaded with protrusions and disseminated cells. Importantly, collagen I induced a similar initial response of protrusions and dissemination in both normal and malignant mammary epithelium. However, dissemination of normal cells into collagen I was transient and ceased as laminin 111 localized to the basal surface, while dissemination of carcinoma cells was sustained throughout culture and laminin 111 was not detected. Despite the large impact of ECM on migration strategy, transcriptome analysis of our 3D cultures revealed few ECM-dependent changes in RNA expression. However, we observed many differences between normal and malignant epithelium, including reduced expression of cell adhesion genes in tumors. We therefore tested whether deletion of an adhesion gene could induce sustained dissemination of non-transformed cells into collagen I. We found that deletion of P-cadherin was sufficient for sustained dissemination, but exclusively into collagen I. Our data reveal that metastatic tumors preferentially disseminate in specific ECM microenvironments. Furthermore, these data suggest that breaks in the basement membrane could induce invasion and dissemination via the resulting direct contact between cancer cells and collagen I.

Introduction

Collective cell migration is an important mechanism for both normal epithelial development and cancer invasion¹. During collective cell migration, cells move in coordinated groups and maintain cell-cell adhesion. In the normal mammary gland, ducts transition from a polarized bilayer into a proliferative, motile, multilayered epithelium and then collectively migrate through the stromal tissue^{2,3}. Mammary carcinomas also originate from a polarized adult epithelium, transition from simple to multilayered organization, and migrate collectively^{4,5}. Despite these similarities, normal ductal morphogenesis in vivo does not involve local dissemination of cells and eventually results in restoration of polarized simple epithelial architecture. In contrast, breast carcinomas continue to grow, disseminate cells locally, and frequently metastasize to distant sites⁶. These observations raise the fundamental question: what features of tumor progression can regulate the transition from a collective to a disseminative phenotype?

Cancer is a genetic disease, and sequencing has revealed that genes encoding cell-cell and cell-matrix adhesion proteins are frequently mutated^{7,8}. However, breast cancer also involves characteristic changes in the extracellular matrix (ECM) and the tumor microenvironment⁹⁻¹². For example, collagen I is enriched and aligned at the stromal border in breast tumors^{10,13}, changes in collagen I organization are independent negative prognostic indicators¹⁴, and increased collagen I crosslinking accelerates progression in experimental cancer models¹⁵. Additionally, basement membrane proteins and their integrin receptors have been shown to regulate carcinoma cell behavior¹⁶⁻¹⁸. A major challenge today is to distinguish the relative contributions of specific genetic and microenvironmental changes to the migration and local dissemination of carcinoma cells.

In vivo, there are vast differences in the soluble signals, the stromal cells, and the ECM microenvironments surrounding carcinomas and normal ducts⁹. It is difficult to manipulate these signals independently in an intact tumor and even more challenging to assess the acute cell behavioral consequences of experimental manipulations. The relative optical inaccessibility of mammalian tissues led our lab and others to establish 3-dimensional (3D) ex vivo models of both normal and malignant mammary epithelial growth^{5,19-24}. We have applied these techniques to test the relative importance of genetic and microenvironmental changes in regulating the pattern of collective cell migration and likelihood of local dissemination.

Results

An epithelial cell in a mammary duct exists in a highly structured 3D environment and receives extensive inputs from cell-cell, cell-matrix, and soluble signals. We previously identified the critical conditions to enable primary mammary epithelium to undergo an organotypic program of branching morphogenesis². We found that despite extensive cell migration, normal mammary morphogenesis in 3D Matrigel cultures and in vivo occurs without ECM-directed protrusions^{2,3}. In contrast, carcinomas in vivo can migrate with protrusions and can disseminate cells locally and to distant sites^{6,25}. Since the tumor microenvironment changes in parallel with genetic changes in the cancer cells¹⁰, it is unclear whether the protrusive migration and dissemination of carcinoma cells are due to cell-intrinsic motility differences or to interactions of the cancer cells with their microenvironment. We therefore exploited organotypic culture techniques to isolate and culture fragments from individual primary human mammary carcinomas in different extracellular matrix microenvironments (Fig. 2-1A and Supplemental Methods). We first optimized the medium conditions to yield consistent branching morphogenesis in normal human breast epithelium samples (Fig. 2-2A-D). We then focused on two ECM environments: a gel composed of basement membrane proteins (Matrigel) to model the normal breast epithelial microenvironment, and 3 mg/mL collagen I to model the stromal matrix encountered by invading mammary carcinomas¹⁰. Although fibrillar collagen I is present near normal mammary ducts, it remains outside an intact basement membrane even during branching morphogenesis, limiting contact with normal epithelial cells²⁶.

Human mammary carcinomas invade and disseminate preferentially into collagen

I

We explanted fragments from primary human mammary carcinomas (n=7 tumors; Fig. 2-2E and Supplemental Methods) into 3D ECM cultures (Fig. 2-1A). The starting point for culture was epithelial fragments of a few hundred to a few thousand cells. We allocated fragments of the same tumor to different 3D ECM microenvironments and observed ECM-dependent carcinoma migration strategies (Fig. 2-1B-C"). In 3D Matrigel, we observed both indolent behavior and collective epithelial migration (Fig. 2-1B-B"). We only rarely observed single cell protrusions from the epithelium in Matrigel and did not observe robust collective protrusive migration. In contrast, fragments from the same primary human mammary carcinoma exhibited protrusive migration and disseminated cells extensively into 3D gels of 3 mg/mL collagen I (Fig. 2-1C-C",H,I). Although the extent of invasion and dissemination varied among tumor fragments (Fig. 2-3A-C), the borders of carcinoma fragments cultured in Matrigel maintained an epithelial appearance without protrusions (150/155 fragments from 5 human tumors; Fig. 2-1H), while the borders of carcinoma fragments in collagen I were protrusive (90/109) and exhibited extensive local dissemination (89/109 fragments from 5 human tumors; Fig. 2-1H,I).

The current, local ECM microenvironment determines the cellular strategy of invasion for primary human mammary carcinomas

We next sought to determine whether protrusive migration and dissemination could be reversed if the ECM composition returned to basement membrane-like composition. To test this concept, we first cultured primary human tumor fragments in either Matrigel or collagen I until the pattern of migration was clear, then digested the ECM and transferred the tumor fragments to a new ECM environment (Fig. 2-1D-G). We tested all reciprocal combinations, including transfer from Matrigel to Matrigel, from Matrigel to collagen I, from collagen I to Matrigel, and from collagen I to collagen I. Transfer between Matrigel and Matrigel resulted in a restarting of collective migration (Fig. 2-1D). Transfer from

Matrigel to collagen I resulted in protrusive migration in the new environment (Fig. 2-1E), whereas transfer from collagen I to Matrigel resulted in a retraction of protrusions and confined, collective growth (Fig. 2-1F). Carcinoma fragments transferred from collagen I to collagen I were protrusive, but were on average less disseminative (Fig. 2-1G-I), suggesting that there may be a limited subpopulation of highly invasive cells in a tumor. However, we cannot exclude the possibility that the more extensive enzymatic digestion required to free epithelial fragments from a collagen I gel may have reduced their invasive behavior. We therefore conclude that the current, local ECM environment determines the migration strategy and likelihood of dissemination.

Collagen I induces protrusive migration and local dissemination of murine carcinoma cells

Our investigations with human breast carcinomas suggested that the local ECM microenvironment is sufficient to induce or repress protrusive and disseminative behavior. However, live primary human carcinoma tissue is scarce, and the details of tumor pathology vary widely from one available sample to the next (Fig. 2-2E). We therefore modeled this regulatory interaction using mouse mammary carcinomas. We selected a mammary carcinoma model in which the mouse mammary tumor virus long terminal repeat drives the expression of the polyoma virus middle T oncogene (*MMTV-PyMT*), as it exhibits progressive cellular and molecular changes that parallel those observed in human breast cancer^{27,28}. Gene expression in this model clusters with the highly aggressive luminal B subtype of human breast cancer²⁹.

We isolated epithelial fragments of 200-1000 cells from advanced murine mammary carcinomas (12-15 weeks, 1.5-2 cm tumors) and embedded them into either Matrigel or collagen I (Fig. 2-4A). Carcinoma fragments in Matrigel culture developed into budded

structures with high efficiency (Fig. 2-4B). Cells within these fragments remained in a stratified organization, without lumens, throughout their time in Matrigel culture, and cells at the ECM border maintained an epithelial appearance, without protrusions (Fig. 2-4B,B'). Although the MMTV-PyMT model metastasizes to the lungs with high efficiency in vivo, 90% of the carcinoma fragments did not disseminate cells into Matrigel (Fig. 2-4D, 45/50 movies). By contrast, carcinoma fragments embedded in 3 mg/mL collagen I developed extensive protrusions and frequently disseminated cells into collagen I (Fig. 2-4C-D; 98%, 47/48 movies). Both the protrusions and dissemination were detectable by transmitted light microscopy (Fig. 2-4C,C'). We conclude that the ECM microenvironment determines the collective cell migratory strategy and the likelihood of local dissemination in both human breast cancer cells and murine mammary carcinoma models.

Normal mammary epithelial cells exhibit protrusive migration and local dissemination in a collagen I microenvironment

We next asked whether a protrusive, disseminative response to collagen I was tumor-specific. We isolated epithelial fragments (organoids) from the mammary glands of FVB mice and cultured them in either Matrigel or 3 mg/mL collagen I (Fig. 2-4E). Again, the cell migratory strategy and likelihood of local dissemination depended on the ECM microenvironment. In Matrigel, normal organoids migrated collectively to accomplish branching morphogenesis, without protrusions into the ECM (Fig. 2-4F,F'), as we previously reported². In collagen I, organoids isolated from the same mouse migrated with extensive protrusions, and cells disseminated locally into the ECM (Fig. 2-4G,G'). To test the reversibility of the ECM-induced changes in migratory program, we next cultured normal epithelial fragments for 90 hours in either Matrigel or collagen I (Fig. 2-5A-C), then recovered and re-embedded the epithelium in either the same or opposite

matrix (Fig. 2-5D). Similar to results observed for human carcinoma fragments (Fig. 2-1G-H), the current, local ECM microenvironment dictated the migratory pattern, with collective epithelial migration in Matrigel (Fig. 2-5E,H) and collective protrusive migration in collagen I (Fig. 2-5F-G).

Mammary carcinomas exhibit sustained local dissemination in collagen I

To better understand how epithelia transition from collective migration to individual cell dissemination, we quantified specific dissemination behaviors. Carcinoma fragments disseminated cells into collagen I throughout culture, with an average of 13 cells observed to leave each tumor mass (612 disseminating cells observed in 48 movies; see Supplemental Methods). We classified the disseminating tumor cells, based on previous morphological definitions^{1,30}, as mesenchymal, amoeboid, or collective (Fig. 2-6A-D). Most carcinoma cells disseminated with a mesenchymal morphology (60%), as they protruded into the ECM and maintained an elongated morphology while migrating through the collagen I matrix (Fig. 2-6A). Other carcinoma cells (34%) disseminated in an amoeboid fashion, as rounded cells that rolled or squeezed through the collagen I matrix (Fig. 2-6B). In a minority of cases (6%), we also observed collective dissemination of groups of cells (Fig. 2-6C). Individual carcinoma fragments typically exhibited both mesenchymal and amoeboid dissemination (Fig. 2-6F). Most disseminated carcinoma cells remained motile during the entire period of observation (69%), but 17% of the disseminated cells died, and 14% rejoined the tumor fragment (Fig. 2-6E). Once in the matrix individual cancer cells were observed to convert between elongated and rounded morphologies, consistent with a previous report on melanoma cells³¹. Despite local dissemination, carcinoma cells localized E-cadherin to intercellular borders in both Matrigel and collagen I (Fig. 2-6H,J).

Protrusive migration and local dissemination are transient responses of normal myoepithelial cells to collagen I

We previously observed no ECM-directed protrusions at the front of elongating mammary ducts in Matrigel or in vivo². In contrast, collagen I induced acute protrusive and disseminative behaviors in both normal and malignant mammary epithelium (Fig. 2-6F-G, 1-50 hrs). We observed dissemination from 79% (34/43 movies) of normal epithelial organoids (Fig. 2-4H), with an average of 5 cells leaving each epithelial group (210 disseminating cells observed in 43 movies), typically at the protrusive borders (Fig. 2-7A,A''). Despite local dissemination, cells in the main epithelial group remained E-cadherin⁺ in both Matrigel and collagen I (Fig. 2-6I,K). The main cell behavioral difference between normal and carcinoma cells was that protrusions and dissemination were both transient in normal epithelial cells (Fig. 2-6G). As normal epithelial organoids ceased protrusive activity and reverted to a program of branching morphogenesis. The protrusive normal cells stained positive for the myoepithelial marker smooth muscle α -actin (SMA; Fig. 2-4G') in 67 of 69 samples. Using a transgenic myoepithelial cell reporter to visualize the protrusive behavior in real-time (Fig. 2-7B; [*Keratin-14::Actin-GFP*]³²), we observed subcellular protrusions extending and retracting from single myoepithelial cells (Fig. 2-7B') as well as multicellular extensions of myoepithelial cells (Fig. 2-7B''). Live imaging revealed that the transition from protrusive to epithelial organization at the ECM interface (Fig. 2-7A') represented a change in cell behavior in individual myoepithelial cells (Fig. 2-7B'). In contrast, in Matrigel, myoepithelial cells remained closely adherent to the luminal epithelial cells and did not extend protrusions into the ECM².

Normal mammary organoids progressively organize a basement membrane in collagen I

We observed a shift from protrusive to smooth, organized basal surfaces in normal mammary organoids cultured in collagen I (Fig. 2-7A-B). To test whether this shift might relate to re-establishment of a basement membrane, we used antibodies to stain for laminin 111, laminin 332, and collagen IV. We observed a negative correlation between protrusions and basement membrane organization. We observed single cell protrusions (Fig. 2-7C,C') and multicellular protrusive groups (Fig. 2-7D,D') that extended through gaps in the laminin 111. Collagen IV staining was diffuse and incomplete in protrusive areas of normal epithelium (Fig. 2-7E,E'). Late in culture in collagen I, normal epithelium typically became covered by a complete basement membrane that stained positive for all three markers (Fig. 2-7F-H'). In contrast, at the ECM border of carcinoma fragments, we observed no laminin 111, only scattered laminin 332, and incomplete collagen IV coverage (Fig. 2-7I-K'). The most striking difference between tumor and normal epithelium in collagen I was the lack of laminin 111 along tumor borders, even late in culture (Fig. 2-7I,I' v. 2-7F,F').

The ECM microenvironment has minor effects on average gene expression

Taken together, our results suggest that the pattern of epithelial migration and local dissemination are constrained by the local ECM microenvironment. We next sought to identify RNA expression changes that could regulate these changes in cell behavior. Accordingly, we collected RNA from normal and malignant epithelium during active growth at day four of culture in either Matrigel or collagen I. Our goal was to compare average gene expression, and so we isolated RNA from whole cultures. We hybridized the resulting RNA to Agilent single color microarrays (Fig. 2-8A), with a minimum of three biologically independent microarray replicates per condition. To test the relative importance of the ECM to gene expression, we performed complete linkage hierarchical clustering. Normal samples clustered together regardless of their ECM

microenvironment, distinct from all tumor samples (Fig. 2-8B). A principal component analysis (PCA) confirmed that the first principal component was whether the epithelium was normal or tumor, and the second principal component was the ECM condition (Fig. 2-8C). Using a criterion for significance of fold change ≥ 2 and a false discovery rate ≤ 0.05 , only 15 or 16 genes were differentially expressed based on ECM condition in normal or tumor epithelium, respectively (Fig. 2-8E-G). However, these genes did not have obvious mechanistic connections to dissemination (Fig. 2-8F-G). Thus, the ECM microenvironment had a relatively small impact on average RNA expression, despite its large effects on migratory strategy and local dissemination. Our experimental design cannot exclude the possibility of changing gene expression within subpopulations of the epithelium.

Normal and malignant epithelium differ in their expression of cell adhesion genes and modifiers of the extracellular microenvironment

In contrast to the modest differences observed between ECM environments, we found significant gene expression differences between normal and malignant epithelium, even when cultured in the same ECM: 1455 genes were differentially expressed between normal and tumor samples in Matrigel, and 599 genes were differentially expressed between normal and tumor samples in collagen I (Fig. 2-8D,E). These data suggest that normal epithelium and tumors accomplish morphologically similar migration processes despite widely different gene expression.

We next sought gene expression signatures that might explain the sustained dissemination of carcinoma cells in collagen I (Fig. 2-9A). The epithelial to mesenchymal transition (EMT) has been proposed as a mechanism for cancer metastasis³³. Conceptual models of EMT center on decreased expression of E-cadherin and

increased expression of genes such as N-cadherin and vimentin³³. However, the local dissemination we observed in collagen I was achieved with membrane-localized E-cadherin (Fig. 2-6J-K). Surprisingly, E-cadherin RNA expression was also not statistically significantly different between any two conditions (Fig. 2-9C). Furthermore, carcinoma cells displayed reduced levels of both N-cadherin and vimentin RNA, and the EMT regulators Snail1, Snail2, and Twist1 were also not differentially expressed (defined as ≥ 2 fold change, $FDR < 0.05$) in any condition (Fig. 2-9C). Our results suggest that a classic molecular EMT program is not activated in the tumor or in response to a collagen microenvironment, despite vigorous dissemination of cells into the ECM.

Importantly, our enrichment analysis revealed large and statistically significant differences between normal tissue and tumors in gene sets for cell adhesion and for proteins that function in the extracellular space (DAVID functional annotation, Fig. 2-9A,B). Analysis of mRNA expression of genes defined by structural motifs related to adhesion (e.g., cadherins and integrins) and of ECM and ECM remodeling genes (e.g., collagens and matrix metalloproteinases (MMPs)) (Fig. 2-9B, 2-10) revealed widespread changes across gene families. Moreover, adhesion gene sets (cadherins, IgCAMs, integrins, lectins, other CAMs) were downregulated in tumor relative to normal epithelium ($p \leq 0.0003$, Wilcoxon rank sum test, ~60% of differentially expressed genes higher in normal epithelium). We specifically observed strong downregulation in the cadherin gene family, with 75% of differentially expressed genes downregulated in tumor relative to normal (Fig. 2-9B; $p \leq 0.0001$, Wilcoxon rank sum test). These data suggest that loss of cell adhesion genes may contribute to the sustained dissemination of carcinoma cells in collagen I.

Reduced intercellular adhesion cooperates with a collagen I microenvironment to permit sustained dissemination of non-transformed cells

Recent breast cancer genome sequencing efforts have revealed mutations in multiple families of cell adhesion genes, including both classical cadherins and protocadherins³⁴. More than 70% of breast tumors in a recent study had mutations in a cell adhesion gene, but few of these mutations occurred in more than one tumor³⁵. We chose to genetically test whether altering cell adhesion was sufficient to enable sustained dissemination of non-transformed cells into collagen I. Since myoepithelial cells were the only protrusive or disseminative cells in our normal epithelial cultures, we focused on P-cadherin (Cdh3), a classical cadherin specifically expressed in myoepithelial but not luminal epithelial cells³⁶. Deletion of P-cadherin in vivo results in precocious alveolar differentiation and luminal epithelial hyperplasia³⁷. We hypothesized that loss of P-cadherin might synergize with a collagen I-rich microenvironment to induce sustained myoepithelial dissemination. In Matrigel, we observed precocious branching (Fig. 2-11A-B) and an increase in branching efficiency (Fig. 2-11C) in P-cadherin null epithelial fragments, but no protrusions or dissemination. In contrast, P-cadherin null epithelial fragments explanted into collagen I disseminated more cells relative to controls, and dissemination was sustained throughout culture (Fig. 2-11D-F). Disseminating cells were myoepithelial in nature (K14⁺, Fig. 2-11H), and they survived and proliferated in collagen I (Fig. 2-11I). Indeed, we frequently observed nearly complete depletion of myoepithelial cells from the surface of P-cadherin null organoids (Fig. 2-11H). We conclude that deletion of a cell adhesion gene is sufficient to induce sustained myoepithelial dissemination in specific ECM microenvironments.

Discussion

In the present study, we sought to isolate the specific role of the ECM in regulating collective epithelial migration and local dissemination by explanting fragments from the same epithelium into different ECM microenvironments. We found that murine and human mammary carcinomas cultured in 3D Matrigel were indolent or migrated collectively as a multilayered epithelium. Surprisingly, we only rarely observed local dissemination in Matrigel, even from metastatic human and murine mammary carcinomas. This result demonstrates that a metastatic genotype is not sufficient for local dissemination in all ECM microenvironments. In contrast, both normal and malignant mammary epithelium disseminated vigorously into collagen I.

Epithelial cells have ECM-specific migration programs

We observed large, ECM-specific differences in the pattern of collective migration and frequency of local dissemination, with fragments from the same epithelium and identical culture medium. Moreover, these large differences in migratory pattern had few corresponding ECM-specific differences in gene expression. Despite the local dissemination of epithelial cells into collagen I, we did not detect a classic molecular EMT response in either normal or tumor tissue. However, all of our transcriptome experiments compared RNA extracted from whole cultures and so our experimental design cannot exclude gene expression or signaling changes in the cells directly in contact with the ECM. Comparable molecular profiling studies comparing in situ and invasive breast cancer at the tissue level have also failed to define a gene signature predictive of invasion³⁸.

Taken together, our data suggest that cancer cells could possess all of the gene expression required for sustained local dissemination and yet remain indolent while the basement membrane remains intact. However, if the basement membrane were disrupted, the resulting direct contact between cancer cells and the stromal collagen I matrix could rapidly induce protrusive and disseminative cell behaviors. Breach of the basement membrane can be accomplished by MMP-based proteolysis by the cancer cells^{10,39}, by immune cells recruited during inflammatory processes, or by the actions of carcinoma-associated macrophages⁴⁰ or fibroblasts⁴¹. Consistent with this model, correlative studies in human breast tumors show that even microscopic breaks in the myoepithelium correlate with poor patient prognosis⁴².

A stromal ECM is not sufficient for sustained dissemination

The acute reaction of normal and carcinoma-derived epithelium to collagen I was very similar, as both exhibited protrusive migration and a mixture of amoeboid and mesenchymal dissemination. All of the individual cell behaviors observed in the tumor fragments were also observed in the normal fragments. However, this similarity was transient: normal epithelium reestablished basement membrane coverage and underwent branching morphogenesis. In contrast, dissemination from carcinoma fragments was sustained throughout culture, and polarized epithelial architecture was not restored. Taken together, our data support a requirement for coordinate changes in both the cancer cell and the microenvironment to enable sustained dissemination. Our data also suggest that the final signal triggering invasion and local dissemination can be provided by changes in the ECM microenvironment, rather than by genetic changes in the cancer cell. This is consistent with recent sequencing efforts that identified similar gene expression and mutations within in situ and invasive breast tumors^{38,43}. Additionally, central fibrosis, which is characterized by high levels of collagen I,

independently correlates negatively with patient outcome even among the most aggressive types of breast cancers⁴⁴.

Cell-cell adhesion and the ECM microenvironment coordinately regulate dissemination

Cell adhesion genes are frequently downregulated or mutated in metastatic human tumors^{7,8} and in our mouse carcinoma model. Our data supports the hypothesis that deletion of a cell adhesion gene can enable sustained dissemination of otherwise normal cells. Since the transiently disseminating normal cells were myoepithelial, we focused on P-cadherin³⁷, the major classical cadherin in myoepithelial cells³⁶. The phenotype of P-cadherin deletion in Matrigel and in vivo was luminal epithelial hyperplasia. However, the phenotype of P-cadherin deletion in collagen I was excess, sustained myoepithelial dissemination. The consequences of molecular perturbations can therefore be qualitatively different in different ECM microenvironments with respect to clinically important variables such as local dissemination. Our data are consistent with recent reports that myoepithelial cells are structurally and molecularly abnormal in non-malignant regions adjacent to primary human breast tumors⁴⁵. Our data suggest that observed changes in the ECM composition of the tumor microenvironment in these regions may help to explain these abnormalities⁴⁵.

Translational implications for breast cancer

Our data indicate that the cellular migratory strategy and the likelihood of local dissemination depend not only on the genetic state of the cancer cells but also on the ECM in the tumor microenvironment. Importantly, we demonstrated through matrix switching experiments that even after an ECM-induced transition to protrusive migration and local dissemination, human malignant carcinomas can revert to confined, non-

protrusive growth in response to basement membrane signals. Our data are consistent with past work on the normalization of tumor architecture by basement membrane signals such as laminin 111^{17,46,47} and on the invasion-associated behavior of cells in collagen I^{10,13,48}.

Future directions

It is now necessary to isolate the molecular basis for the differential effects of different ECM microenvironments on collective cell migration and dissemination. Collagen I and Matrigel have distinct rigidity, protein composition, and supramolecular organization. It remains unclear which of these variables is most important to dissemination, though past studies suggest a role for increased matrix rigidity in cancer progression¹⁰. Our data also suggest that deletion of a single adhesion gene is sufficient to induce sustained dissemination of non-transformed cells into a stromal matrix such as collagen I. It will be important to determine whether deletion of other adhesion genes will similarly promote local dissemination. Since the collective migration strategy of epithelial cells is different in different ECMs, it is also possible that specific genetic perturbations will contribute to invasion and dissemination only in specific microenvironmental contexts.

Materials and Methods

Isolation of primary murine mammary organoids. We isolated mouse mammary organoids from normal mice using previously described techniques^{2,49}. Briefly, we dissected the #3 and #4 mammary glands and digested this tissue into epithelial fragments by a combination of mechanical disruption and collagenase/trypsin digestion. We then separated these fragments from single cells by differential centrifugation. The final pellet was composed of epithelial fragments, each containing several hundred cells, which we term organoids. Tumors were harvested from mice at 12-16 weeks of age, coinciding with poorly differentiated carcinomas. We surgically isolated the largest tumor in each mouse and processed it as above. Any incompletely digested large tumor fragments were removed prior to differential centrifugation. We also added additional rounds of differential centrifugation as needed to remove single cells. This protocol was further adapted for isolation of organoids from primary human mammary tumor.

Primary murine mammary organoid culture. We embedded organoids derived from normal and tumor epithelium in 3D Matrigel (BD Biosciences 354230) or rat tail collagen I (BD Biosciences 354236). Cultures were set up in 24-well coverslip bottom plates (E&K Scientific EK-42892), or 2-well or 4-well coverslip bottom chambers (Nunc 155383). Acid solubilized rat tail collagen I gels (3 mg/mL collagen I, pH 7-7.5) were prepared as described in the Supplemental Methods. For each matrix, organoids were mixed to yield a suspension of 2-3 organoids/ μ l. A 100 μ l suspension of organoids was plated in each well on a 37°C heating block, followed by incubation at 37°C for 45 min to allow polymerization. Epithelial fragments in collagen I were plated on top of an underlay of cell-free collagen I of the same concentration. Murine samples were cultured in 1 mL of 2.5 nM FGF2 in murine organoid media².

Time-lapse DIC microscopy. Live imaging of normal and tumor murine organoids was conducted using a Zeiss Cell Observer system with a Zeiss AxioObserver Z1 and an AxioCam MRM camera. In general, images were collected at 20-minute intervals with exposure times of approximately 250 ms. Some of the human tumor movies were collected on a Zeiss Axiovert S-100 microscope and a Cohu CCD camera, as previously reported². Temperature was held at 37°C and CO₂ at 5%.

Gene expression analysis of normal and tumor fragments in parallel ECM conditions. In total, four unique conditions were profiled (tumor vs. normal; collagen I vs. Matrigel), each replicated at least 3 times with biologically independent experiments. Sample preparation, labeling, and array hybridizations were performed according to standard protocols from the UCSF Shared Microarray Core Facilities and Agilent Technologies (<http://www.arrays.ucsf.edu> and <http://www.agilent.com>). Equal amounts of Cy3-labeled target were hybridized to Agilent whole mouse genome 4x44K Ink-jet arrays (Agilent). Arrays were scanned using the Agilent microarray scanner (Agilent), and raw signal intensities were extracted with Feature Extraction v. 9.1 software (Agilent). Samples were confirmed to be of good quality and were quantile normalized using R/Bioconductor packages. Pairwise differentially expressed genes were detected using the limma package in R. Q-values ≤ 0.05 were deemed statistically significant. A standalone program written in Java was developed to interface with the R program via the command-line to generate heatmaps for publication (available upon request). Genes ≥ 2 fold changed and with q-values ≤ 0.05 were used as input for DAVID Gene Set Analysis⁵⁰. Gene sets associated with structurally similar gene families (including cell-cell adhesion, cytoskeletal networks, and actin-myosin contractility) were manually curated from Mouse Genome Informatics and Interpro (available upon request). Cell

adhesion gene lists were further cross-referenced with OKCAM, an online cell adhesion database⁵¹. Microarray data has been made available on the NCBI's GEO database (Series GSE39173).

***P-cadherin* deletion experiments.** The *P-cadherin* and *mT/mG* mouse lines were acquired from the Jackson Laboratory, while the *Keratin-14::Actin-GFP* transgenic line was a kind gift of Dr. Elaine Fuchs^{32,37,52}. *P-cad^{-/-}* and *P-cad^{+/-};mT/mG;K14::Actin-GFP* mammary organoids were isolated as described above. Organoids were grown in Matrigel or collagen I with 2.5 nM FGF2. Branching in Matrigel was quantified on day 7 in 3 independent biological replicates and scored as 3 or more buds per organoid. Organoids were grown in 3 mg/mL collagen I for 4-5 days and cell dissemination was quantified from DIC and confocal time-lapse movies in 3 independent biological replicates.

Supporting Information

Additional materials and methods are described in *Supporting Information*, available online at <http://www.pnas.org/content/suppl/2012/08/22/1212834109.DCSupplemental>. Movies are available via the American Society for Cell Biology (ASCB) Cell: An Image Library, <http://www.cellimagelibrary.org> (accession nos. 42151–42168).

Author contribution

E.R.S. principally designed, performed, and analyzed the *P-cadherin* experiments. E.R.S. also contributed to writing the manuscript.

References

- 1 Friedl, P. & Gilmour, D. Collective cell migration in morphogenesis, regeneration and cancer. *Nat Rev Mol Cell Biol* **10**, 445-457 (2009).
- 2 Ewald, A. J., Brenot, A., Duong, M., Chan, B. S. & Werb, Z. Collective epithelial migration and cell rearrangements drive mammary branching morphogenesis. *Dev Cell* **14**, 570-581 (2008).
- 3 Ewald, A. J. *et al.* Mammary collective cell migration involves transient loss of epithelial features and individual cell migration within the epithelium. *Journal of Cell Science* (2012).
- 4 Hanahan, D. & Weinberg, R. A. The hallmarks of cancer. *Cell* **100**, 57-70 (2000).
- 5 Friedl, P. *et al.* Migration of coordinated cell clusters in mesenchymal and epithelial cancer explants in vitro. *Cancer Res* **55**, 4557-4560 (1995).
- 6 Nguyen, D. X., Bos, P. D. & Massague, J. Metastasis: from dissemination to organ-specific colonization. *Nat Rev Cancer* **9**, 274-284 (2009).
- 7 Vogelstein, B. & Kinzler, K. W. The multistep nature of cancer. *Trends Genet* **9**, 138-141 (1993).
- 8 Wood, L. D. *et al.* The genomic landscapes of human breast and colorectal cancers. *Science* **318**, 1108-1113 (2007).
- 9 Egeblad, M., Nakasone, E. S. & Werb, Z. Tumors as organs: complex tissues that interface with the entire organism. *Dev Cell* **18**, 884-901 (2010).
- 10 Egeblad, M., Rasch, M. G. & Weaver, V. M. Dynamic interplay between the collagen scaffold and tumor evolution. *Curr Opin Cell Biol* **22**, 697-706 (2010).
- 11 Polyak, K., Haviv, I. & Campbell, I. G. Co-evolution of tumor cells and their microenvironment. *Trends in Genetics* **25**, 30-38 (2009).
- 12 Egeblad, M. *et al.* Visualizing stromal cell dynamics in different tumor microenvironments by spinning disk confocal microscopy. *Dis Model Mech* **1**, 155-167; discussion 165 (2008).
- 13 Provenzano, P. P. *et al.* Collagen reorganization at the tumor-stromal interface facilitates local invasion. *BMC Med* **4**, 38 (2006).
- 14 Conklin, M. W. *et al.* Aligned collagen is a prognostic signature for survival in human breast carcinoma. *Am J Pathol* **178**, 1221-1232 (2011).
- 15 Levental, K. R. *et al.* Matrix crosslinking forces tumor progression by enhancing integrin signaling. *Cell* **139**, 891-906 (2009).
- 16 Petersen, O. W., Ronnov-Jessen, L., Howlett, A. R. & Bissell, M. J. Interaction with basement membrane serves to rapidly distinguish growth and differentiation pattern of normal and malignant human breast epithelial cells. *Proc Natl Acad Sci U S A* **89**, 9064-9068 (1992).
- 17 Weaver, V. M. *et al.* Reversion of the malignant phenotype of human breast cells in three-dimensional culture and in vivo by integrin blocking antibodies. *J Cell Biol* **137**, 231-245 (1997).
- 18 Hagios, C., Lochter, A. & Bissell, M. J. Tissue architecture: the ultimate regulator of epithelial function? *Philos Trans R Soc Lond B Biol Sci* **353**, 857-870 (1998).
- 19 Debnath, J. & Brugge, J. S. Modelling glandular epithelial cancers in three-dimensional cultures. *Nat Rev Cancer* **5**, 675-688 (2005).
- 20 Griffith, L. G. & Swartz, M. A. Capturing complex 3D tissue physiology in vitro. *Nat Rev Mol Cell Biol* **7**, 211-224 (2006).
- 21 Ewald, A. J. in *Imaging in Developmental Biology* Vol. 3 (eds R. Wong & J. Sharpe) In Press (Cold Spring Harbor Laboratory Press, 2010).

- 22 Simian, M. *et al.* The interplay of matrix metalloproteinases, morphogens and growth factors is necessary for branching of mammary epithelial cells. *Development* **128**, 3117-3131 (2001).
- 23 Gudjonsson, T., Ronnov-Jessen, L., Villadsen, R., Bissell, M. J. & Petersen, O. W. To create the correct microenvironment: three-dimensional heterotypic collagen assays for human breast epithelial morphogenesis and neoplasia. *Methods* **30**, 247-255 (2003).
- 24 Nelson, C. M. & Bissell, M. J. Modeling dynamic reciprocity: engineering three-dimensional culture models of breast architecture, function, and neoplastic transformation. *Semin Cancer Biol* **15**, 342-352 (2005).
- 25 Friedl, P., Hegerfeldt, Y. & Tusch, M. Collective cell migration in morphogenesis and cancer. *Int J Dev Biol* **48**, 441-449 (2004).
- 26 Williams, J. M. & Daniel, C. W. Mammary ductal elongation: differentiation of myoepithelium and basal lamina during branching morphogenesis. *Dev Biol* **97**, 274-290 (1983).
- 27 Guy, C. T., Cardiff, R. D. & Muller, W. J. Induction of mammary tumors by expression of polyomavirus middle T oncogene: a transgenic mouse model for metastatic disease. *Mol Cell Biol* **12**, 954-961 (1992).
- 28 Lin, E. Y. *et al.* Progression to malignancy in the polyoma middle T oncoprotein mouse breast cancer model provides a reliable model for human diseases. *Am J Pathol* **163**, 2113-2126 (2003).
- 29 Herschkowitz, J. I. *et al.* Identification of conserved gene expression features between murine mammary carcinoma models and human breast tumors. *Genome Biol* **8**, R76 (2007).
- 30 Calvo, F. *et al.* RasGRF suppresses Cdc42-mediated tumour cell movement, cytoskeletal dynamics and transformation. *Nat Cell Biol* **13**, 819-826 (2011).
- 31 Sanz-Moreno, V. *et al.* Rac activation and inactivation control plasticity of tumor cell movement. *Cell* **135**, 510-523 (2008).
- 32 Vaezi, A., Bauer, C., Vasioukhin, V. & Fuchs, E. Actin cable dynamics and Rho/Rock orchestrate a polarized cytoskeletal architecture in the early steps of assembling a stratified epithelium. *Dev Cell* **3**, 367-381 (2002).
- 33 Yang, J. & Weinberg, R. A. Epithelial-mesenchymal transition: at the crossroads of development and tumor metastasis. *Dev Cell* **14**, 818-829 (2008).
- 34 Leary, R. J. *et al.* Integrated analysis of homozygous deletions, focal amplifications, and sequence alterations in breast and colorectal cancers. *Proc Natl Acad Sci U S A* **105**, 16224-16229 (2008).
- 35 Velculescu, V. E. Defining the blueprint of the cancer genome. *Carcinogenesis* **29**, 1087-1091 (2008).
- 36 Daniel, C. W., Strickland, P. & Friedmann, Y. Expression and functional role of E- and P-cadherins in mouse mammary ductal morphogenesis and growth. *Dev Biol* **169**, 511-519 (1995).
- 37 Radice, G. L. *et al.* Precocious mammary gland development in P-cadherin-deficient mice. *Journal of Cell Biology* **139**, 1025-1032 (1997).
- 38 Polyak, K. Molecular markers for the diagnosis and management of ductal carcinoma in situ. *J Natl Cancer Inst Monogr* **2010**, 210-213 (2010).
- 39 Wolf, K. *et al.* Multi-step pericellular proteolysis controls the transition from individual to collective cancer cell invasion. *Nat Cell Biol* **9**, 893-904 (2007).
- 40 DeNardo, D. G. *et al.* CD4(+) T cells regulate pulmonary metastasis of mammary carcinomas by enhancing protumor properties of macrophages. *Cancer Cell* **16**, 91-102 (2009).

- 41 Gaggioli, C. *et al.* Fibroblast-led collective invasion of carcinoma cells with differing roles for RhoGTPases in leading and following cells. *Nat Cell Biol* **9**, 1392-1400 (2007).
- 42 Man, Y. G. & Sang, Q. X. The significance of focal myoepithelial cell layer disruptions in human breast tumor invasion: a paradigm shift from the "protease-centered" hypothesis. *Exp Cell Res* **301**, 103-118 (2004).
- 43 Miron, A. *et al.* PIK3CA mutations in in situ and invasive breast carcinomas. *Cancer Res* **70**, 5674-5678 (2010).
- 44 Kreike, B. *et al.* Gene expression profiling and histopathological characterization of triple-negative/basal-like breast carcinomas. *Breast Cancer Research* **9** (2007).
- 45 Trujillo, K. A. *et al.* Markers of fibrosis and epithelial to mesenchymal transition demonstrate field cancerization in histologically normal tissue adjacent to breast tumors. *Int J Cancer* **129**, 1310-1321 (2010).
- 46 Nelson, C. M. & Bissell, M. J. Of extracellular matrix, scaffolds, and signaling: tissue architecture regulates development, homeostasis, and cancer. *Annu Rev Cell Dev Biol* **22**, 287-309 (2006).
- 47 Gudjonsson, T. *et al.* Normal and tumor-derived myoepithelial cells differ in their ability to interact with luminal breast epithelial cells for polarity and basement membrane deposition. *J Cell Sci* **115**, 39-50 (2002).
- 48 Greenburg, G. & Hay, E. D. Epithelia suspended in collagen gels can lose polarity and express characteristics of migrating mesenchymal cells. *J Cell Biol* **95**, 333-339 (1982).
- 49 Fata, J. E. *et al.* The MAPK(ERK-1,2) pathway integrates distinct and antagonistic signals from TGFalpha and FGF7 in morphogenesis of mouse mammary epithelium. *Dev Biol* (2007).
- 50 Huang, D. W., Sherman, B. T. & Lempicki, R. A. Systematic and integrative analysis of large gene lists using DAVID bioinformatics resources. *Nat Protoc* **4**, 44-57 (2009).
- 51 Li, C. Y. *et al.* OKCAM: an ontology-based, human-centered knowledgebase for cell adhesion molecules. *Nucleic Acids Res* **37**, D251-D260 (2009).
- 52 Muzumdar, M. D., Tasic, B., Miyamichi, K., Li, L. & Luo, L. A global double-fluorescent Cre reporter mouse. *Genesis* **45**, 593-605 (2007).

Figure 2-1. ECM microenvironments modulate the pattern of collective migration and local dissemination in human mammary carcinomas. (A) Schematic description of isolation and 3D culture of human mammary carcinoma fragments. In the first round of culture, tumor fragments were embedded in either 3D Matrigel or collagen I. In the second round of culture, the same tumor fragments were freed from the 3D gels and re-embedded in either the same or the other microenvironment. (B-C'') Representative DIC time-lapse sequence of human mammary carcinomas in (B) Matrigel or (C) collagen I. (B' and C') Insets at 30 h in (B) and (C) showing the smooth and protrusive leading fronts, respectively. (B'' and C'') Micrographs of the border of the same mammary carcinoma embedded in Matrigel or collagen I, stained with Phalloidin (F-actin) and DAPI. (D-G) Representative frames of DIC time-lapse movies of human mammary carcinomas switched from (D) Matrigel to Matrigel (M-M), (E) Matrigel to collagen I (M-C), (F) collagen I to Matrigel (C-M), or (G) collagen I to collagen I (C-C) at 0 or 1 h in culture (Left) or at 45 h in culture (Right). (H-I) Bar graphs outlining the percentage of tumor fragments in each ECM condition with protrusive migration (H) or local dissemination (E) relative to the number of primary human tumor fragments analyzed in each condition.

Figure 2-1

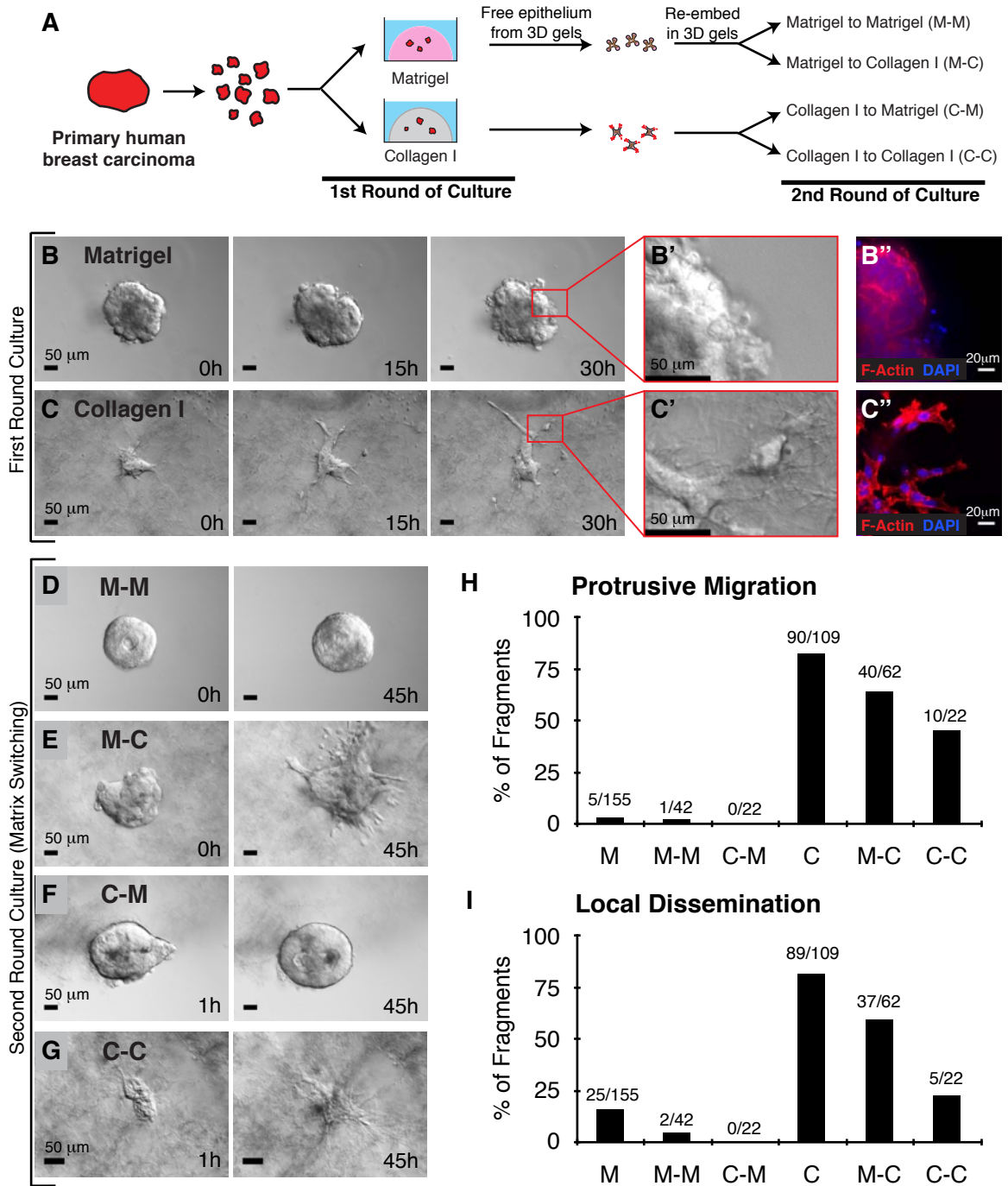


Figure 2-2

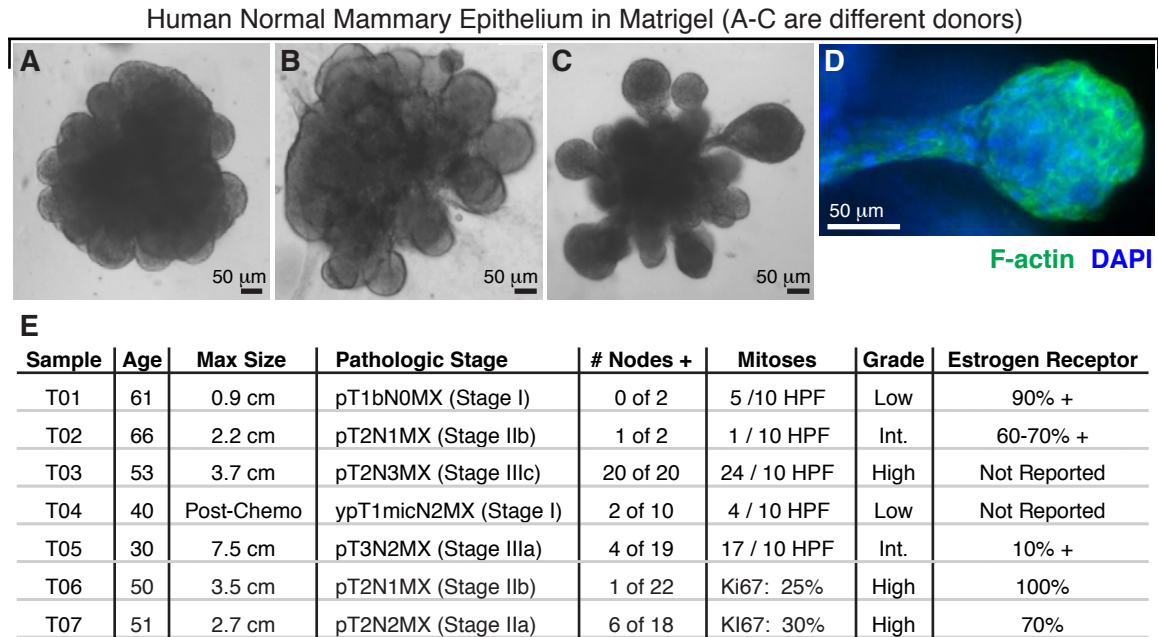


Figure 2-2. Normal human mammary epithelium undergoes branching morphogenesis in Matrigel. (A-C) Representative bright-field images of human mammary branching morphogenesis in Matrigel. (D) F-actin and DAPI staining showing the non-protrusive front of a human mammary end bud in Matrigel. (E) Pathologic stage and characteristics of human tumor samples used in this study. Six of these samples grew well in culture and exhibited strong ECM dependence in migration strategy and dissemination frequency (T01-03 and T05-T07). T04 was from a patient who had previously received chemotherapy, and the residual tissue was largely intermediate ductal carcinoma in situ and fibroadenoma. T04 explants did not grow well in 3D culture. Human tissue was acquired from the Collaborative Human Tissue Network and the Johns Hopkins Hospital.

Figure 2-3

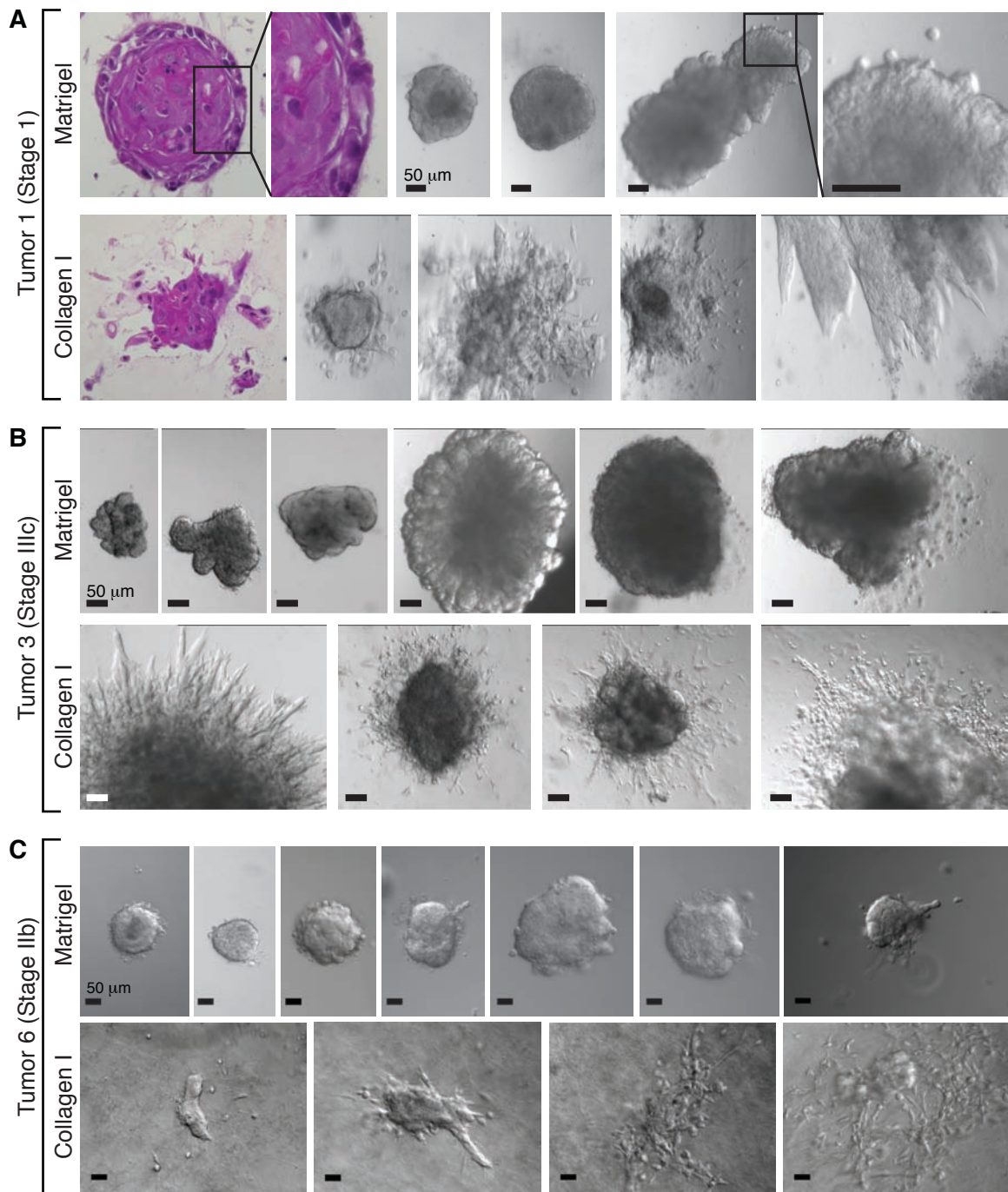


Figure 2-3. Despite intra- and inter-tumor heterogeneity, the ECM microenvironment regulates collective migration and dissemination in human breast tumors. (A-C) Representative images are presented for the range of morphologies observed in epithelial fragments from 3 human tumors when cultured in either Matrigel (top row) or collagen I (bottom row). All scale bars are 50 μm .

Figure 2-4. The ECM governs the migratory pattern and disseminative behavior of both tumor and normal murine mammary epithelium. (A) Schematic description of isolation and 3D culture of murine tumor fragments. (B-C) Representative DIC time-lapse movies of tumor fragments in (B) Matrigel and (C) collagen I. Black arrowheads indicate disseminated cells, some of which are observed to proliferate (white arrowhead). (B' and C') Localization of actin, SMA, and DAPI in tumor fragments in (B') Matrigel and (C') collagen I. White arrowheads mark the leading fronts. (D) Percent of tumor fragments showing cell dissemination in Matrigel and collagen I. *n*, total number of movies (4 biological replicates, Student's t-test, two-tailed, unequal variance). (E) Schematic description of isolation and 3D culture of normal mammary organoids. (F-G) Representative DIC time-lapse movies of normal organoids in (F) Matrigel and (G) collagen I. (F'-G') Localization of actin, SMA, and DAPI in normal organoids in (F') Matrigel and (G') collagen I. White arrowheads demarcate the shape of leading fronts. Yellow arrowhead indicates myoepithelial cell dissemination. (H) Percent of normal organoids showing dissemination in Matrigel and collagen I. *n*, total number of movies (4 biological replicates, Student's t-test, two-tailed, unequal variance).

Figure 2-4

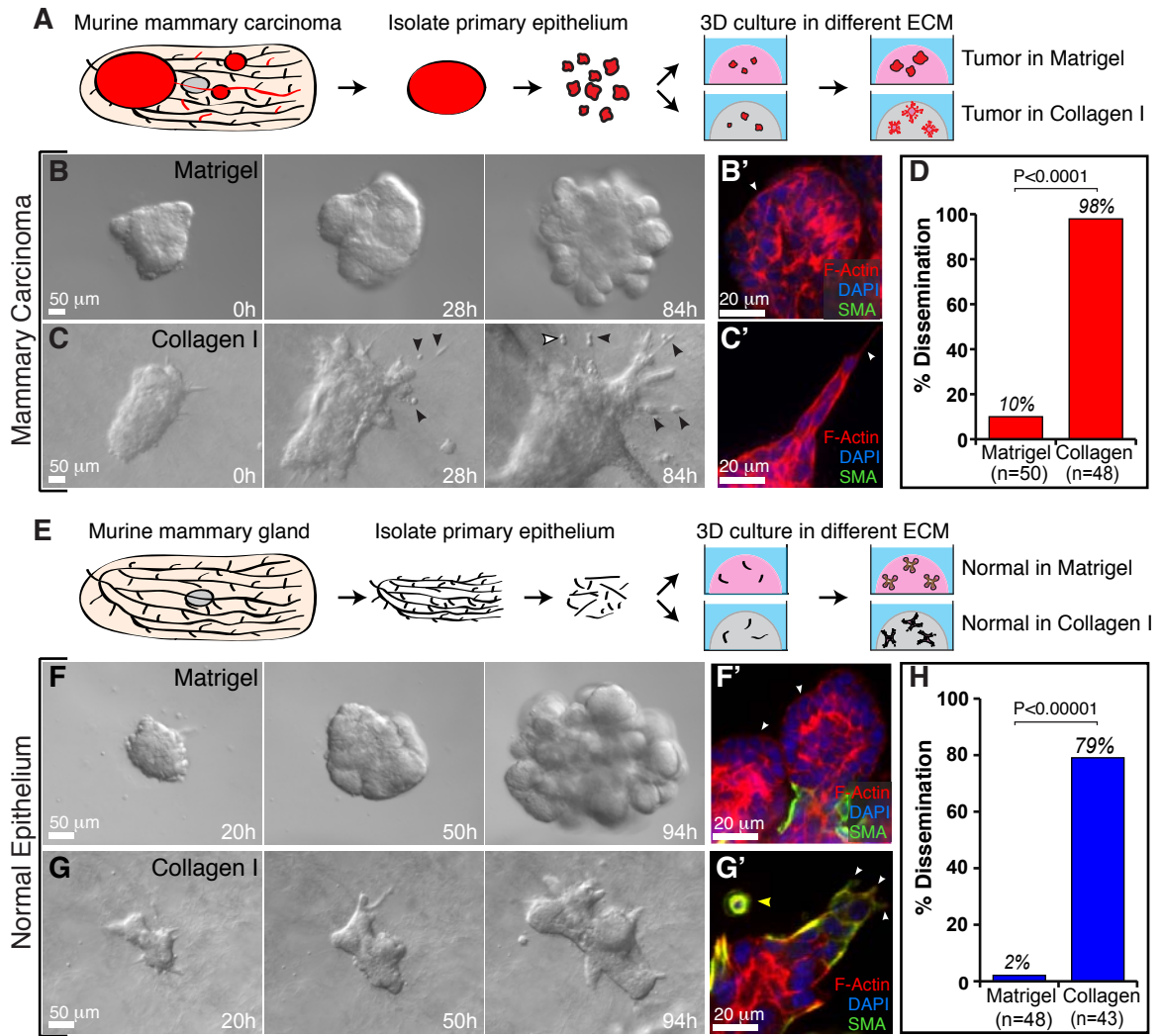


Figure 2-5. The current, local ECM microenvironment determines the collective migration pattern of murine mammary epithelium. (A) Schematic description of isolation and 3D culture of normal mammary organoids. (B-C) Representative bright-field time-lapse movies of normal organoids in (B) Matrigel and (C) collagen I. (D) Schematic description of epithelial fragment isolation and matrix switching. (E-H) Representative bright-field time-lapse movies of normal organoids switched from (E) Matrigel to Matrigel (M-M), (F) Matrigel to collagen I (M-C), (G) collagen I to Matrigel (C-M), and (H) collagen I to collagen I (C-C).

Figure 2-5

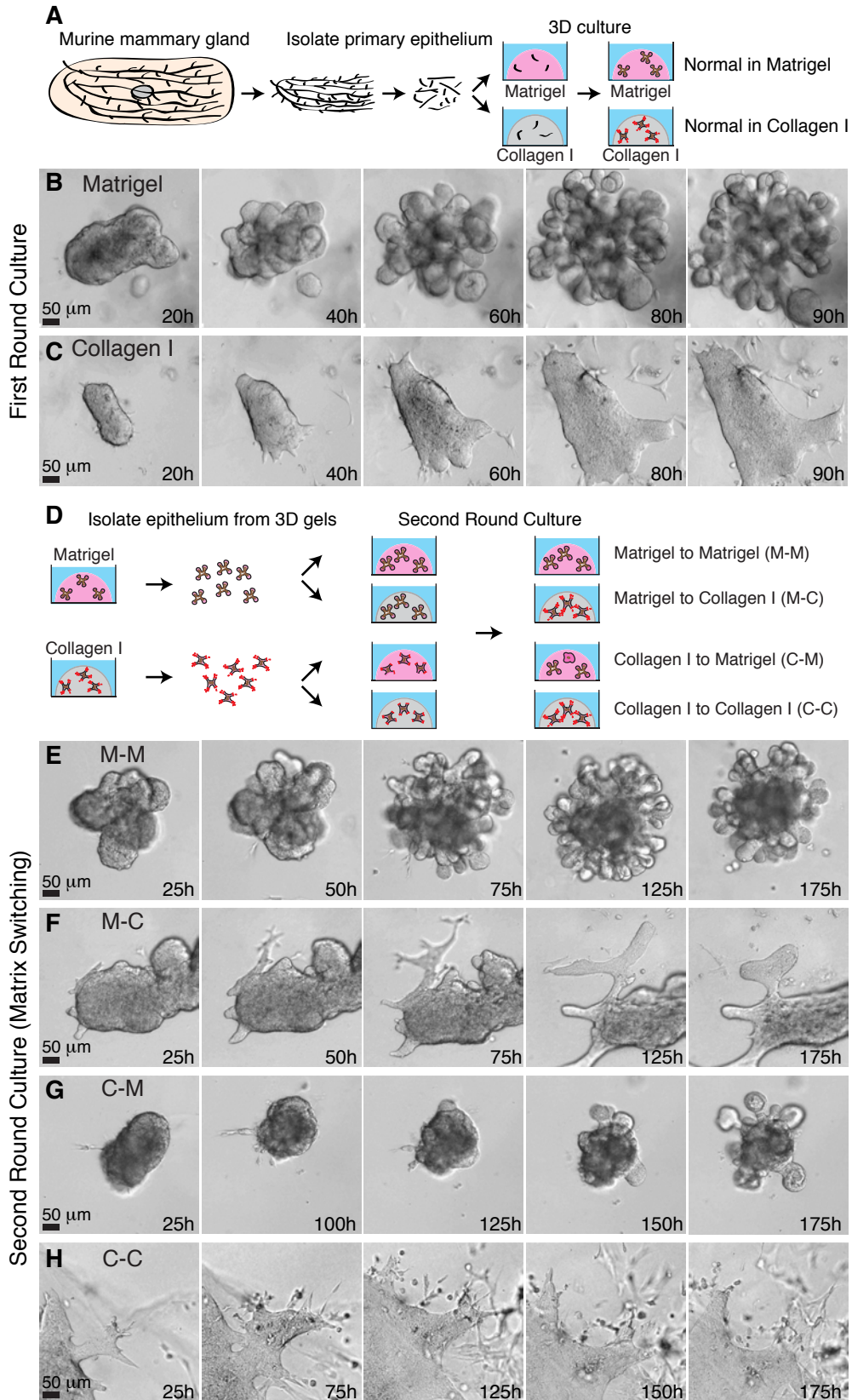


Figure 2-6

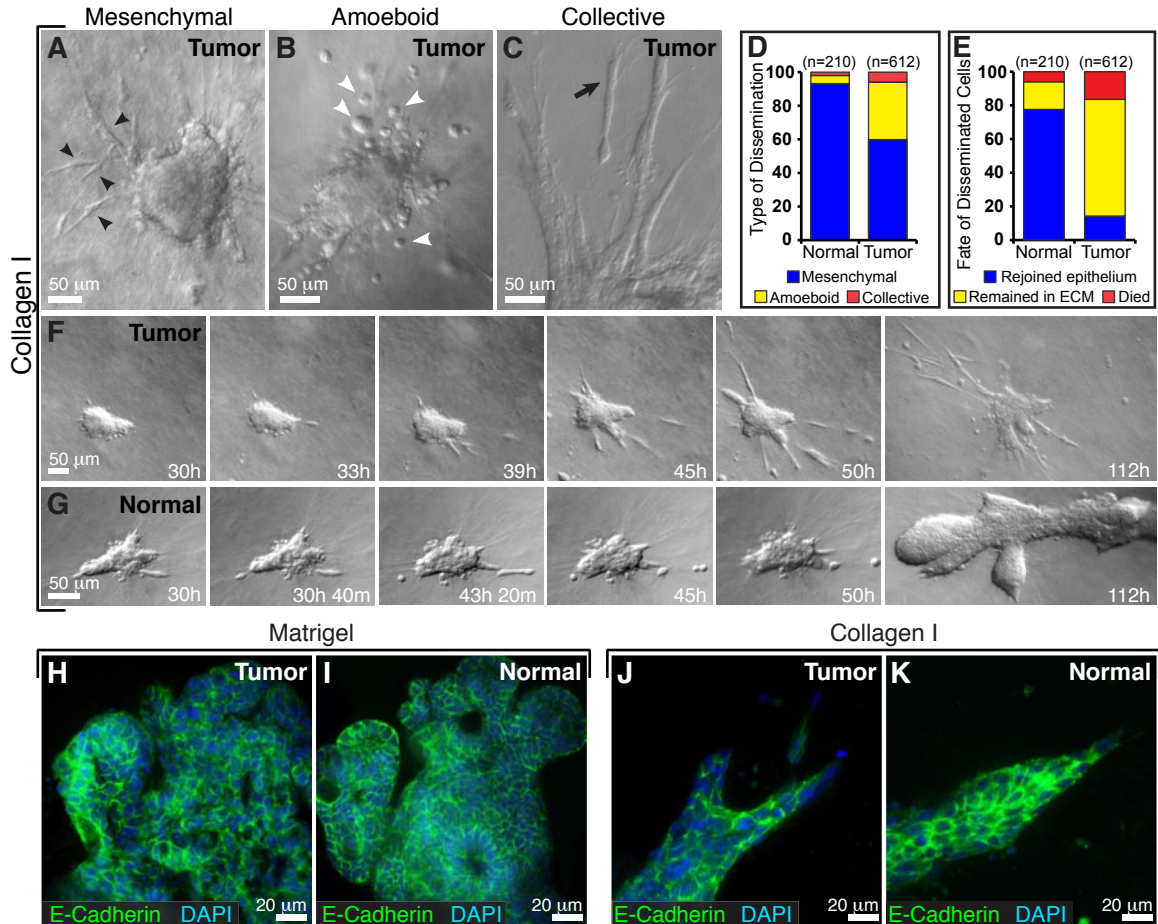


Figure 2-6. Cell dissemination into collagen I is persistent in tumor and transient in normal epithelium. (A-C) Tumor cells disseminate with mesenchymal (black arrowheads) (A), amoeboid (white arrowheads) (B), and collective (black arrow) (C) morphologies. (D-E) Distribution of morphological types of dissemination (D) and fate of disseminated cells in normal and tumor organoids (E) in collagen I. *n*, total number of disseminated cells observed in each condition. (F-G) Representative frames from DIC time-lapse movies of tumor (F) and normal organoids (G) in collagen I. (H-I) Localization of E-cadherin and DAPI in tumor (H) and normal organoids (I) cultured in Matrigel. (J-K) Localization of E-cadherin and DAPI in tumor (J) and normal organoids (K) cultured in collagen I.

Figure 2-7. Normal epithelium transiently protrudes and disseminates into collagen I but reestablishes a complete basement membrane. (A) Representative DIC time-lapse movie of a normal organoid grown in collagen I. (A') Higher magnification of a transition from a protrusive to a smooth border with ECM. (A'') Higher magnification of reintegration of disseminated cells with the epithelial group. (B) Representative confocal time-lapse movie of a normal organoid grown in collagen I. (B') Higher magnification of transient protrusions within single myoepithelial cells. Arrows indicate individual protrusions, retractions, and epithelial reorganization. (B'') Higher magnification of a multicellular extension of myoepithelial cells (blue arrows) at the leading front. (C-G) Normal epithelia in collagen reform a multi-component basement membrane. (C-D' and F-F') Localization of actin, DAPI and laminin 111 in a merge of all channels (C, D, F) and in a single channel of laminin 111 (C', D', F') in a normal organoid with a single cell protrusion (C'), a multicellular extension (D'), and a normal organoid after reorganization (F'). (E-E' and G-G') Localization of actin, DAPI and collagen IV in a merge of all channels (E, G), a single channel of collagen IV (E', G') in a normal organoid with multicellular extensions (E') and after reorganization (G'). (H-H') Localization of DAPI and laminin 332 in a merge of two channels (H) and in a single channel of laminin 332 (H'). (I-K') Tumor epithelia display incomplete basement membrane coverage. Single channels show the localization of actin (I, J, K), laminin 111 (I'), collagen IV (J'), and laminin 332 (K') in tumor organoids in collagen I. Red and green arrowheads indicate actin-based protrusions and signals of basement membrane components, respectively.

Figure 2-7

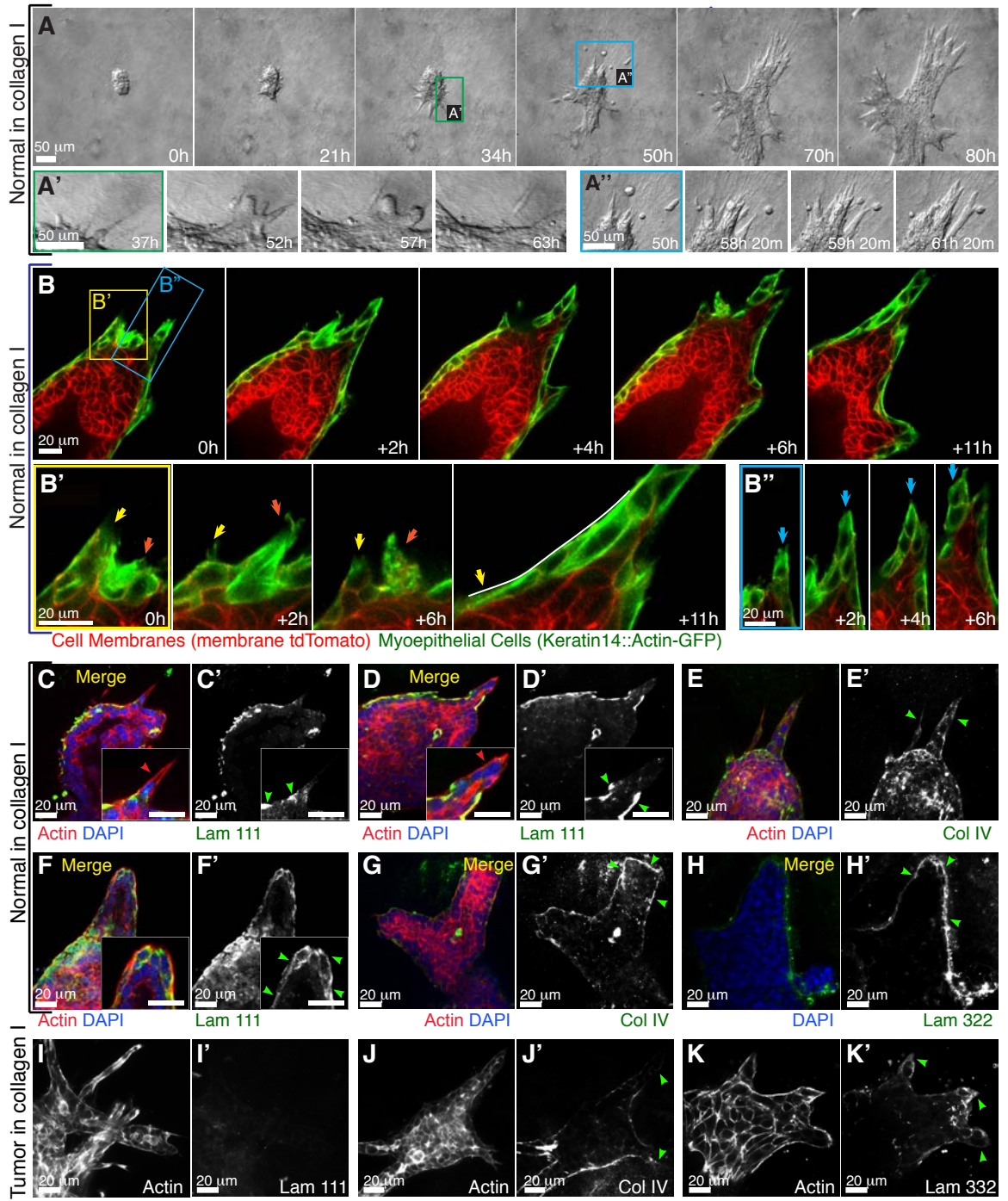


Figure 2-8

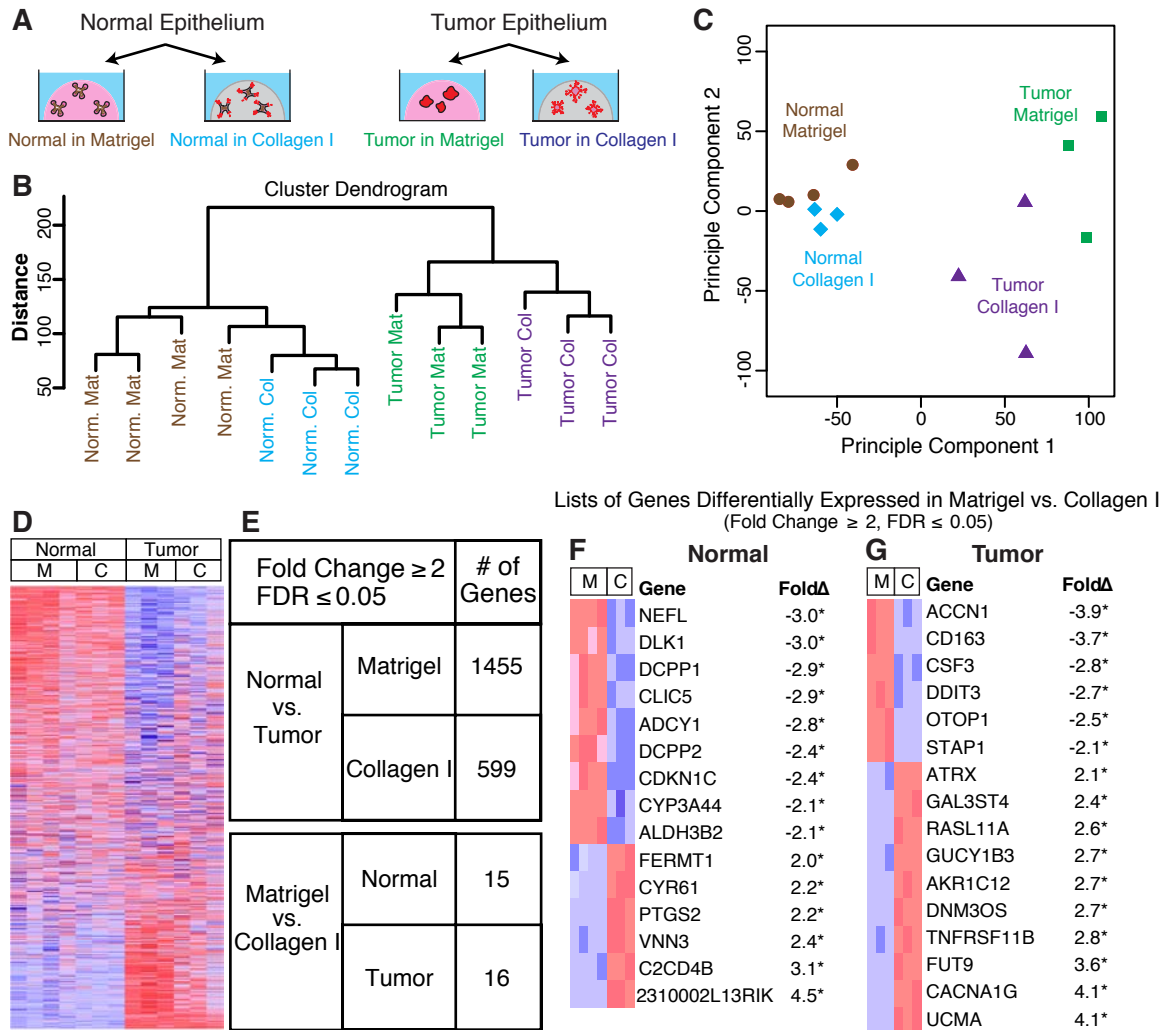


Figure 2-8. Tumor and normal epithelium remain transcriptionally distinct despite morphological similarities induced by the ECM. (A) Schematic description of 3D cultures of normal and tumor murine epithelial fragments in Matrigel and collagen I for mRNA expression analyses. $n =$ at least 3 biological replicates. (B) Complete linkage hierarchical clustering of the experimental conditions. (C) Principal component analysis of the experimental conditions. (D) Heatmap representation of the 19693 genes included in the microarray (blue and red indicate lower and higher expression, respectively). (E) Summary of differentially expressed genes with fold changes ≥ 2 and $FDR \leq 0.05$. (F-G) Genes differentially expressed based on ECM condition in normal (F) and tumor (G). *M*, Matrigel; *C* = collagen I.

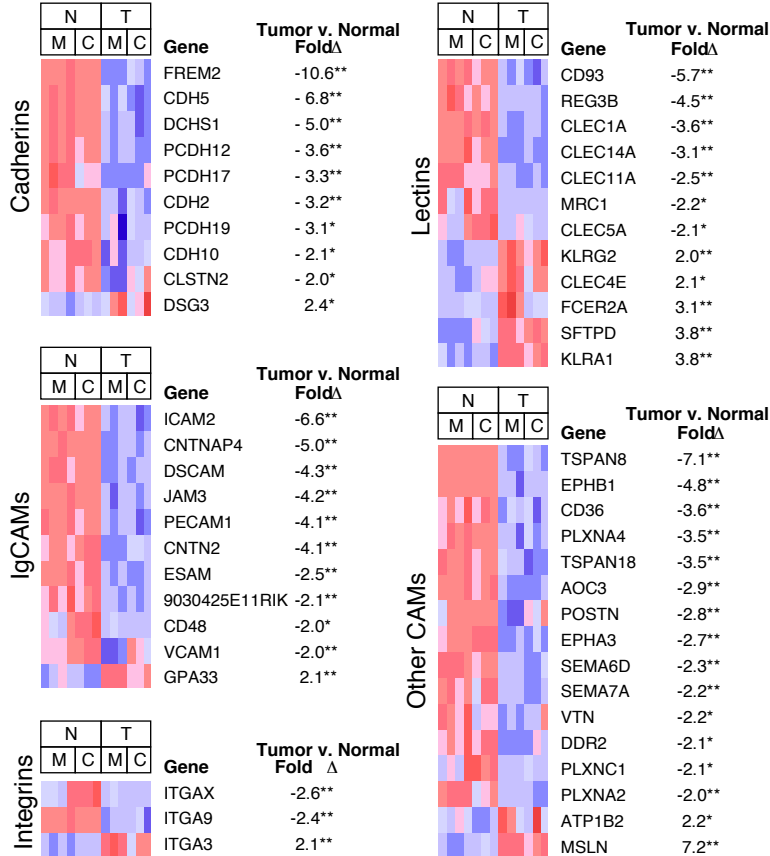
Figure 2-9. Cell-cell adhesion and extracellular genes are downregulated in tumor epithelium. (A) Analysis using DAVID functional annotation clustering. Genes with fold changes ≥ 2 and FDR ≤ 0.05 were used as input into DAVID. The top enriched categories include genes whose protein products are involved in cell adhesion, are localized to the extracellular space, or are involved in the inflammatory response. (B) Expression of structurally related genes implicated in cell-cell and cell-matrix adhesion. (C) Expression of genes associated with epithelial to mesenchymal transition (EMT). EMT genes are either upregulated in normal or are not significantly differentially expressed. For all heatmaps, * denotes p-value < 0.05 ; ** denotes p-value < 0.001 .

Figure 2-9

A

Enrichment	Cluster #	Gene Ontology (GO) Category	# of Genes	Enrichment Score	FDR
Matrigel	Higher in Normal	1 Cell Adhesion (GO:007155)	64	10.9	9.4×10^{-11}
		2 Extracellular Region (GO:0005576)	137	8.1	7.9×10^{-12}
		3 Blood Vessel Development (GO:0001568)	31	5.3	6.4×10^{-5}
		4 Heparin Binding (GO:008201)	38	4.6	6.0×10^{-3}
	Higher in Tumor	1 Extracellular Region (GO:0005576)	138	19.3	3.3×10^{-21}
		2 Inflammatory Response (GO:0006954)	58	7.6	4.1×10^{-7}
		3 Ectoderm Development (GO:0007398)	25	3.3	7.9×10^{-3}
Collagen I	Higher in Normal	1 Extracellular Region (GO:0044421)	65	12.0	1.4×10^{-13}
		2 Cell Adhesion (GO:0007155)	44	8.7	6.9×10^{-9}
		3 Blood Vessel Development (GO:0001568)	27	8.6	1.5×10^{-7}
		4 Carbohydrate Binding (GO:0030246)	26	5.1	7.5×10^{-6}
		5 Regulation of Cell Migration (GO:0030334)	13	3.8	2.3×10^{-3}
		6 Growth Factor Binding (GO:0019838)	14	3.6	6.3×10^{-3}
	Higher in Tumor	1 Extracellular Region (GO:0005576)	41	6.7	6.6×10^{-9}

B Cell Adhesion Families Gene Expression



C EMT Gene Expression

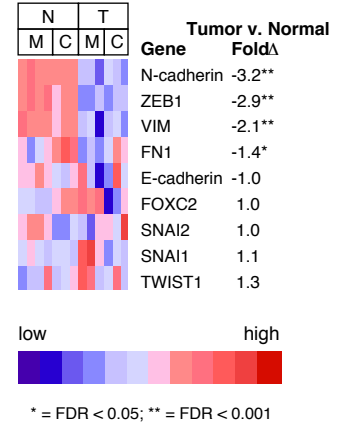


Figure 2-10

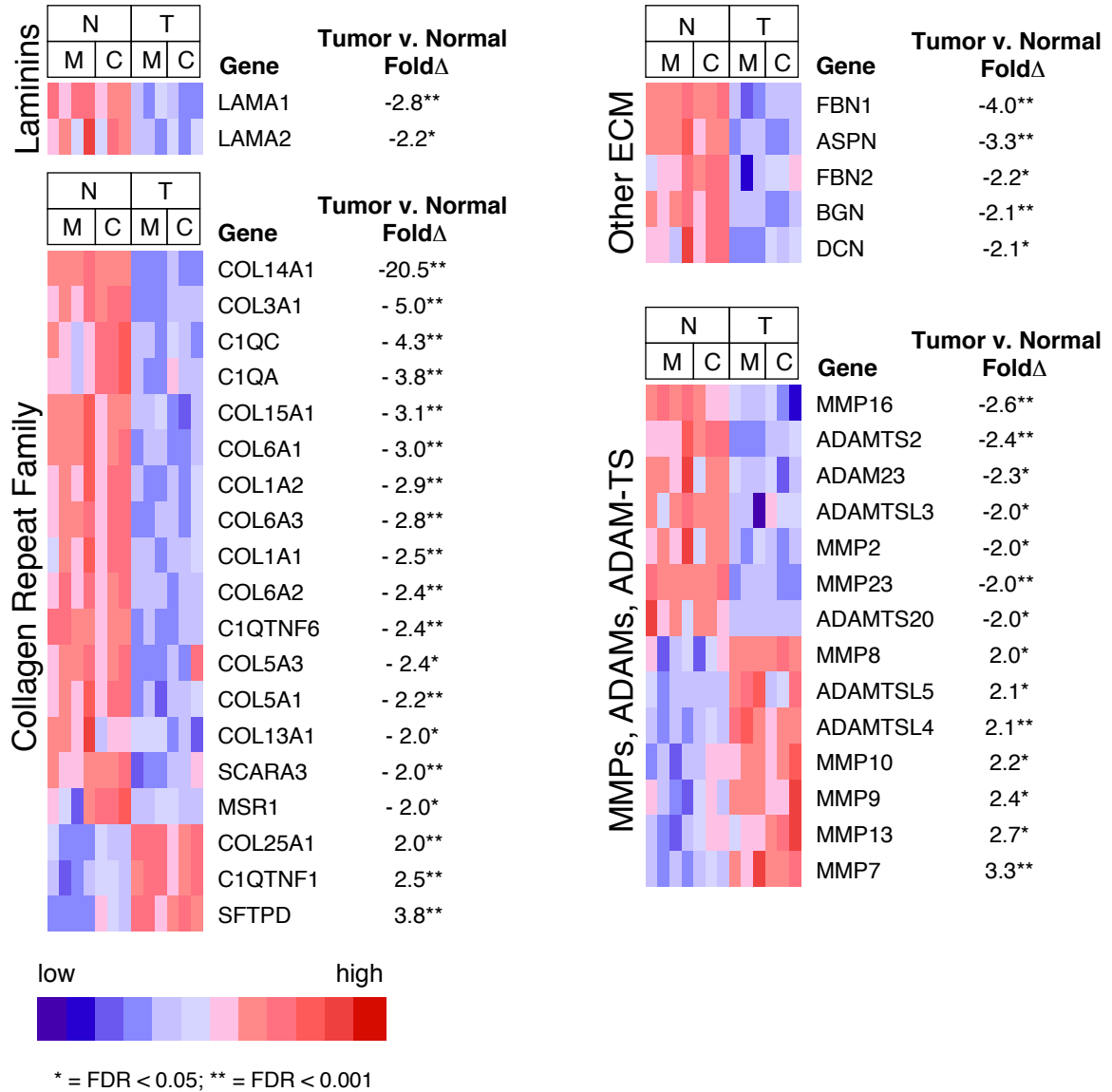
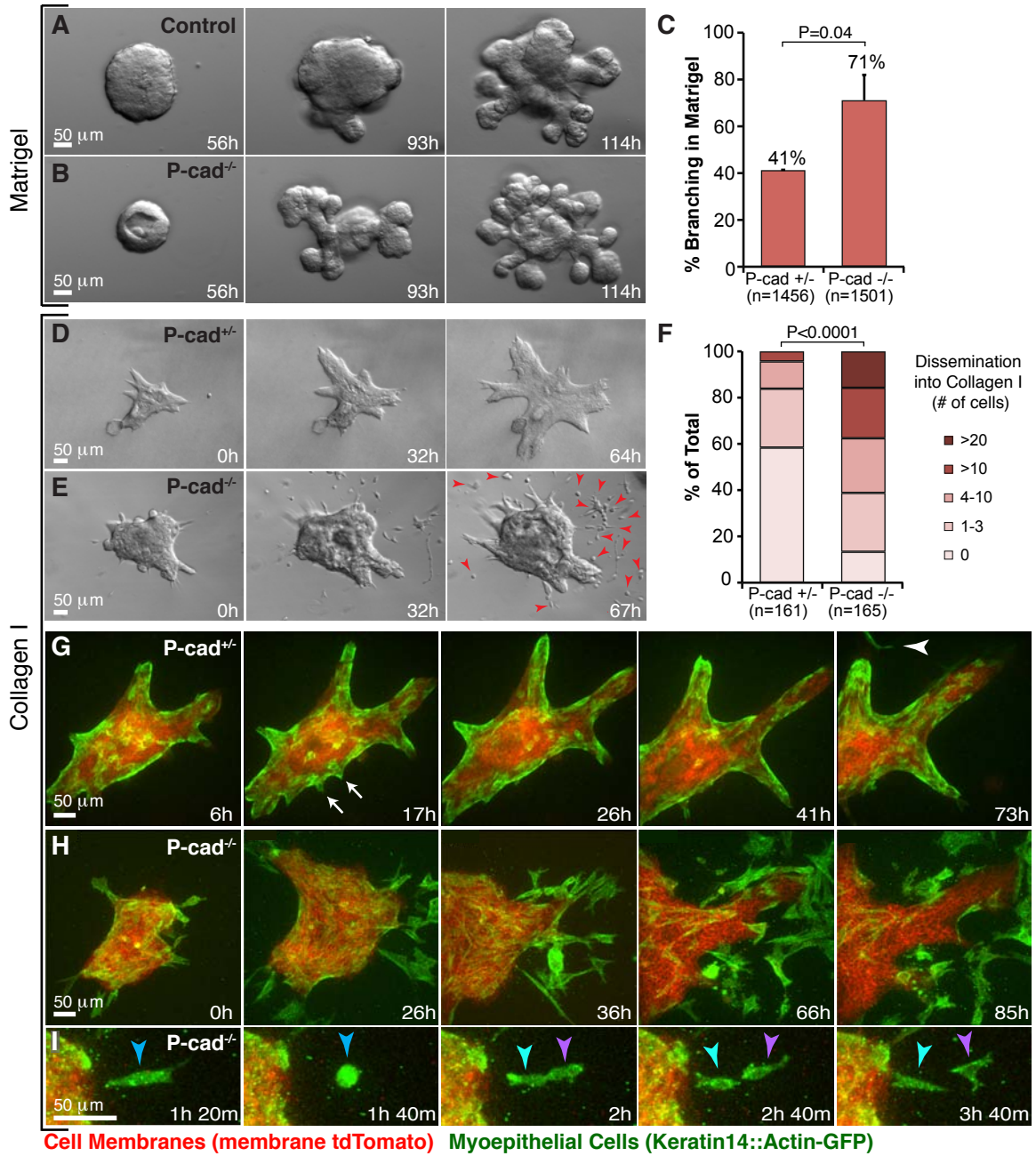


Figure 2-10. Extracellular matrix genes and metalloproteinases are differentially expressed by normal and tumor epithelium. The majority of differentially expressed genes in laminin, collagen, and other ECM gene sets were upregulated in normal epithelium. Approximately equal numbers of differentially expressed metalloproteinase genes were downregulated in normal and tumor epithelium. For all heatmaps, * denotes p-value < 0.05; ** denotes p-value < 0.001.

Figure 2-11. Loss of P-cadherin causes precocious branching morphogenesis in Matrigel and enhanced, sustained dissemination into collagen I. (A-B) Representative DIC time-lapse movies of (A) control (*P-cad*^{+/+}) and (B) *P-cad*^{-/-} epithelium grown in parallel in Matrigel. (C) Percent of *P-cad*^{+/+} and *P-cad*^{-/-} organoids branching in Matrigel on day 7. *n*, total number of organoids counted (3 biological replicates; *P = 0.04; Student's t-test, two-tailed, unequal variance). (D-E) Representative DIC time-lapse movies of (D) *P-cad*^{+/+} and (E) *P-cad*^{-/-} epithelium grown in parallel in collagen I. Arrowheads indicate persistent cell dissemination. (F) Distribution of number of disseminated cells per organoid in *P-cad*^{+/+} and *P-cad*^{-/-} epithelia. *n*, total number of movies (3 biological replicates; *P < 0.0001; upper one-sided chi-squared test). (G) Representative confocal time-lapse movie of *P-cad*^{+/+}; *mT/mG*; *K14::Actin-GFP* epithelium in collagen I. Arrows indicate transient, myoepithelial-led protrusions. Arrowhead indicates a single disseminated myoepithelial cell. (H) Representative confocal time-lapse movie of enhanced myoepithelial dissemination into collagen I by *P-cad*^{-/-}; *mT/mG*; *K14::Actin-GFP* epithelium. (I) Proliferation of a disseminated *P-cad*^{-/-} myoepithelial cell.

Figure 2-11



CHAPTER 3

3D culture assays of murine mammary

branching morphogenesis and epithelial invasion

(Modified from Nguyen-Ngoc et al., *Methods Mol Biol* 2014)

Abstract

Epithelia are fundamental tissues that line cavities, glands, and outer body surfaces. We use three-dimensional (3D) embedded culture of primary murine mammary epithelial ducts, called “organoids”, to recapitulate in days in culture epithelial programs that occur over weeks deep within the body. Modulating the composition of the extracellular matrix (ECM) allows us to model cell- and tissue-level behaviors observed in normal development, such as branching morphogenesis, and in cancer, such as invasion and dissemination. Here, we describe a collection of protocols for 3D culture of mammary organoids in different ECMs and for immunofluorescence staining of 3D culture samples and mammary gland tissue sections. We illustrate expected phenotypic outcomes of each assay and provide troubleshooting tips for commonly encountered technical problems.

1. Introduction

Mammary gland development occurs postnatally from a simple epithelial rudiment^{1,2}. During puberty, this rudiment undergoes stratification and initiates branching morphogenesis to form a network of epithelial tubes. The functional unit of elongation is a proliferative, multilayered front called the terminal end bud (TEB)^{3,4}. Behind the TEB, repolarization to a mature duct reestablishes a simple, bi-layered architecture, characterized by an inner layer of luminal epithelial cells and an outer layer of myoepithelial cells. These fundamental programs involve concurrent changes in cell proliferation, migration, polarity, and tissue architecture and are modulated by signaling cues from stromal cells and the extracellular matrix (ECM)⁵.

Because mammary epithelium develops within a fat pad with limited optical accessibility,

various groups have used 3D culture to facilitate direct observation and manipulation of epithelial cell behaviors⁶⁻¹⁴. Cultures of primary mammary tissues were first developed half a century ago^{15,16}, but the past decade has seen significant improvements in and increasing utilization of 3D culture models¹⁷⁻²⁰. While many conventional methods rely on immortalized cell lines or primary single cells, we use freshly isolated, murine mammary epithelial ducts, which we term “organoids”. The organoid assay arose from a series of papers published in the Bissell and Werb Labs^{17-19,21}. There are technical differences among the papers, but all involve mechanical disruption, enzymatic digestion, and differential centrifugation to separate mammary epithelial organoids from surrounding adipocytes and stromal cells. Purified organoids can be embedded in various ECMs to model distinct epithelial programs.

Our recent studies have revealed many of the cellular mechanisms driving epithelial morphogenesis and demonstrated that the ECM microenvironment regulates the migration and dissemination of mammary epithelial cells^{17,22-24}. Normal development in vivo occurs within a basement membrane, and we use Matrigel, a basement membrane-rich ECM, as an experimentally convenient model for the normal ductal microenvironment. Culture of organoids in basal medium, without supplemental growth factors, induces formation of simple, bi-layered cysts, while culture with growth factor induces a stereotyped program of branching morphogenesis. In contrast, cancer progression involves breaks in the basement membrane, and the microenvironment around a tumor is enriched in collagen I²⁵⁻³⁰. We demonstrated that collagen I-rich microenvironments induce a conserved program of invasion and dissemination in normal and malignant mammary epithelium²³. Conversely, defined mixtures of Matrigel and collagen I can reproduce a more physiological organization of the elongating TEB²⁴.

Building on our previously published methods^{17,22,23,31}, this protocol seeks to provide a comprehensive guide to utilizing the mammary organoid assay (Fig. 3-1A). We introduce several variations on the assay in different ECMs and growth conditions that model different aspects of epithelial development and disease. We also provide optimized protocols for immunofluorescence staining of organoids in 3D embedded culture and of tissue sections of whole mammary glands.

2. Materials

2.1 Mice

We have successfully isolated and cultured organoids from mice ranging in age from E18.5 through 1.5 years of age. There are variations in response to growth factors with age and strain. All protocols below are optimized for FVB mice between 8-12 weeks of age. Once euthanized, mammary tissue is optimally isolated and cultured immediately, but successful organoid cultures have been established from mice sacrificed and then kept at 4°C overnight.

2.2 Reagents

1. Collagenase solution in DMEM/F12: 2 mg/mL collagenase, 2 mg/mL trypsin, 5% v/v fetal bovine serum (FBS), 5 µg/mL insulin, and 50 µg/mL gentamicin.
 - a. Collagenase from *Clostridium histolyticum* (Sigma C2139): Dissolve 1 g in 10 mL DMEM/F12, and make 200 µL aliquots. Store at -20°C.
 - b. Trypsin: Dissolve 1 g in 10 mL DMEM/F12, and make 200 µL aliquots. Store at -20°C.
2. Dulbecco's phosphate buffered saline (DPBS, with Ca²⁺, Mg²⁺).
3. Phosphate buffered saline (PBS, without Ca²⁺, Mg²⁺).

4. BSA solution: 2.5% bovine serum albumin (BSA) in DPBS.
5. 2000 U DNase (Sigma D4263): Dissolve in 1 mL of PBS, and make 40 μ L aliquots. Store at -20°C.
6. Organoid medium in DMEM/F12: 1% penicillin/streptomycin and 1% insulin-transferrin-selenium-X (ITS) (GIBCO 51500).
7. FGF2, 25 μ g (Sigma F0291): Dissolve in 250 μ L of PBS, and make 20 μ L aliquots. Store at -20°C.
8. Growth Factor Reduced Matrigel (BD Biosciences 354230).
9. Rat tail collagen I (BD Biosciences 354236).
10. DMEM 10X, low glucose.
11. 1.0 N NaOH.
12. 4% paraformaldehyde (PFA) in DPBS.
13. OCT compound.
14. 0.5% Triton X-100 in DPBS.
15. 10% FBS in DPBS.
16. Mounting Medium (Sigma F4680-25ML).
17. Primary antibodies.
18. Secondary antibodies conjugated to fluorescent probes.

2.3 Instructions for Preparing Solutions

Prepare solutions as follows:

1. Collagenase solution (10 mL per mouse): Combine 9 mL DMEM/F12, 500 μ L FBS, 5 μ L insulin (10 mg/mL stock), 10 μ L gentamicin (50 mg/mL stock), 200 μ L collagenase (100 mg/mL stock), and 200 μ L trypsin (100 mg/mL stock) in a 15 mL tube. Filter sterilize through a 0.2 μ m filter into a new tube. This solution should be made fresh for each experiment.

2. BSA solution: Combine 46 mL DPBS and 4.1 mL BSA (30% stock solution). Filter sterilize, and store at 4°C. This solution can be reused for several experiments if kept sterile but should be monitored for contamination.
3. Organoid medium: Remove 10 mL of DMEM/F12 from a 500 mL bottle of medium. Add 5 mL penicillin/streptomycin (10,000 units penicillin and 10 mg streptomycin/mL stock) and 5 mL ITS. For the branching morphogenesis assays (**Sections 3.10.2** and **3.10.3**) and the invasion assay (**Section 3.10.4**), supplement organoid medium with growth factor at the desired concentration. Diverse growth factors induce branching in the 1-10 nM range, including EGF ligands (EGF, TGF- α , amphiregulin, heregulin, neuregulin), FGF ligands (FGF2, FGF7), and HGF. We typically use 2.5 nM FGF2 for 8–12-week-old FVB mice. It is necessary to optimize the growth factor concentration for the specific age and strain of mouse.

2.4 Tools and instruments

1. One Spencer Ligature scissors, delicate pattern (Fine Science Tools (FST) 14028-10): *For mouse exterior*.
2. One standard forceps, narrow pattern (FST 11003-12): *For mouse exterior*.
3. One Iris scissors, straight pattern (FST 14060-09): *For mouse interior (sterile)*.
4. One Graefe forceps (FST 11051-10): *For mouse interior (sterile)*.
5. Sterile scalpel, #10 blade.
6. Polystyrene Petri dish.
7. Benchtop incubator orbital shaker (Thermo Scientific MaxQ 4450).
8. Incublock™ microtube incubator with two blocks set to 37°C (Denville Scientific Inc I0540).
9. Ice bucket.
10. Centrifuge tubes, 15 mL and 50 mL.

11. Chambered coverglass, 2-well and 4-well (Nunc, Lab-Tek, Thermo Scientific).
12. SensoPlate, black, 24W multiwell plate, glass bottom, sterile, w/lid (Greiner Bio-One 662892).
13. 24-well glass plate cover (MatTek Corp P24GTOP-1.5-F).
14. Disposable base molds: 15x15x5 mm, 24x24x5 mm, and 30x24x5 mm (Fisher Scientific).
15. Superfrost® Plus Gold precleaned microscope slides (Fisher Scientific 15-188-48).
16. Cover glass, 50 x 22 mm.
17. Orbital Shaker (Reliable Scientific, Inc.).
18. StainTray with black lid (Simport M920-2).
19. Cryostat.

3. Methods

3.1 Collecting mouse mammary glands

Mice have five pairs of mammary glands located beneath the skin and outside the peritoneum. This section describes how to collect glands #3, #4, and #5 for organoid isolation and how to limit contamination by other tissues.

1. Generally, use female mice between 8 to 12 weeks old.
2. Sterilize the dissecting area with 70% Ethanol.
3. Sterilize the dissecting tools by heat in a glass bead sterilizer.
4. Euthanize the mouse in a CO₂-saturated chamber for 3-5 minutes followed by cervical dislocation.
5. Pin the mouse face up to a protected Styrofoam board.
6. Wet the mouse thoroughly with 70% EtOH. Use the back of the standard forceps to smooth down the fur. Wipe away any feces with a 70% EtOH damp Kimwipe.

7. Use the standard forceps to grasp the skin above the groin.
8. Use the Spencer Ligature scissors to cut along the ventral midline from the groin to the chin (Fig. 3-1B). Be careful to cut only the skin and not the peritoneum underneath.
9. Make four incisions from the midline cut towards the four legs (Fig. 3-1B).
10. Use the standard forceps to pull back the skin one side at a time to expose the mammary glands (Fig. 3-1C). Use the back of the Graefe forceps to help separate the skin from the peritoneum (Fig. 3-1D).
11. Push back a thin yellow layer of muscle located on top of gland #3 to expose the mammary gland (Fig. 3-1E-E').
12. Use the Graefe forceps to remove the inguinal lymph node located at the intersection of three blood vessels in gland #4 (Fig. 3-1F-F').
13. Use the Graefe forceps and Iris scissors to grasp and pull out mammary glands #3, #4, and #5 from both right and left sides. Pool glands in a sterile Petri dish (Fig. 3-2A) (see **Note 1**).

3.2 Isolating mammary epithelial organoids

Mammary epithelium is embedded inside a fat pad containing adipose tissue and collagen-rich stroma. This section describes how to purify fragments of mammary epithelium (“organoids”) using enzymatic and mechanical digestion. All centrifugation speeds refer to a Sorvall Legend X1R benchtop swinging bucket centrifuge (1500 rpm, 1250 rcf). We have achieved similar results with 1500 rpm spins in similar benchtop centrifuges from other manufacturers.

1. In a sterile hood, mince mammary glands with a scalpel, ~25-50 times per mouse, until the tissue relaxes (Fig. 3-2A,A'). Use a separate scalpel for each mouse type.

2. Use the scalpel to transfer the minced glands to collagenase solution in a 15 mL or 50 mL tube (Fig. 3-2B). We use 10 mL of collagenase solution per mouse.
3. Shake the suspension at 110 rpm for 30-40 min (see **Note 2**) at 37°C until the tissue breaks up into smaller pieces and is relatively dispersed (Fig. 3-2B') but not overdigested (Fig. 3-2B''). We typically use a Thermo Scientific MaxQ 4450 for this purpose.
4. Spin the tube in a centrifuge at 1500 rpm for 10 min at room temperature. The tube will have 3 layers: a fatty layer on top, an aqueous layer in the middle, and a red pellet of epithelium on the bottom (Fig. 3-2C).
6. Precoat (Fig. 3-3A) (see **Note 3**) a 15 mL tube with BSA solution. Use one tube per mouse type. For all subsequent steps, precoat all pipette tips and tubes with BSA solution prior to contact with mammary tissue (Fig. 3-3).
7. To recover additional epithelial tissue, use a pipette to transfer the opaque fatty layer into the BSA-coated 15 mL tube. Add DMEM/F12 up to 10 mL. Pipette up and down vigorously to disperse the fatty layer (Fig. 3-2D). Spin the tube at 1500 rpm for 10 min at room temperature. Aspirate the supernatant, and save the pellet (Fig. 3-2E).
8. Aspirate (see **Note 4**) the aqueous layer in the tube with the original pellet.
9. Add 10 mL DMEM/F12 to the tube with the original pellet, and transfer to the 15 mL "fatty layer" tube (step 7). Pipette up and down vigorously to resuspend and combine the two pellets.
10. Spin the tube at 1500 rpm for 10 min at room temperature.
11. Aspirate the supernatant, and add up to 4 mL DMEM/F12 to the combined pellet (Fig. 3-2F). At this stage during isolation, the suspension contains small clusters of organoids and stromal cells attached to one another (Fig. 3-2F-F').

12. Add 40 μL DNase (2 U/ μL) into the 4 mL organoid suspension, and gently invert by hand for 2-5 min at room temperature to break up the clusters and detach organoids from single cells (Fig. 3-2G'-G'').
13. Add 6 mL of DMEM/F12, and pipette up and down thoroughly.
14. Spin the tube at 1500 rpm for 10 min at room temperature. The pellet should now appear red and more compact (Fig. 3-2H-H').

Next perform differential centrifugation to wash out enzymes and separate single stromal cells from the epithelial organoids. The protocol suggests aspiration of the supernatant assuming that the stromal cells will be discarded. If recovery of mammary stromal populations is desired, then transfer the supernatant after each spin to a 50 mL tube.

15. Aspirate the supernatant to the 0.5 mL mark.
16. Resuspend the pellet in 10 mL DMEM/F12, and mix thoroughly.
17. Pulse to 1500 rpm, and stop the centrifuge 3-4 sec after it reaches speed.
18. Repeat step 15-17 three more times (see **Note 5**).
19. The final pellet should be off-white and consist mostly of organoids, without single cells (Fig. 3-2I-I',J). However, the organoid suspension may be contaminated with other tissue types, most commonly nerve bundles (Fig. 3-2K) and muscle (Fig. 3-2L).

3.3 Organoid density determination

This section describes how to determine the density of the organoid suspension and the overall yield.

1. Resuspend the pellet in 10 mL DMEM/F12 to form a homogeneous mixture (see **Note 6**).

2. Mix thoroughly (e.g. by rocking the tube by hand), and transfer 50 μL of the suspension to a 30 mm Petri dish. Count the number of organoids in this sample volume under a microscope (Fig. 3-2I',J).
3. Calculate the total number of organoids collected according to the following formula. For example, if 20 organoids were counted in a 50 μL sample removed from a 10 mL total volume (9950 μL remaining), then the total number of organoids would be $(20/50) \times 9950 = 3980$ organoids.

Total number of organoids	=	$\frac{\text{Number of organoids}}{\text{Sample Volume (e.g. 50 } \mu\text{L})}$	X	Remaining volume (e.g. 9950 μL)
---------------------------------	---	--	---	--

4. Calculate the organoid density (see **Note 7**), and re-adjust to 1000 organoids/mL to simplify allocation to ECM gels.
5. Calculate the number of organoids and the respective volume of suspension required for each experiment.
6. Aliquot the required volumes of organoid suspension into BSA-coated 1.5 mL microcentrifuge tubes (Fig. 3-3C), and spin the tubes at 1500 rpm for 5 min at room temperature.
7. Carefully remove the supernatant so as not to disturb the pellet (see **Note 8**).
8. Calculate the volume of ECM solution required to reach a final density of 2 organoids/ μL (see **Note 9**).

3.4 Plating mammary organoids in Matrigel

Mammary epithelium develops in vivo within a basement membrane. 3D culture in Matrigel, a basement membrane-rich gel, recapitulates important features of epithelial development^{17,19,22,23}. This section describes how to embed organoids in 3D Matrigel.

1. Thaw Matrigel at 4°C for 3-4 h prior to plating. If the Matrigel is put at 4°C to thaw at the start of the prep, it will be ready to use by the end of the prep. During plating, always keep Matrigel on ice.
2. Use a plate with a coverglass bottom for time-lapse imaging.
3. Pre-incubate the plate at 37°C for 5 min.
4. Set up the tissue culture hood in preparation for plating (Fig. 3-4A).
5. Set the heating block to 37°C, and place the plate in direct contact with the block (Fig. 3-4B-C') (see **Note 10**).
6. Add the required volume of liquid Matrigel to a microcentrifuge tube with organoids. Since Matrigel is quite viscous, first pipette up and down slowly a few times to coat the tip and ensure an accurate volume.
7. Keep the Matrigel-containing tube on ice or in a cold block. Resuspend the organoid pellet gently to avoid introducing air bubbles. Do not try to take up the entire volume into the pipette tip while mixing.
8. Plate the appropriate volume of Matrigel/organoid suspension into the wells according to the following table (Fig. 3-5A). Pipette up and down to resuspend the organoids before plating each sample, and pipette out only until the first stop.

Type of plate	Volume of gel / well (µL)	Volume of medium / well (µL)
24-well plate	50 – 150	750 – 1000
4-well chamber	50 – 75	750 – 1000
2-well chamber	150 – 300	1500 – 2000

9. Keep the plate on the heating block for several minutes to allow further gelation before returning it to the incubator.
10. Incubate the plate at 37°C, 5% CO₂ for 30-60 min.

11. Gently add pre-warmed organoid medium to the wells. For the cyst formation assay (**Section 3.10.1**), use basal medium without supplemental growth factors. For the branching morphogenesis assay (**Section 3.10.2**), supplement the medium with nanomolar concentrations of growth factor. A variety of growth factors may be used, including EGF ligands (EGF, TGF- α , amphiregulin, heregulin, neuregulin), FGF ligands (FGF2, FGF7), and HGF. We most commonly use 2.5 nM FGF2.
12. Add sterile water or PBS to the empty wells to prevent desiccation.
13. Label the wells. Return the plate to the incubator.
14. If the plate will be used for DIC imaging, use a glass plate cover for better image quality.

3.5 Preparing collagen I solution

Collagen I solubilized from rat tail is commonly used to study 3D migration of many cell types³². However, the properties of collagen I gels vary depending on multiple factors during preparation, such as temperature, pH, and collagen concentration. We demonstrated that the extent of collagen fiber assembly correlated strongly with invasive behavior²⁴. This section describes how we prepare collagen I (Fig. 3-5B).

1. Rat tail collagen I is used to prepare a collagen solution according to the following formula. The steps below describe how to make a 250 μ L solution. Scale up the volume as needed.

Total volume (μ L)	250	500	1000	2000	5000
1.0 N NaOH (μ L)	8	16	32	64	160
DMEM 10X (μ L)	25	50	100	200	500
collagen I stock (μ L)	217	434	868	1763	4340

2. Perform all steps on ice. To work with a large volume of collagen solution, use a 1000 μ L extra long pipette tip to avoid the collagen solution getting stuck to the filter barrier during pipetting.
3. First, combine 25 μ L DMEM 10X and 8 μ L NaOH, and mix well. The solution will turn a dark pink color (Fig. 3-5C₁).
4. Add 217 μ L collagen I (Fig. 3-5C₂) (see **Note 11**). Since collagen I is quite viscous, pipette up and down slowly a few times to coat the pipette tip.
5. Mix the solution well until the color remains stable. When the pH changes from acidic \rightarrow neutral \rightarrow basic, the color changes from light green/yellow \rightarrow light pink/orange \rightarrow dark pink, respectively (Fig. 3-5C₃₋₇). The desired color is light pink or salmon, which corresponds to a pH of 7.0-7.5 (see **Note 12**). The pH can be tested using pH strips.
6. Use DMEM 1X to adjust the neutralized collagen I solution to the desired collagen concentration (see **Note 13**). For the invasion assay (**Section 3.10.4**), we use a collagen concentration of 3 mg/mL.

3.6 Plating mammary organoids in collagen I

Fibrillar collagen I, the most abundant structural protein in mammary glands, plays an important role in normal development as well as in breast cancer. Our previous studies have demonstrated that collagen I induces a conserved response of protrusive invasion in both normal and tumor organoids²³. This section describes how to properly prepare pre-assembled collagen I and embed mammary organoids in a 3D gel.

1. Use a plate with a glass bottom for time-lapse imaging.
2. Use 20-30 μ L of neutralized collagen to make a thin underlay on the coverglass of the well at room temperature (Fig. 3-5E). The underlay helps the top collagen/organoid suspension attach better to the coverglass.
3. Incubate the plate with the underlays at 37°C until ready for plating.

4. Pre-incubate the neutralized collagen I solution (used for the top gel) on ice for 60-120 min for pre-assembly²⁴ (see **Note 14**). The collagen I solution will turn cloudy and fibrous (Fig. 3-5D₁₋₆) (see **Note 15**), a state we term pre-assembled collagen I.
5. Set up the tissue culture hood in preparation for plating (Fig. 3-4A).
6. Set the heating block to 37°C, and place the plate on top, in direct contact with the block (Fig. 3-4B-C') (see **Note 10**).
7. Always keep the collagen I solution (or a Matrigel/collagen I mix) on ice. Add the desired amount of pre-assembled collagen I to the organoid pellet in a microcentrifuge tube. Since collagen I is quite viscous, first pipette up and down slowly a few times to coat the tip and ensure an accurate volume.
8. Keep the tube on ice or in a cold block. Resuspend the organoid pellet gently to avoid introducing air bubbles. Do not try to take up the entire volume into the pipette tip while mixing.
9. Plate the appropriate volume of collagen/organoid suspension (see table in **Section 3.4**) on top of the underlay (Fig. 3-5E'). Pipette up and down to resuspend the organoids before plating each sample, and pipette out only until the first stop.
10. Keep the plate on the heating block for several minutes to allow further gelation before returning it to the incubator (see **Note 16**).
11. Incubate the plate at 37°C, 5% CO₂ for 45-60 min. After gelation, collagen I fibrils are visible under the microscope at 10X and 40X (Fig. 3-5F-F').
12. Gently add pre-warmed organoid medium supplemented with growth factor to the wells. A variety of growth factors may be used, including EGF ligands (EGF, TGF- α , amphiregulin, heregulin, neuregulin), FGF ligands (FGF2, FGF7), and HGF. We most commonly use 2.5 nM FGF2.
13. Add sterile water or PBS to the empty wells to prevent desiccation.

14. Label the wells. Return the plate to the incubator.
15. If the plate will be used for DIC imaging, use a glass plate cover for better image quality.

3.7 Plating mammary organoids in a mixture of Matrigel and collagen I

A mixture of Matrigel and collagen I represents a more physiological ECM microenvironment for mammary branching morphogenesis. The presence of collagen I significantly improves epithelial ductal elongation and myoepithelial coverage²⁴. We do not observe epithelial protrusions into mixed Matrigel/collagen I gels²⁴. This section describes how to properly prepare a mixture of Matrigel and pre-assembled collagen I and how to embed mammary organoids in this mixed matrix.

1. Prepare collagen I solution as described in **Section 3.5**.
2. Repeat steps 1-4 in **Section 3.6** to make underlays and prepare pre-assembled collagen I.
3. Combine Matrigel and pre-assembled collagen I at the desired ratio. Gently pipette up and down a few times to form a homogeneous solution (Fig. 3-5B').
4. Always keep the mixed matrix solution on ice. Add the desired amount to the organoid pellet in a microcentrifuge tube.
5. Plate the mixed matrix/organoid suspension as described in steps 5 – 15 in **Section 3.6** (Fig. 3-5E').

3.8 Immunofluorescence staining of 3D culture samples

The thickness of 3D gels and the multicellular structure of mammary organoids often results in reduced antibody accessibility for immunofluorescence (IF) staining and poor visualization during imaging. This section describes two methods for performing IF staining in 3D culture samples. First, fix gels as follows:

1. Remove organoid medium from the wells.
2. Fix samples with 4% PFA for 10-15 min at room temperature (see **Note 17**) on an orbital shaker at 20 rpm.
3. Remove PFA, and wash samples 2-3X 10 min with DPBS.

From here, you can perform antibody staining directly in intact 3D gels or on cut sections on slides. The whole gel staining works well with high-quality antibodies and probes such as Phalloidin (stains for F-actin), smooth muscle actin (SMA), and keratin 14. For many other antibodies, staining sections on slides is preferable.

3.8.1 Staining whole gels

1. Permeabilize the gel with 0.5% Triton X-100 for 30-60 min.
2. After permeabilization, immediately block samples with 10% FBS (see **Note 18**) for 1-3 h at room temperature or overnight at 4°C.
3. Remove the blocking solution, add primary antibody in 10% FBS (see **Note 18**) at the desired ratio, and incubate for 2-3 h at room temperature or overnight at 4°C.
4. Remove the primary antibody solution, and wash samples 3X 10 min with 10% FBS or DPBS at room temperature.
5. Optional: Block the samples again with 10% FBS for 30-60 min at room temperature.
6. Add secondary antibody in 10% FBS (see **Note 18**) at the desired ratio, and incubate for 1-2 h at room temperature.
7. Wash 3X 10 min with DPBS at room temperature.
8. Store samples in DPBS at 4°C, but remove DPBS before imaging. If the gel has detached from the coverslip, leaving the DPBS in the well causes the gel to wiggle or float and go out of focus.

3.8.2 Staining sections on slides

1. Gently detach the gel from the culture plate and transfer to a small disposable base mold (15x15x5 mm) filled with a thin layer of OCT.
2. Freeze the mold at -80°C for 5-10 min.
3. Fill up the mold with OCT to cover the sample, and return to -80°C for long-term storage.
4. During sectioning, store molds on dry ice. Set up the cryostat with OT at -20°C and CT at -20°C.
5. Remove an OCT block from its mold, and cut sections at 20-100 μm thickness.
6. Transfer sections to slides using a fine camel hair brush or a pair of forceps.
7. Keep slides at -80°C for long-term storage.
8. For antibody staining, thaw slides at room temperature (see **Note 19**).
9. Wash slides 2-3X 10 min with DPBS to remove OCT.
10. Permeabilize with 0.5% Triton X-100 for 30-60 min (see **Note 20**).
11. Wash 2X 10 min with DPBS to remove Triton.
12. Block slides with 10% FBS for 2 h at room temperature or overnight at 4°C.
13. Remove the blocking solution, add primary antibody in 10% FBS, and incubate for 2-3 h at room temperature or overnight at 4°C (see **Note 21**).
14. Wash 3X 10 min with 10% FBS or DPBS.
15. Add secondary antibody in 10% FBS, and incubate for 2 h at room temperature or overnight at 4°C.
16. Wash 3X 10 min with DPBS.
17. Mount slides with mounting medium and 50 x 22 mm coverslips. Let the slides dry at room temperature in a dry StainTray or in a dark drawer before imaging.

3.9 Immunofluorescence staining of mammary gland tissue sections

The opacity and thickness of the mammary fat pad limits the accessibility of mammary epithelium to whole gland staining and imaging. This section describes how to perform IF staining in mammary gland tissue sections.

1. Collect mouse mammary glands #3 and/or #4, as described in **Section 3.1**, taking care to keep the entire gland intact (see **Note 22**). Spread out the gland on the bottom of a 1- or 2-well chambered coverglass.
2. Fix the tissue with 4% PFA for 4 h at room temperature or overnight at 4°C.
3. Wash 3X 15 min with DPBS to remove PFA.
4. Transfer the gland to a medium (24x24x5 mm) or large (30x24x5 mm) disposable base mold filled with a thin layer of OCT.
5. Freeze the mold at -80°C for 5-10 min.
6. Fill up the mold with OCT to cover the gland, and return to -80°C for long-term storage.
7. During sectioning, store molds on dry ice. Set up the cryostat with OT at -40°C and CT at -30°C.
8. Remove an OCT block from its mold, and cut sections at 50-200 μm thickness.
9. Transfer sections to slides using a fine camel hair brush or a pair of forceps.
10. Keep slides at -80°C for long-term storage.
11. Repeat steps 8-17 in **Section 3.8.2** for IF staining (see **Note 23**).

3.10 Assays

In vivo, mammary epithelium develops within a basement membrane surrounded by collagen-rich stromal tissue. The ability to manipulate the ECM microenvironment in 3D organotypic culture allows us to isolate the effects of individual matrix components on mammary epithelial cell behaviors. This section describes four assays that use different ECM compositions or growth conditions to model distinct epithelial programs (Fig. 3-6A).

3.10.1 Cyst formation assay

In 3D Matrigel in basal medium, mammary organoids reorganize from a multilayered fragment to establish a simple bi-layered epithelium with an internal lumen, termed a cyst (Fig. 3-6B, Fig. 3-7A). The extent of lumen formation varies with the initial size of the organoid and with the mouse strain (Fig. 3-7A₁-A₄). The resulting morphologies include a minimal or barely detectable lumen (Fig. 3-7A₁), a partial lumen (Fig. 3-7A₂), a complete lumen in a small cyst (Fig. 3-7A₃), and a complete lumen in a large cyst (Fig. 3-7A₄). Epithelial cells in the cyst always maintain a smooth basal surface with the ECM (Fig. 3-7A₄). We have observed that C57BL6 organoids form cysts with complete lumens (Fig. 3-6B) more efficiently than FVB organoids. Although the appearance of the lumen varies by light microscopy, immunofluorescence staining for SMA and F-actin can confirm establishment of a simple bi-layered structure of internal luminal epithelial cells and basal myoepithelial cells (Fig. 3-8A). We use this assay to model the formation of mammary epithelial ducts in vivo (Fig. 3-8D).

3.10.2 Branching morphogenesis assay in Matrigel

In 3D Matrigel, nanomolar concentrations of growth factor induce mammary organoids to undergo branching morphogenesis (Fig. 3-6C). The branching program includes sequential steps of lumen clearing, stratification, bud initiation, and bud elongation (Fig. 3-6C)¹⁷. We observe variation in morphology depending on the extent of progression through this program. Organoids that only complete stratification or bud initiation (Fig. 3-7B₁), or that form fewer than three buds (Fig. 3-7B₂-B₄), are not scored as “branched” (Fig. 3-7B). Only organoids with three or more elongated buds are scored as “branched” (Fig. 3-7C). However, the morphology of branched organoids varies based on the initial size of the organoid, the mouse strain, and the types of growth factors added. Here, we

present four examples of branching in Matrigel (Fig. 3-7C₁-C₄). The first two show organoids with multiple multilayered, elongating buds without any regions of repolarization (Fig. 3-7C₁-C₂). In contrast, the second two show organoids that have re-established simple epithelial architecture in the central lumen (Fig. 3-7C₃) or within buds (Fig. 3-7C₄). During bud elongation in Matrigel, the leading front of the bud is always non-protrusive (Fig. 3-7B₄,C₄). Notably, these buds lack or are incompletely covered by myoepithelial cells (SMA⁺, Fig. 3-8B). These gaps in myoepithelial coverage can be observed *in vivo*, particularly in side branches of the mammary ductal tree (Fig. 3-8E).

3.10.3 Branching morphogenesis assay in a mix of Matrigel and collagen I

In a mixture of Matrigel and collagen I, mammary organoids undergo a similar program of branching morphogenesis to that in Matrigel alone, with several notable differences²⁴ (Fig. 3-6D). Branched organoids in the mixed matrix generally have fewer buds, but the buds elongate much further into the ECM. We have demonstrated that ratios of 5:5 and 3:7 Matrigel to collagen I induce the highest average bud lengths²⁴. Here, we present four examples of branching in the mixed matrices. Organoids may contain both short and long buds, without repolarization (Fig. 3-7D₁) or with partial repolarization (Fig. 3-7D₂,D₄). We also observe bifurcation at the ends of elongated buds (Fig. 3-7D₃). As in Matrigel alone, the leading front of the bud is always non-protrusive (Fig. 3-7D₄). Importantly, a mix of 3:7 Matrigel to collagen I yields a high percentage of epithelial buds that maintain complete myoepithelial coverage throughout bud initiation and elongation (Fig. 3-8C). This phenomenon more closely models elongation of the terminal end bud *in vivo* (Fig. 3-8F).

3.10.4 Invasion assay

Collagen I induces a conserved protrusive response in mammary epithelium (48 h, Fig. 3-6E). Organoids invade collectively into collagen I, with branches varying in shape and length, from short and thin (Fig. 3-7E₁-E₂) to elongated and wide (Fig. 3-7E₃-E₄). Initially, we observe extensive subcellular protrusions. However, these protrusions cease, and the epithelium reestablishes a smooth basal surface upon formation of a basement membrane between the epithelium and ECM (Fig. 3-6E)²³. The extent of invasion and epithelial reorganization varies, even within the same organoid. At day 5 in culture, we observe both protrusive (orange arrowheads, Fig. 3-7E₄) and non-protrusive, round tips (violet arrowheads, Fig. 3-7E₁-E₄) at the ends of multicellular invasive structures. We also observe single cell dissemination into collagen I (blue arrowheads, Fig. 3-7E₁,E₄).

3.11 Technical Issues

Here we present several technical problems that we commonly encounter during 3D culture. First, epithelial organoids located very close to the cover glass tend to lose their 3D structure and spread out in 2D as sheets of cells (Fig. 3-7F₁-F₂). Second, organoids may be surrounded by protrusive or stringy cells, which likely results from stromal or other non-epithelial cells attaching to organoids during their isolation (Fig. 3-7F₃). Non-epithelial contaminating species appear distinct and behave differently from organoids. We have observed groups of dead cells (Fig. 3-7F₄), clusters of protrusive stromal cells (Fig. 3-7F₅), and nerve bundles (Fig. 3-7F₆), which tend to locally disseminate cells into the matrix.

4. Notes

1. Mammary gland #1 is very small. Mammary gland #2 is located in the neck and is hard to distinguish from other tissues. Generally, do not collect these glands so as to

- avoid contamination by other tissues (e.g. muscle or epithelial glands) (Fig. 3-2L).
2. Incubation in collagenase solution can require up to 60 min to adequately break up the fat pad. Check the status of the suspension after 30 min of shaking. We have observed incorrect incubation times increase the amount of contaminating tissues in the final organoid suspension (Fig. 3-2K). If shaking is done in an incubator that is also used for bacterial cultures, wipe the outside of the tube with 70% ethanol before bringing it into the biosafety cabinet.
 3. Always precoat new pipette tips and tubes with BSA solution to prevent organoids from sticking to the plastic. This precoating (Fig. 3-3) is critical to achieving a high final yield of organoids, especially at younger ages or with C57BL6 mice.
 4. Never aspirate the supernatant completely to avoid sucking up the pellet.
 5. Carefully examine the pellet after each quick spin before aspirating the supernatant. If the organoids are not well pelleted, mix the suspension thoroughly again, and increase the centrifugation time.
 6. The appropriate volume of DMEM/F12 to use for counting varies depending on the estimated yield. If the yield is low, add less medium. If the yield is high, dilute the suspension further 2-10X.
 7. The yield varies significantly with mouse strain and age. We generally obtain 2000-4000 organoids per FVB mouse and 500-2000 organoids per C57BL6 mouse.
 8. Always check the pellet after every centrifugation. Be careful not to disturb the pellet when removing the supernatant. Use small pipette tips if necessary.
 9. The optimal density of organoids in the gel differs for different ECMs and mouse strains. For example, C57BL6 organoids tend to be more contractile than FVB organoids when embedded in collagen I, resulting in contraction of the gel and detachment from the glass bottom if plated too densely.

10. In a 24-well plate, the glass bottom is slightly recessed from the edge of the plastic wall. When both blocks are present in the heating block (Fig. 3-4B), there is a small gap between the plate and the heating block surface, resulting in a temperature at the glass bottom less than 37°C. To establish direct contact between the glass bottom and the heating block, remove one of the blocks and set up the plate as in Fig. 3-4C-C'.
11. When preparing the collagen I solution, always wait for the solution to come down to the tip, and pipette it out completely. This is particularly important during collagen I neutralization to ensure an accurate volume and concentration of collagen.
12. Since the concentration and pH of rat tail collagen I vary among batches, adjust the pH using small volumes of collagen stock (up to 30 µL) or small amounts of 1.0 N NaOH (<0.5 µL).
 - a. If the adjustment requires addition of a large amount of collagen I stock, you will need to add more DMEM 10X to maintain ionic balance. However, this complicates calculation of the final concentration of neutralized collagen solution.
 - b. If you find that your collagen I stock is more basic, prepare the collagen solution with 7.0-7.5 µL of 1.0 N NaOH per 250 µL, and then adjust the final pH with small volumes of 1.0 N NaOH. This will avoid the need to add large volumes of collagen I stock to achieve the appropriate pH.
13. If you are concerned about the accuracy of the final collagen concentration, try to use the same pipette tip for mixing throughout neutralization and pH adjustment to limit loss of collagen solution inside the pipette tip.
14. The pre-incubation time will determine the density of pre-assembled collagen fibrils. Due to batch variability in collagen stocks, the time required to obtain a gel with visible collagen fibrils varies considerably from 45-120 min. To examine the extent of

- fibril formation during pre-incubation, plate 30 μ L of collagen solution onto a small Petri dish, let it gel for several minutes, and examine under the microscope.
15. If the neutralized collagen I solution is pre-incubated for more than 3-4 h on ice, it will become very cloudy and fibrous (Fig. 3-5D₆), and the resulting gel will be less transparent, impairing visibility during imaging.
 16. Collagen I gels tend to detach from the coverglass when kept too long on the heating block. Therefore, if you have Matrigel and collagen I gels on the same plate, plate the Matrigel samples first and the collagen I samples last.
 17. In PFA, Matrigel becomes very fragile, especially after more than 4 days in culture. To avoid disintegration of the gel, reduce the PFA concentration to 2% with lighter shaking or incubate the gel with 4% PFA for 8-10 min.
 18. In our lab, we have identified two successful approaches for performing antibody staining that use slightly different solutions and incubation times. The first one, described in **Sections 3.8** and **3.9**, uses 10% FBS in DPBS as both the blocking buffer and the dilution buffer for antibodies. The other method uses 10% FBS, 1% BSA in DPBS as a blocking buffer and 1% FBS, 1% BSA in DPBS as the dilution buffer for antibodies.
 19. From this step on, slides are kept in a StainTray with a black lid filled with a shallow layer of water to prevent desiccation and photo-bleaching of fluorescent probes.
 20. If you plan to stain for extracellular proteins, such as basement membrane components, permeabilize the samples before embedding into OCT and sectioning. Direct permeabilization on slides can extract too many of these proteins.
 21. To conserve primary antibodies, especially ones that require a high concentration, use a PAP pen to draw a hydrophobic border around the section, and add primary antibody solution within this area.

22. For mice less than 4 weeks of age, we typically use only gland #4 and remove the fat pad distal to the lymph nodes. Since the glands at this age are very small, pool several glands into one OCT block for sectioning.
23. To improve antibody staining in mammary gland tissue sections, it is sometimes useful to significantly increase the incubation times. For example, we sometimes permeabilize with Triton X-100 for 1 h at room temperature; incubate with primary antibody for 48 h at 4°C; and incubate with secondary antibody for 6 h at room temperature or overnight at 4°C. In addition, for incubation with antibodies, it is preferable to draw a hydrophobic border around the tissue with a PAP pen to reduce the volume of solution required and to ensure that the tissue is always immersed in solution. Do not let samples air-dry.

References

- 1 Sternlicht, M. D. Key stages in mammary gland development: the cues that regulate ductal branching morphogenesis. *Breast Cancer Res* **8**, 201 (2006).
- 2 Hogg, N. A., Harrison, C. J. & Tickle, C. Lumen formation in the developing mouse mammary gland. *J Embryol Exp Morphol* **73**, 39-57 (1983).
- 3 Williams, J. M. & Daniel, C. W. Mammary ductal elongation: differentiation of myoepithelium and basal lamina during branching morphogenesis. *Dev Biol* **97**, 274-290 (1983).
- 4 Hinck, L. & Silberstein, G. B. Key stages in mammary gland development: the mammary end bud as a motile organ. *Breast Cancer Res* **7**, 245-251 (2005).
- 5 Sternlicht, M. D., Kouros-Mehr, H., Lu, P. & Werb, Z. Hormonal and local control of mammary branching morphogenesis. *Differentiation* **74**, 365-381 (2006).
- 6 Mroue, R. & Bissell, M. J. Three-dimensional cultures of mouse mammary epithelial cells. *Methods Mol Biol* **945**, 221-250 (2012).
- 7 Vidi, P. A., Bissell, M. J. & Lelievre, S. A. Three-dimensional culture of human breast epithelial cells: the how and the why. *Methods Mol Biol* **945**, 193-219 (2012).
- 8 Griffith, L. G. & Swartz, M. A. Capturing complex 3D tissue physiology in vitro. *Nat Rev Mol Cell Biol* **7**, 211-224 (2006).
- 9 Gudjonsson, T., Ronnov-Jessen, L., Villadsen, R., Bissell, M. J. & Petersen, O. W. To create the correct microenvironment: three-dimensional heterotypic collagen assays for human breast epithelial morphogenesis and neoplasia. *Methods* **30**, 247-255 (2003).
- 10 Nelson, C. M. & Bissell, M. J. Modeling dynamic reciprocity: engineering three-dimensional culture models of breast architecture, function, and neoplastic transformation. *Semin Cancer Biol* **15**, 342-352 (2005).
- 11 Nelson, C. M., Inman, J. L. & Bissell, M. J. Three-dimensional lithographically defined organotypic tissue arrays for quantitative analysis of morphogenesis and neoplastic progression. *Nat Protoc* **3**, 674-678 (2008).
- 12 Wozniak, M. A. & Keely, P. J. Use of three-dimensional collagen gels to study mechanotransduction in T47D breast epithelial cells. *Biol Proced Online* **7**, 144-161 (2005).
- 13 Provenzano, P. P., Eliceiri, K. W., Inman, D. R. & Keely, P. J. Engineering three-dimensional collagen matrices to provide contact guidance during 3D cell migration. *Curr Protoc Cell Biol* **Chapter 10**, Unit 10 17 (2010).
- 14 Debnath, J., Muthuswamy, S. K. & Brugge, J. S. Morphogenesis and oncogenesis of MCF-10A mammary epithelial acini grown in three-dimensional basement membrane cultures. *Methods* **30**, 256-268 (2003).
- 15 Ichinose, R. R. & Nandi, S. Lobuloalveolar Differentiation in Mouse Mammary Tissues in Vitro. *Science* **145**, 496-497 (1964).
- 16 Ichinose, R. R. & Nandi, S. Influence of hormones on lobulo-alveolar differentiation of mouse mammary glands in vitro. *J Endocrinol* **35**, 331-340 (1966).
- 17 Ewald, A. J., Brenot, A., Duong, M., Chan, B. S. & Werb, Z. Collective epithelial migration and cell rearrangements drive mammary branching morphogenesis. *Dev Cell* **14**, 570-581 (2008).
- 18 Simian, M. *et al.* The interplay of matrix metalloproteinases, morphogens and growth factors is necessary for branching of mammary epithelial cells. *Development* **128**, 3117-3131 (2001).

- 19 Fata, J. E. *et al.* The MAPK(ERK-1,2) pathway integrates distinct and antagonistic signals from TGF α and FGF7 in morphogenesis of mouse mammary epithelium. *Dev Biol* **306**, 193-207 (2007).
- 20 Nelson, C. M., Vanduijn, M. M., Inman, J. L., Fletcher, D. A. & Bissell, M. J. Tissue geometry determines sites of mammary branching morphogenesis in organotypic cultures. *Science* **314**, 298-300 (2006).
- 21 Sternlicht, M. D. *et al.* Mammary ductal morphogenesis requires paracrine activation of stromal EGFR via ADAM17-dependent shedding of epithelial amphiregulin. *Development* **132**, 3923-3933 (2005).
- 22 Ewald, A. J. *et al.* Mammary collective cell migration involves transient loss of epithelial features and individual cell migration within the epithelium. *J Cell Sci* **125**, 2638-2654 (2012).
- 23 Nguyen-Ngoc, K. V. *et al.* The ECM microenvironment regulates collective migration and local dissemination in normal and malignant mammary epithelium. *PNAS* **109**, E2595-E2604 (2012).
- 24 Nguyen-Ngoc, K. V. & Ewald, A. J. Mammary ductal elongation and myoepithelial migration are regulated by the composition of the extracellular matrix. *J Microsc* (2013).
- 25 Provenzano, P. P. *et al.* Collagen reorganization at the tumor-stromal interface facilitates local invasion. *BMC Med* **4**, 38 (2006).
- 26 Provenzano, P. P. *et al.* Collagen density promotes mammary tumor initiation and progression. *BMC Med* **6**, 11 (2008).
- 27 Conklin, M. W. *et al.* Aligned collagen is a prognostic signature for survival in human breast carcinoma. *Am J Pathol* **178**, 1221-1232 (2011).
- 28 Egeblad, M., Rasch, M. G. & Weaver, V. M. Dynamic interplay between the collagen scaffold and tumor evolution. *Curr Opin Cell Biol* **22**, 697-706 (2010).
- 29 Paszek, M. J. *et al.* Tensional homeostasis and the malignant phenotype. *Cancer Cell* **8**, 241-254 (2005).
- 30 Levental, K. R. *et al.* Matrix crosslinking forces tumor progression by enhancing integrin signaling. *Cell* **139**, 891-906 (2009).
- 31 Ewald, A. J. Isolation of mouse mammary organoids for long-term time-lapse imaging. *Cold Spring Harb Protoc* **2013** (2013).
- 32 Wolf, K. *et al.* Collagen-based cell migration models in vitro and in vivo. *Semin Cell Dev Biol* **20**, 931-941 (2009).

Figure 3-1. Collection of mouse mammary glands for organoid isolation and 3D culture. (A) Schematic description of isolation and 3D culture of mouse mammary organoids. (B) Scheme for surgically accessing the mammary glands. Numbers indicate the order of cuts. (C) Locations of the ten mammary glands. (D) Expose glands #3, #4, and #5 by pushing back the abdomen (blue dotted line) with the back of the Graefe forceps. (E-E') A thin layer of muscle partially covers gland #3 (E) and should be pushed back before dissection (E'). Dotted line in (E') indicates the region of gland #3 to be collected. (F) Use the Graefe forceps to pluck out the lymph node in gland #4. Dotted line in (F') indicates the approximate region of glands #4 and #5 to be collected.

Figure 3-1

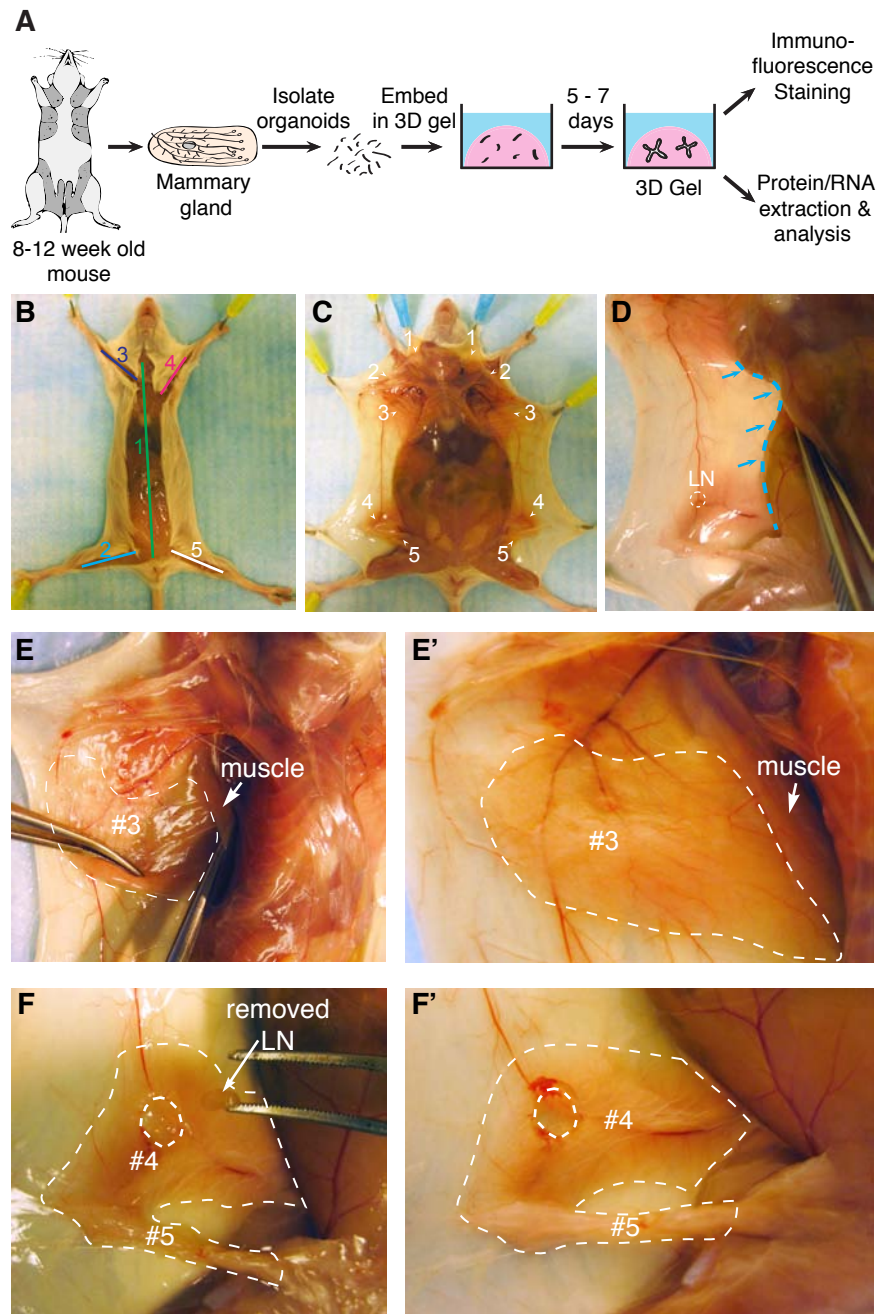


Figure 3-2. Mammary organoid isolation. (A-A') Collected mammary glands are pooled in a Petri dish (A) and minced until the tissue relaxes, typically 25-50 cuts (A'). (B-B'') Incubation in collagenase solution breaks up the fat pad (B) into smaller pieces that are relatively dispersed (B'). Too long of a digestion (B'') will cause organoids to be too small and not grow well. (C) Following incubation in collagenase solution, centrifugation separates the suspension into three layers, with a top opaque layer of fat and a pellet (#1) of epithelium and stroma. (D) The fatty layer is transferred to a new tube and resuspended in 10 mL DMEM/F12. (E) Centrifugation of the dispersed fatty layer recovers additional epithelium in the pellet (#2). (F-F'') The combined pellets from (C) and (E) are resuspended in 4 mL DMEM/F12 with DNase (F). Before DNase treatment, organoids (pink arrowheads) are loosely attached to each other and to stromal cells (F'), forming visible clusters in the tube (F''). (G-G'') DNase treatment causes organoids (pink arrowheads) to detach from one another (G') and the clusters to disappear (G''). (H-H') Centrifugation of the suspension in (G) results in a compact red pellet (H'). (I-I'') Differential centrifugation removes single cells from the suspension (I') and results in an off-white pellet of purified epithelial organoids (I''). Organoids (pink arrowheads) may appear rounded and small or more elongated and even branched (I'). Larger organoids typically survive and branch more efficiently in our assays. (J) Close-up view of an organoid. (K-L) Non-epithelial tissues can be observed in the final suspension, including nerve bundles (K) and muscle (L).

Figure 3-2

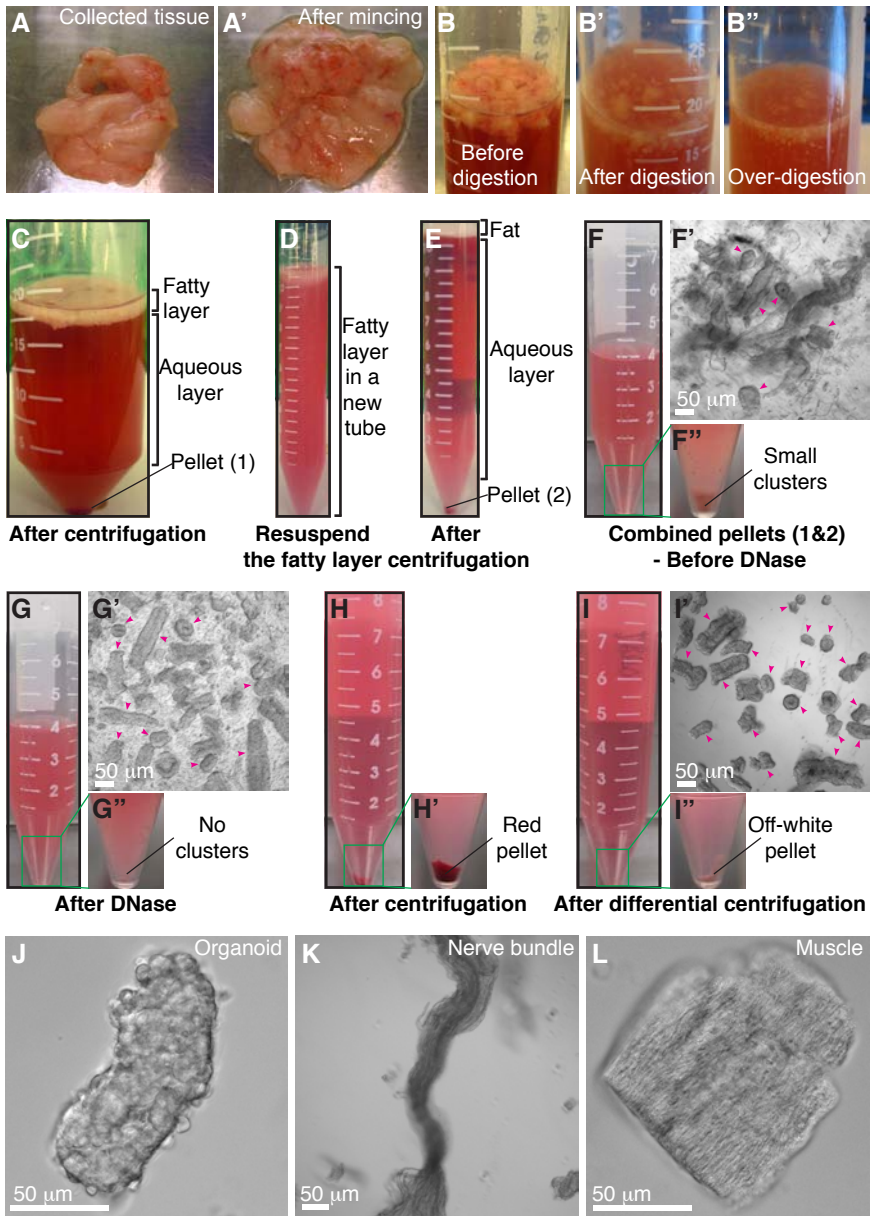


Figure 3-3

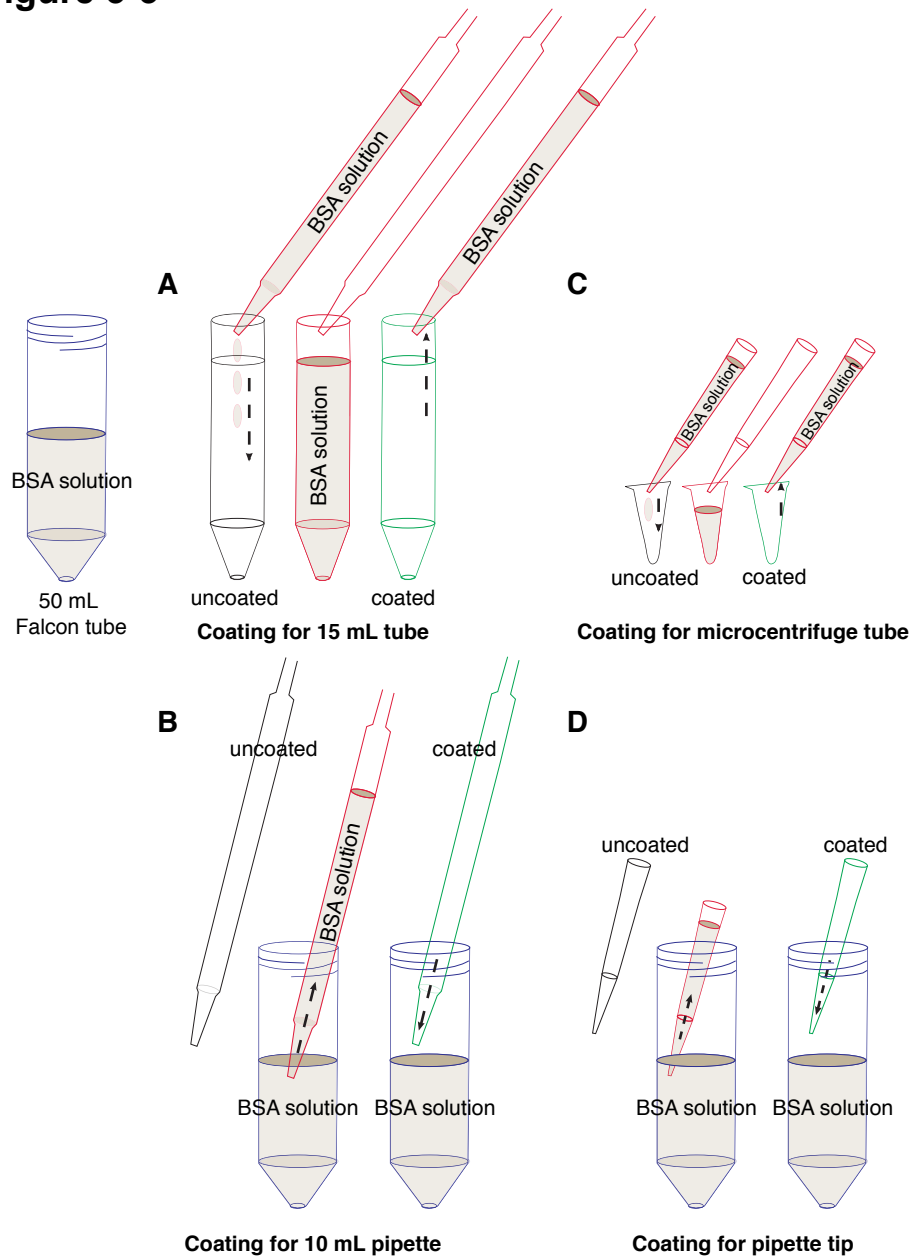
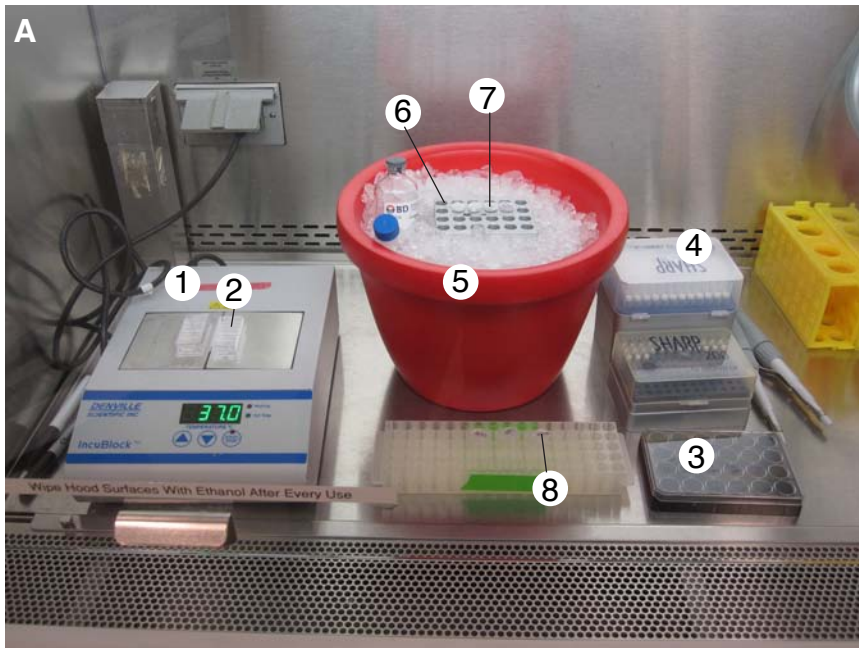


Figure 3-3. Precoating tubes and pipette tips with BSA. Tissue can adhere to uncoated plastic surfaces, and this protocol involves many pipetting steps. Accordingly, it is essential to precoat plastic surfaces with BSA solution to maximize final organoid yield. (A) Precoat a 15 mL tube by filling the tube with BSA solution, inverting the tube to precoat the cap, and removing the BSA solution. (B) Precoat a 10 mL pipette tip by taking up BSA solution to fill the entire pipette and ejecting back out. (C-D) Use the same approach to precoat a microcentrifuge tube (C) and a small pipette tip (D).

Figure 3-4



- | | | |
|-------------------|-------------------------|---|
| 1. Heating block | 4. 1 mL extra long tips | 7. Collagen I solution
being pre-incubated |
| 2. 4-well chamber | 5. Ice bucket | |
| 3. 24-well plate | 6. Cold block | 8. Organoid samples |

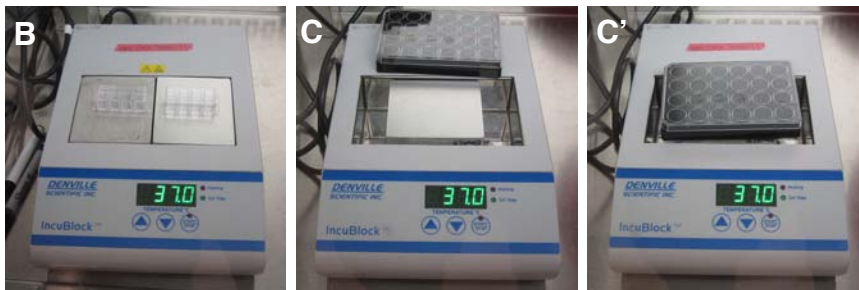


Figure 3-4. Setting up the tissue culture hood for plating. (A) Sample layout of reagents, tools, and equipment used for plating 3D culture samples. (B) Heating block set-up for plating in 2-well or 4-well chambers. (C-C') To plate in a 24-well dish, remove one of the blocks from the heating block (C) to establish direct contact between the remaining block and the plate bottom (C').

Figure 3-5. Plating organoids in 3D Matrigel and collagen I. (A) Schematic description of plating organoids in Matrigel. (B-B') Schematic description of preparing pre-assembled collagen I (B), which can be used alone or mixed with Matrigel (B'). (C₁-C₇) Color indicators for the pH of the collagen I solution during neutralization. (D₁-D₆) Decreasing transparency of the collagen I solution during pre-incubation on ice. (E-E') Schematic description of plating organoids in 3D collagen I or in a mixture of Matrigel and collagen I. (E) A top view for making an underlay on the coverglass. (E') A side view of how to plate the organoid/collagen I suspension on top of the gelled underlay. (F-F') Representative DIC images of collagen I fibers at low (F) and high (F') magnification.

Figure 3-5

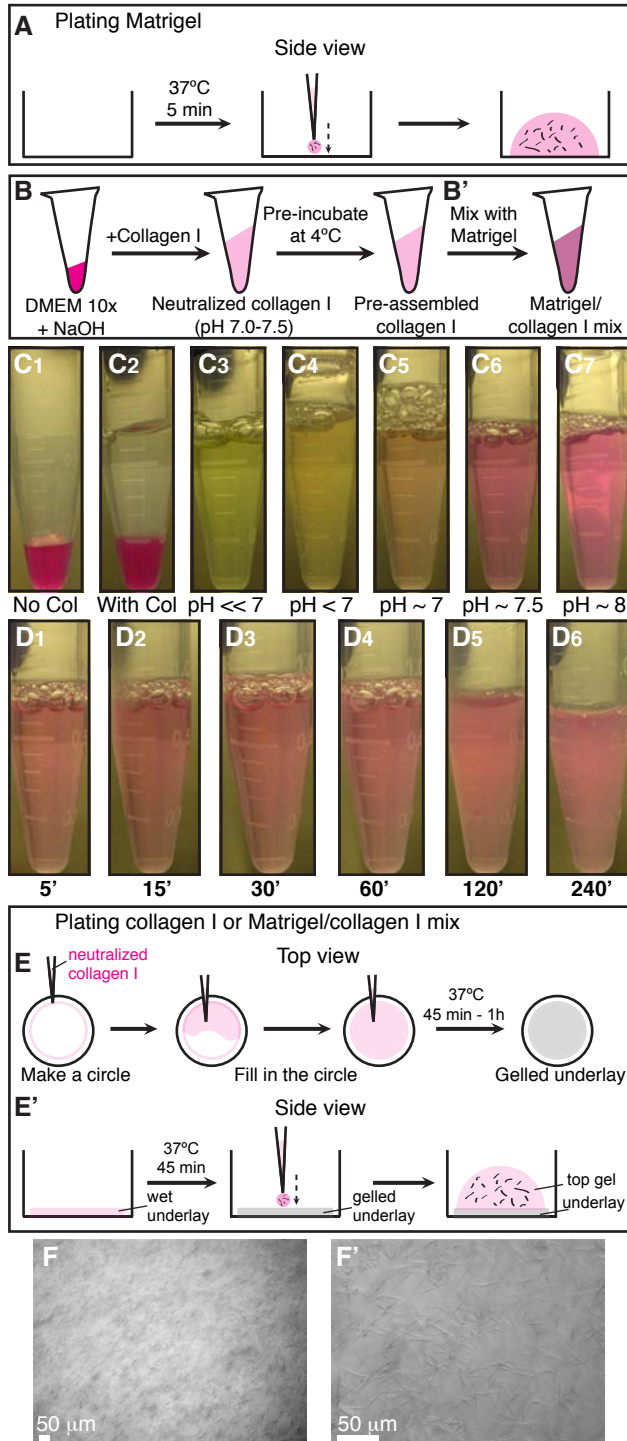


Figure 3-6

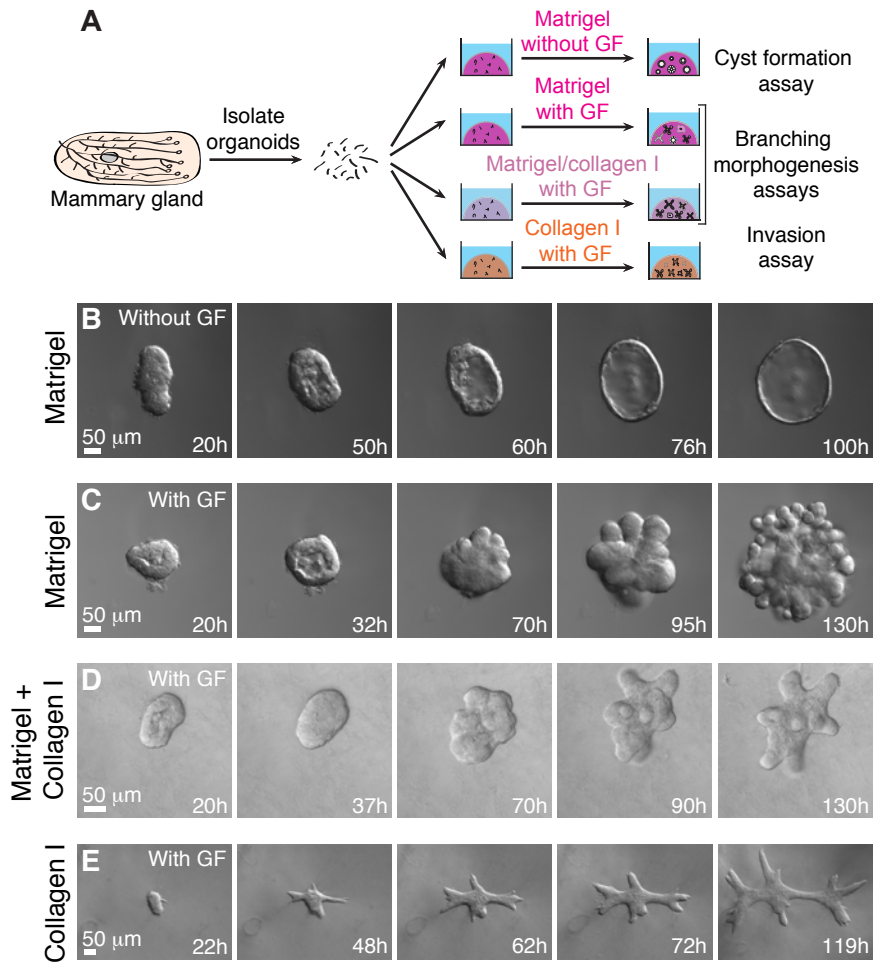
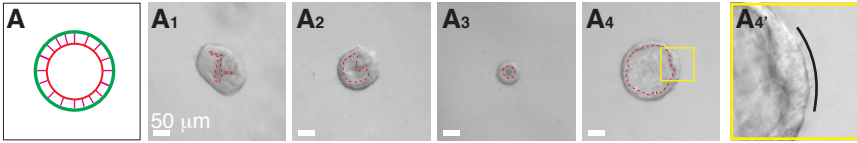


Figure 3-6. 3D organotypic culture assays. (A) Schematic description of four assays that use different extracellular matrix compositions to model specific epithelial behaviors. (B-E) Representative frames of DIC time-lapse movies showing cyst formation in Matrigel in basal medium (B), branching morphogenesis in Matrigel induced by FGF2 (C), branching morphogenesis in a mixture of Matrigel and collagen I induced by FGF2 (D), and epithelial cell invasion into pure collagen I induced by FGF2 (E).

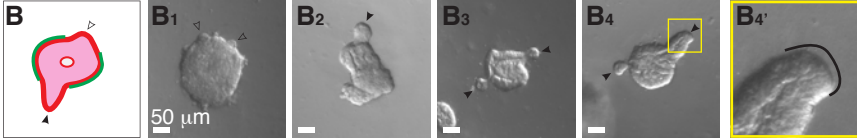
Figure 3-7. Phenotypic variability in assay outcomes. (A) Schematic description of a cyst. (A₁-A₄) DIC images showing variation in cyst morphology. (A₄') An inset of (A₄) showing a smooth basal surface with Matrigel. (B) Schematic description of a stratified, unbranched organoid. (B₁-B₄) DIC images showing examples of stratified, unbranched organoids in Matrigel. (B₄') An inset of (B₄) showing a smooth basal surface with Matrigel. (C) Schematic description of a branched organoid in Matrigel. (C₁-C₄) DIC images showing variation in branching morphology. (C₄') An inset of (C₄) showing a smooth basal surface with Matrigel. (D) Schematic description of a branched organoid in a mixture of Matrigel and collagen I. (D₁-D₄) DIC images showing variation in branching morphology. (D₄') An inset of (D₄) showing a smooth basal surface with the mixed matrix. (E) Schematic description of an organoid with protrusive tips in collagen I. (E₁-E₄) DIC images showing variation in protrusive invasion. (E₄') An inset of (E₄) showing protrusive tips into collagen I. (F) DIC images showing commonly observed technical issues. (F₁-F₂) Organoids lose their 3D organization in Matrigel (F₁) and collagen I gels (F₂) when they make contact with the cover glass. (F₃) Non-epithelial species (red arrowheads) attached to organoids may appear elongated and mesenchymal (ECM: Matrigel). (F₄) A group of dead cells beside a branching organoid (ECM: collagen I). (F₅) A cluster of elongated, non-epithelial cells (ECM: Matrigel). (F₆) A nerve bundle disseminating single cells into the surrounding matrix (ECM: Matrigel).

Figure 3-7

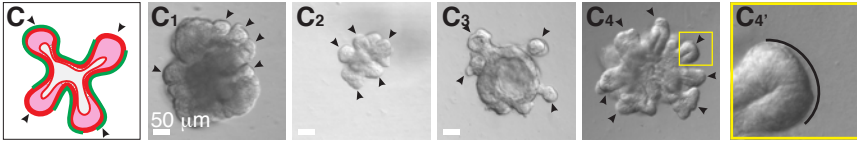
Matrigel, without GF: Variation in cyst morphology



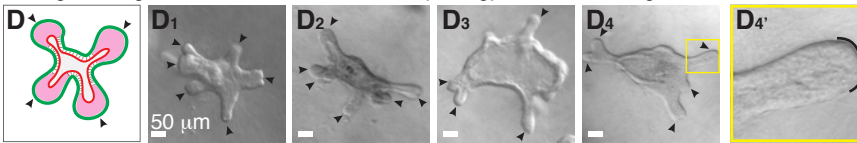
Matrigel, with GF: Stratified, but not branched organoids



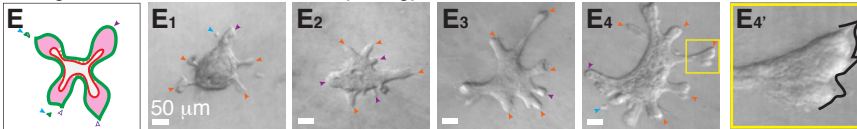
Matrigel, with GF: Variation in morphology of branched organoids



Matrigel/collagen I, with GF: Variation in morphology of branched organoids



Collagen I, with GF: Variation in morphology of multicellular invasive structures



Myoepithelial cell ▷ unscored buds ▶ scored buds
 Luminal epithelial cell ▶ protrusive tip ▶ round tip ▶ disseminated cell

Technical issues

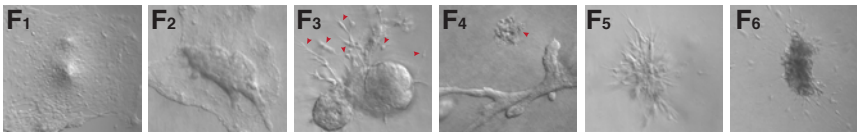


Figure 3-8

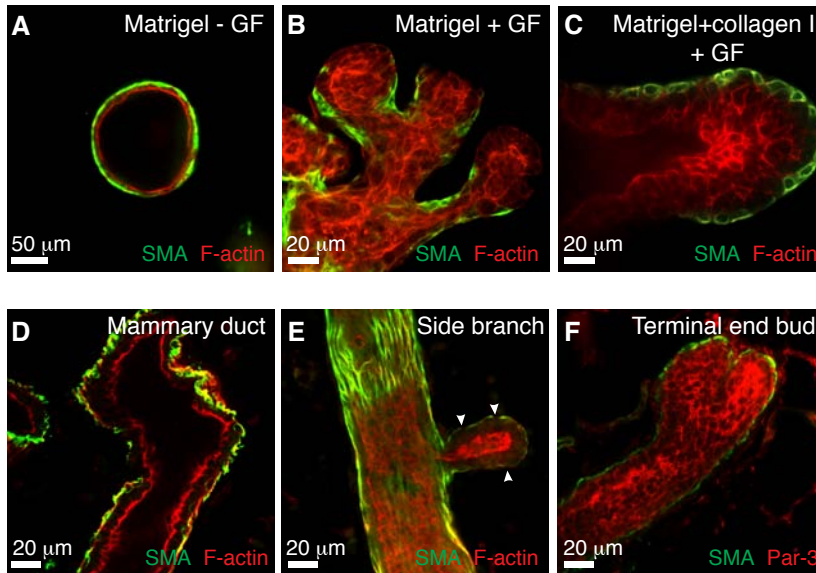


Figure 3-8. Correlation between epithelial morphologies in 3D organotypic assays and in vivo. (A-C) Representative confocal images of a cyst in Matrigel (A), branched buds in Matrigel (B), and a stratified, elongating bud in a mixture of Matrigel and collagen I (C). (D-F) Representative confocal images from mammary gland tissue sections of a bilayered duct (D), a side branch (E), and a terminal end bud (F).

CHAPTER 4

Twist1-induced dissemination preserves epithelial identity
and requires E-cadherin

(Modified from Shamir et al., *J Cell Biol* 2014)

Abstract

Dissemination of epithelial cells is a critical step in metastatic spread. Molecular models of dissemination focus on loss of E-cadherin or repression of cell adhesion through an epithelial to mesenchymal transition (EMT). We sought to define the minimum molecular events necessary to induce dissemination of cells out of primary murine mammary epithelium. Deletion of *E-cadherin* disrupted epithelial architecture and morphogenesis but only rarely resulted in dissemination. In contrast, expression of the EMT transcription factor *Twist1* induced rapid dissemination of cytokeratin-positive epithelial cells. *Twist1* induced dramatic transcriptional changes in extracellular compartment and cell-matrix adhesion genes but not in cell-cell adhesion genes. Surprisingly, we observed disseminating cells with membrane-localized E-cadherin and β -catenin, and *E-cadherin* knockdown strongly inhibited *Twist1*-induced single cell dissemination. Dissemination can therefore occur with retention of epithelial cell identity. The spread of cancer cells during metastasis could similarly involve activation of an epithelial motility program without requiring a transition from epithelial to mesenchymal character.

Introduction

Metastasis is the primary cause of death in breast cancer, and patient outcomes correlate negatively with the extent of metastatic spread at diagnosis^{1,2}. Metastasis initiates with dissemination, the escape of epithelial cancer cells from the primary tumor into the surrounding stroma³. As dissemination requires loss of epithelial cell-cell junctions, a change in the expression of intercellular adhesion genes could be the initiating event^{4,5}. Two related molecular models for dissemination have been proposed on this basis: genomic loss of cell adhesion genes^{1,6,7} and repression of cell adhesion genes through an epithelial to mesenchymal transition (EMT)^{8,9}.

These molecular models converge on the cell adhesion gene *E-cadherin* (*E-cad*, *Cdh1*). *E-cad* is essential for early embryonic development¹⁰; *E-cad* expression is frequently lost in human breast cancer¹¹; and *E-cad* loss in experimental cancer models accelerates metastatic progression^{12,13}. However, a gap exists in our understanding of the relationship between the normal role of *E-cad* in adult tissues and its function during cancer metastasis. Analyses of *E-cad*'s requirement in adult epithelial tissues using Cre-mediated deletion¹⁴ have revealed highly varied *E-cad* null phenotypes. Conditional *E-cad* deletion in the mammary gland results in cell death during lactation¹⁴, while conditional *E-cad* deletion in the skin results in hyperproliferation of some cell types and premature degeneration of others¹⁵. *E-cad* deletion in these developmental contexts is not associated with systemic dissemination. Nevertheless, transcriptional repression of *E-cad* by EMT transcription factors such as Twist1 remains a central concept in cancer metastasis^{8,9}. Twist1 regulates metastasis in a mouse mammary tumor model¹⁶, and its expression is upregulated in both invasive lobular and invasive ductal breast cancer^{16,17}.

Collectively, prior publications have demonstrated that E-cad functions as an invasion suppressor and that induction of EMT transcription factors can accelerate malignant progression^{1,5,6,8,12,18}. However, human breast tumors typically contain thousands of mutations in both signaling and structural genes^{19,20}. These co-existing mutations obscure the contribution of individual genetic events to discrete steps in the metastatic cascade. Specifically, the presence of additional mutations in cancer cell lines has made it difficult to distinguish the individual sufficiency of *E-cad* deletion or *Twist1* expression for dissemination. Importantly, dissemination can be induced in developmental contexts such as neural crest migration, suggesting that its molecular regulation may be distinct from other aspects of neoplasia²¹.

We sought to define the minimum molecular perturbations necessary to induce dissemination of normal mammary epithelial cells. To accomplish these goals, we utilized a combination of organotypic culture, Cre-lox based genetic models, inducible expression systems, lentiviral gene knockdown, and time-lapse imaging to test the sufficiency of *E-cad* deletion or *Twist1* expression to induce dissemination in primary mammary epithelium. Our results demonstrate that E-cad is required for simple epithelial architecture and branching morphogenesis, but its loss is not associated with significant dissemination in 3D culture or in vivo. In contrast, *Twist1* expression induces rapid epithelial dissemination. Moreover, *Twist1*-induced dissemination occurs without loss of epithelial gene expression and requires E-cad.

Results

E-cad is required for simple mammary epithelial architecture

We first assayed the acute consequences of *E-cad* deletion in primary mammary epithelial cells using the “organoid” assay, in which mammary ducts are explanted into 3D extracellular matrix (ECM; Matrigel)²² (Fig. 4-1A). In basal medium without growth factors, normal organoids form polarized cysts²² (Fig. 4-1A,B). We isolated organoids from mice carrying floxed *E-cad* alleles¹⁴ and a ubiquitously-expressed, tamoxifen-inducible Cre recombinase²³ (*Cre-ER;E-cad^{fl/fl}* mice). Organoids from the same mouse were divided into a control group and an experimental group in which *E-cad* deletion was induced with 50 nM tamoxifen.

Control organoids efficiently formed polarized cysts, with E-cad localized to lateral points of cell-cell contact and zona occludens 1 (ZO-1) localized in apical puncta (58.2%, Fig. 4-1B,D,E,E'). In contrast, E-cad⁻ organoids either failed to establish simple epithelial architecture (66%) or transiently established and then lost simple epithelial architecture (33%) (Fig. 4-1C,D). E-cad⁻ organoids had a multilayered organization and lacked morphologically evident lumens (Fig. 4-1E,F). Interestingly, a subset of lateral cell-cell contact surfaces within E-cad⁻ organoids had continuous ZO-1 staining (Fig. 4-1F,F'). Immunofluorescence (Fig. 4-1F) and western blotting (Fig. 4-1G) confirmed loss of E-cad protein by day 6 in culture. E-cad loss coincided with a reduction in α E-catenin and β -catenin (Fig. 4-1G) but not with a significant change in N-cadherin (N-cad) (Fig. 4-2A,B). By immunofluorescence, α E-catenin was absent from most internal cell-cell contact surfaces (Fig. 4-2C-C'').

E-cad⁻ cells are excluded from regions of simple epithelial organization but rarely

disseminate

We next used time-lapse microscopy to observe the cell dynamics driving loss of simple organization following *E-cad* deletion. We monitored recombined cells using the genetically encoded Cre biosensor *mT/mG*²⁴. Without Cre activity, all cells in *mT/mG* mice express a membrane-localized red fluorescent protein. Cre activity excises the red gene and induces heritable expression of a membrane-localized green fluorescent protein. We could thereby distinguish in real-time the behaviors of E-cad⁺ (red) versus E-cad⁻ (green) cells. Loss of simple epithelial architecture in E-cad⁻ organoids correlated with a reduction in luminal volume (Fig. 4-1H), consistent with a loss of tight junctions. This tissue-level change was accompanied by a change in E-cad⁻ cell shape from simple columnar to round (Fig. 4-1H',H''). Round cells shifted internally, inducing a transition from a single to multiple luminal epithelial cell layers (arrowheads in Fig. 4-1H',H'').

We next monitored whether *E-cad* deletion was sufficient to induce dissemination into the ECM. Normal epithelial cysts maintain a smooth basal surface with the ECM (Fig. 4-3A). Conversely, E-cad⁻ cells accumulated on the basal surface and collectively migrated into Matrigel as single file columns (Fig. 4-3B,B',G,G') and as disorganized masses (Fig. 4-3E,E',F,F'). Single file migration initiated from basally positioned E-cad⁻ cells that rounded up but maintained cell-cell contact (Fig. 4-3C). As additional cells changed shape, the initiating cell migrated further into the ECM and led a column of closely connected E-cad⁻ cells. However, despite contact with the ECM and high motility, E-cad⁻ cells rarely disseminated into the matrix. Each organoid consists of 300-500 cells; yet, on average, only one cell disseminated from each E-cad⁻ organoid (n=206 organoids imaged by time-lapse across 9 biologically independent replicates). Most E-cad⁻ cells remained adherent to other epithelial cells. The few E-cad⁻ cells that did disseminate were rounded, migrated minimally, and had no detectable membrane

protrusions.

E-cad⁻ cells remain adherent despite reductions in multiple classes of intercellular junctions

To analyze the effects of mosaic E-cad loss, we utilized adenovirally delivered Cre (Adeno-Cre) to induce *E-cad* deletion in a subset of cells within *E-cad^{fl/fl};mT/mG* organoids (Fig. 4-3D). We confirmed that green, Cre⁺ cells stained negative for E-cad protein (Fig. 4-3E,E') and that loss of E-cad was accompanied by loss of β -catenin from the membrane (Fig. 4-3F,F'). In these genetic mosaic organoids, E-cad⁻ cells were observed both basally at the cell-ECM interface and in interior positions apical to polarized E-cad⁺ cells (Fig. 4-3D-F). The basally positioned E-cad⁻ cells were frequently observed past the cell-derived basement membrane (laminin 332 immunofluorescence, Fig. 4-3G,G'). E-cad⁺ cells within the same organoid localized β -catenin to points of cell-cell contact and were inside the basement membrane (Fig. 4-3E-G).

We next sought to identify adhesion systems that could allow epithelial cells to remain adherent despite loss of E-cad and membrane-localized β -catenin. Desmosomes represent a major class of intercellular junctions in mammary epithelial cells²⁵. However, E-cad inhibition can induce reductions in both desmosomes and tight junctions²⁶. We therefore utilized transmission electron microscopy (TEM) to quantify the effect of E-cad loss on intercellular junctions in organoids from *E-cad^{fl/fl}* and *E-cad^{fl/+}* littermates. We induced recombination with Adeno-Cre and focused our analysis on basally positioned cells (Fig. 4-3H). E-cad⁻ cells typically lacked both punctate ZO-1 immunoreactivity (Fig. 4-1F) and ultrastructurally identifiable tight junctions. Compared to normal, E-cad⁺ epithelium, E-cad⁻ epithelium also had a statistically significant, almost 8-fold reduction

in desmosomes (Fig. 4-3I). However, we still detected small desmosomes connecting E-cad⁻ cells, even within single file migration columns (Fig. 4-3J,J'). Taken together, our data reveal that loss of E-cad results in loss of simple epithelial architecture, reductions in multiple classes of cell-cell junctions, and both apical and basal exclusion of E-cad⁻ cells from E-cad⁺ simple epithelium. However, E-cad loss was not sufficient for robust single cell dissemination into the 3D ECM.

E-cad is required for branching morphogenesis in 3D culture

Normal mammary branching morphogenesis begins with a transition from simple to multilayered architecture and a concurrent reduction in apico-basal polarity and intercellular junctions^{22,27}. Therefore, it was plausible that E-cad⁻ cells could participate in branching morphogenesis. We thus assayed the effects of *E-cad* deletion under culture conditions that utilize FGF2 to induce branching morphogenesis (²² and Fig. 4-4A).

We first induced *E-cad* deletion in most epithelial cells using Adeno-Cre and monitored effects on branching by time-lapse microscopy. Control, E-cad⁺ organoids underwent normal branching morphogenesis (Fig. 4-4B). Specifically, they initiated and elongated numerous mammary buds and maintained a smooth border with the ECM. In contrast, E-cad⁻ organoids did not undergo branching morphogenesis and instead rapidly developed a disorganized and uneven basal epithelial surface (Fig. 4-4C,D). Cells at the basal ECM border were rounded and displayed extensive, uncoordinated motility (Fig. 4-4C'). These cells were Cre biosensor⁺ (green) and E-cad⁻ by immunofluorescence (Fig. 4-4E,E') and lacked β -catenin at points of cell-cell contact (Fig. 4-4F,F').

We next induced genetic mosaic *E-cad* deletion and observed some normal, smooth epithelial buds emerging from disorganized cell surfaces. We hypothesized that these

buds were composed of E-cad⁺ cells that had escaped recombination (Fig. 4-4G). Consistent with this model, we observed groups of red, E-cad⁺ cells coalesce and initiate new buds from within large disorganized groups of green, E-cad⁻ cells (Fig. 4-4H,H'). Our data demonstrate that E-cad⁻ cells remain motile and adherent but fail to incorporate into epithelial buds. Furthermore, in genetic mosaic mixtures, E-cad⁺ cells can initiate buds from predominantly E-cad⁻ organoids (Fig. 4-4G,H).

E-cad⁻ cells are excluded from polarized ducts and the body cell compartment of the terminal end bud in vivo

Our genetic mosaic analysis in 3D culture revealed that E-cad⁻ cells lost simple epithelial architecture and most intercellular junctions but remained adherent to each other. However, the presence of E-cad⁻ cells in an organoid did not prevent the initiation of E-cad⁺ epithelial buds. Accordingly, we predicted that, in vivo, genetic mosaic *E-cad* deletion would result in exclusion of E-cad⁻ cells from regions of active branching morphogenesis and accumulation of disorganized E-cad⁻ cell groups both apically and basally. To test this prediction, we isolated organoids from control, *E-cad*^{+/+}; *mT/mG* mice and from *E-cad*^{fl/fl}; *mT/mG* mice, induced mosaic recombination with Adeno-Cre, and transplanted the organoids into contralateral, cleared mammary fat pads of 3-week-old NOD/SCID mice (Fig. 4-5A,D, respectively). Glands were harvested and analyzed 6 weeks post-transplantation.

Mammary ducts during puberty are elongated by specialized epithelial structures known as terminal end buds (TEBs)²⁸. TEBs are composed of a single, basally positioned layer of cap cells and multiple, apically positioned body cell layers²⁹. Cap cells give rise to myoepithelial lineages while body cells give rise to luminal epithelial lineages. Only body cells express *E-cad*³⁰. Ductal outgrowths from control, genetic mosaic *mT/mG*

transplants had both red and green cells in the body and cap cell regions of the TEB (Fig. 4-5B,B') and in the luminal and myoepithelial cell layers of polarized ducts (Fig. 4-5C,C'). In contrast, outgrowths from genetic mosaic *E-cad^{fl/fl};mT/mG* transplants displayed a striking exclusion of E-cad⁻ cells from the body cell region of the TEB (Fig. 4-5E,E') and from the luminal layer of ducts (Fig. 4-5F,F'). Myoepithelial cells were red and green in *E-cad^{fl/fl};mT/mG* genetic mosaic outgrowths (Fig. 4E', green arrowheads), but myoepithelial cells express *P-cadherin* instead of *E-cad*³⁰.

Despite their exclusion from polarized ducts and body cells, E-cad⁻ cells were observed in vivo at 6 weeks post-transplantation. Groups of E-cad⁻ cells were detected on the basal surfaces of polarized E-cad⁺ ducts in the gland periphery (Fig. 4-5F,F') and on the basal surfaces of polarized E-cad⁺ epithelium near the transplantation site (Fig. 4-5G,G'). We also observed small clusters of exclusively E-cad⁻ cells, surrounded by myoepithelial cells (smooth muscle actin⁺ (SMA)) (Fig. 4-5H,H'). Consistent with our 3D culture data, green, Cre⁺ cells in vivo were validated by antibody staining to lack membrane-localized E-cad (Fig. 4-2D-F) and β -catenin (Fig. 4-2G).

We next tested the in vivo consequences of *E-cad* deletion in polarized mammary epithelium. We isolated and transplanted organoids from *Cre-ER;E-cad^{fl/fl};mT/mG* mice into cleared mammary fat pads, waited 6 weeks for mature ductal outgrowths, and induced *E-cad* deletion by tamoxifen injection (Fig. 4-5I). Glands were harvested and analyzed 2-6 weeks post-tamoxifen injection. E-cad⁻ cells (by immunofluorescence) were observed apically inside duct lumens (Fig. 4-5J,J') and basally as single cells or disorganized groups on duct surfaces (Fig. 4-5J,J''). Basally positioned E-cad⁻ cells were typically still surrounded by myoepithelial cells.

We conclude that E-cad is required in mammary epithelial cells to establish and maintain simple epithelial architecture and to initiate and elongate new buds, both in 3D culture and in vivo. E-cad⁻ cells are viable in both contexts but extrude apically and basally from polarized epithelium and fail to contribute to mammary branching morphogenesis in the luminal cell compartment.

Twist1 induces robust cell dissemination of otherwise normal primary epithelial cells

Our data reveal that E-cad loss is not sufficient for robust cell dissemination in 3D culture or in vivo. This conclusion has implications for our conceptual understanding of EMT, as repression of *E-cad* is considered a core effector of EMT^{9,16,31,32}. The bHLH transcription factor Twist1 has emerged as a candidate regulator of EMT in cancer and is thought to act through regulation of *E-cad*^{8,16,31}. We sought to test the hypothesis that acute expression of *Twist1* would induce epithelial dissemination.

We isolated organoids from mice carrying a ubiquitously expressed reverse tetracycline transactivator (rtTA) and a Tet-responsive *Twist1* allele (Fig. 4-6A, *CMV::rtTA;TRE-Twist1*)³³. In basal medium, control organoids maintained a smooth basal surface (Fig. 4-6B). In contrast, *Twist1* expression induced rapid dissemination of protrusive, individual cells out of the epithelium as early as 24 h following *Twist1* induction (Fig. 4-6C,C'). We next tested the relationship between branching morphogenesis and dissemination. In FGF2-containing medium, control organoids branched efficiently (Fig. 4-6D). In contrast, *Twist1* expression inhibited FGF2-induced branching morphogenesis in 99% of organoids and induced robust dissemination in 97% of organoids (Fig. 4-6D-F). In the presence of FGF2, disseminated cells proliferated to form secondary epithelial sites within the ECM (Fig. 4-6E'). Immunofluorescent staining for cell type-specific

cytokeratins revealed that both luminal epithelial (K8⁺) and myoepithelial (K14⁺) cells disseminated in response to *Twist1* induction (Fig. 4-6G). Interestingly, both cells within the epithelial structure and disseminated cells displayed nuclear Twist1 immunoreactivity (Fig. 4-6H,H'). The Twist1⁺ epithelial group displayed abnormal internal localization of myoepithelial cells (SMA⁺) and basement membrane (laminin 332) and corresponding gaps in basal myoepithelial and basement membrane coverage (Fig. 4-6I).

Epithelial cell behaviors are restored when *Twist1* expression is turned off

We next tested the consequences of transient expression of *Twist1*. We induced *Twist1* for 48 h and then turned off *Twist1* by removing doxycycline (Fig. 4-7A). In basal medium, disseminated single cells stopped migrating within 48 h of doxycycline removal (Fig. 4-7B,B'). In FGF2-containing medium, organoids initiated branching morphogenesis within 70 h of doxycycline removal (Fig. 4-7C,D), and disseminated single cells were observed to reintegrate with the epithelial group (Fig. 4-7E). Remarkably, by day 7, the resulting branched structures had normalized epithelial organization, with internal luminal cells and basally positioned myoepithelial cells (Fig. 4-7F). We conclude that epithelial cells can rapidly re-establish normal developmental programs, such as branching morphogenesis, when *Twist1* expression ceases.

Twist1-induced dissemination is cell autonomous

We demonstrated that ubiquitous *Twist1* activation induced rapid epithelial dissemination. We next sought to test whether a single Twist1⁺ cell could escape a mostly Twist1⁻ epithelium. We reasoned that Twist1⁻ cells could serve as a barrier to dissemination. Alternatively, Twist1⁺ cells could induce the dissemination of neighboring Twist1⁻ cells. To achieve mosaic activation of *Twist1*, we utilized a *Lox-Stop-Lox-rtTA* (*R26::LSL-rtTA*³⁴) and varying titers of Adeno-Cre to modulate the fraction of cells

capable of activating *Twist1*. We again used the *mT/mG* reporter²⁴ to distinguish between Cre⁺rtTA⁺ cells (green) and Cre⁻rtTA⁻ cells (red). We monitored the resulting genetic mosaic tissue for dissemination in our branching morphogenesis assay (Fig. 4-8A).

Without doxycycline or *Twist1* induction, organoids formed branched structures with a mix of red and green cells (Fig. 4-8B). Conversely, *Twist1* induction resulted in dissemination of green (Cre⁺rtTA⁺Twist1⁺) cells across a wide range of viral titers, even in organoids in which most cells were Cre⁻rtTA⁻Twist1⁻ (Fig. 4-8C,D). Epithelium that was mostly Twist1⁻ had a high frequency of branching morphogenesis despite the dissemination of Twist1⁺ cells (Fig. 4-8E). As the fraction of rtTA⁺Twist1⁺ cells per organoid increased, we observed a decrease in the percentage of branching organoids (Fig. 4-8E), consistent with the branching inhibition observed in epithelium with constitutive *Twist1* expression (Fig. 4-6F). We never observed dissemination of red, rtTA⁻ cells, indicating that Twist1-induced dissemination is cell autonomous.

Twist1 is sufficient to induce local dissemination in vivo

Our 3D culture data predicted that Twist1 would induce epithelial dissemination in vivo. To test this prediction, we transplanted genetic mosaic organoids containing a mixture of red, Twist1⁻ and green, Twist1⁺ cells into cleared mammary fat pads of 3-week-old NOD/SCID mice (Fig. 4-8F). *Twist1* was induced in culture and maintained in vivo using doxycycline feed. Consistent with our 3D culture data, we observed local dissemination of green, Twist1⁺ cells into the surrounding stroma (Fig. 4-8G-G’). We did not detect dissemination of red, Twist1⁻ cells. Importantly, we observed groups of 10-20 green, Twist1⁺ epithelial cells in the stroma (Fig. 4-8H,H’). We hypothesize that these groups represent secondary epithelial sites formed from disseminated Twist1⁺ cells. We

conclude that *Twist1* expression is sufficient for epithelial dissemination in 3D culture and in vivo.

Twist1 induces dissemination without complete loss of adherens junction components

Our genetic analyses revealed that loss of E-cad and expression of *Twist1* induced distinct cell behaviors and tissue-level phenotypes. *E-cad* deletion resulted in loss of polarized epithelial architecture, while *Twist1* expression induced dissemination of luminal and myoepithelial cells (Fig. 4-9A-G). We next used immunoblotting to compare levels of cell-cell adhesion proteins between normal (–Dox) and *Twist1*-expressing (+Dox) tissue. We observed significant reductions in E-cad, α E-catenin, β -catenin, and N-cad (Fig. 4-9H, 4-10A,B) but detected protein in all cases. This reduction in N-cad is inconsistent with a cadherin switch model in which increases in N-cad levels induce migration³⁵. We next used immunofluorescence to localize E-cad and β -catenin during dissemination. Consistent with our western blot results, E-cad staining appeared weaker in cells expressing *Twist1*. However, we observed E-cad and β -catenin localized at points of cell-cell contact in cells prior to dissemination (Fig. 4-9I,L); E-cad and β -catenin localized to the rear of recently disseminated cells (Fig. 4-9J,M); and E-cad and β -catenin localized to the membranes of cells migrating in the ECM (Fig. 4-9K,N). We also observed E-cad[–] cells in the matrix, consistent with the dissemination of K14⁺ myoepithelial cells, which would not normally express E-cad. We conclude that *Twist1* can induce dissemination of cells with membrane-localized adherens junction proteins.

Twist1 induces transcriptional changes in cell-matrix adhesion but does not fundamentally alter epithelial identity

We next sought to identify the early transcriptional changes downstream of *Twist1*. We isolated organoids from three *CMV::rtTA;TRE-Twist1* mice and three *rtTA*⁻ littermate controls (*TRE-Twist1*), cultured these organoids for 24 h in basal medium, added doxycycline for 48 h, and then extracted RNA during active dissemination (Fig. 4-11A). RNA-seq analysis identified 183 genes that were differentially expressed (DE) between control and *Twist1*-expressing tissue at genome-wide significance ($p=2.7\times 10^{-6}$).

Surprisingly, none of the canonical EMT genes were significantly differentially expressed at the RNA level, including *E-cad* ($p=0.35$). However, both *Snai1* ($p=3.2\times 10^{-6}$) and *Fn1* ($p=4.6\times 10^{-6}$) were close to genome-wide significance (Fig. 4-11B). We next analyzed the expression of 127 genes involved in cell-cell adhesion and intercellular junctions. Of these genes, only 5 were differentially expressed (*Celsr1*, *Cldn2*, *Fat4*, *Frem2*, and *Pcdh18*). No classical cadherins, desmosomal cadherins, catenins, or cytokeratins were significantly dysregulated at the RNA level. We conclude that *Twist1* induces dissemination without loss of epithelial identity. This observation is consistent with the positive immunoreactivity for cytokeratin, E-cad, and β -catenin protein in disseminated cells.

We next analyzed Gene Ontology (GO) Slim annotations to characterize biological process (Fig. 4-11C), cellular component (Fig. 4-11E), and molecular function terms (Fig. 4-13A) associated with our 183 DE genes³⁶. Relevant GO biological processes with several DE genes included cell adhesion (Fig. 4-11D), transport (Fig. 4-12A), cell differentiation (Fig. 4-12B), lipid metabolic process (Fig. 4-12C), and signal transduction (Fig. 4-12D). Of these, the cell adhesion, cell differentiation, and ECM organization GO categories were statistically significantly enriched for DE genes relative to genes overall. Importantly, the DE cell adhesion genes were primarily associated with cell-substrate,

not cell-cell, adhesion and with cell migration, cell projections, and ECM organization (Fig. 4-11D). We observed significantly more DE genes than expected in GO cellular component categories for extracellular region, extracellular space, and proteinaceous ECM (Fig. 4-11F). DE genes were also associated with the cytoplasm (Fig. 4-12E), plasma membrane (Fig. 4-12F), and nucleus.

To complement the GO analysis of DE genes at genome-wide significance, we also performed a more general test of differential expression. Because we observed discordant expression changes within pathways, we employed a joint test of upregulation and downregulation by calculating the absolute value of the z-score for differential expression of each gene, followed by a *t* test for genes within versus outside each pathway. Gene sets from pathway databases (canonical pathways) were augmented to include gene lists from the literature (curated pathways). We found 8 significant canonical pathways, all related to the cell interface with the extracellular space: focal adhesion, integrins, axon guidance, collagen formation, ECM-receptor interactions, and ECM organization (Fig. 4-14A). We found 51 significant curated gene sets, 13 of which we characterized as cancer-related (Fig. 4-14B). Out of 183 DE genes, 33 were associated with at least 3 cancer-related gene sets (Fig. 4-14B). We conclude that our data identify a novel set of genes regulated by Twist1 during dissemination that collectively reprogram the extracellular environment and cell interactions with the ECM. Importantly, some of the DE genes have enzymatic activity, are upregulated in human cancers, and may represent novel targets for inhibiting dissemination (Fig. 4-14B, 4-13B).

E-cad loss blocks single cell dissemination of Twist1⁺ cells

We observed that Twist1 induced dissemination of cells with membrane-localized E-cad

and β -catenin and that Twist1 did not affect E-cad RNA levels. It was therefore possible that E-cad was contributing to Twist1-induced dissemination. Accordingly, we tested whether *E-cad* knockdown (KD) would inhibit single cell dissemination. We used lentiviral shRNA and puromycin selection to knock down *Luciferase (Luc)* or *E-cad* in *CMV::rtTA;TRE-Twist1* organoids isolated from the same mouse (Fig. 4-15A). We confirmed E-cad loss by immunoblotting (Fig. 4-15B) and used *Luc* KD organoids as a negative control. Consistent with our *E-cad* deletion experiments, we observed a tandem reduction in α E-catenin and β -catenin.

We next used time-lapse microscopy to quantify dissemination following *Twist1* induction in *Luc* KD and *E-cad* KD organoids. Surprisingly, *E-cad* knockdown resulted in a strong inhibition of single cell dissemination (Fig. 4-15C-F). Many *Twist1*-induced, *Ecad* KD organoids had no detectable disseminated cells (Fig. 4-15E). Instead, concurrent *Twist1* expression and *E-cad* knockdown induced migration of long chains of cells into the ECM (Fig. 4-15G-G''). *Twist1*-induced, *Ecad* KD cells retained nuclear Twist1⁺ protein (Fig. 4-15H,H'), were cytokeratin⁺ (Fig. 4-15I,I'), and were organized in collective groups (Fig. 4-15H-I'). We conclude that Twist1 requires E-cad for efficient single cell dissemination.

Discussion

Our goal was to define the molecular requirements for dissemination of primary, normal epithelial cells. We utilized genetic techniques to contrast deletion of the cell adhesion gene *E-cad* with expression of the EMT transcription factor *Twist1*. We focused on *E-cad* as it is frequently mutated in human cancer^{6,11}, and loss of E-cad can synergize with loss of p53 to promote metastasis¹². In our experiments, *E-cad* deletion throughout the mammary epithelium resulted in loss of most intercellular junctions, loss of simple epithelial architecture, and inhibition of branching morphogenesis. However, E-cad⁺ cells within genetic mosaic epithelium were able to initiate and elongate normal mammary buds in 3D culture and in vivo. The associated E-cad⁻ cells were viable and remained adherent to each other but did not contribute to polarized luminal ducts. Therefore, mammary epithelial cells must be able to maintain contact through alternate adhesion systems such as desmosomal cadherins or protocadherins. We conclude that E-cad is required for normal mammary development but that its loss alone is not sufficient for robust dissemination.

We next evaluated the consequences of *Twist1* expression as *Twist1* can regulate multiple aspects of metastasis and is thought to function primarily through *E-cad* repression^{9,16,33,37,38}. Our data reveal that *Twist1* expression is sufficient to induce normal epithelial cells to disseminate out of an epithelium, migrate through the ECM, and establish secondary epithelial sites. Surprisingly, the disseminating cells retained cytokeratin expression, and many displayed membrane-localized E-cad and β -catenin. Transcriptional profiling revealed essentially no changes in the RNA expression of epithelial-specific cadherins, catenins, or keratins. Instead, *Twist1* regulated many genes that mediate cell-matrix adhesion or modify the extracellular compartment. Since *Twist1*

regulates distinct targets depending on its bHLH dimer partner³⁹, it is likely that its regulated genes vary in different experiments. However, since our experimental induction of *Twist1* was sufficient to induce dissemination, our 183 differentially expressed genes are likely particularly important in regulating the transition from adherent to motile epithelial cell phenotypes.

The conceptual framework for EMT was developed in response to classic experiments by Elizabeth Hay in which definitive epithelial tissues lost polarity and disseminated as single cells into collagen I gels^{40,41}. The appearance of these cells was most similar to that of embryonic mesenchymal cells, leading to the concept of an epithelial to mesenchymal transition. We are observing a similar migration of cells out of an epithelial tissue and into the surrounding ECM. However, we do not observe a loss of epithelial-specific gene expression, and the migratory cells are readily able to re-establish epithelial organization, both spontaneously and following cessation of *Twist1* expression. Interestingly, we observed reductions in protein but not RNA levels of E-cad, β -catenin, and α E-catenin, suggesting post-translational regulation of adherens junction components following *Twist1* induction⁴². However, we demonstrated that complete knockdown of *E-cad* dramatically inhibited *Twist1*-induced single cell dissemination. We speculate that the exact protein levels of E-cad may critically regulate whether *Twist1* expression results in single cell dissemination or collective cell migration.

Accordingly, our data support the concept of a *Twist1*-dependent epithelial migratory program rather than a transition to mesenchymal cell fate or gene expression. Consistent with this framework, *Twist1* regulates genes important for interactions with the stromal ECM environment. Our concept of an epithelial migratory program also finds

support in breast cancer. Human breast tumors can express *E-cad* in both the primary tumor and in distant metastases⁴³, and primary breast tumor cells positive for the EMT transcription factor Slug can express high levels of E-cad⁴⁴.

Most cancer therapies target the increased proliferation of cancer cells relative to normal tissues and not the cell behaviors driving invasion, dissemination, and metastasis. Few of these drugs have proven clinical benefit in metastatic breast cancer patients⁴⁵. *Twist1* is overexpressed in multiple metastatic human cancers and appears to specifically regulate metastatic cell behaviors in multiple experimental cancer models^{16,33,37,46}. *Twist1* therefore represents an attractive conceptual target for developing anti-metastatic therapies. However, it is very difficult to target a transcription factor with small molecule therapeutics. Our observation that *Twist1* regulates many proteins in the extracellular compartment suggests that there may be essential, druggable effectors downstream of *Twist1* whose repression could inhibit dissemination. Our inducible mouse model revealed that disseminated single cells rapidly cease migration following loss of *Twist1* expression, suggesting that interfering with the *Twist1* program could be an effective anti-cancer strategy. We envision our *Twist1*-induced dissemination assay as a rapid, reproducible, and scalable platform to build a new molecular model for effectors of *Twist1* and to identify novel therapeutic compounds to antagonize cancer invasion and dissemination.

Materials and methods

Mouse strains. The *R26::Cre-ER* mouse line²³ was a kind gift of Jeremy Nathans (Johns Hopkins University, Baltimore, MD). The *CMV::rtTA* transgenic line was a kind gift of Feng Cong and Harold Varmus (National Cancer Institute, Bethesda, MD). The *Twist1-tetO₇-luc (TRE-Twist1)* transgenic line was previously described³³. *E-cad^{fl/fl14}*, *mT/mG²⁴*, and *R26::Lox-Stop-Lox-rtTA-IRES-EGFP (R26::LSL-rtTA)*³⁴ mouse lines were acquired from the Jackson Laboratory (Bar Harbor, ME). Mouse husbandry and procedures were all conducted under an IACUC-approved animal protocol.

Isolation and 3D culture of primary mammary epithelial organoids. We used mechanical disruption, collagenase/trypsin digestion, and differential centrifugation to purify fragments of primary mammary epithelial ducts, termed “organoids”, as previously described^{22,27,47}. Briefly, mammary glands were harvested from mice 8-12 weeks of age, minced with a scalpel, and shaken for 40 min at 37°C in collagenase solution: DMEM (10565-018; Gibco) with 2 mg/mL collagenase (C2139; Sigma), 2 mg/mL trypsin (27250-018; Gibco), 5% fetal bovine serum (F0926; Sigma), 5 µg/mL insulin (I9278; Sigma), and 50 µg/mL gentamicin (15750; Gibco). Suspensions were centrifuged at 1250 rcf to remove a floating layer of adipocytes, and pellets were treated with 2 U/µL DNase (D4263; Sigma) to detach organoids from stromal cells. Enzymes and single cells were removed by four quick spins at 1250 rcf such that the final pellet consisted mostly of organoids, each containing several hundred cells. Organoids were embedded in 3D Matrigel (354230; BD Biosciences) at 2-3 organoids/µL and plated as 100 µL suspensions in 24-well coverslip-bottomed plates (662892; Greiner Bio-One) over a 37°C heating block. Gels were allowed to polymerize for 30 min at 37°C and then cultured in organoid medium: DMEM with 1% Insulin-Transferrin-Selenium (51500-056;

GIBCO) and 1% Penicillin-Streptomycin (P4333; Sigma). Basal organoid medium was used to induce cyst formation while addition of 2.5 nM FGF2 (F0291; Sigma) was used to induce branching morphogenesis. Branching was scored as organoids with three or more elongated buds. Cysts were scored as unbranched organoids with lumens detectable by light microscopy. Dissemination was scored as organoids with one or more adjacent single cells that were clearly separated from the epithelial group.

Tamoxifen-inducible Cre-mediated deletion in 3D culture. Cre activity was induced in *Cre-ER;E-cad^{fl/fl};mT/mG* epithelium by culturing organoids overnight with 50 nM tamoxifen once embedded in Matrigel. To wash out tamoxifen, samples were rinsed with PBS, incubated in organoid medium for 20 min at 37°C, and then cultured in fresh organoid medium. The tamoxifen-inducible system resulted in Cre activity in almost all cells and did not affect branching morphogenesis in control organoids (for example, *Cre-ER;E-cad^{fl/+};mT/mG*).

Adenoviral delivery of Cre recombinase. Prior to embedding in Matrigel, mammary organoids were infected with Adeno-Cre (1045; Vector Biolabs) at a ratio of approximately 1×10^7 PFU per 1,000 organoids. Infections were conducted in 50 μ L of DMEM for 1-2 h at 37°C to yield recombination in 50-75% of cells. Percent recombination was raised by increasing viral titer or by overnight incubation with virus.

***Twist1* activation in 3D culture.** *Twist1* expression was induced in 3D Matrigel cultures by supplementing organoid medium with 5 μ g/mL doxycycline (Shanghai RenYoung Pharmaceutical Co., Ltd). Because doxycycline is labile, medium was replaced every 48 h. To turn *Twist1* expression off, doxycycline-containing medium was removed, and

samples were rinsed with sterile PBS. Samples were then incubated with organoid medium without doxycycline for 20 min at 37°C. This medium was then discarded, samples were rinsed again with PBS, and fresh organoid medium without doxycycline was added back.

Mammary fat pad transplantation. For transplantation of genetic mosaic E-cad or Twist1 tissue, we isolated organoids, induced recombination with Adeno-Cre, and washed organoids twice with 500 μ L of DMEM to remove viral particles. For all experiments, organoids were incubated at 37°C overnight in organoid medium with 2.5 nM FGF2 in Nunc HydroCell 96-well microplates (174907; Thermo Scientific). For *Twist1* experiments, organoid medium was supplemented with 5 μ g/mL doxycycline. The next day, organoids were resuspended in a 50% DMEM / 50% Matrigel solution at a density of 20-40 organoids/ μ L and stored on ice. We conducted orthotopic transplantation into 3-week-old NOD/SCID mice in a sterile hood. Briefly, mice were anesthetized with 2-2.5% isoflurane and immobilized, and the surgical site was cleaned with ethanol. A 1 cm incision was made at the midline and a 0.5 cm incision from the midline to one hip. The skin was retracted to expose the no. 4 mammary gland. The no. 5 mammary fat pad and the region of the no. 4 mammary fat pad proximal to the lymph node were removed. The organoid suspension was loaded into a Hamilton syringe (702RN (7636-01); custom 1" needles, 26 gauge), and 10-20 μ L were injected into the cleared no. 4 fat pad. The skin was then locally infiltrated with 5-10 μ L of 0.25% Bupivacaine. The same procedure was repeated for the contralateral mammary gland. For each mouse, we transplanted control organoids (e.g. *mT/mG*) in one gland and experimental organoids (*E-cad^{fl/fl};mT/mG*, *Cre-Er;Ecad^{fl/fl};mT/mG*, or *R26::LSL-rtTA;TRE-Twist1;mT/mG*) in the other. The surface of the peritoneum was wet with PBS (without Ca²⁺, Mg²⁺), and wounds were closed with 9

mm autoclips. Triple Antibiotic Ointment was applied to the incision site as needed. For *Twist1* experiments, IP injections of 100 μg of doxycycline in PBS (without Ca^{2+} , Mg^{2+}) were also performed at the time of surgery. *Twist1* activation in vivo was maintained with doxycycline feed (TD.01306, Harlan Laboratories). For deletion of *E-cad* in mature ductal networks, *Cre-ER;E-cad^{fl/fl};mT/mG* organoids were transplanted into NOD/SCID mice and allowed to grow for 6 weeks. To induce *E-cad* deletion, we injected tamoxifen IP every other day for 5 days (3 total injections) using a 1 mL syringe and a 30G1/2 needle (305106; BD). Each injection consisted of 100 μL of 10 mg/mL tamoxifen dissolved in sunflower seed oil. Glands were harvested 2-6 weeks post injection.

Differential interference contrast microscopy. Time-lapse imaging of mammary organoids was conducted using a Zeiss LD Plan-Neofluar 20X/0.4 Korr Ph2 objective lens and a Zeiss Cell Observer system with a Zeiss AxioObserver Z1 and an AxioCam MRM camera. In general, we recorded 100-200 positions in parallel for 5-7 days, with images acquired at 20-min intervals. Temperature was maintained at 37°C and CO_2 at 5%. AxioVision (Zeiss) was used to acquire and analyze time-lapse movies, place scale bars, and export individual TIFFs. Adobe Photoshop CS5 was used to adjust levels on entire images to maximize image clarity.

Confocal microscopy. Confocal imaging was performed on a Solamere Technology Group spinning-disk confocal microscope with an XR/MEGA-10 S30 camera (Standard Photonics, Inc.), as previously described^{48,49}. A Zeiss Fluor 20X/0.75 objective lens was used for intermediate magnification images. A Zeiss LD C-Apochromat 40X/1.1 W Korr objective lens was used for high magnification single and time-lapse image acquisition, with water and oil used as the imaging mediums, respectively. Acquisition of both fixed

and time-lapse images was performed using a combination of μ Manager⁵⁰ and Piper (Stanford Photonics, Inc.). For time-lapse imaging, images were collected at 20-min intervals for 2-4 days, and temperature was maintained at 37°C and CO₂ at 5%. Imaris (Bitplane) was used to analyze time-lapse movies, place scale bars, and export individual TIFFs. Adobe Photoshop CS5 was used as needed to adjust levels and gamma for each channel on entire images to maximize image clarity.

High-pressure freezing and freeze substitution processing. We isolated epithelium from *E-cad*^{fl/fl} and *E-cad*^{fl/+} littermates, induced recombination with Adeno-Cre, and cultured organoids for 5-7 days in Matrigel. Embedded organoids were then fixed in 3% glutaraldehyde to preserve for shipping to Lawrence Berkeley Labs (Berkeley, CA). There, samples were placed in 1 mm wide by 200 μ m deep aluminum freezing hats and, prior to freezing, were surrounded with 20% bovine serum albumin, here used as a cryo-protectant. Samples were then cryo-immobilized using a BAL-TEC HPM-010 high-pressure freezer (BAL-TEC, Inc., Carlsbad, CA) and freeze-substituted in 1% osmium tetroxide and 0.1% uranyl acetate in acetone with 5% DDH₂O, as previously described⁵¹. Upon completion of freeze-substitution, samples were progressively infiltrated with an Epon-Araldite resin⁵². Polymerization in Epon-Araldite resin was performed by flat-embedding between two glass slides to allow for precise localization of features of interest⁵³.

Transmission electron microscopy. Samples were sectioned into 70-100 nm thin and 500 nm thick sections using a Leica UC6 Ultramicrotome (Leica Microsystems, Wetzlar, Germany). Sections were then collected onto formvar-coated, rhodium-enforced copper 2 mm slot grids. The grids were post-stained with 2% uranyl acetate followed by

Reynold's lead citrate, 5 minutes each. The sections were imaged using a FEI Tecnai 12 TEM (FEI, Hillsboro, OR), operated between 690X and 11000X magnification at 120 kV under normal conditions. Images were recorded using an Orius SC1000B CCD with Digital Micrograph 3 software (Gatan Inc., Pleasanton, CA). Serial EM software was used to collect wide-field montages for overview TEM images of complete organoid cross sections⁵⁴. ImageJ software⁵⁵ and Adobe Photoshop CS4 were used to crop images, place scale bars, and adjust brightness and contrast on entire images, as needed.

Desmosome quantification. Desmosomes were counted among basally positioned cells in 5 *E-cad*^{fl/fl} organoids and 4 *E-cad*^{fl/+} organoids imaged by TEM. For each organoid, we selected 1-4 regions of 20-30 cells that were no more than 2 cells deep from the organoid-ECM interface. Regions were free of single file columns or epithelial buds. For desmosomes located between cells in the second and third layers deep to the surface, we counted the desmosome but not the third-layer cell. Adobe Photoshop CS4 was used to track the desmosomes and regions used for quantification.

Immunofluorescence. Organoids grown in 3D Matrigel were fixed in 4% paraformaldehyde for 10 min, rinsed three times in PBS for 10 min, embedded in Optimal Cutting Temperature compound (OCT), and frozen at -80°C. OCT blocks were sectioned at 50 µm thickness by cryostat at -20°C. Sections were placed on Superfrost® Plus Gold Microscope Slides (15-188-48; Fisherbrand) and stored at -80°C. For antibody staining, samples were thawed at room temperature, rinsed twice in PBS for 10 min to remove OCT, permeabilized with 0.5% Triton X-100 for 1 h, and rinsed twice in PBS for 10 min. Samples were blocked for 1-3 h with 10% FBS / 1% BSA, incubated with primary antibodies overnight at 4°C in 1% FBS / 1% BSA, and rinsed

three times in 1% FBS / 1% BSA for 15 min. Incubation with secondary antibodies was conducted in 1% FBS / 1% BSA overnight at 4°C or for 2 h at room temperature. Slides were rinsed three times in PBS for 10 min, mounted with Fluoromount (F4680; Sigma-Aldrich), and sealed with coverslips. F-Actin was stained with Alexa Fluor Phalloidin (1:100) (Invitrogen), and nuclei were stained with DAPI (1:1,000) (D3571; Invitrogen). Immunofluorescence staining for each antibody was performed at least three independent times for a minimum of 10-15 organoids. Primary antibodies used were rat anti-E-cadherin (1:250) (13-1900; Invitrogen), rabbit anti-ZO-1 (1:500) (40-2300; Invitrogen), rabbit anti- β -catenin (1:1,000) (C2206; Sigma-Aldrich), mouse anti- α E-catenin (1:100) (ALX-804-101; Enzo Life Sciences, Inc.), rabbit anti-laminin 332 (1:1,000) (gifts of Peter Marinkovich, Stanford University, Stanford, CA and Monique Aumailley, University of Cologne, Cologne, Germany), rat anti-cytokeratin-8 (1:100) (TROMA-I; Developmental Studies Hybridoma Bank, Iowa City, IA), rabbit anti-cytokeratin-14 (1:500) (PRB-155P; Covance), mouse anti-smooth muscle α -actin (1:250) (A5228; Sigma-Aldrich), and mouse anti-Twist1 (1:50) (sc-81417; Santa Cruz). Secondary antibodies used were all Alexa Fluor-conjugated antibodies (1:200) (Invitrogen).

Transplanted no. 4 mammary glands were dissected, fixed in 4% paraformaldehyde for 4 h at room temperature, rinsed three times in PBS for 15 min, and embedded in OCT. OCT blocks were sectioned at 50-100 μ m thickness by cryostat with OT at -40°C and CT at -30°C. Samples on slides were stained as above but incubated in primary antibody for 48 h at 4°C and in secondary antibody for 24 h at 4°C or for 6-8 h at room temperature.

Protein extraction. Lysis buffer for protein extraction was prepared by diluting 10X

RIPA buffer (20-188; Millipore) in ultrapure water and chilling the mixture at 4°C for at least 2 h. Immediately prior to use, lysis buffer was supplemented with 0.1% SDS, 5% glycerol, 3 mM EDTA, 1 mM NaF, 1 mM PMSF, 1.5 mM NaVO₄, Aprotinin (A6279; Sigma-Aldrich), and a mini protease inhibitor tablet (11836153001; Roche). Organoids embedded in 3D Matrigel were collected using freshly made PBS/EDTA buffer (5 mM, 1 mM NaVO₄, 1.5 mM NaF, 1mM PMSF in PBS). Medium was aspirated from 3D culture wells, and all wells were rinsed once quickly with 1 mL of cold PBS. Approximately 1 mL of cold PBS/EDTA buffer was used to dissolve two 100 µL gels. Solutions were transferred to centrifuge tubes and mixed well by pipetting. Tubes were left on a 4°C shaker for 1 h to dissolve the Matrigel and then centrifuged at 400 rcf for 5 min at 4°C. Supernatants were removed, and, if necessary, pellets were washed with additional PBS/EDTA to remove residual Matrigel. After another 5 min spin, pellets were resuspended in 100 µL of RIPA lysis buffer, vortexed, and left on ice for 30-40 min. Tubes were centrifuged for 10 min at 18,400 rcf at 4°C and supernatants transferred to new centrifuge tubes and stored at -80°C. For lentivirus experiments, organoids were collected following 3-day puromycin selection, washed once with cold PBS to remove trace medium, and resuspended in RIPA lysis buffer as described.

Western blotting. Whole cell protein lysates were thawed on ice for 20 min, vortexed, and centrifuged for 5 min at 18,400 rcf at 4°C. Samples in Laemmli Sample Buffer (161-0747; Bio-Rad) and β-mercaptoethanol were heated at 70°C for 10 min and loaded for equal protein based on BCA analysis (Thermo Scientific Pierce) in 4-15% Mini-PROTEAN TGX precast gels (456-1084; Bio-Rad). SDS-PAGE was performed at 40 V for 30 min and 80 V for ~90 min until the dye front ran off the gels. Gels were transferred onto nitrocellulose membranes (45-000-948; GE Healthcare) at 100 V for 1 h at 4°C. Membranes were blocked with 5% milk in TBST (03-500-537; Fisher Scientific) for 1 h at

room temperature. Primary antibodies were prepared in blocking buffer and added overnight at 4°C. Primary antibodies used were rat anti-E-cadherin (1:1000) (13-1900; Invitrogen), rabbit anti-β-catenin (1:2000) (C2206; Sigma-Aldrich), mouse anti-αE-catenin (1:1000) (ALX-804-101; Enzo Life Sciences, Inc.), rabbit anti-N-cadherin (1:1000) (ab18203; Abcam), mouse anti-Twist1 (1:500) (sc-81417; Santa Cruz), and mouse anti-β-actin (1:1000) (A2228; Sigma-Aldrich). The N-cadherin antibody detected protein by western blotting but not by immunofluorescence. Membranes were washed three times with TBST for 5 min and incubated with HRP-conjugated secondary antibodies (1:2000) (Invitrogen) in blocking buffer for 1 h at room temperature. Bands were detected with ECL reagents (34075 or 34095; Thermo Scientific), and membranes were imaged using an Alpha-InnoTec imager and software. Band intensities acquired under auto-exposure were quantified using Fiji. To probe for more than one protein, membranes were incubated with stripping buffer (21059, Thermo Scientific) for 30 min at 37°C, washed three times with TBST for 5 min, and re-blocked. Primary antibodies used on the same membrane were from different hosts.

***E-cad* knockdown experiments.** Approximately 1,000 *CMV::rtTA;TRE-Twist1* organoids resuspended in 200 μL basal organoid medium were added to each of four wells of a Nunc HydroCell 96-well microplate. Organoids were allowed to settle for 1 h at 37°C. Lentiviral transduction particles were thawed on ice: (1) MISSION pLKO.1-puro *Luciferase* shRNA (1x10⁶ TU/ml, SHC007V, Sigma-Aldrich); (2) MISSION pLKO.1-puro *Cdh1* shRNA #1 (1x10⁶ TU/ml, TRCN0000042578, Sigma-Aldrich); (3) MISSION pLKO.1-puro *Cdh1* shRNA #2 (1x10⁶ TU/ml, TRCN0000042581, Sigma-Aldrich). In separate centrifuge tubes, 3 μL ViroMag R/L nanoparticles (RL40200, OZ Biosciences) were mixed with 47 μL lentivirus and incubated at room temperature for 30 min. In three

of the organoid wells, 150 μL of medium were carefully removed, and 50 μL of the ViroMag/lentivirus mix were added. Suspensions were mixed well to disperse the organoids and prevent aggregation. The fourth organoid well served as a no-virus, puromycin control to evaluate killing efficiency. The 96-well plate was incubated on top of a magnetic plate (MF10000, OZ Biosciences) at 37°C for 1.5 h, then taken off the magnet and incubated overnight at 37°C. On day 2, ~70 μL of medium were removed from each well with virus, 200 μL of fresh organoid medium were added, and the suspensions were mixed well to redisperse the organoids. On day 3, ~200 μL of medium were removed from all wells, and 200 μL of organoid medium with 2.5 nM FGF2 and 4 $\mu\text{g}/\text{mL}$ puromycin were added. Selection was performed for 3 days, and the surviving virus-treated organoids were collected for 3D culture and imaged by DIC time-lapse microscopy. In parallel, *TRE-Twist1* (rtTA⁻) organoids from littermate controls were treated with lentiviruses and, following selection, used for protein extraction to evaluate *E-cad* knockdown efficiency. Time-lapse movies were used to track and count cells that had disseminated by 100 h of *Twist1* induction in each of the three treatment groups. A cell was considered disseminated if it had a clear space between itself and the main organoid (visible ECM) and was observed to be migrating away persistently. Cells within collective chains that temporarily detached in only a few frames were not counted as disseminated.

RNA isolation and sequencing. Organoids were isolated from three *CMV::rtTA;TRE-Twist1* mice (“Twist1”) and three *TRE-Twist1* (rtTA⁻, “Control”) littermates (all inbred FVB/N). For each mouse, organoids were embedded in 3D Matrigel at 3-10 organoids/ μL and plated as six 50 μL suspensions in a 35-mm dish. Organoids were cultured in basal organoid medium for 24 h and in basal organoid medium supplemented

with 5 $\mu\text{g}/\text{mL}$ doxycycline for an additional 48 h. All *CMV::rtTA;TRE-Twist1* samples were disseminating at 48 h of *Twist1* induction while no control samples were disseminating. Total RNA was extracted using 1 mL TRIzol per dish (15596-026; Life Technologies) and Qiagen RNeasy. With 10-100 ng of RNA collected per sample, we generated barcoded NuGen RNA-seq v.2 libraries and ran paired end, 75 bp, 50 cycle sequencing on a HiSeq 2000 (JHMI Deep Sequencing and Microarray Core Facility, Baltimore, MD).

Paired-end, non-strand-specific RNA-seq reads were mapped to the mouse reference genome (GRCM build 38) using read mapper Bowtie⁵⁶ and splice junction mapper TopHat⁵⁷. We achieved an average of 51.4 million uniquely mapped reads per sample and estimated the number of reads mapped to each gene using HTSeq⁵⁸, with gene coordinates from the reference genome Generic Feature Format file. Raw counts were normalized and p-values were calculated for *Twist1* versus Control differential expression from negative binomial distributions using DESeq⁵⁹. Based on the number of genes tested, the genome-wide significance level for 0.05 family-wise error rate was 2.74×10^{-6} , and 183 genes were significant at this level. Sequence data has been uploaded to the Sequence Read Archive (Project Accession SRP033275).

Gene Ontology analysis. Significant genes were characterized using GO Slim categories for biological process, cellular component, and molecular function³⁶ (GO file downloaded on 9/12/13, mapping from 3/5/13). We first computed the overall fraction of genes that were upregulated ($f_{\text{up}}=107/18,260$) and downregulated ($f_{\text{down}}=76/18,260$). For each GO term, we then calculated the number of genes n annotated to the category and also among the 18,260 genes sequenced. Categories with $n < 2$ were not considered further. For categories with $n \geq 2$, we conducted separate two-sided tests corresponding

to enrichment or depletion based on Poisson distributions for upregulated (expected number = $f_{up}n$) and downregulated (expected number = $f_{down}n$) DE genes. For each of the three ontologies, the p-value threshold for 0.05 family-wise error rate was set to $0.05/(4 * \text{number of categories tested})$. This conservative approach was selected as more computationally convenient than the corresponding Fisher's exact tests.

Pathway-level differential expression. To assess pathway-level differential expression, we used gene sets available through MSigDB v4.0⁶⁰. The 1,320 canonical gene sets within MSigDB are aggregated from major pathway databases: BioCarta, KEGG, Reactome, the Pathway Interaction Database (PID), the SigmaAldrich database, the Signaling Gateway database, the Signal Transduction KE database, and the SuperArray database. These are then augmented to 4,722 curated gene sets by including gene lists from published studies, the L2L gene sets from mammalian microarray studies⁶¹, the MYC Target Gene Database⁶², and other public resources. For each gene, including genes not differentially expressed at genome-wide significance, the p-value from DESeq was converted to the equivalent z-score for a two-sided test, with $z > 0$ for Twist1 > Control and $z < 0$ for Twist1 < Control. Each pathway was tested using a one-sided Student's *t*-test of $|z|$ within pathway > $|z|$ outside pathway, corresponding to an increased number of differentially expressed genes without regard to direction (up or down in Twist1 versus Control). Significance thresholds for 0.05 family-wise error rates at the pathway level were estimated using 500 permutations of gene z-scores, recording the best p-value from each permutation, and taking the 25th-best p-value as the 0.05 FWER threshold. The resulting thresholds were 1.44×10^{-13} for canonical gene sets and 5.31×10^{-19} for curated gene sets. These thresholds are more stringent than a standard Bonferroni correction.

References

- 1 Bogenrieder, T. & Herlyn, M. Axis of evil: molecular mechanisms of cancer metastasis. *Oncogene* **22**, 6524-6536 (2003).
- 2 Polyak, K. Molecular markers for the diagnosis and management of ductal carcinoma in situ. *J Natl Cancer Inst Monogr* **2010**, 210-213 (2010).
- 3 Nguyen, D. X., Bos, P. D. & Massague, J. Metastasis: from dissemination to organ-specific colonization. *Nat Rev Cancer* **9**, 274-284 (2009).
- 4 Nelson, W. J. Remodeling epithelial cell organization: transitions between front-rear and apical-Basal polarity. *Cold Spring Harb Perspect Biol* **1**, a000513 (2009).
- 5 Polyak, K. & Weinberg, R. A. Transitions between epithelial and mesenchymal states: acquisition of malignant and stem cell traits. *Nat Rev Cancer* **9**, 265-273 (2009).
- 6 Hirohashi, S. Inactivation of the E-cadherin-mediated cell adhesion system in human cancers. *American Journal of Pathology* **153**, 333-339 (1998).
- 7 Jeanes, A., Gottardi, C. J. & Yap, A. S. Cadherins and cancer: how does cadherin dysfunction promote tumor progression? *Oncogene* **27**, 6920-6929 (2008).
- 8 Yang, J. & Weinberg, R. A. Epithelial-mesenchymal transition: at the crossroads of development and tumor metastasis. *Dev Cell* **14**, 818-829 (2008).
- 9 Peinado, H., Olmeda, D. & Cano, A. Snail, Zeb and bHLH factors in tumour progression: an alliance against the epithelial phenotype? *Nat Rev Cancer* **7**, 415-428 (2007).
- 10 Larue, L., Ohsugi, M., Hirchenhain, J. & Kemler, R. E-cadherin null mutant embryos fail to form a trophectoderm epithelium. *Proc Natl Acad Sci U S A* **91**, 8263-8267 (1994).
- 11 Berx, G. *et al.* E-cadherin is inactivated in a majority of invasive human lobular breast cancers by truncation mutations throughout its extracellular domain. *Oncogene* **13**, 1919-1925 (1996).
- 12 Derksen, P. W. *et al.* Somatic inactivation of E-cadherin and p53 in mice leads to metastatic lobular mammary carcinoma through induction of anoikis resistance and angiogenesis. *Cancer Cell* **10**, 437-449 (2006).
- 13 Onder, T. T. *et al.* Loss of E-cadherin promotes metastasis via multiple downstream transcriptional pathways. *Cancer Res* **68**, 3645-3654 (2008).
- 14 Boussadia, O., Kutsch, S., Hierholzer, A., Delmas, V. & Kemler, R. E-cadherin is a survival factor for the lactating mouse mammary gland. *Mechanisms of Development* **115**, 53-62 (2002).
- 15 Tinkle, C. L., Lechler, T., Pasolli, H. A. & Fuchs, E. Conditional targeting of E-cadherin in skin: insights into hyperproliferative and degenerative responses. *Proc Natl Acad Sci U S A* **101**, 552-557 (2004).
- 16 Yang, J. *et al.* Twist, a master regulator of morphogenesis, plays an essential role in tumor metastasis. *Cell* **117**, 927-939 (2004).
- 17 Mironchik, Y. *et al.* Twist overexpression induces in vivo angiogenesis and correlates with chromosomal instability in breast cancer. *Cancer Res* **65**, 10801-10809 (2005).
- 18 Berx, G. & Van Roy, F. The E-cadherin/catenin complex: an important gatekeeper in breast cancer tumorigenesis and malignant progression. *Breast Cancer Res* **3**, 289-293 (2001).
- 19 Wood, L. D. *et al.* The genomic landscapes of human breast and colorectal

- cancers. *Science* **318**, 1108-1113 (2007).
- 20 Stephens, P. J. *et al.* Complex landscapes of somatic rearrangement in human breast cancer genomes. *Nature* **462**, 1005-1010 (2009).
- 21 Barrallo-Gimeno, A. & Nieto, M. A. The Snail genes as inducers of cell movement and survival: implications in development and cancer. *Development* **132**, 3151-3161 (2005).
- 22 Ewald, A. J., Brenot, A., Duong, M., Chan, B. S. & Werb, Z. Collective epithelial migration and cell rearrangements drive mammary branching morphogenesis. *Dev Cell* **14**, 570-581 (2008).
- 23 Badea, T. C., Wang, Y. & Nathans, J. A noninvasive genetic/pharmacologic strategy for visualizing cell morphology and clonal relationships in the mouse. *J Neurosci* **23**, 2314-2322 (2003).
- 24 Muzumdar, M. D., Tasic, B., Miyamichi, K., Li, L. & Luo, L. A global double-fluorescent Cre reporter mouse. *Genesis* **45**, 593-605 (2007).
- 25 Bissell, M. J. & Bilder, D. Polarity determination in breast tissue: desmosomal adhesion, myoepithelial cells, and laminin 1. *Breast Cancer Res* **5**, 117-119 (2003).
- 26 Gumbiner, B., Stevenson, B. & Grimaldi, A. The Role of the Cell-Adhesion Molecule Uvomorulin in the Formation and Maintenance of the Epithelial Junctional Complex. *J. Cell Biol.* **107**, 1575-1587 (1988).
- 27 Ewald, A. J. *et al.* Mammary collective cell migration involves transient loss of epithelial features and individual cell migration within the epithelium. *J Cell Sci* **125**, 2638-2654 (2012).
- 28 Williams, J. M. & Daniel, C. W. Mammary ductal elongation: differentiation of myoepithelium and basal lamina during branching morphogenesis. *Dev Biol* **97**, 274-290 (1983).
- 29 Hinck, L. & Silberstein, G. B. Key stages in mammary gland development: the mammary end bud as a motile organ. *Breast Cancer Res* **7**, 245-251 (2005).
- 30 Daniel, C. W., Strickland, P. & Friedmann, Y. Expression and functional role of E- and P-cadherins in mouse mammary ductal morphogenesis and growth. *Dev Biol* **169**, 511-519 (1995).
- 31 Vesuna, F., van Diest, P., Chen, J. H. & Raman, V. Twist is a transcriptional repressor of E-cadherin gene expression in breast cancer. *Biochem Biophys Res Commun* **367**, 235-241 (2008).
- 32 Thiery, J. P., Acloque, H., Huang, R. Y. & Nieto, M. A. Epithelial-mesenchymal transitions in development and disease. *Cell* **139**, 871-890 (2009).
- 33 Tran, P. T. *et al.* Twist1 suppresses senescence programs and thereby accelerates and maintains mutant Kras-induced lung tumorigenesis. *PLoS Genet* **8**, e1002650 (2012).
- 34 Belteki, G. *et al.* Conditional and inducible transgene expression in mice through the combinatorial use of Cre-mediated recombination and tetracycline induction. *Nucleic Acids Res* **33**, e51 (2005).
- 35 Nieman, M. T., Prudoff, R. S., Johnson, K. R. & Wheelock, M. J. N-cadherin promotes motility in human breast cancer cells regardless of their E-cadherin expression. *J. Cell Biol.* **147**, 631-643 (1999).
- 36 Ashburner, M. *et al.* Gene ontology: tool for the unification of biology. The Gene Ontology Consortium. *Nat Genet* **25**, 25-29 (2000).
- 37 Tsai, J. H., Donaher, J. L., Murphy, D. A., Chau, S. & Yang, J. Spatiotemporal Regulation of Epithelial-Mesenchymal Transition Is Essential for Squamous Cell Carcinoma Metastasis. *Cancer Cell* **22**, 725-736 (2012).
- 38 Vesuna, F., Lisok, A., Kimble, B. & Raman, V. Twist modulates breast cancer

- stem cells by transcriptional regulation of CD24 expression. *Neoplasia* **11**, 1318-1328 (2009).
- 39 Barnes, R. M. & Firulli, A. B. A twist of insight - the role of Twist-family bHLH factors in development. *Int J Dev Biol* **53**, 909-924 (2009).
- 40 Greenburg, G. & Hay, E. D. Epithelia suspended in collagen gels can lose polarity and express characteristics of migrating mesenchymal cells. *J Cell Biol* **95**, 333-339 (1982).
- 41 Hay, E. D. & Zuk, A. Transformations between epithelium and mesenchyme: normal, pathological, and experimentally induced. *Am J Kidney Dis* **26**, 678-690 (1995).
- 42 Reynolds, A. B. p120-catenin: Past and present. *Biochim Biophys Acta* **1773**, 2-7 (2007).
- 43 Kowalski, P. J., Rubin, M. A. & Kleer, C. G. E-cadherin expression in primary carcinomas of the breast and its distant metastases. *Breast Cancer Res* **5**, R217-222 (2003).
- 44 Come, C. *et al.* Snail and slug play distinct roles during breast carcinoma progression. *Clin Cancer Res* **12**, 5395-5402 (2006).
- 45 Carey, L. A. Through a glass darkly: advances in understanding breast cancer biology, 2000-2010. *Clin Breast Cancer* **10**, 188-195 (2010).
- 46 Morel, A. P. *et al.* EMT inducers catalyze malignant transformation of mammary epithelial cells and drive tumorigenesis towards claudin-low tumors in transgenic mice. *PLoS Genet* **8**, e1002723 (2012).
- 47 Nguyen-Ngoc, K. V. *et al.* The ECM microenvironment regulates collective migration and local dissemination in normal and malignant mammary epithelium. *PNAS* **109**, E2595-E2604 (2012).
- 48 Ewald, A. J. Practical considerations for long-term time-lapse imaging of epithelial morphogenesis in three-dimensional organotypic cultures. *Cold Spring Harb Protoc* **2013** (2013).
- 49 Ewald, A. J., Werb, Z. & Egeblad, M. Dynamic, long-term in vivo imaging of tumor-stroma interactions in mouse models of breast cancer using spinning-disk confocal microscopy. *Cold Spring Harb Protoc* **2011**, pdb top97 (2011).
- 50 Edelstein, A., Amodaj, N., Hoover, K., Vale, R. & Stuurman, N. Computer control of microscopes using microManager. *Curr Protoc Mol Biol* **Chapter 14**, Unit14 20 (2010).
- 51 McDonald, K. L. & Webb, R. I. Freeze substitution in 3 hours or less. *J Microsc* **243**, 227-233 (2011).
- 52 McDonald, K. & Muller-Reichert, T. Cryomethods for thin section electron microscopy. *Methods Enzymol* **351**, 96-123 (2002).
- 53 Muller-Reichert, T., Hohenberg, H., O'Toole, E. T. & McDonald, K. Cryoimmobilization and three-dimensional visualization of *C. elegans* ultrastructure. *J Microsc* **212**, 71-80 (2003).
- 54 Mastronarde, D. N. Automated electron microscope tomography using robust prediction of specimen movements. *J Struct Biol* **152**, 36-51 (2005).
- 55 Abramoff, M. D., Magalhaes, P. J. & Ram, S. J. Image processing with ImageJ. *Biophotonics International* **11**, 36-42 (2004).
- 56 Langmead, B., Trapnell, C., Pop, M. & Salzberg, S. L. Ultrafast and memory-efficient alignment of short DNA sequences to the human genome. *Genome Biol* **10**, R25 (2009).
- 57 Trapnell, C., Pachter, L. & Salzberg, S. L. TopHat: discovering splice junctions with RNA-Seq. *Bioinformatics* **25**, 1105-1111 (2009).
- 58 Anders, S. *HTSeq: Analysing high-throughput sequencing data with Python*,

- <<http://www-huber.embl.de/users/anders/HTSeq/doc/index.html>> (2010).
- 59 Anders, S. & Huber, W. Differential expression analysis for sequence count data. *Genome Biol* **11**, R106 (2010).
- 60 Subramanian, A. *et al.* Gene set enrichment analysis: a knowledge-based approach for interpreting genome-wide expression profiles. *Proc Natl Acad Sci U S A* **102**, 15545-15550 (2005).
- 61 Newman, J. C. & Weiner, A. M. L2L: a simple tool for discovering the hidden significance in microarray expression data. *Genome Biol* **6**, R81 (2005).
- 62 Zeller, K. I., Jegga, A. G., Aronow, B. J., O'Donnell, K. A. & Dang, C. V. An integrated database of genes responsive to the Myc oncogenic transcription factor: identification of direct genomic targets. *Genome Biol* **4**, R69 (2003).

Figure 4-1. *E-cad* deletion induced loss of simple epithelial architecture. (A) *E-cad* deletion was induced in half of *Cre-ER;E-cad^{fl/fl}* organoids with tamoxifen. (B) Control, *E-cad*⁺ organoids (–Tam) formed cysts. (C) *E-cad*[–] organoids (+Tam) failed to form cysts (28/42 movies, 3 biological replicates) or transiently established and then lost lumens (14/42 movies). (D) *E-cad* deletion blocked cyst formation. *n*, total # of organoids; *r*, # of biological replicates. Error bars indicate SD. ****P*=0.0004, Student's *t* test, 2-tailed, equal variance. (E) Control organoids formed cysts with enrichment of *E-cad* and ZO-1 along apico-lateral membranes (E'). (F) *E-cad*[–] organoids were multilayered, lacked *E-cad* immunoreactivity, and displayed abnormal ZO-1 localization. Arrow indicates rare *E-cad*⁺ cells. (G) By western blot, *E-cad* deletion (+Tam) resulted in complete loss of *E-cad* protein and significant reductions in α *E-catenin* and β -catenin (see Fig. 4-2A,B). Whole cell lysate samples were loaded for equal protein based on BCA analysis. (H) The Cre biosensor *mT/mG* was used to observe *E-cad*[–] cell behaviors by confocal microscopy. *Cre*⁺, *E-cad*[–] cells (green) changed shape, from columnar to round, before shifting apically (arrowheads in H',H''). Gamma adjustments were performed in panels (E) and (F) to improve image clarity. Bars: (B, C) 20 μ m; (E, F, H) 10 μ m.

Figure 4-1

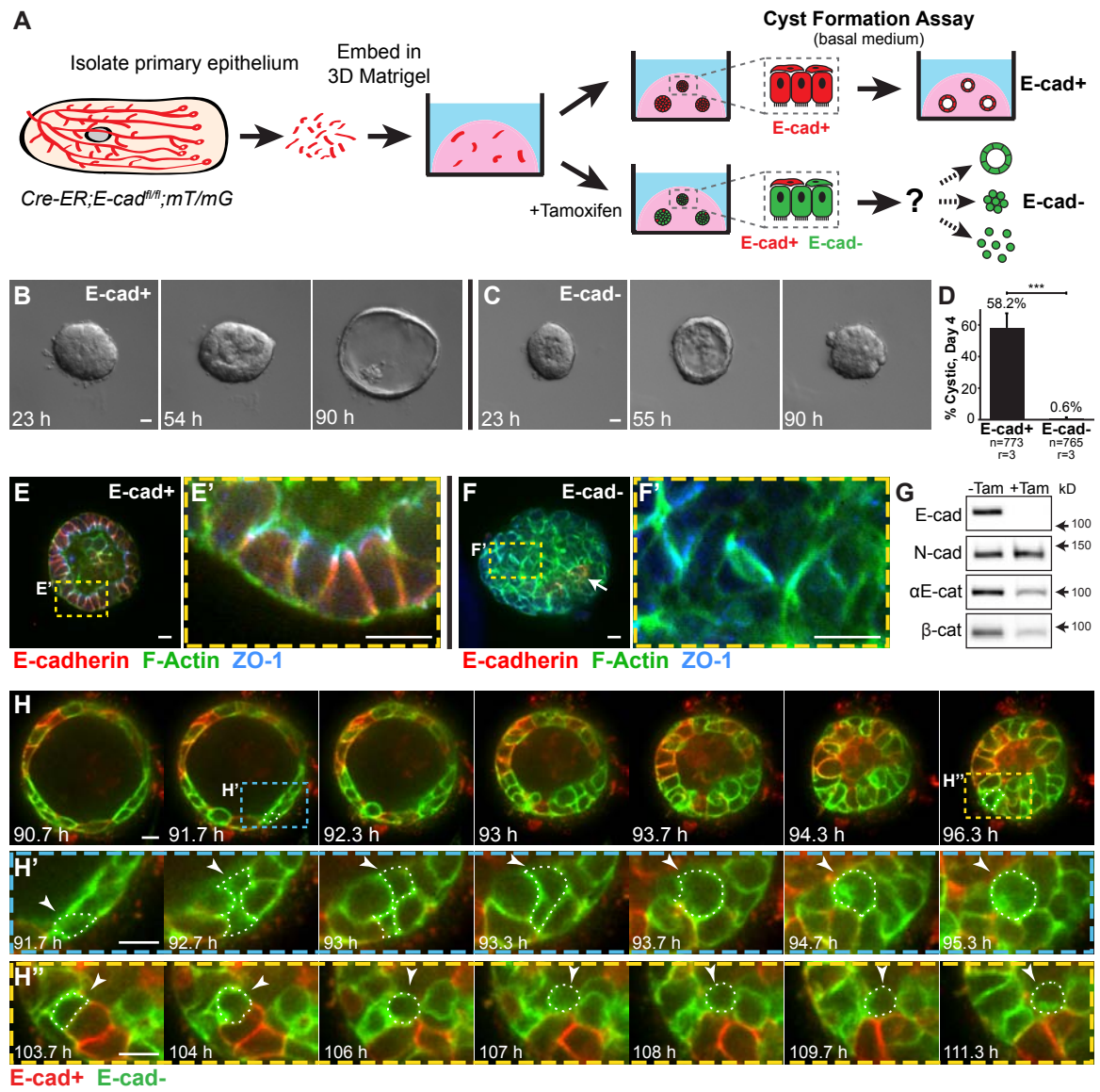
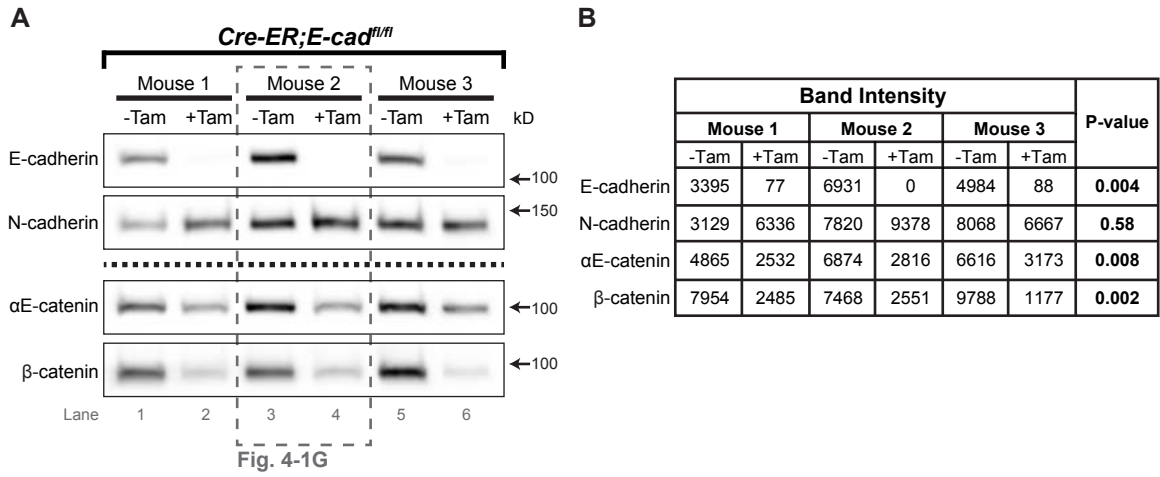


Figure 4-2. *E-cad* deletion induced loss of adherens junction proteins in 3D culture and in vivo. (A) Organoids were isolated from three *Cre-ER;E-cad^{fl/fl}* mice, and *E-cad* deletion was induced with tamoxifen in half of the organoids from each mouse. Protein was extracted on day 6 in culture and assayed for levels of adherens junction components by western blot. Whole cell lysate samples were loaded for equal protein based on BCA analysis. The dotted line indicates two separate blots, prepared from the same samples in parallel, each probed with different antibodies. (B) Fiji was used to quantify intensity of all bands in (A). *E-cad* was essentially absent following gene deletion (** $P=0.004$, Student's *t* test, 1-tailed, equal variance). α E-catenin and β -catenin were significantly reduced, while N-cad did not change (Student's *t* test, 2-tailed, equal variance). (C) Tamoxifen-treated *Cre-ER;E-cad^{fl/fl}* organoids on day 6 had membrane-localized α E-catenin in a subset of cells near the basal surface. Most internal cells were α E-catenin⁻. (D-G) In genetic mosaic *E-cad^{fl/fl};mT/mG* outgrowths in vivo, green, *Cre*⁺ cells reliably lacked membrane-localized *E-cad* (D-F) and β -catenin (G). *E-cad*⁻ luminal cells were excluded from buds (D, green arrowheads) and from polarized epithelium (E,E') and were observed as unpolarized clusters at the injection site (F,G). Bars, 10 μ m.

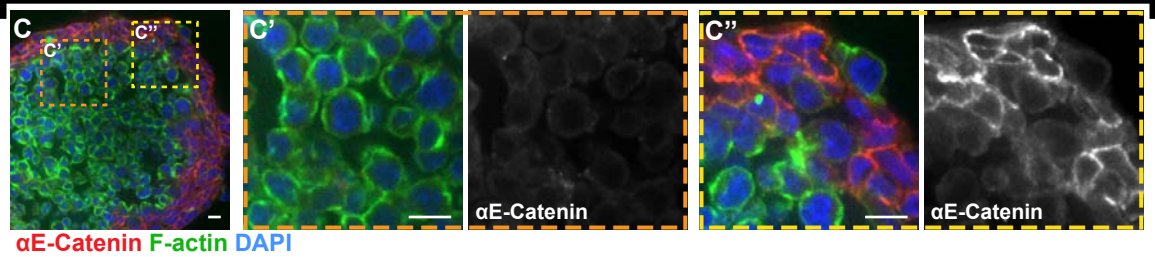
Figure 4-2



B

	Band Intensity						P-value
	Mouse 1		Mouse 2		Mouse 3		
	-Tam	+Tam	-Tam	+Tam	-Tam	+Tam	
E-cadherin	3395	77	6931	0	4984	88	0.004
N-cadherin	3129	6336	7820	9378	8068	6667	0.58
αE-catenin	4865	2532	6874	2816	6616	3173	0.008
β-catenin	7954	2485	7468	2551	9788	1177	0.002

Cre-ER;E-cad^{fl/fl}, +Tam



E-cad^{fl/fl};mT/mG Donor Tissue: 6 weeks in vivo

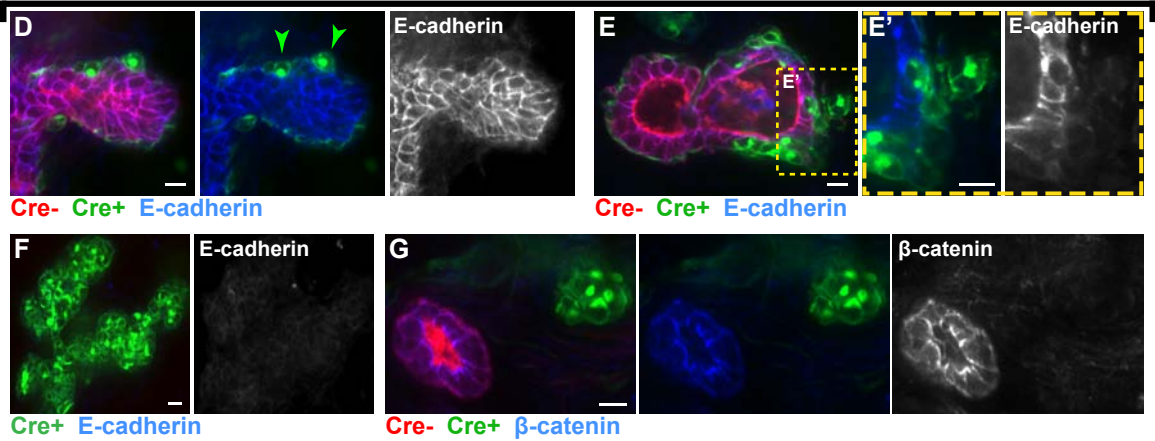


Figure 4-3. E-cad⁻ cells displayed reductions in multiple classes of intercellular junctions. *Cre-ER;E-cad^{fl/+}* and *Cre-ER;E-cad^{fl/fl}* organoids were isolated, and widespread recombination was induced with tamoxifen. (A) Control organoids (E-cad⁺) maintained a smooth basal epithelial border. (B) E-cad⁻ organoids collectively migrated into Matrigel as single file columns (B', red arrowhead). (C) Basally positioned E-cad⁻ cells (white arrowhead) were observed to round up and initiate single file cell columns. (D) Adeno-Cre was used to generate genetic mosaic organoids with a mixture of E-cad⁺ and E-cad⁻ cells. (E,F) Green, Cre⁺ cells reliably lacked E-cad (E,E') and β -catenin (F,F'). (G) Basally positioned E-cad⁻ cells were located beyond the basement membrane protein laminin 332. Arrows in (G') indicate a single file column. (H) TEM was used to quantify desmosomes in Adeno-Cre-transduced *E-cad^{fl/+}* (control) and *E-cad^{fl/fl}* organoids. Red outline indicates a representative region used for analysis. (I) E-cad⁻ epithelium had significantly fewer desmosomes compared to control, E-cad⁺ epithelium. Error bars indicate SD. ***P=0.0008; Student's *t* test, 2-tailed, equal variance. (J) Small desmosomes (J', yellow arrowheads) were detected connecting cells in single file columns. Gamma adjustments were performed in panels (E) and (F) to improve image clarity. Bars: (A, B) 20 μ m; (C, E-G) 10 μ m; (H) 5 μ m; (J) 0.5 μ m.

Figure 4-3

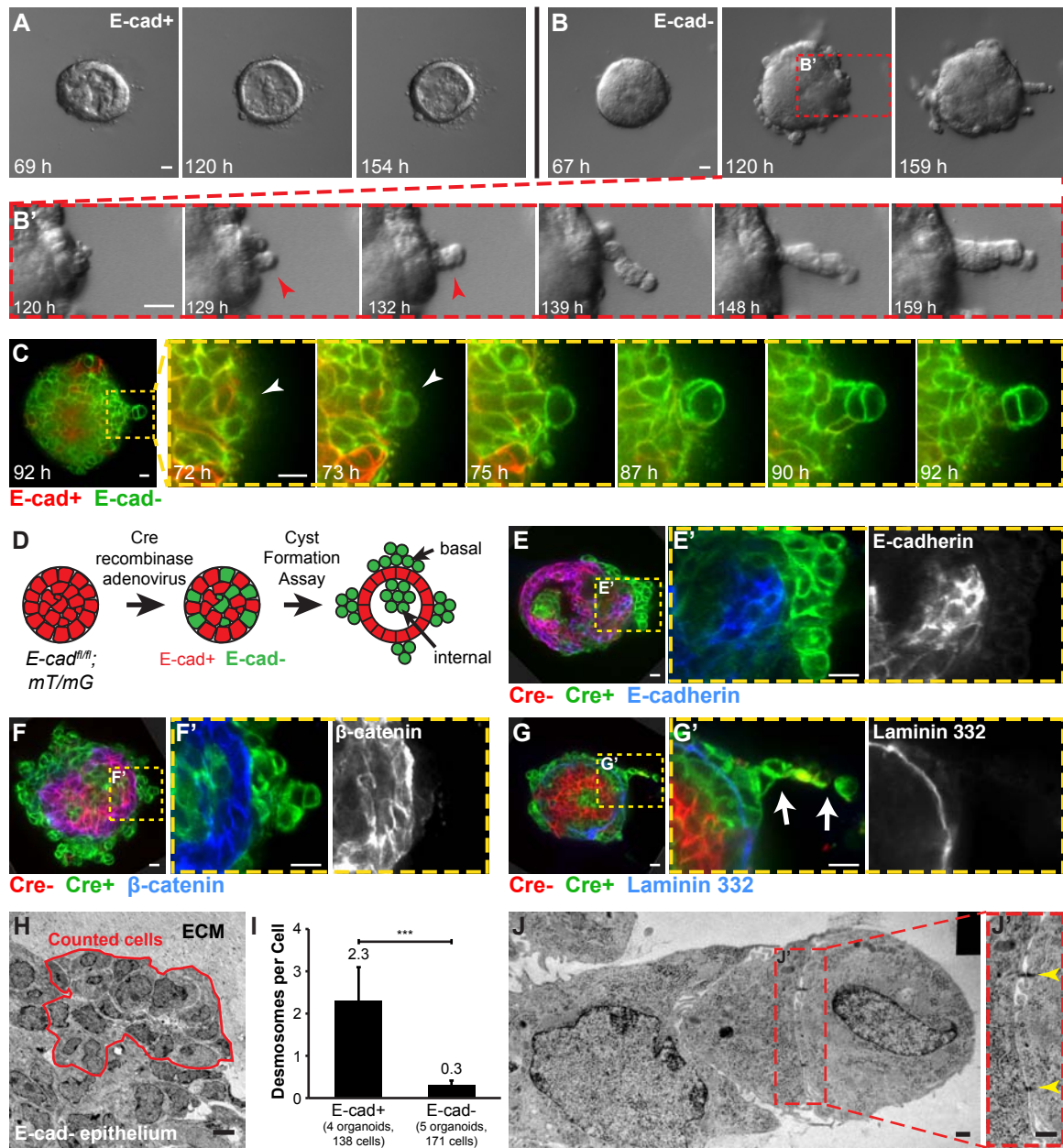


Figure 4-4. Loss of E-cad inhibited branching morphogenesis and induced epithelial disorganization in 3D culture. (A) *E-cad^{+/+};mT/mG* and *E-cad^{fl/fl};mT/mG* organoids were isolated, recombination was induced with Adeno-Cre, and branching morphogenesis was induced with FGF2. (B) *E-cad⁺* organoids completed branching morphogenesis. (C) *E-cad⁻* organoids developed a disorganized basal surface composed of rounded cells (C'). (D) This disorganized surface morphology was observed in 94% of *E-cad⁻* organoids. *n*, # of time-lapse movies; *r*, # of biological replicates. (E,F) Basally positioned cells were green (*Cre⁺*), *E-cad⁻* (E), and β -catenin⁻ (F). (G,H) In genetic mosaic organoids with a mixture of *E-cad⁺* and *E-cad⁻* cells, *E-cad⁺* cells (red) were observed to initiate new buds (white arrowheads, H'). Bars: (B, C) 20 μ m; (E, F, H) 10 μ m.

Figure 4-4

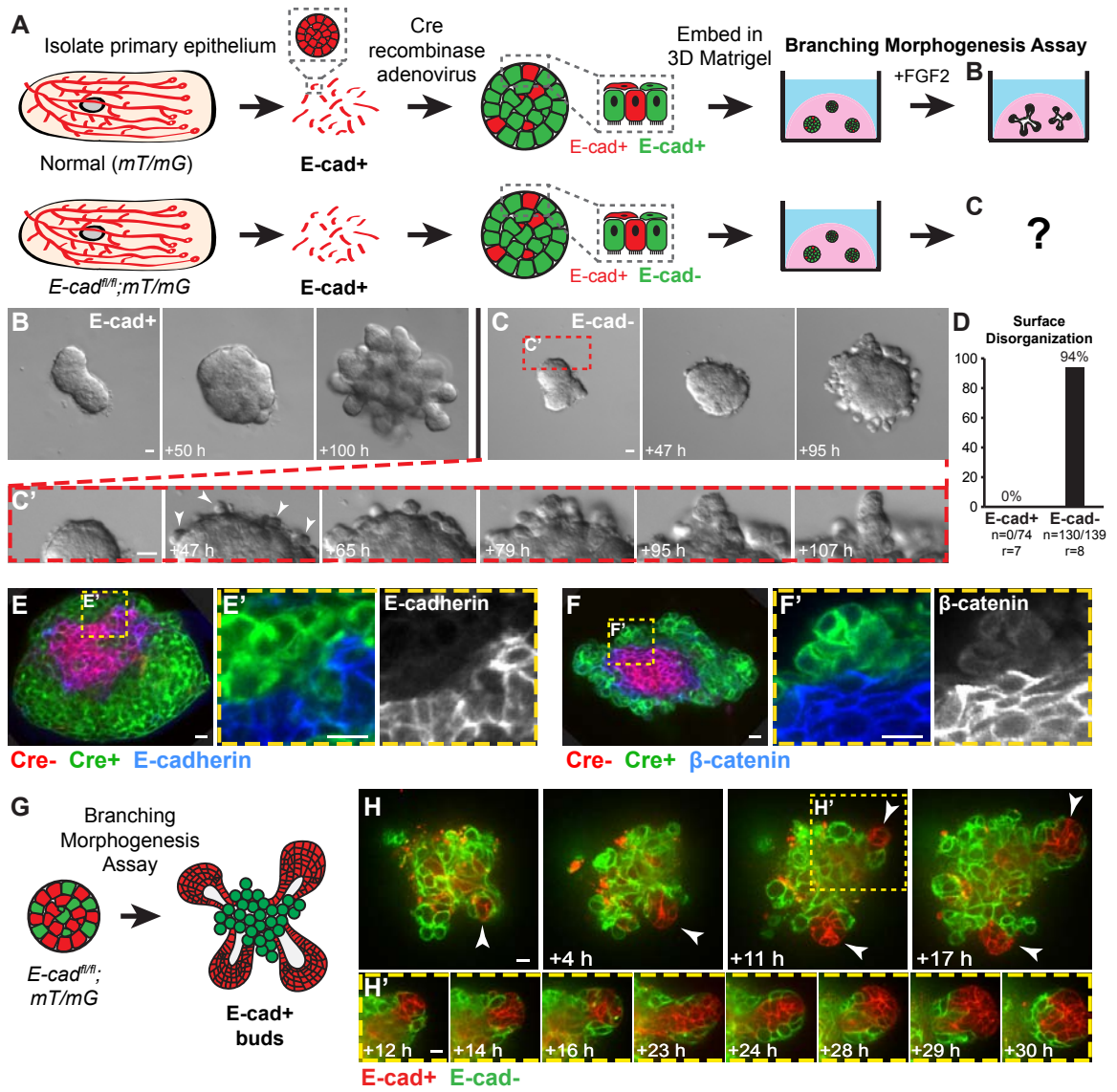


Figure 4-5. E-cad⁻ cells were excluded from polarized ducts and the body cell compartment of the terminal end bud in vivo. (A) Adeno-Cre-transduced *mT/mG* organoids (E-cad⁺) were transplanted into cleared mammary fat pads, and glands were harvested after 6 weeks. (B,C) Both TEBs (B) and polarized ducts (C) contained a mixture of red and green cells in the luminal and myoepithelial cell layers. (D) Adeno-Cre-transduced *E-cad^{fl/fl};mT/mG* organoids were transplanted into contralateral no. 4 glands. (E) E-cad⁻ luminal cells were markedly excluded from the body cell region of the TEB in ductal outgrowths. Arrowheads indicate green cells in the cap cell layer. (F-G) E-cad⁻ luminal cells were observed on the basal surfaces of polarized epithelium in the gland periphery (F) and near the injection site (G). (H) E-cad⁻ cells were also observed in disorganized clusters surrounded by myoepithelial cells (H', SMA⁺). (I) *Cre-ER;E-cad^{fl/fl};mT/mG* organoids (E-cad⁺) were transplanted into cleared mammary fat pads and allowed to grow out for 6 weeks. Tamoxifen was injected to induce *E-cad* deletion, and glands were harvested after 2-6 weeks. (J) E-cad⁻ cells were observed in the lumens (J') and on the basal surfaces (J'') of E-cad⁺ polarized ducts (9 glands). Bars, 10 μm.

Figure 4-5

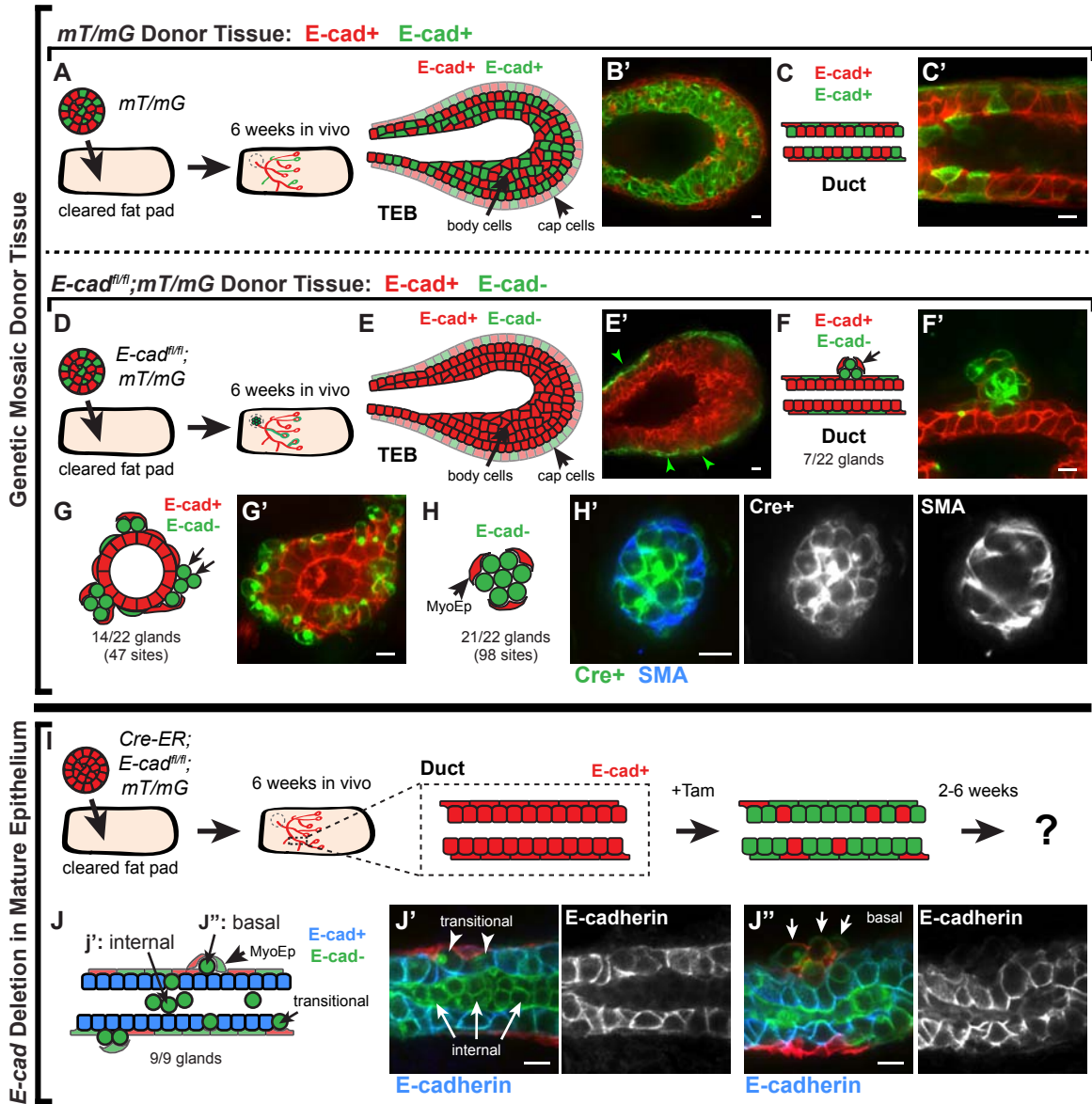


Figure 4-6. Twist1 induced robust dissemination of normal epithelial cells.

(A) Organoids were isolated from *CMV::rtTA;TRE-Twist1* mice, and *Twist1* was induced in half of the organoids with doxycycline. (B,C) In basal medium, control organoids maintained epithelial organization (B), while *Twist1* expression induced robust dissemination (C). Disseminating cells (red arrowheads) migrated away from the epithelium with extensive protrusions (C'). (D,E) In FGF2-containing medium, control organoids completed branching morphogenesis (D), while *Twist1* expression blocked branching and induced robust dissemination (E). Red arrowheads in (E) indicate disseminated cells. With FGF2, disseminated cells proliferated to form secondary epithelial sites (blue arrows and E', 6/9 biological replicates). (F) Less than 1% of *Twist1*⁺ organoids branched (**P=0.0006, Student's *t* test, 2-tailed, equal variance) while 97% disseminated (****P=4x10⁻⁷, Student's *t* test, 2-tailed, equal variance). *n*, total # of organoids; *r*, # of biological replicates. Error bars indicate SD. (G) Both luminal (K8⁺, red arrows) and myoepithelial (K14⁺, green arrows) cells disseminated. (H) Both disseminated single cells and cells within the main epithelial group were *Twist1*⁺. (I) Myoepithelial cells (SMA⁺) and basement membrane (laminin 332; white arrows) were inappropriately localized to the organoid interior. Gamma adjustments were performed in panels (H-I) to improve image clarity. Bars: (B-E) 20 μm; (G-I) 10 μm.

Figure 4-6

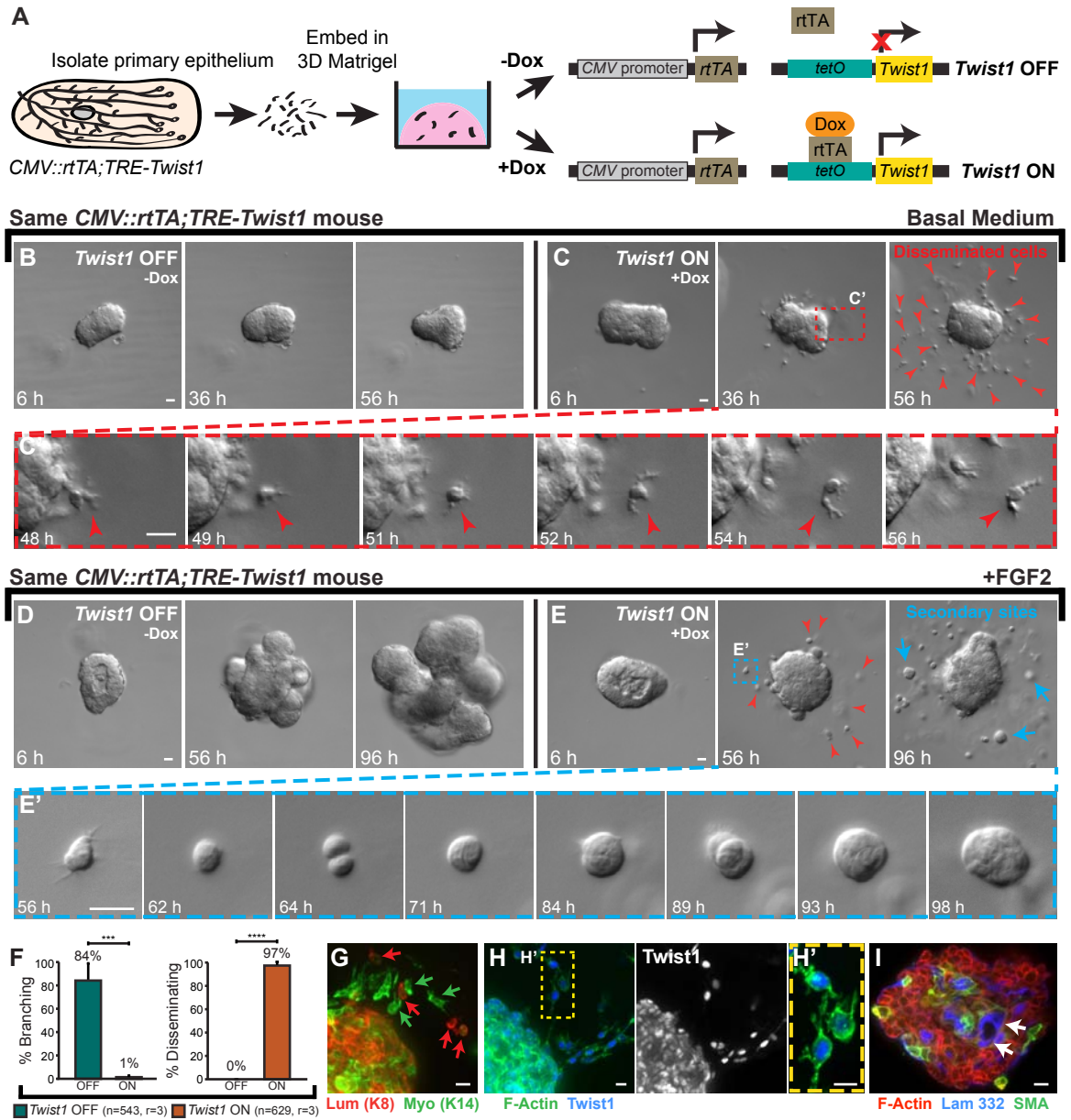


Figure 4-7. Organoids recovered epithelial behaviors when *Twist1* was turned off.

(A) *Twist1* was transiently activated in *CMV::rtTA;TRE-Twist1* epithelium by a 48 h pulse of doxycycline. (B) In basal medium, organoids transiently disseminated, but disseminated cells stopped migrating after doxycycline removal (arrowheads). (C-E) In the presence of FGF2, organoids initiated new buds after doxycycline removal (D), and disseminated cells reintegrated with the main organoid (E). (F) Branched organoids displayed normal mammary epithelial organization, with inner luminal epithelial cells (K8⁺) and outer myoepithelial cells (K14⁺). Bars, 20 μ m.

Figure 4-7

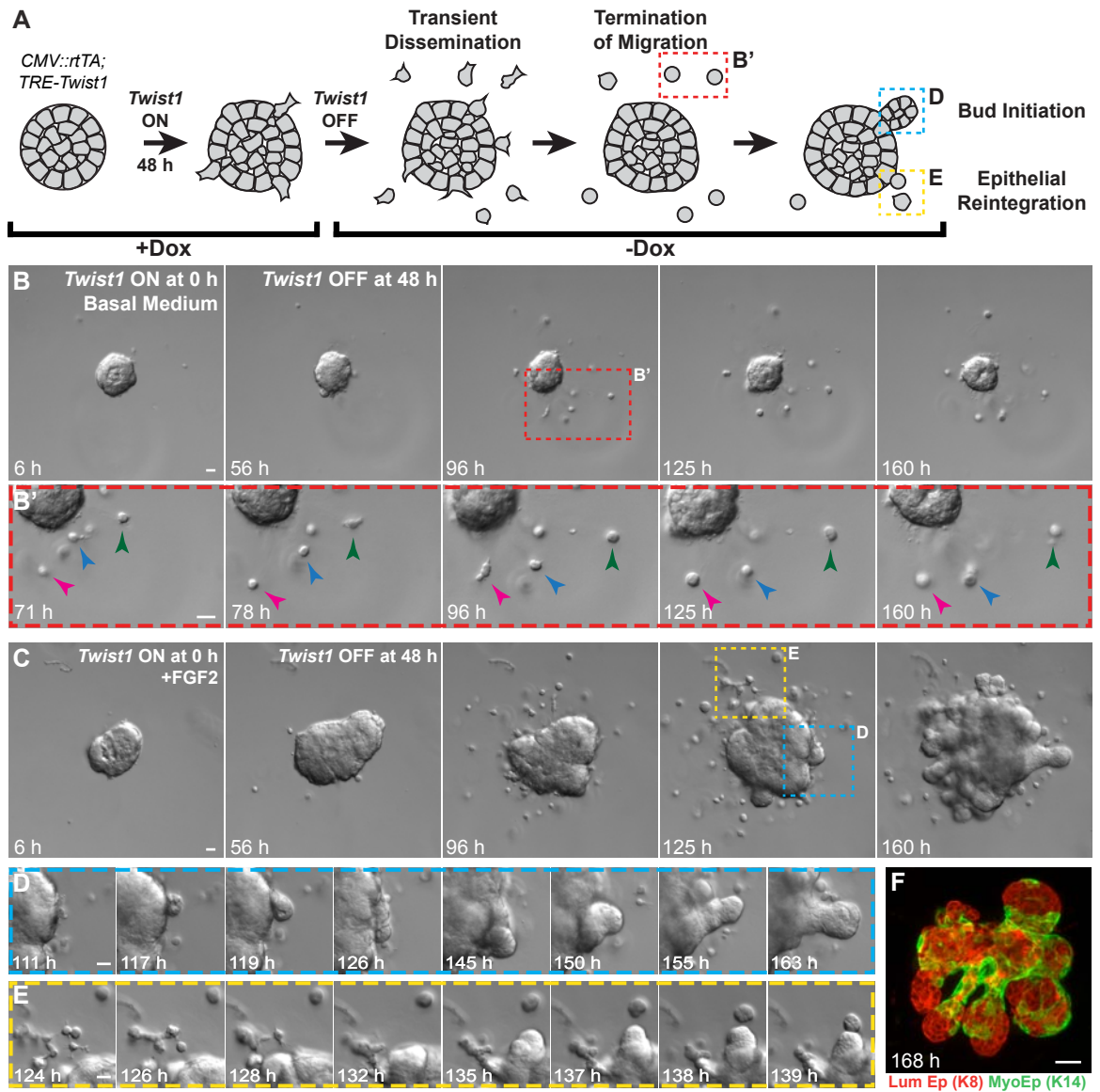


Figure 4-8. Twist1-induced dissemination was cell autonomous, and Twist1 was sufficient for dissemination in vivo. (A) A Cre-inducible rtTA (*R26::Lox-Stop-Lox-rtTA-IRES-EGFP*) and varying titers of Adeno-Cre were used to activate *rtTA* and *Twist1* expression in a labelled subset of epithelial cells. The *mT/mG* biosensor was used as an indirect marker of *rtTA*⁺ cells (green), and dissemination was monitored in the branching morphogenesis assay. (B) Without doxycycline, *Twist1* expression was off, and organoids branched normally, with a mixture of red and green cells. (C) With doxycycline, *Twist1* expression was induced in green, *rtTA*⁺ cells, and organoids exclusively disseminated green cells. Red, *rtTA*⁻*Twist1*⁻ cells formed normal branched structures and did not disseminate. (D-E) The dose of Adeno-Cre was titrated to vary the number of *rtTA*⁺ cells per organoid, and branching and dissemination were quantified on day 7 in culture. With doxycycline, a high percentage of organoids disseminated cells, even at Adeno-Cre titers that produced few *rtTA*⁺*Twist1*⁺ cells per organoid (D). Increasing the number of *rtTA*⁺*Twist1*⁺ cells per organoid resulted in a decrease in branching (E). *n*, total # of organoids; *r*, # of biological replicates. Error bars indicate SD. (F) Adeno-Cre-transduced *R26::LSL-rtTA;TRE-Twist1;mT/mG* organoids were transplanted into cleared mammary fat pads of 3-week-old NOD/SCID mice. *Twist1* expression was induced prior to transplantation by overnight incubation with doxycycline and maintained in vivo with doxycycline feed for 2 weeks. (G) Red, *Twist1*⁻ cells maintained epithelial organization. Green, *Twist1*⁺ cells appeared mesenchymal and protrusive and disseminated locally into the fat pad. (H) Small, disorganized clusters of exclusively green cells containing *Twist1*⁺ cells. Gamma adjustments were performed in panels (G) and (H) to improve image clarity. Bars: (B, C) 20 μm; (G', G'', H') 10 μm.

Figure 4-8

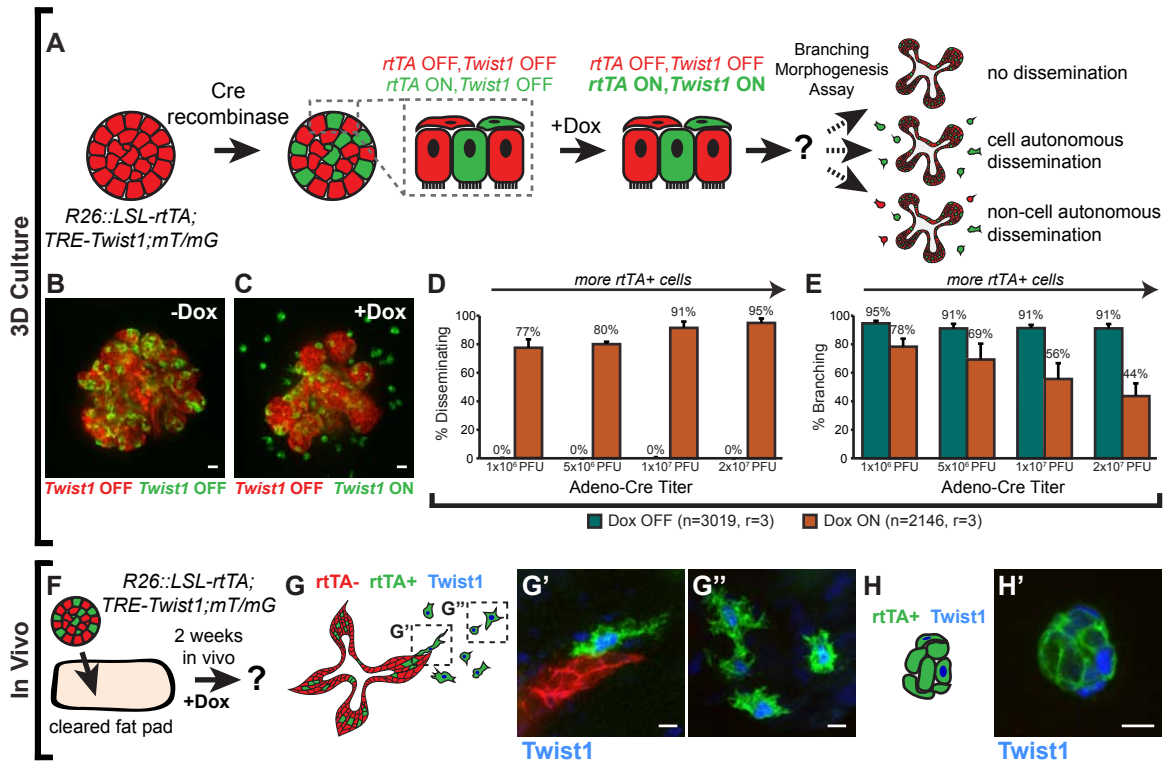


Figure 4-9. Twist1 induced single cell dissemination despite membrane-localized adherens junction proteins. (A,B) *E-cad* deletion blocks branching and induces epithelial disorganization. (C) Rare *E-cad*⁻ disseminated cells maintain a rounded morphology. (D,E) *Twist1* expression blocks branching and induces single cell dissemination (red arrowheads). (F) Disseminated *Twist1*⁺ cells exhibit extensive actin-rich protrusions (red arrows). (G) In time-lapse movies, *E-cad*⁻ cells were only rarely observed to disseminate. In contrast, >100 cells per *Twist1*⁺ organoid were routinely observed to disseminate. *n*, # of time-lapse movies; *r*, # of biological replicates. (H) By western blot, *Twist1* expression resulted in reductions in protein levels of *E-cad*, *N-cad*, α *E-catenin*, and β -*catenin* (see Fig. 4-10A,B). Whole cell lysate samples were loaded for equal protein based on BCA analysis. (I-N) Membrane-localized *E-cad* and β -*catenin* (white arrowheads) were detected in basally positioned cells protruding into the ECM (I, L), in cells that had just disseminated (J, M), and in disseminated cells migrating through the ECM (K, N). Bars: (B, E) 20 μ m; (C, F, I-N) 10 μ m.

Figure 4-9

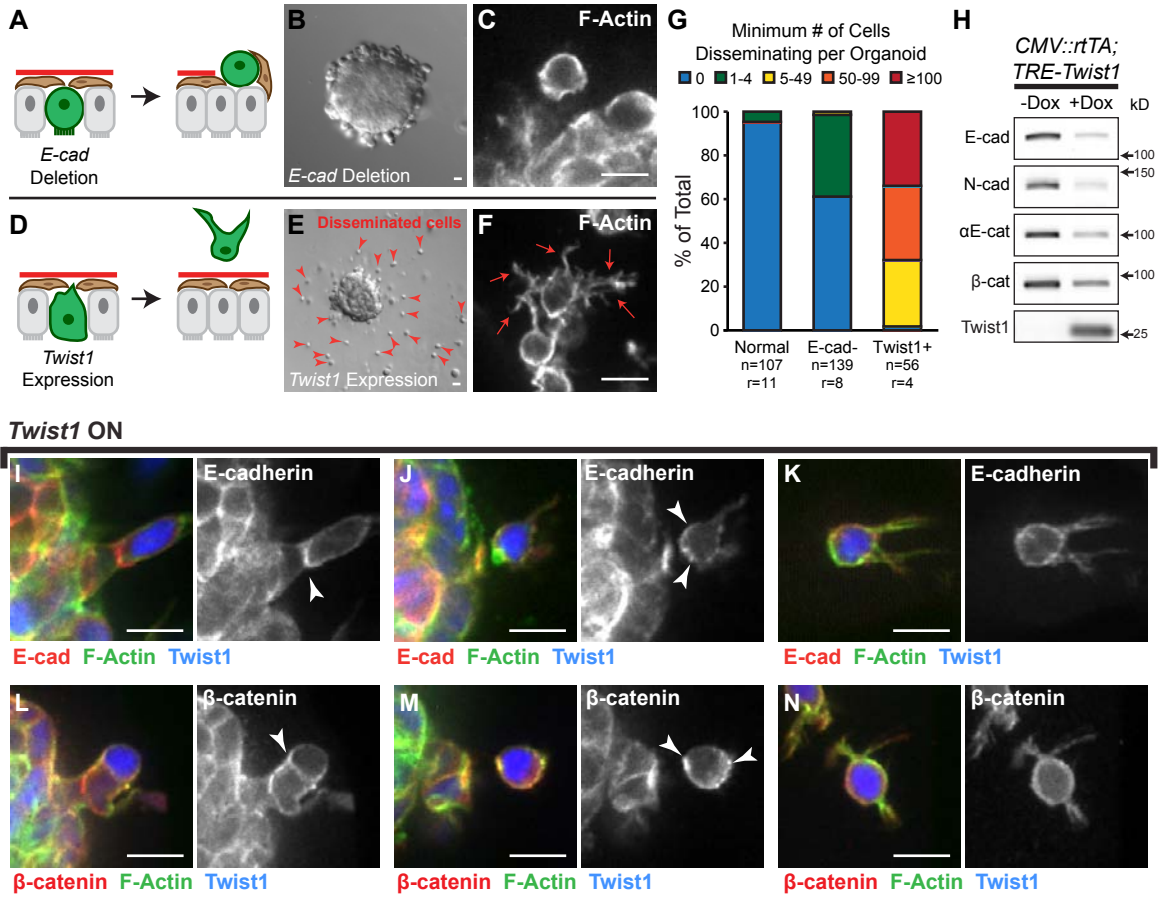
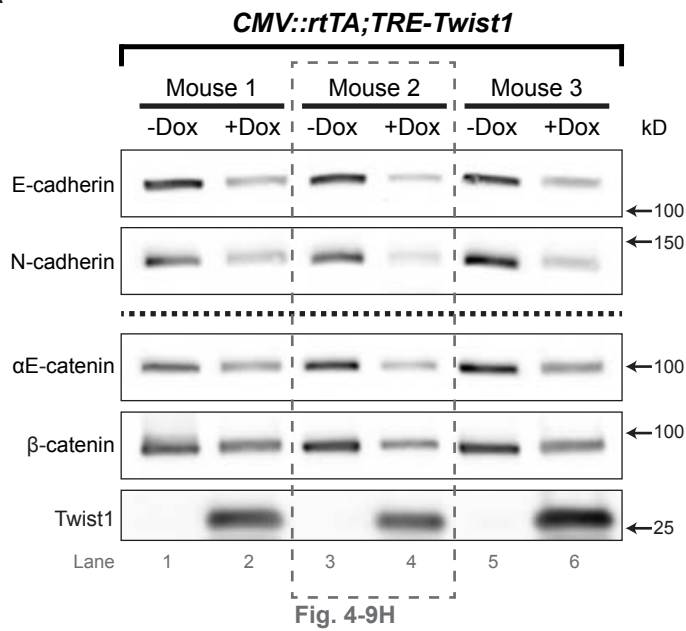


Figure 4-10. Adherens junction protein levels were partially reduced in *Twist1*-expressing tissue. (A) Organoids were isolated from three *CMV::rtTA;TRE-Twist1* mice, and *Twist1* expression was induced with doxycycline in half of the organoids from each mouse. Protein was extracted after 5 days of *Twist1* induction and assayed for levels of adherens junction components by western blot. Whole cell lysate samples were loaded for equal protein based on BCA analysis. The dotted line indicates two separate blots, prepared from the same samples in parallel, each probed with different antibodies. (B) Fiji was used to quantify intensity of all bands in (A). *Twist1* protein was verified to be absent without doxycycline ($***P=0.001$, Student's *t* test, 1-tailed, equal variance). E-cad, N-cad, α E-catenin, and β -catenin were all significantly reduced in *Twist1*-expressing tissue (Student's *t* test, 2-tailed, equal variance).

Figure 4-10

A



B

	Band Intensity						P-value
	Mouse 1		Mouse 2		Mouse 3		
	-Dox	+Dox	-Dox	+Dox	-Dox	+Dox	
E-cadherin	5618	2086	4941	1002	4725	2025	0.002
N-cadherin	4854	2237	4831	1109	7006	2091	0.01
αE-catenin	4163	2724	4940	1626	5876	3468	0.03
β-catenin	8057	5683	7208	3499	7299	5397	0.02
Twist1	218	9331	113	7443	175	12348	0.001

Figure 4-11. Twist1 induced changes in genes regulating cell-ECM interactions and the extracellular space. (A) RNA-seq was used to compare gene expression 48 h after *Twist1* induction in control versus *Twist1*⁺ organoids. (B) Heat map of canonical EMT genes. Only *Twist1* was significantly differentially expressed. Genes are sorted by increasing p-value. (C-F) The 183 DE genes were mapped to direct associations with GO Slim biological process (C) and cellular component (E) terms. Black vertical bars indicate the expected number of DE genes per category. Asterisks specify significantly enriched terms. (D) DE genes associated with “cell adhesion”. (F) DE genes associated with “extracellular space”, “extracellular region”, and “proteinaceous ECM”. Genes are sorted by descending fold change in (D) and (F). BP, biological process; CC, cellular component.

Figure 4-11

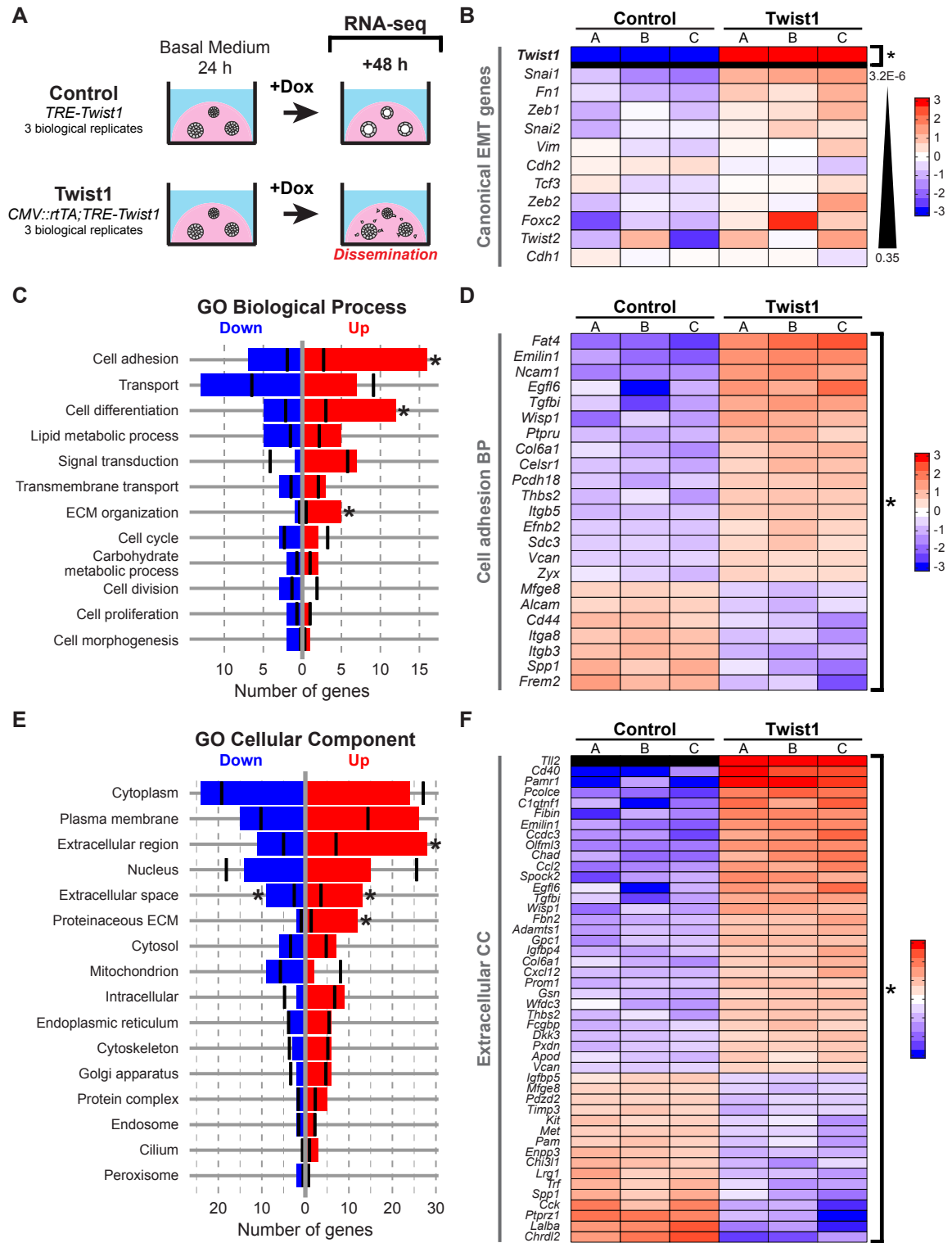


Figure 4-12. Heat maps of DE genes within relevant GO Slim biological process and cellular component categories. (A-D) Heat maps of DE genes associated with the GO biological process categories: transport (A), cell differentiation (B), lipid metabolic process (C), and signal transduction (D). (E-F) Heat maps of DE genes associated with the GO cellular component categories: cytoplasm (E) and plasma membrane (F). Genes are sorted by descending fold change. BP, biological process; CC, cellular component.

Figure 4-12

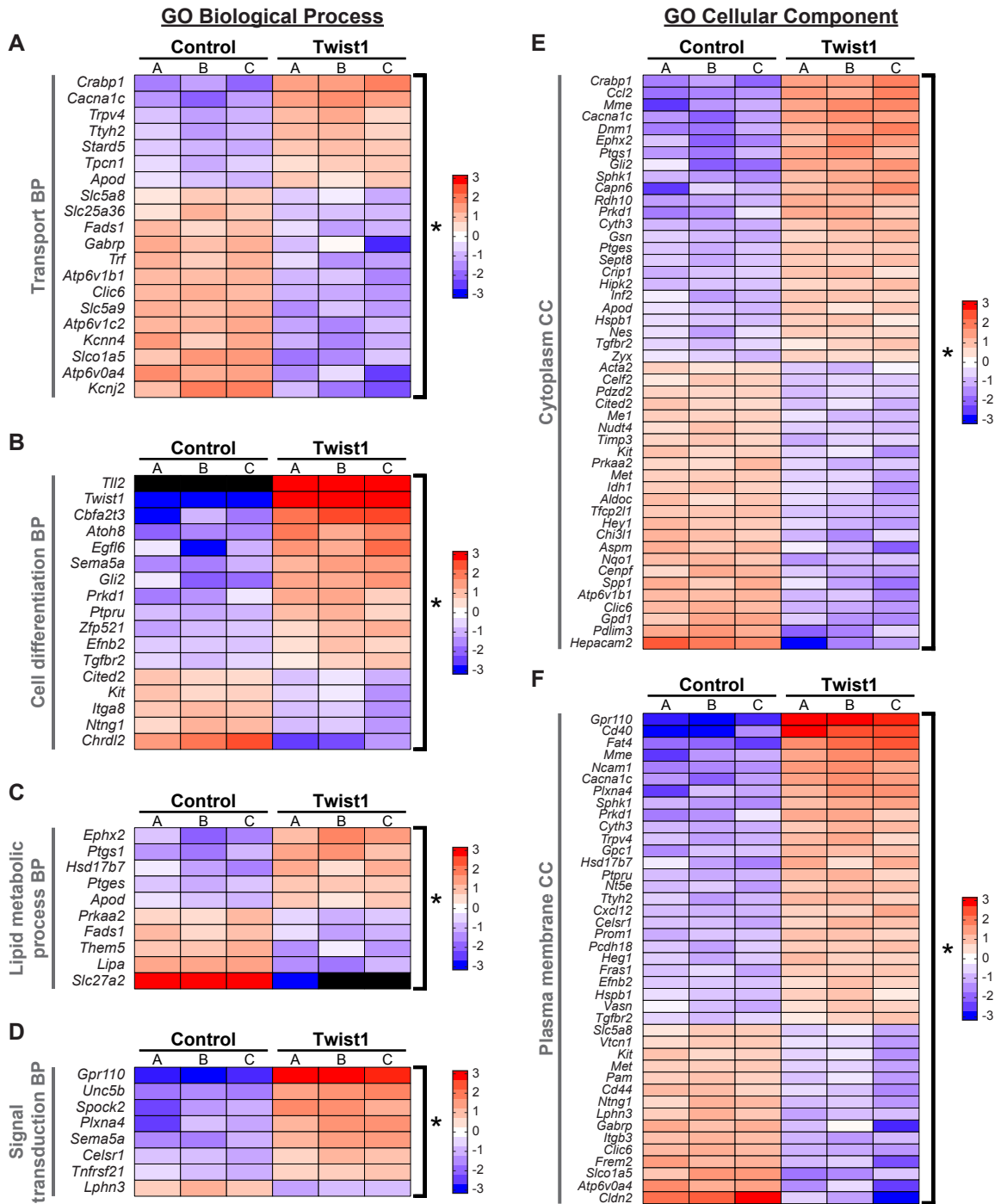


Figure 4-13. Enzymatic activities upregulated by Twist1 offer candidate targets for blocking dissemination. (A) The 183 DE genes were mapped to direct associations with GO Slim molecular function terms. Black vertical bars indicate the expected number of DE genes per category. No terms were significantly enriched. (B) Heat map of DE genes associated with kinase activity and phosphatase activity. Genes are sorted by descending fold change. MF, molecular function.

Figure 4-13

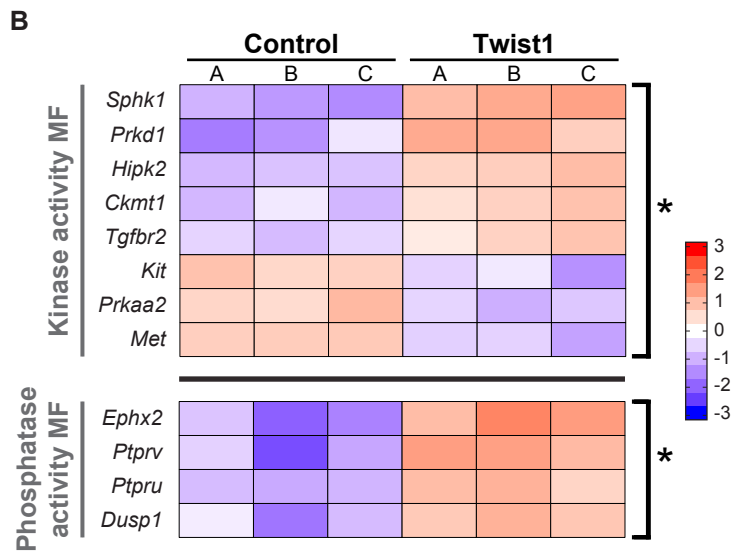
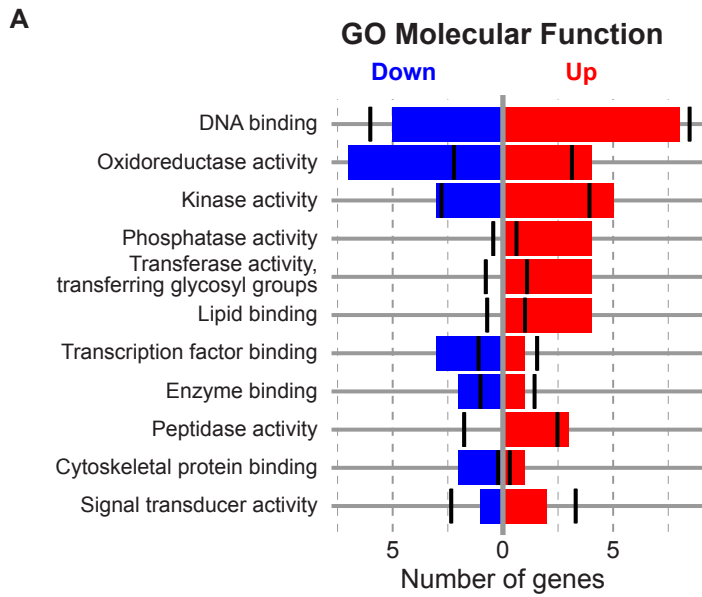


Figure 4-14. Significantly enriched pathways relate to cell-matrix adhesion. (A-B)
Gene set enrichment analysis (GSEA) identified 8 significant canonical pathways (A), all related to cell-matrix adhesion and ECM organization, and 51 significant curated gene sets, 13 of which were characterized as cancer-related (B). The Circos plots depict DE genes associated with each gene set. PID, Pathway Interaction Database.

Figure 4-14

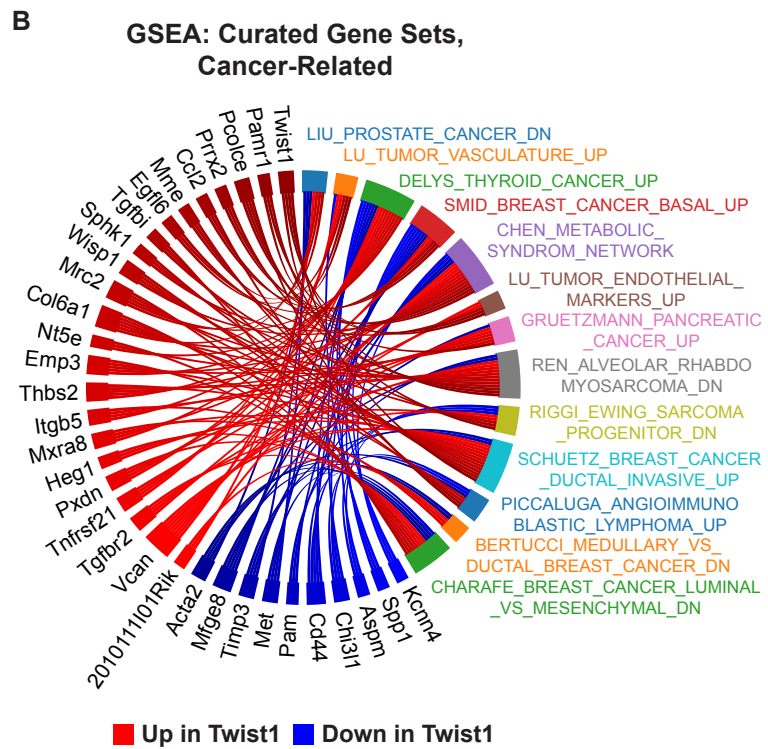
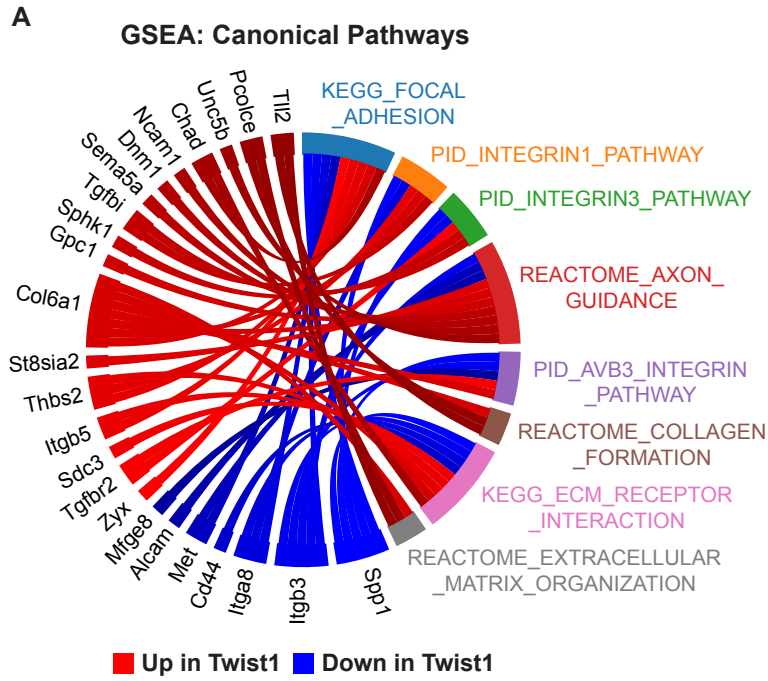
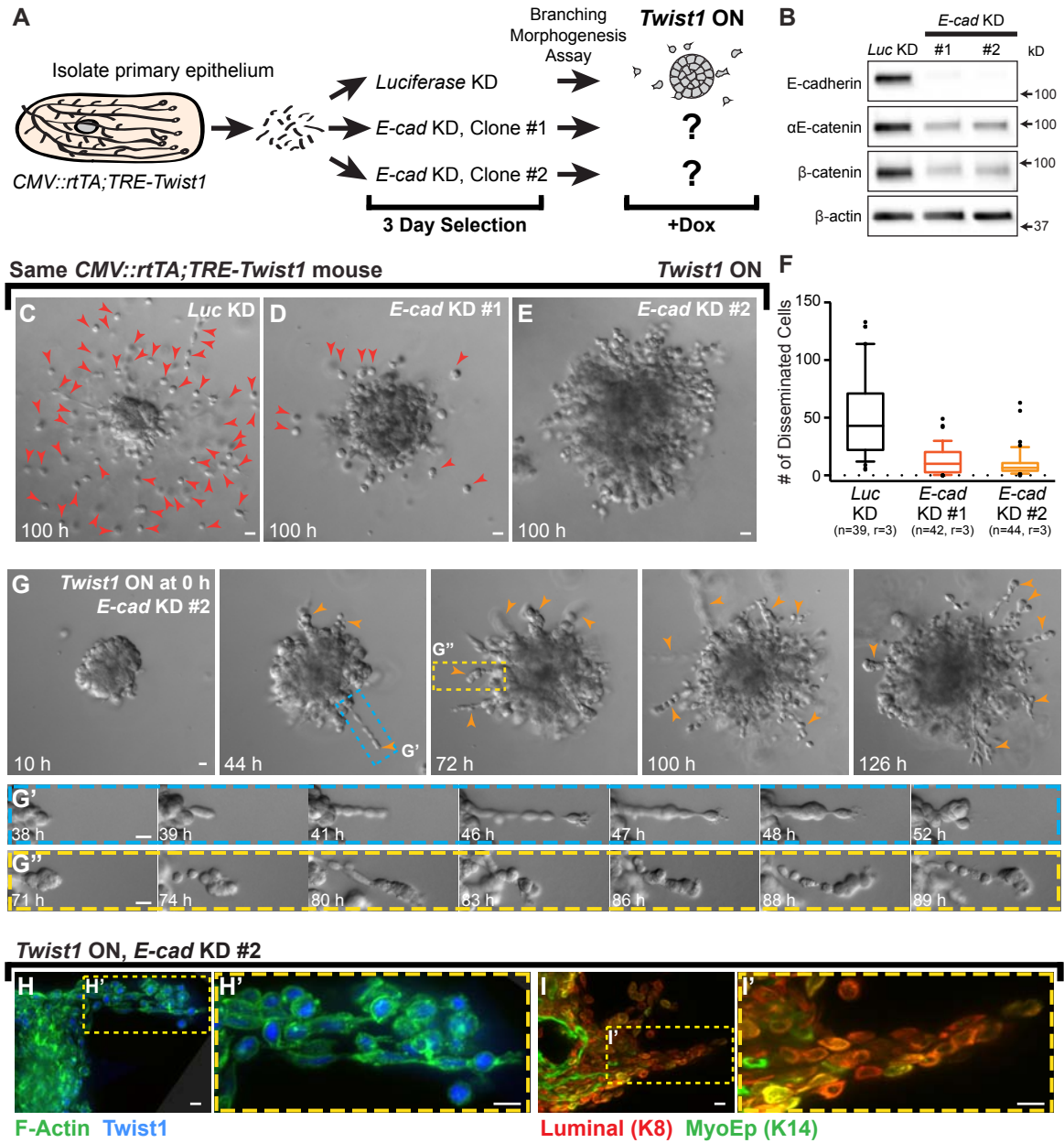


Figure 4-15. E-cad is required for Twist1-induced single cell dissemination. (A) Organoids from *CMV::rtTA;TRE-Twist1* mice were divided into three groups for treatment with lentiviral shRNA against *Luc* or *E-cad* (two clones). Puromycin was used to select for transduced cells. Organoids were monitored for dissemination following *Twist1* induction. (B) *E-cad* shRNA induced loss of E-cad protein and reductions in α E-catenin and β -catenin. Whole cell lysate samples were loaded for equal protein based on BCA analysis. (C-E) In FGF2-containing medium with doxycycline, *E-cad* KD organoids disseminated significantly fewer cells than *Luc* KD organoids. Red arrowheads in (C) and (D) indicate disseminated cells. (F) Disseminated cells per organoid were quantified from movies after 100 h of *Twist1* induction. *E-cad* knockdown significantly reduced single cell dissemination. Box-and-whisker plots are drawn with the box extending from the 25th to 75th percentiles and whiskers at the 10th and 90th percentiles. n, # of time-lapse movies; r, # of biological replicates. ****P<0.0001 between *Luc* shRNA and *E-cad* shRNA #1 or #2; *P=0.014 between *E-cad* shRNA #1 and #2 (Negative Binomial Generalized Estimating Equations model). (G) *E-cad* KD organoids extended collective chains of cells into the matrix (orange arrowheads) (G',G''). (H,I) Cells within collective chains stained positive for Twist1 and luminal (K8⁺) and/or myoepithelial (K14⁺) cytokeratins. Bars: (C-E, G) 20 μ m; (H, I) 10 μ m.

Figure 4-15



CHAPTER 5

Dissemination of Twist1⁺ epithelial cells involves directional amoeboid migration and is regulated by heterotypic cell-cell dynamics

Abstract

Cancer metastasis requires the dissemination and migration of cancer cells away from the primary tumor. However, the difficulty in visualizing cell and tissue dynamics in vivo has made it challenging to understand how cells accomplish this task. To date, most of our insight into cellular mechanisms of 3D migration comes from studies of fibroblasts embedded in gels of extracellular matrix (ECM). No in vitro model has allowed for direct, real-time observation of migration by epithelial cells starting from a whole tissue. We recently described a novel assay to study this process, in which acute, inducible expression of the transcription factor *Twist1* is sufficient to induce rapid and robust dissemination of otherwise normal cells out of primary mouse mammary epithelium. Here, we leveraged this model to study how *Twist1*⁺ epithelial cells initially detach from a multicellular, adherent tissue and migrate through the ECM as single cells. We found that these cells disseminated and migrated by filopodal, amoeboid motility, and their initial migration path showed high directional persistence. Using electron microscopy, we observed that *Twist1*⁺ cells at the basal tissue surface and in the ECM appear to clear the surrounding matrix at sites of protrusive activity, consistent with our previous findings that *Twist1* significantly regulates genes in the extracellular compartment. We hypothesize that *Twist1*⁺ cells may use proteolysis and ECM remodeling to facilitate forward motility at the leading edge. Another fundamental component of dissemination is that it arises from a heterogeneous cell population. Using cell type-specific fluorescent reporters, we found that other epithelial cells can serve as regulators of dissemination. In particular, our data provide support that basal myoepithelial cells can restrict the dissemination of inner luminal cells, the primary cell of origin in breast cancer.

Introduction

Cell migration plays an essential role in the morphogenesis of a variety of tissue types and also in the pathogenesis of disease processes such as cancer metastasis. A rich literature has demonstrated that cells migrate on 2D substrates via planar protrusions called lamellipodia that form due to actin polymerization. In contrast, there has been an increasing recognition of a diversity and plasticity of cell migration modes in 3D extracellular matrix (ECM) environments^{1,2}. Broadly, these modes can be subdivided into single cell versus collective cell migration. Single cell migration is further distinguished by amoeboid versus mesenchymal motility, which differ in the degree of cell adhesion to the ECM and the distribution of Rac and Rho/ROCK activity¹. Mesenchymal typically describes cells with a fibroblast-like, spindle-shaped morphology, a high level of focalized adhesion to the matrix, cytoskeletal contractility, and movement like fibroblasts¹. In contrast, amoeboid typically describes cells with a rounded or ellipsoid morphology and movement generated by cortical filamentous actin, without mature focal contacts, stress fibers, and focalized proteolytic activity¹. Studies of cell migration in 3D have also demonstrated that the composition and organization of the ECM can determine whether cells migrate by proteolytic mechanisms that remodel the ECM or by non-proteolytic mechanisms that involve shape changes to pass through the ECM^{1,3}. Importantly, much of the insight into 3D migratory mechanisms has relied upon studies that start from single cells, such as leukocytes, fibroblasts, and cancer cells. They do not model the process of dissemination and migration away from an intact epithelium, the first step in cancer metastasis.

We recently demonstrated that acute *Twist1* expression was sufficient to induce rapid and robust dissemination of otherwise normal, single mammary epithelial cells out of a

tissue (*CMV::rtTA;TRE-Twist1* mouse)⁴. Furthermore, we found that fluorescently labelled, genetic mosaic expression of *Twist1* resulted in cell autonomous dissemination of *Twist1*⁺ cells (*R26::LSL-rtTA;TRE-Twist1;mT/mG* mouse)^{1,4}. We next sought to characterize the migratory strategy of disseminating cells and the dynamic interactions between disseminating cells and cells remaining in the epithelium. We used fluorescent reporters to track in real-time the behavior of *Twist1*⁺ cells or specific mammary epithelial cell types following *Twist1* activation. Our data demonstrate that *Twist1*⁺ cells migrate by filopodal, amoeboid motility, and their migration path away from the epithelium is remarkably persistent. In addition, while dissemination is cell autonomous, non-cell autonomous cellular regulators within the tissue, including *Twist1*⁻ cells and basal myoepithelial cells, appear to limit whether dissemination is successfully accomplished.

Results

Twist1⁺ cells extrude from the basal layer and detach by forward filopodal protrusions and rear retraction

We first sought to identify the sequence of events as *Twist1*-expressing cells leave an epithelium. We used a Cre-inducible rtTA (*R26::LSL-rtTA*^{1,5}), a fluorescent Cre biosensor (*mT/mG*^{1,6}), and a low titer of Adeno-CMV-Cre to induce rare, genetic mosaic activation of *Twist1* such that we could track the behavior of individual rtTA⁺Twist1⁺ cells (green) in real-time (Fig. 5-1A). In culture medium with doxycycline, red, Cre⁻ cells were consistently Twist1⁻, whereas green, Cre⁺ cells were Twist1⁺ (Fig. 5-1B-B').

We used time-lapse microscopy to monitor the behavior of isolated Twist1⁺ cells within genetic mosaic organoids. Dissemination of Twist1⁺ cells was observed to occur even from epithelium that was mostly Twist1⁻ and organized into polarized, simple architecture (Fig. 5-1C). We distinguished two key steps in initial cell escape. First, Twist1⁺ cells near the basal surface extended protrusions into the ECM perpendicular to the plane of the epithelium. As these forward protrusions lengthened, the main cell body appeared to progressively squeeze out of the epithelium, until the cell had completely extruded from the basal layer onto the surface of the organoid (Fig. 5-D-D'). Second, the extruded cell again elaborated forward protrusions and squeezed the cell body at the rear to fully detach from the epithelium (Fig. 5-1E-E'). Morphologically, protrusions consistently appeared filopodal and the shape and behavior of the cell body appeared amoeboid.

Protrusive cells at the basal surface appear well connected to the main epithelium by multiple classes of cell-cell junctions

We previously observed that *Twist1*⁺ cells retained membrane-localized E-cadherin and β -catenin at every stage of dissemination: protrusion into the ECM, detachment from the epithelium, and migration in the ECM^{1,3,4}. E-cadherin and β -catenin were particularly concentrated at the rears of cells that had just detached. To further resolve the junctions at these cell-cell borders, we sought to define the ultrastructure of cells during dissemination.

In order to reliably identify and characterize disseminating cells by transmission electron microscopy (TEM), we analyzed epithelium in which *Twist1* is ubiquitously expressed (*CMV::rtTA;TRE-Twist1* organoids cultured with doxycycline). We focused our analysis on basally positioned cells that were protruding into the ECM (Fig. 5-2A,B). Surprisingly, protrusive cells appeared closely apposed to neighboring cells. Moreover, we observed desmosomes (Fig. 5-2A') and other morphologically distinct junctions (Fig. 5-2A'',D-D'',E,F, yellow arrowheads) connecting protrusive cells to other cells within the epithelium. Some of these junctions appear tight junction-like, but we will require higher resolution TEM and immunofluorescence to definitively identify their composition. Nevertheless, combined with the positive immunoreactivity for adherens junction proteins, these data suggest that *Twist1*⁺ cells retain multiple classes of cell-cell junctions during active dissemination.

We next used TEM to examine the cell surfaces in contact with ECM. Normal epithelium maintains a smooth, organized basal tissue surface, without any protrusions into the ECM^{4,7}. In contrast, the leading edges of protrusive *Twist1*⁺ cells contained extensive submicron membrane protrusions, both in regions of nascent protrusive activity (Fig. 5-2A''',C, red arrowheads) and in more elongated filopodia (Fig. 5-2A''''', red arrowheads).

In the ECM proximate to these protrusions, we commonly observed matrix clearing, characterized by a decrease in electron density relative to the surrounding Matrigel (Fig. 5-2C, orange dashed line). We expect that these protrusions and matrix modification reflect the consequences of *Twist1*'s significant transcriptional regulation of genes in the extracellular compartment⁴.

Luminal cells can disseminate through gaps in the myoepithelium

Mature mammary epithelium forms simple, bi-layered ducts composed of an inner luminal epithelial cell layer and an outer myoepithelial cell layer. We previously observed that constitutive *Twist1* expression induces dissemination of both major mammary cell types, using immunofluorescence for cell type-specific cytokeratins⁴. Furthermore, we detected disrupted tissue organization within the main epithelial group, with internal localization of myoepithelial cells and basement membrane and corresponding gaps in myoepithelial and basement membrane coverage at the basal tissue surface in contact with ECM. We next sought to correlate the integrity of the myoepithelium with luminal cell dissemination.

We used a genetically encoded, myoepithelial-specific fluorescent reporter (*K14::Actin-GFP*) and a ubiquitous membrane fluorescent marker (*mT/mG*) to characterize the dynamic interactions between luminal and myoepithelial cells in *CMV::rtTA;TRE-Twist1* epithelium (Fig. 5-3A). In real-time, we observed that luminal cells (red) disseminated through gaps in the myoepithelium (green) (Fig. 5-3B, white arrows indicate gaps). Interestingly, non-disseminating myoepithelial cells at the basal surface appeared to restrain luminal cell dissemination (Fig. 5-3C). Some luminal cells that invaded past the myoepithelium successfully disseminated (Fig. 5-3C, orange arrowhead) whereas others were dynamically covered and contained by myoepithelial cells (Fig. 5-3C, purple

arrowhead). Taken together, our data suggest that the integrity of the myoepithelium may regulate the ability of internal luminal cells to disseminate.

Myoepithelial cell ingression results in internal myoepithelial-lined tunnels

We next sought to identify the mechanism by which myoepithelial cells are internally localized in response to constitutive *Twist1* expression (Fig. 5-4A). We observed by immunofluorescence that myoepithelial cells ($K14^+$) formed multicellular networks within the epithelium and appeared to enclose acellular internal spaces (Fig. 5-4B). We anticipated two possibilities: (1) phenotypic conversion of internal luminal cells to a myoepithelial program; or (2) myoepithelial ingression from the basal surface. Using the myoepithelial-specific fluorescent reporter (*K14::Actin-GFP*), we observed that individual basal myoepithelial cells migrated inward into internal epithelial layers (Fig. 5-4C-D). These cells could appear elongated and protrusive, and they dynamically detached from and reattached to cells within the basal myoepithelium (Fig. 5-4C'-C''). This type of ingression resulted in single, isolated, internal myoepithelial cells (Fig. 5-4C'-C''). Alternatively, ingressing myoepithelial cells were also observed to form interconnected networks that spanned the length of the organoid, such that it was difficult to distinguish individual cells (Fig. 5-4D'-D''). *Twist1* may therefore induce a migratory program in myoepithelial cells reflected as both dissemination away from the epithelium and ingression into the epithelium. Another possibility is that increased cell-matrix adhesion in $Twist1^+$ luminal epithelial cells results in a general scrambling of tissue architecture (Zev Gartner, personal communication, 2014). While the cellular mechanism remains unknown, the resulting tissue organization compromises the integrity of the basally positioned myoepithelium as a putative barrier between luminal cells and the ECM.

We next used TEM to resolve the ultrastructure of internal myoepithelial cells in *CMV::rtTA;TRE-Twist1* organoids. Although we broadly observed disrupted tissue organization and polarity, we at times observed lumens that were electron lucid and surrounded by polarized cells. These cells contained microvilli and characteristic junctional distribution, with apically localized tight junctions and more distal desmosomes and adherens junctions (Fig. 5-5A-A’). In contrast, we frequently observed internal, electron-dense spaces, which we termed “tunnels” for their characteristically rounded morphology (Fig. 5-5A,C). Cells that lined these tunnels lacked apicobasal polarity and microvilli and instead maintained a smooth cell surface in contact with the tunnel interior, without detectable protrusions (Fig. 5-5B,C’,C’’,D). A single cell often extended around and enclosed at least half of the circumference of the tunnel (Fig. 5-5B,C’). The types of junctions connecting these cells to their neighbors were distinct from those observed in normal lumens and included long stretches of tight junction-like structures (Fig. 5-5B’, yellow arrowheads). Tunnels were also more electron-dense than normal lumens (Fig. 5-5A) and contained what appeared to be secreted material (Fig. 5-5D’). While we cannot identify with certainty that the cells lining these spaces are myoepithelial in origin, their morphology and localization is consistent with our observations by light microscopy. Moreover, the high electron density and likely secretory material within these tunnels correlates with our immunofluorescence staining of basement membrane adjacent to internal myoepithelial cells⁴.

Twist1⁻ cells can initiate re-epithelialization of disseminated Twist1⁺ cells

We anticipated that dissemination might be regulated not only by interactions between different mammary epithelial cell types but also by interactions between *Twist1*-expressing cells and wild-type cells. We therefore examined the heterotypic cell-cell interactions between Twist1⁻ and Twist1⁺ cells in genetic mosaic epithelium (*R26::LSL-*

rtTA;TRE-Twist1;mT/mG). In epithelium with a high fraction of Twist1⁺ cells, we observed extensive dissemination, with organoids mostly dissociating into single cells (green) but retaining a residual Twist1⁻ epithelial core (red) (Fig. 5-6A-B). Twist1⁻ cells within the epithelium were stretched basally into the ECM as they maintained contact with green, protrusive Twist1⁺ cells that appeared in the process of disseminating (Fig. 5-6B'-B''). We next used confocal microscopy to observe the real-time dynamics between these two cell populations. Interestingly, we identified a surprising behavior in which Twist1⁻ cells extended into the ECM and reinitiated attachment to disseminated Twist1⁺ cells (Fig. 5-6C-C''). In turn, the Twist1⁺ cell became less protrusive and rounded up upon reestablishment of this cell-cell border (Fig. 5-6C'-C''). Accordingly, we conclude that dynamic interactions between Twist1⁺ and Twist1⁻ cells may limit the ability of disseminated Twist1⁺ cells to migrate away from the epithelium.

Twist1⁺ cells migrate in the ECM with amoeboid motility

We next sought to describe the migratory behavior of disseminated cells. The *K14::Actin-GFP* reporter allowed us to directly observe the actin dynamics during migration (Fig. 5-7A,B). Cells squeezed through the matrix in stereotypic cycles, with a protrusive filopodia at the front and a smooth, rounded cell body at the rear. During each cycle, the main cell body gradually redistributed from the rear to the front, with constriction in the middle (Fig. 5-7A',B'). In the final retraction phase, actin was concentrated at the rear of the cell (Fig. 5-7A,B, red arrowheads). When stationary, cells were observed to sometimes have multiple protrusions in different directions, as if sampling their surroundings. When migrating, the protrusions were consistently localized at the front, leading the cell body. Consistent with this morphology, by TEM, we observed filopodia at the migrating fronts of disseminated cells (Fig. 5-7C,D, blue arrowheads). Interestingly, we identified electron dense, membrane-bound structures

both internal to the cell, near the filopodium (Fig. 5-7C'), and external to the cell, outside the main cell body (Fig. 5-7D') and at the filopodal front (Fig. 5-7D''). Similar to our analysis of protrusive cells at the basal tissue surface (Fig. 5-2C), we identified matrix clearing around membrane protrusions (Fig. 5-7C'', orange dashed line) and particularly around regions of these darkly staining extracellular vesicles (Fig. 5-7D'-D'', orange dashed lines). We hypothesize that these structures may be exosomes and thus play a role in remodeling the ECM. Such paracellular proteolysis and ECM modification would be consistent with Twist1's significant regulation of genes involved in ECM composition and organization⁴.

Disseminating Twist1⁺ cells demonstrate high persistence in their initial migration path away from the epithelium

We next asked to what extent dissemination involved random versus directional cell migration. Using DIC time-lapse movies from three biological replicates of *CMV::rtTA;TRE-Twist1* epithelium, we tracked the migration paths of a minimum of ten disseminating cells per organoid in eleven organoids (Fig. 5-8A-B shows tracks for Organoid #5). Tracking was performed from initial, discernable epithelial detachment for a minimum of 10 hours, with an average duration of 17 hours across all organoids. We generally focused on the earliest disseminating cells to easily distinguish the tracked cell from other migrating cells nearby. Persistence was calculated as the displacement divided by the total track length and averaged among tracked cells for each organoid. The mean of the mean persistence across organoids was 0.61 with a standard deviation of 0.04 (Fig. 5-8C), indicating a remarkable consistency across organoids and biological replicates. A persistence of 0.61 can be visually interpreted in an organoid (#5) with a mean persistence equal to this value (Fig. 5-8A-B) and in an individual migrating cell with a persistence equal to this value (Fig. 5-8D). In conclusion, disseminating Twist1⁺

cells appear to have relatively high directional persistence in a radial migration pattern away from the main organoid.

Discussion

In this study, we sought to describe the cellular basis for dissemination and migration of Twist1⁺ epithelial cells. Twist1, a bHLH transcription factor, has emerged as a major putative regulator of metastasis and is thought to operate by causing cells to undergo an epithelial-to-mesenchymal transition. However, we recently demonstrated that Twist1 induced dissemination of normal mammary epithelial cells that expressed cytokeratin and adhesion proteins and maintained epithelial-specific gene expression⁴. Thus, dissemination occurred with retention of epithelial identity at the molecular level. Here, our data provide further support for the concept that disseminating cells can also retain epithelial character at the cellular level. Twist1 did not induce a transition to mesenchymal morphology or migration strategy. Rather, disseminating epithelial cells displayed an amoeboid mode of migration with filopodal kinetics at the cell front.

By TEM, we observed matrix clearing around ECM-directed protrusions and around darkly staining extracellular vesicles, which we speculate may be exosomes. ECM proteolysis at the leading edge is not normally coupled with amoeboid morphology. Nevertheless, we previously found that Twist1 significantly regulated genes important in the composition and organization of the extracellular matrix. In turn, we hypothesize that these transcriptional changes may manifest as Twist1⁺ cells digesting the matrix to clear a path forward. Interestingly, our tracking of cells as they disseminate revealed a high persistence in their initial migration path. Stabilized, actin-rich filopodia can maintain the orientation of a cell's leading edge⁸. We speculate that the observed protrusive activity and ECM remodeling at the front of Twist1⁺ cells may together accomplish directionally persistent migration away from the epithelium during dissemination.

A major unresolved question from our previous work was why some Twist1⁺ cells disseminated while many remained in the epithelium. Our data now suggest that cell dissemination is regulated by at least two distinct heterotypic cell-cell interactions between (1) myoepithelial and luminal cells, and (2) Twist1⁻ and Twist1⁺ cells. In epithelium with constitutive *Twist1* expression, myoepithelial cells that remain at the basal surface appear to contain luminal cells invading into the ECM. In turn, we observed luminal cell dissemination through gaps in the myoepithelium. Together, our observations support the hypothesis that the integrity of the myoepithelium may influence the ability of luminal cells to disseminate. Interestingly, focal disruptions in the myoepithelium serve as a negative prognostic indicator in clinical management of ductal carcinoma in situ⁹, and myoepithelial cells have been posited to function as suppressors of tumor cell invasion^{10,11}. We expect that Twist1-induced myoepithelial dissemination and ingression result in gaps in the basal myoepithelial layer that directly expose luminal cells to the ECM and may facilitate their escape. Furthermore, we speculate that retention of a normal (Twist1⁻) myoepithelium may physically obstruct Twist1⁺ cell dissemination. This would be consistent with our finding that Twist1⁻ cells within a genetic mosaic epithelium initiate contact with disseminated Twist1⁺ cells and mediate their re-epithelialization. While we cannot distinguish the specific cell type of these Twist1⁻ cells in real-time, our data collectively suggest that they may be normal myoepithelial cells. Future studies would need to validate this putative barrier function through myoepithelial-specific genetic or chemical perturbation. More broadly, the ability of such heterotypic cell-cell interactions to limit cell escape has implications for our conceptual understanding of breast cancer metastasis and which cells within a tumor are likely protective versus invasive.

Materials and methods

Mouse strains. The *CMV::rtTA* transgenic line was a kind gift of Feng Cong and Harold Varmus (National Cancer Institute, Bethesda, MD). The *K14::Actin-GFP* transgenic line¹² was a kind gift of Elaine Fuchs (The Rockefeller University, New York, NY). The *Twist1-tetO₇-luc* (*TRE-Twist1*) transgenic line was previously described¹³. *mT/mG*⁶ and *R26::Lox-Stop-Lox-rtTA-IRES-EGFP* (*R26::LSL-rtTA*)⁵ mouse lines were acquired from the Jackson Laboratory. Mouse husbandry and procedures were all conducted under an IACUC-approved animal protocol.

Isolation and 3D culture of primary mammary epithelial organoids. We used a combination of mechanical disruption, collagenase/trypsin digestion, and differential centrifugation to purify fragments of primary mammary epithelial ducts, termed “organoids”, as previously described^{4,7,14,15}. Organoids were embedded in 3D Matrigel (354230; BD Biosciences) at 2-3 organoids/ μ L and plated as 100 μ L suspensions in 24-well coverslip-bottomed plates (662892; Greiner Bio-One) over a 37°C heating block. Gels were allowed to polymerize for 30 min at 37°C and then cultured in organoid medium: DMEM (D6546; Sigma) with 1% Insulin-Transferrin-Selenium (51500-056; GIBCO) and 1% Penicillin-Streptomycin (P4333; Sigma). Branching morphogenesis was induced with 2.5 nM FGF2 (F0291; Sigma). To generate genetic mosaic *Twist1* expression, prior to embedding in Matrigel, *R26::LSL-rtTA;TRE-Twist1;mT/mG* organoids were infected with Adeno-Cre (Vector Biolabs #1045), as previously described⁴. Viral titer was adjusted in order to modulate the percent recombination. For all experiments, *Twist1* expression was induced by supplementing organoid medium with 5 μ g/mL doxycycline (Shanghai RenYoung Pharmaceutical Co., Ltd), and medium was replaced every 48 h.

Confocal microscopy. Confocal imaging was performed on a spinning-disk confocal microscope (Solamere Technology Group) with an XR/MEGA-10 S30 camera (Stanford Photonics, Inc.), as previously described^{16,17}. An LD C-Apochromat 40X/1.1 W Korr objective lens (Carl Zeiss) was used for high magnification single and time-lapse image acquisition, with water and oil used as the imaging mediums, respectively. Acquisition of both fixed and time-lapse images was performed using a combination of μ Manager¹⁸ and Piper (Stanford Photonics, Inc.). Imaris (Bitplane) was used to analyze time-lapse movies, place scale bars, and export individual TIFFs. Adobe Photoshop CS5 was used as needed to adjust levels for each channel on entire images to maximize image clarity.

Differential interference contrast (DIC) microscopy. Time-lapse imaging of mammary organoids was conducted using an LD Plan-Neofluar 20X/0.4 Korr Ph2 objective lens and a Cell Observer system with an AxioObserver Z1 and an AxioCam MRM camera (Carl Zeiss). Images were acquired at 20-min intervals for 5-7 days. Temperature was maintained at 37°C and CO₂ at 5%. AxioVision (Carl Zeiss) was used to analyze time-lapse movies, place scale bars, and export individual TIFFs. Adobe Photoshop CS5 was used to adjust levels on entire images to maximize image clarity.

Glycosaminoglycan staining with ruthenium red. We isolated epithelium from a *CMV::rtTA;TRE-Twist1* mouse and cultured organoids for 5 d in Matrigel in medium with 2.5 nM FGF2 and 5 μ g/mL doxycycline. Embedded organoids were then fixed in 3% glutaraldehyde to preserve for shipping to Lawrence Berkeley National Laboratory. There, samples were high-pressure frozen either unstained or stained using Luft's Ruthenium Red (RR) method¹⁹ in combination with microwave-assisted processing. All microwaving procedures were carried out using a Pelco Biowave microwave oven with a

Pelco ColdSpot insert cooled by a Pelco SteadyTemp chilled cooling system (Ted Pella Inc., Redding, CA). Briefly, samples were microwaved in 0.05% RR in 0.1 M sodium cacodylate buffer at 150 W for 1-min-ON, 1-min-OFF, 1-min-ON and rinsed three times by microwaving in fresh buffer for 40 s at 150 W. Samples were then microwaved in 0.05% RR and 1% osmium tetroxide for 1-min-ON, 1-min-OFF, 1-min-ON at 150 W and rinsed three times by microwaving in fresh buffer for 40 s at 150 W. Samples were stored in 0.1 M sodium cacodylate buffer at 4°C until high-pressure freezing.

High-pressure freezing, freeze substitution, and resin embedding. Both unstained and RR-stained samples were placed in 1-mm-wide by 200- μ m-deep aluminum freezing hats and, before freezing, were surrounded with 20% BSA, used as a cryoprotectant. Samples were then cryoimmobilized using a high-pressure freezer (HPM-010; Bal-tec, Inc.) and freeze-substituted in 1% osmium tetroxide and 0.1% uranyl acetate in acetone, as previously described²⁰. Upon completion of freeze substitution, samples were progressively infiltrated with an epon-araldite resin using a quick infiltration procedure, as previously described²¹. Polymerization in epon-araldite resin was performed by flat embedding between two glass slides at 60°C overnight to allow for precise localization of features of interest²².

TEM. Samples were sectioned into 70–90-nm-thin sections using an Ultramicrotome (UC6; Leica). Sections were then collected onto formvar-coated, rhodium-enforced copper 2-mm slot grids. The grids were post-stained with 2% uranyl acetate followed by Reynold's lead citrate, for 5 min each. The sections were imaged using a Tecnai 12 TEM (FEI), operated between 480x and 18500x at 120 kV under normal conditions. Images were recorded using an Orius SC1000B CCD with Digital Micrograph 3 software (Gatan Inc.).

Montaging TEM images. SerialEM software was used to collect wide-field montages for overview imaging of complete organoid cross-sections, as well as for high-magnification imaging of large regions of interest containing multicellular features²³. The mosaic of images obtained by SerialEM was reconstructed using the *blendmont* utility in the IMOD software package, which aligns the smaller images and blends overlapping edges²⁴. ImageJ software²⁵ and Photoshop CS4 (Adobe Systems Inc., San Jose, CA) were used to crop images, place scale bars, and adjust brightness and contrast on entire images, as needed.

Immunofluorescence. Organoids grown in Matrigel were fixed in 4% paraformaldehyde for 10 min, rinsed three times in PBS for 10 min, embedded in Optimal Cutting Temperature compound (OCT), and frozen at -80°C. OCT blocks were sectioned at 50- μ m thickness by cryostat at -20°C. Sections were placed on Superfrost Plus Gold microscope slides (15-188-48; Fisherbrand) and stored at -80°C. For antibody staining, samples were thawed at room temperature, rinsed twice in PBS for 10 min to remove OCT, permeabilized with 0.5% Triton X-100 for 1 h, and rinsed twice in PBS for 10 min. Samples were blocked for 1–3 h with 10% FBS/1% BSA, incubated with primary antibodies overnight at 4°C in 1% FBS/1% BSA, and rinsed three times in 1% FBS/1% BSA for 15 min. Incubation with secondary antibodies was conducted in 1% FBS/1% BSA overnight at 4°C. Slides were rinsed three times in PBS for 10 min, mounted with Fluoromount (F4680; Sigma-Aldrich), and sealed with coverslips. Primary antibodies used were rat anti-cytokeratin-8 (1:100; TROMA-I; Developmental Studies Hybridoma Bank), rabbit anti-cytokeratin-14 (1:500; PRB-155P; Covance), and mouse anti-Twist1 (1:50; sc-81417; Santa Cruz Biotechnology Inc.). Secondary antibodies used were all Alexa Fluor-conjugated antibodies (1:200; Invitrogen).

Cell tracking. Imaris (Bitplane) was used to perform tracking on at least 10 cells per movie in a total of 11 movies of *CMV::rtTA;TRE-Twist1* organoids across three biological replicates. All organoids were cultured in organoid medium with 2.5 nM FGF2 and 5 $\mu\text{g}/\text{mL}$ doxycycline. Tracks were generated for cells that could be followed from initial detachment over at least 10 h. The center of the main cell body was used as the reference point across frames. Cells were tracked until they were not longer visible (e.g., migrated out of focus) or alternatively began to divide or form a secondary site. Cells were excluded if they significantly interacted with surrounding disseminated cells. Persistence was calculated as the displacement divided by the total track length and averaged the persistence across all cells within a single movie.

References

1. Friedl, P. & Wolf, K. Plasticity of cell migration: a multiscale tuning model. *J. Cell Biol.* **188**, 11–19 (2010).
2. Friedl, P., Sahai, E., Weiss, S. & Yamada, K. M. New dimensions in cell migration. *Nat. Rev. Mol. Cell Biol.* **13**, 743–747 (2012).
3. Wolf, K. *et al.* Multi-step pericellular proteolysis controls the transition from individual to collective cancer cell invasion. *Nat. Cell Biol.* **9**, 893–904 (2007).
4. Shamir, E. R. *et al.* Twist1-induced dissemination preserves epithelial identity and requires E-cadherin. *J. Cell Biol.* **204**, 839–856 (2014).
5. Belteki, G. *et al.* Conditional and inducible transgene expression in mice through the combinatorial use of Cre-mediated recombination and tetracycline induction. *Nucleic Acids Res.* **33**, e51 (2005).
6. Muzumdar, M. D., Tasic, B., Miyamichi, K., Li, L. & Luo, L. A global double-fluorescent Cre reporter mouse. *genesis* **45**, 593–605 (2007).
7. Ewald, A. J. *et al.* Mammary collective cell migration involves transient loss of epithelial features and individual cell migration within the epithelium. *J. Cell. Sci.* **125**, 2638–2654 (2012).
8. Petrie, R. J., Doyle, A. D. & Yamada, K. M. Random versus directionally persistent cell migration. *Nat. Rev. Mol. Cell Biol.* **10**, 538–549 (2009).
9. Man, Y.-G. & Sang, Q.-X. A. The significance of focal myoepithelial cell layer disruptions in human breast tumor invasion: a paradigm shift from the ‘protease-centered’ hypothesis. *Exp. Cell Res.* **301**, 103–118 (2004).
10. Polyak, K. & Hu, M. Do myoepithelial cells hold the key for breast tumor progression? *J Mammary Gland Biol Neoplasia* **10**, 231–247 (2005).
11. Sternlicht, M. D. & Barsky, S. H. The myoepithelial defense: a host defense against cancer. *Med. Hypotheses* **48**, 37–46 (1997).
12. Vaezi, A., Bauer, C., Vasioukhin, V. & Fuchs, E. Actin cable dynamics and Rho/Rock orchestrate a polarized cytoskeletal architecture in the early steps of assembling a stratified epithelium. *Dev. Cell* **3**, 367–381 (2002).
13. Tran, P. T. *et al.* Twist1 Suppresses Senescence Programs and Thereby Accelerates and Maintains Mutant Kras-Induced Lung Tumorigenesis. *PLoS Genet* **8**, e1002650 (2012).
14. Ewald, A. J., Brenot, A., Duong, M., Chan, B. S. & Werb, Z. Collective epithelial migration and cell rearrangements drive mammary branching morphogenesis. *Dev. Cell* **14**, 570–581 (2008).
15. Nguyen-Ngoc, K.-V. *et al.* ECM microenvironment regulates collective migration and local dissemination in normal and malignant mammary epithelium. *Proc Natl Acad Sci USA* **109**, E2595–604 (2012).
16. Ewald, A. J., Werb, Z. & Egeblad, M. Dynamic, Long-Term In Vivo Imaging of Tumor-Stroma Interactions in Mouse Models of Breast Cancer Using Spinning-Disk Confocal Microscopy. *Cold Spring Harbor Protocols* **2011**, pdb.top97–pdb.top97 (2011).
17. Ewald, A. J. Practical Considerations for Long-Term Time-Lapse Imaging of Epithelial Morphogenesis in Three-Dimensional Organotypic Cultures. *Cold Spring Harbor Protocols* **2013**, pdb.top072884–pdb.top072884 (2013).
18. Edelstein, A. A., Amodaj, N. N., Hoover, K. K., Vale, R. R. & Stuurman, N. N. Computer control of microscopes using μ Manager. *Audio, Transactions of the IRE Professional Group on Chapter 14*, Unit14–Unit20 (2010).
19. Luft, J. H. Ruthenium red and violet. II. Fine structural localization in animal

- tissues. *Anat. Rec.* **171**, 369–415 (1971).
20. McDonald, K. L. & Webb, R. I. Freeze substitution in 3 hours or less. *J Microsc* **243**, 227–233 (2011).
 21. McDonald, K. L. Out with the old and in with the new: rapid specimen preparation procedures for electron microscopy of sectioned biological material. *Protoplasma* **251**, 429–448 (2014).
 22. Müller-Reichert, T., Hohenberg, H., O'Toole, E. T. & McDonald, K. Cryoimmobilization and three-dimensional visualization of *C. elegans* ultrastructure. *J Microsc* **212**, 71–80 (2003).
 23. Mastronarde, D. N. Automated electron microscope tomography using robust prediction of specimen movements. *J. Struct. Biol.* **152**, 36–51 (2005).
 24. Kremer, J. R., Mastronarde, D. N. & McIntosh, J. R. Computer visualization of three-dimensional image data using IMOD. *J. Struct. Biol.* **116**, 71–76 (1996).
 25. Abramoff, M. D., Magalhaes, P. J. & Ram, S. J. Image Processing with ImageJ. *Biophotonics* **11**, 36–42 (2004).

Figure 5-1

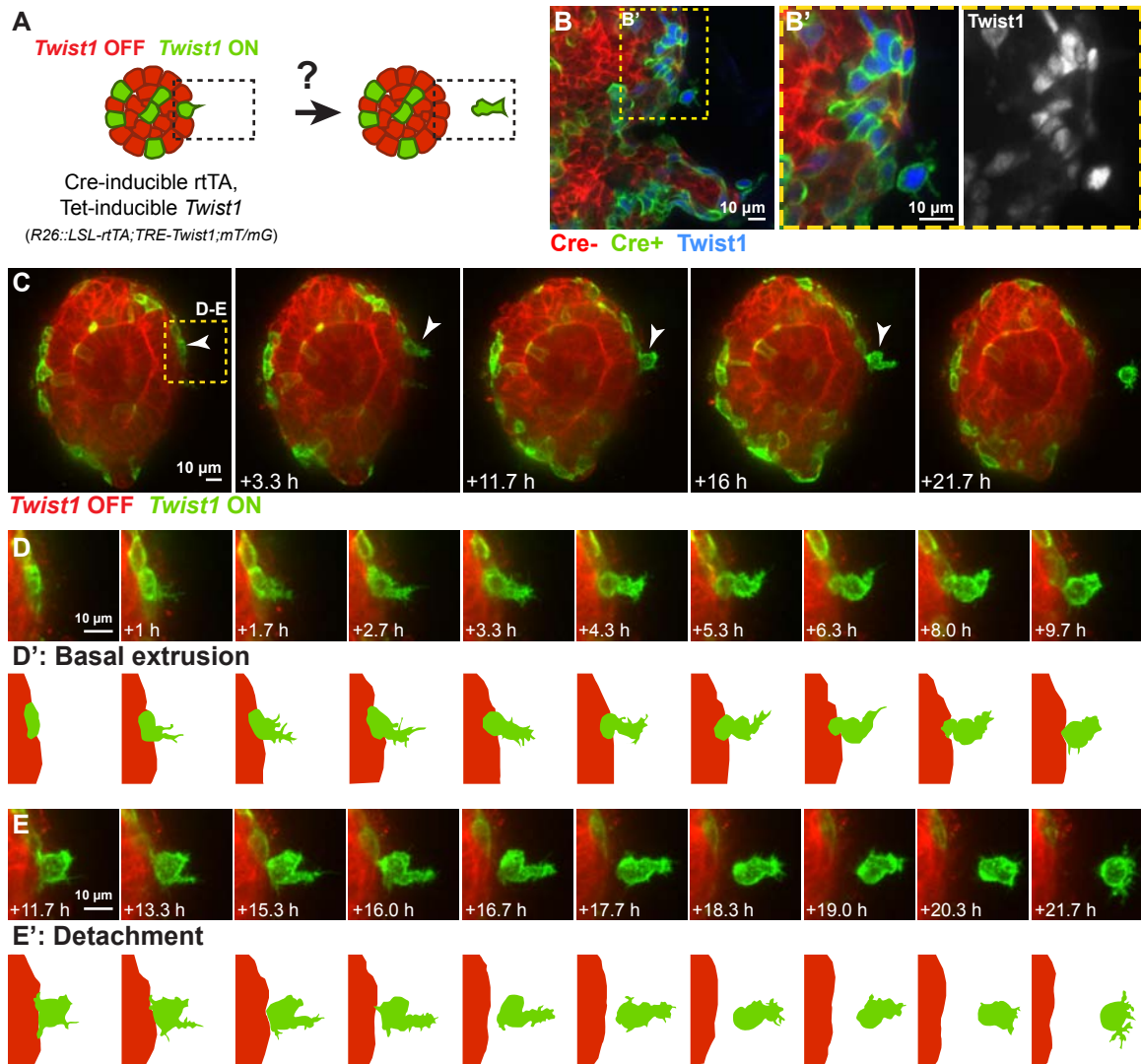


Figure 5-1. *Twist1*⁺ cells disseminated by successive basal extrusion and epithelial detachment. (A) A low titer of Adeno-CMV-Cre was used to induce rare genetic mosaic activation of *Twist1* in isolated *R26::LSL-rTA;TRE-Twist1;mT/mG* organoids. Dissemination of rTA⁺*Twist1*⁺ cells was monitored by confocal microscopy. (B) With doxycycline, green (Cre⁺) cells were *Twist1*⁺. (C-E) Rare *Twist1*⁺ cells were observed to disseminate from mostly *Twist1*⁻ epithelium by initial extrusion from the basal epithelial layer (D) followed by epithelial detachment (E).

Figure 5-2. Basal, protrusive Twist1⁺ cells were connected to the epithelium by multiple classes of intercellular junctions. TEM was used to examine the ultrastructure of basally positioned cells in *CMV::rtTA;TRE-Twist1* organoids cultured with doxycycline. (A) Protrusive cells maintained junctional connections to adjacent cells (A'-A'', yellow arrowhead) and extended membrane protrusions (A'''-A''''', red arrowheads) and filopodia (A''''') into the ECM. (B-C) Sites of membrane protrusion (C, red arrowheads) often corresponded with matrix clearing (C, orange dashed line). (D-F) Multiple cell-cell junctions with distinct ultrastructure, including long stretches of tight junction-like structures (D-D''), could be observed near the rear of a protrusive cell. Green pseudocolor in D demarcates a neighboring cell. Yellow arrowheads indicate intercellular junctions. All TEM images are from high-pressure frozen, freeze-substituted samples that were pre-fixed with 3% glutaraldehyde. The sample shown in panels B-F was stained with ruthenium red. Des, desmosome.

Figure 5-2

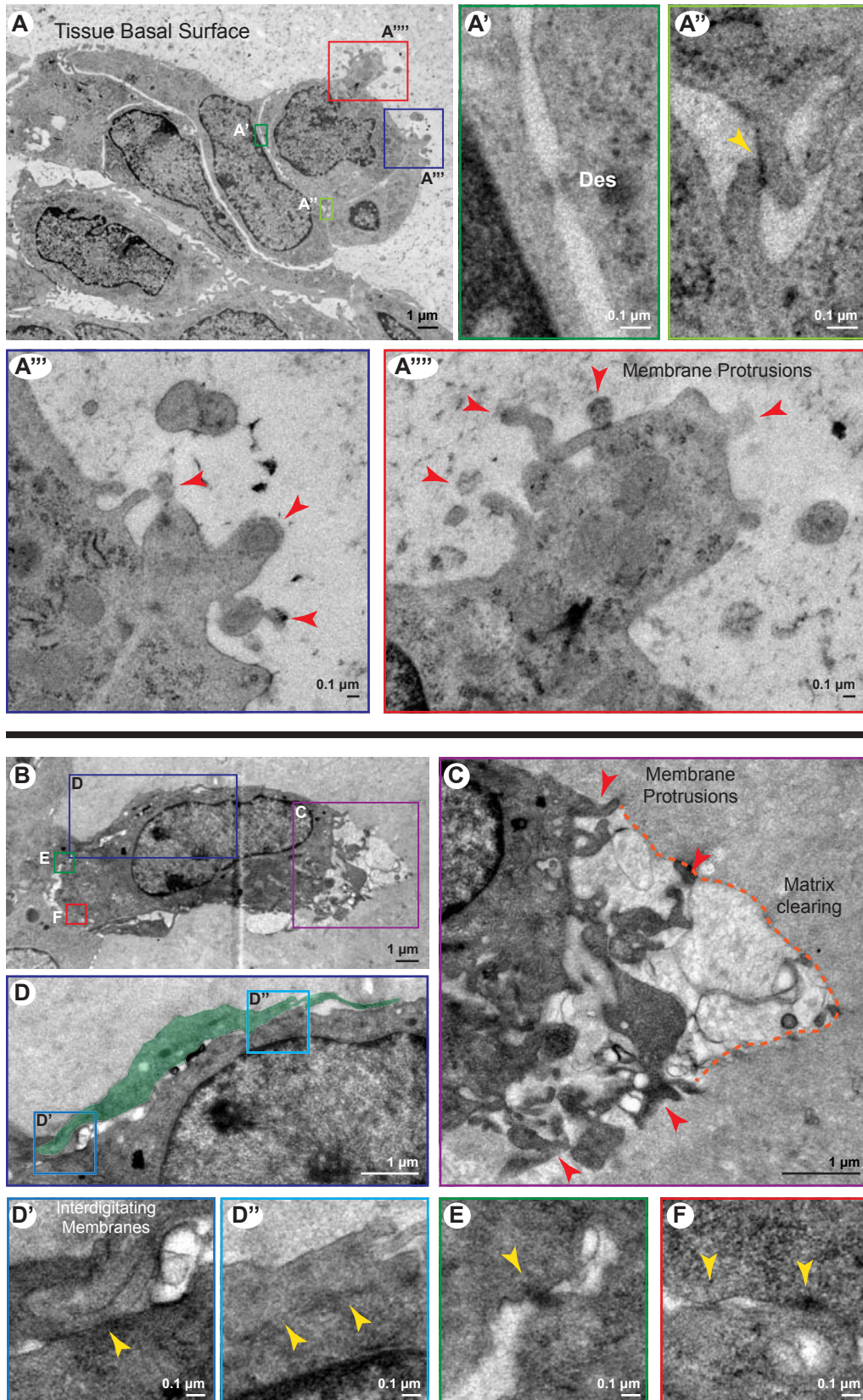


Figure 5-3

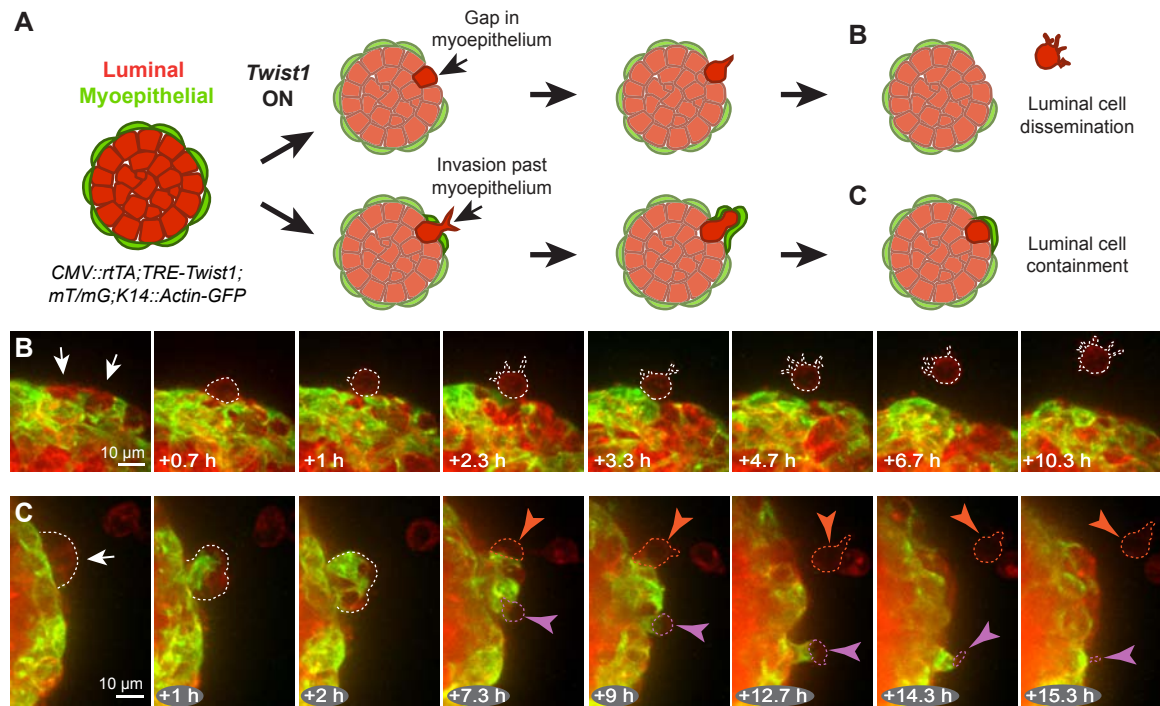


Figure 5-3. The status of the myoepithelium could influence luminal cell dissemination. (A) Fluorescent reporters were used to distinguish the real-time interactions between myoepithelial cells (*K14::Actin-GFP*, green) and luminal cells (*mT/mG*, red) in epithelium with constitutive *Twist1* expression. (B) Luminal cells (white dotted line) were observed to disseminate through gaps in the myoepithelium (white arrows). (C) Luminal cells that invaded past a seemingly intact myoepithelium (white arrow) sometimes disseminated (orange dotted line and arrowhead) and other times were contained (purple dotted line and arrowhead) by myoepithelial cells.

Figure 5-4. Twist1 induced myoepithelial ingression into the epithelium. (A) A myoepithelial-specific fluorescent reporter (*K14::Actin-GFP*, green) was used to identify the cellular mechanism driving internal myoepithelial cell localization in organoids with constitutive *Twist1* expression. (B) By immunofluorescence, myoepithelial cells ($K14^+$) frequently lined acellular internal spaces. (C-D) By confocal microscopy, myoepithelial cells were observed to migrate inward from the basal surface and exhibit dynamic individual cell motility (C-C'') or establish multicellular networks with other ingressing myoepithelial cells (D-D'').

Figure 5-4

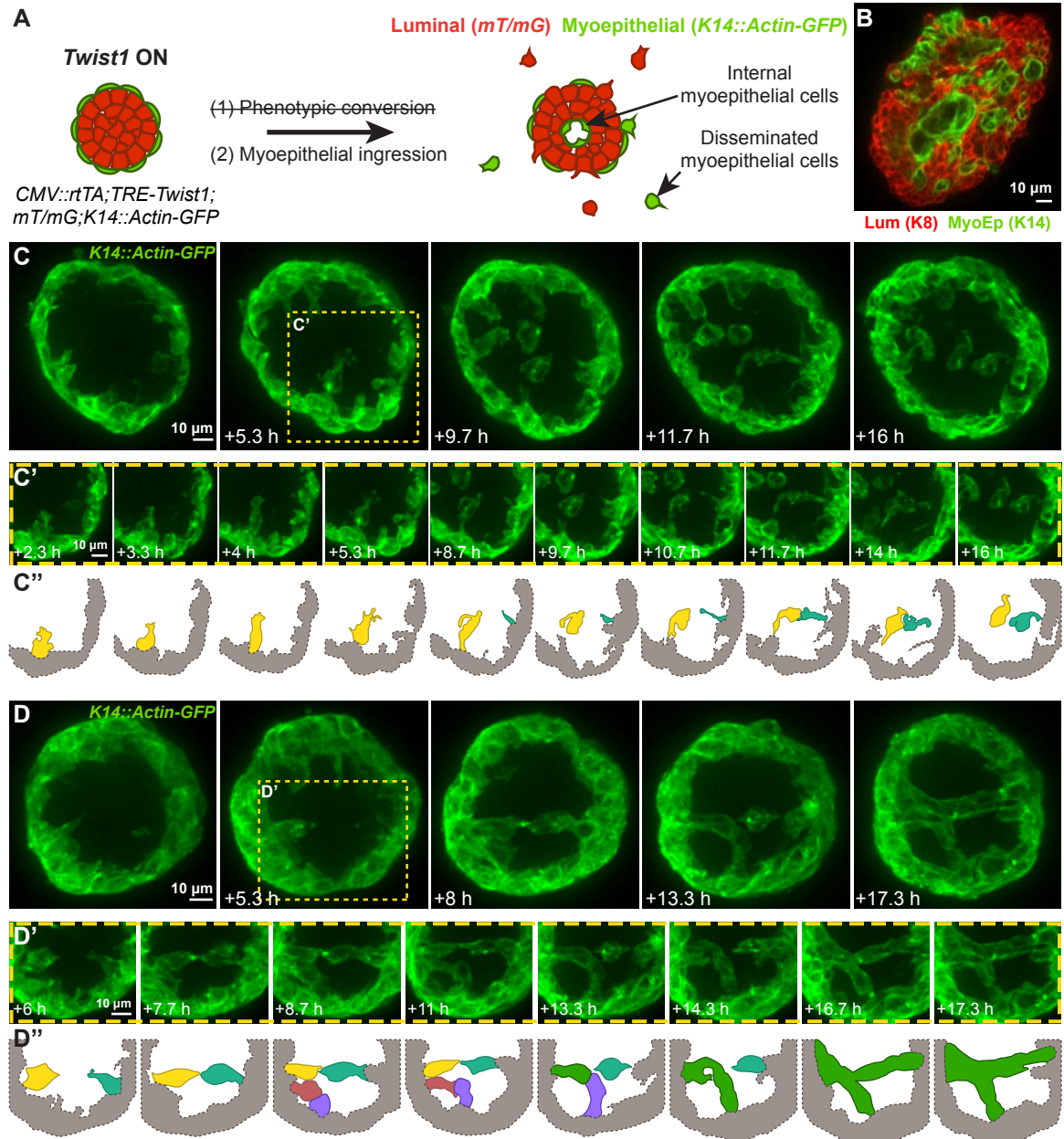


Figure 5-5. *Twist1*-expressing epithelium frequently contained electron-dense tunnels. (A) *CMV::rtTA;TRE-Twist1* epithelium had rare, morphologically normal lumens that were surrounded by cells with microvilli (A') and normal spatial configuration of intercellular junctions (A'-A''). (B-D) More commonly, the epithelium contained multiple abnormally shaped "tunnels" that were more electron-dense than normal lumens. Cells that lined these tunnels lacked microvilli, possessed distinct junctions with adjacent cells (B', yellow arrowheads), and appeared elongated and extended around the surface area of the tunnel (B, C', C'', D, pseudocolors). (D') Tunnels had dark and irregularly staining secretory material. All TEM images are from high-pressure frozen, freeze-substituted samples that were pre-fixed with 3% glutaraldehyde and stained with ruthenium red. Des, desmosome; TJ, tight junction; AJ, adherens junction.

Figure 5-5

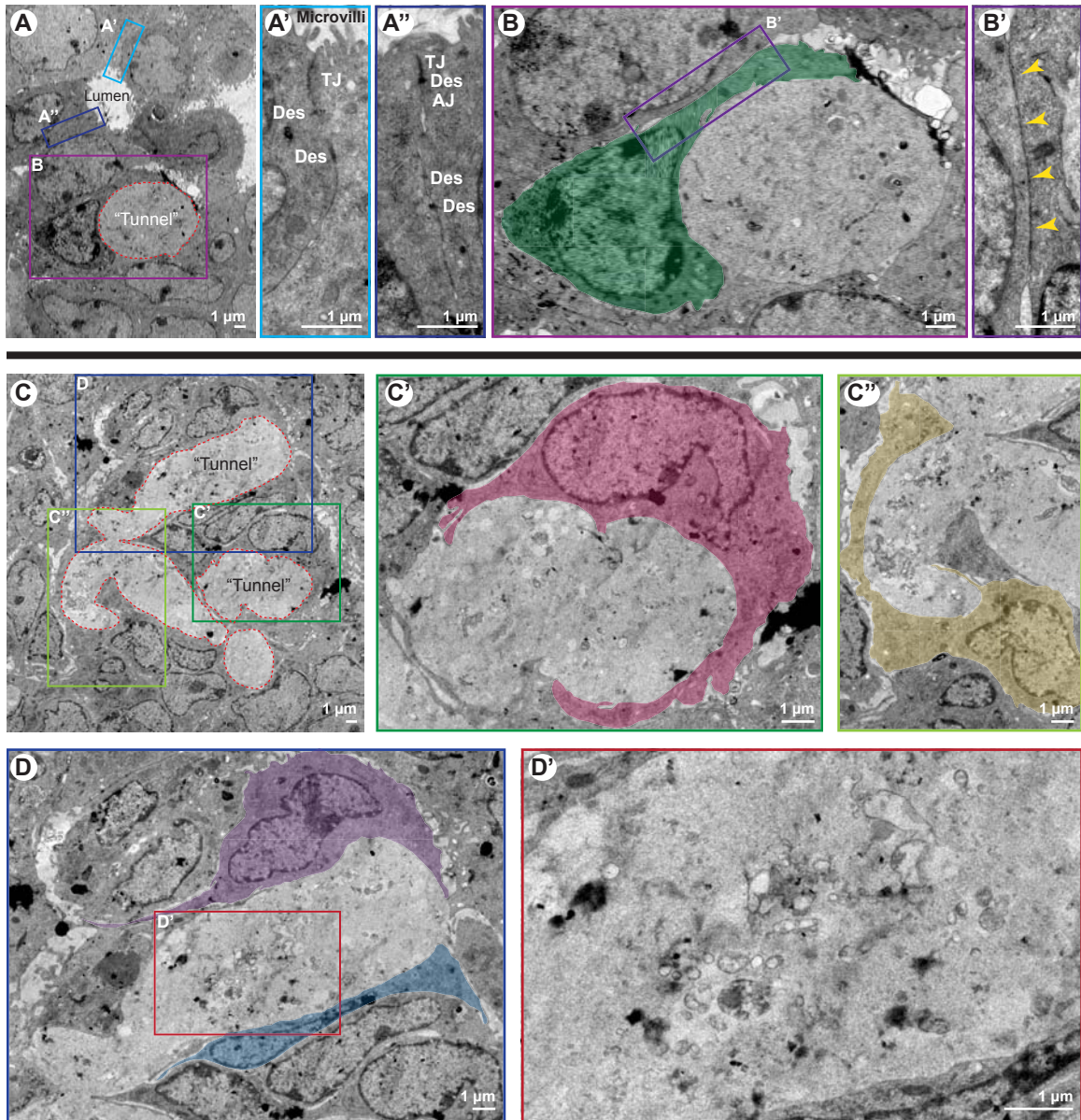


Figure 5-6

R26::LSL-rtTA;TRE-Twist1;mT/mG

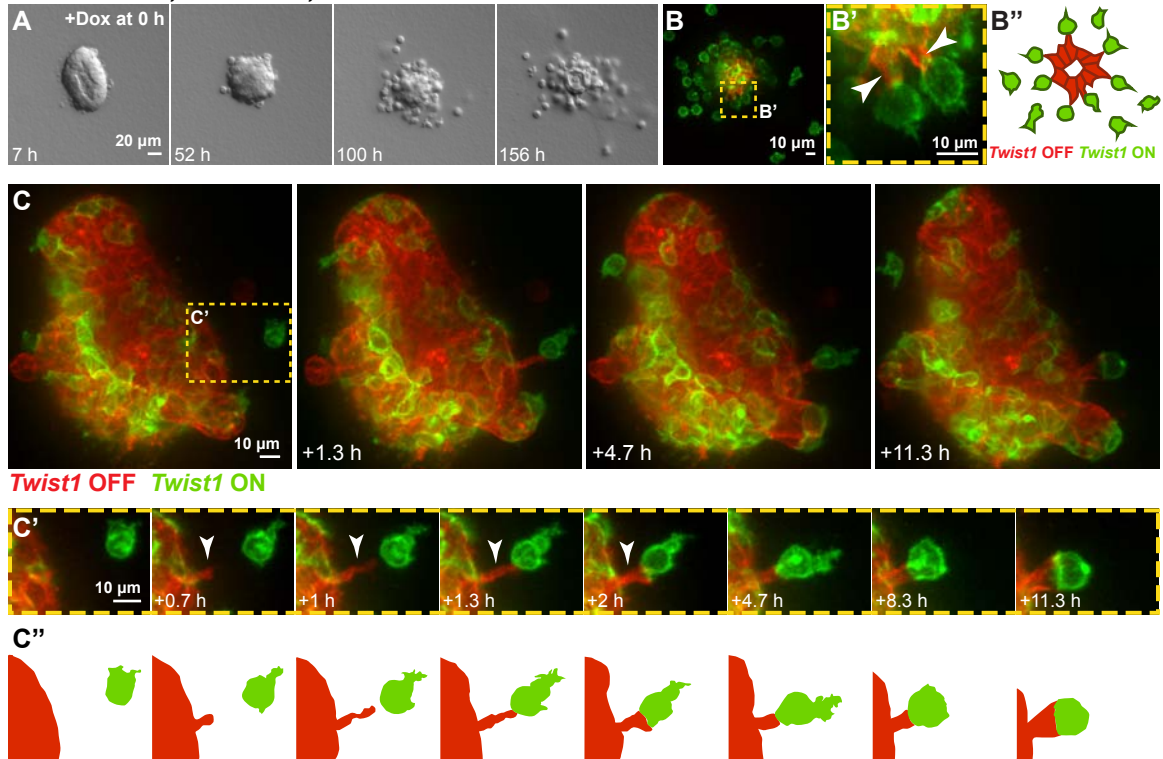
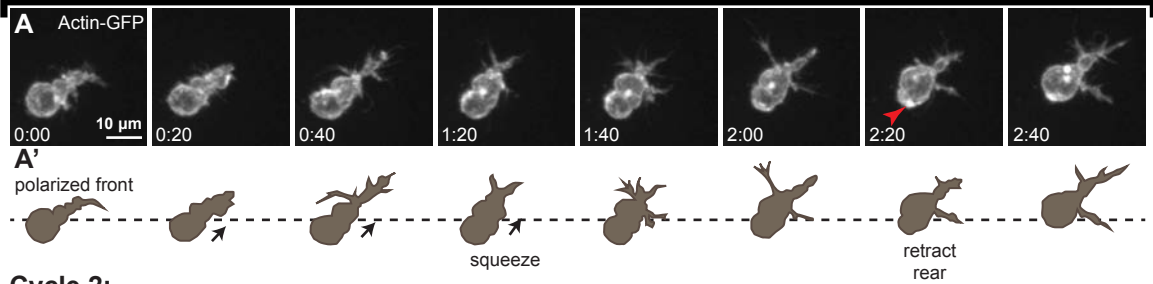


Figure 5-6. *Twist1*⁻ cells reattached to disseminated *Twist1*⁺ cells. (A) Adeno-CMV-Cre titers were used to induce a high percentage of *rtTA*⁺*Twist1*⁺ cells in isolated *R26::LSL-rtTA;TRE-Twist1;mT/mG* epithelium. Organoids mostly dissociated into single cells, but retained a cystic core. (B) Cre reporter activity confirmed that the epithelial core of the organoid in A was composed of red, *Twist1*⁻ cells, which appeared to be stretched basally into the ECM (white arrowheads) by green, *Twist1*⁺ cells (B'-B''). (C-C'') In real-time, *Twist1*⁻ were observed to reinitiate contact with disseminated *Twist1*⁺ cells and induce re-epithelialization.

Figure 5-7. Disseminated Twist1⁺ cells migrate by filopodal, amoeboid motility. (A-B) The *K14::Actin-GFP* reporter was used in *CMV::rtTA;TRE-Twist1* epithelium to visualize actin dynamics during cell migration in the ECM. Cells exhibited amoeboid motility and completed cycles of leading edge protrusion and cell body retraction, with actin accumulation at the rear (red arrowheads). (C-D) Filopodia were detected at the front of disseminated cells (blue arrowheads). Darkly staining, membrane-bound structures were observed just beneath the cell surface (C') and released into the ECM (D'-D''). Matrix clearing was visible around these structures (D'-D'') and around membrane protrusions (C'') (orange dashed lines). All TEM images are from high-pressure frozen, freeze-substituted samples that were pre-fixed with 3% glutaraldehyde. The black triangle in the bottom right corner of D is a region of the image mosaic where no pixels were collected.

Figure 5-7

Cycle 1:



Cycle 2:

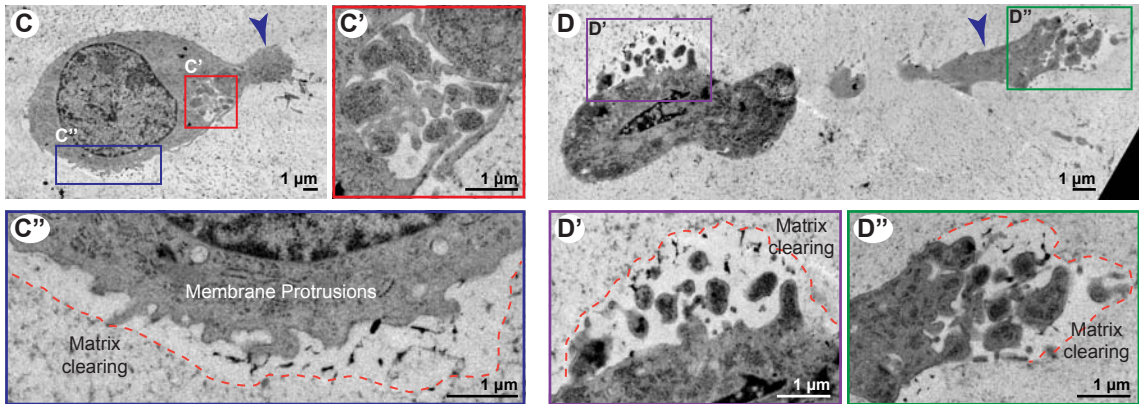
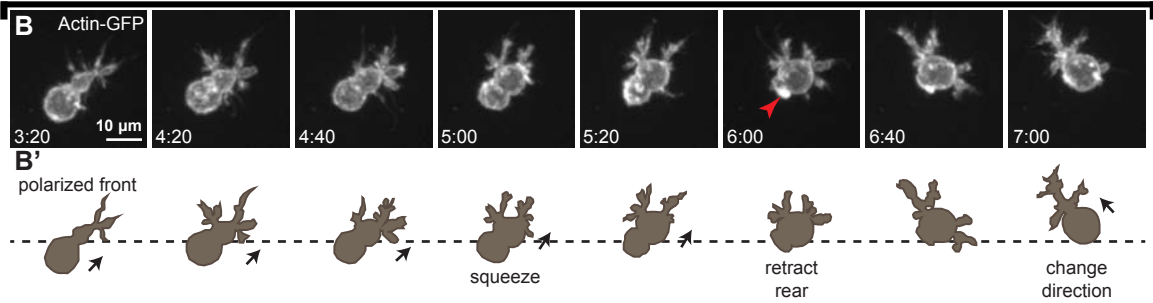


Figure 5-8

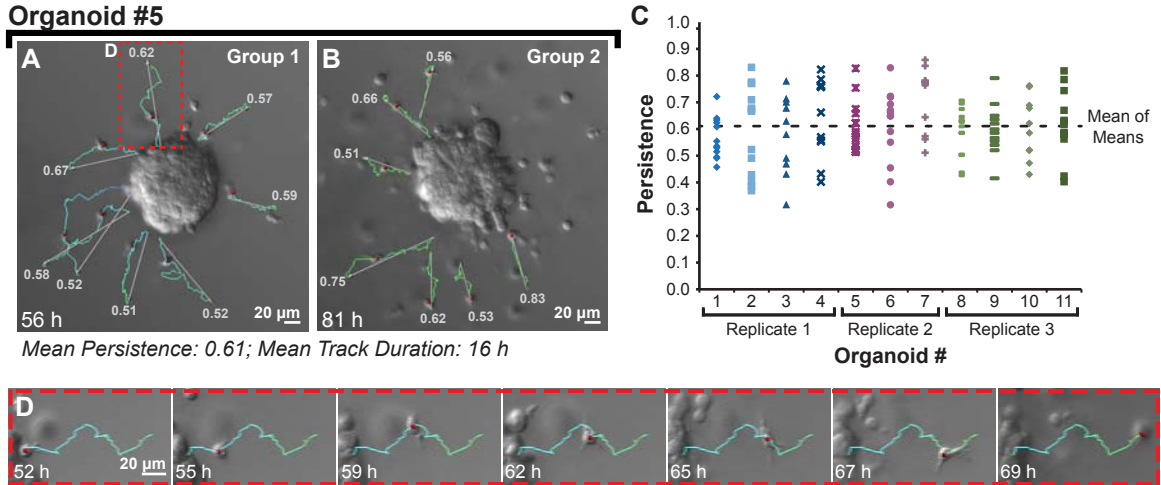


Figure 5-8. *Twist1*⁺ cells disseminate from the epithelium with high directional persistence. (A-B) In DIC time-lapse movies of *CMV::rtTA;TRE-Twist1* organoids, individual cells were tracked for at least 10 h following initial detachment from the basal epithelial surface. Grey arrows indicate the displacement vector while colored lines indicate the total path of the cell. Red spheres indicate the position of the cell on the track at the time point of the frame. Numbered labels at the end of each track indicate the persistence. (C) Cells were tracked in 11 movies taken from three biological replicates. Persistence values for each cell tracked are plotted within an individual movie. The horizontal dashed line (persistence = 0.61) indicates the mean of the mean persistence of migration among all sampled organoids. (D) A single tracked cell with persistence equal to the overall mean.

CHAPTER 6

Myoepithelial and luminal cell-cell interactions
appear to regulate epithelial invasion and dissemination

Introduction

Human tumors are composed of a heterogeneous population of cells, only a small fraction of which locally disseminate and metastasize¹. It is largely unclear which cells are most capable of dissemination and in what tissue context. Normal mammary epithelium forms a bilayered architecture consisting of two major cell types: inner luminal and outer myoepithelial cells². Most breast tumors arise from luminal epithelial cells, and the integrity of the myoepithelium is the major diagnostic criteria used to distinguish ductal carcinoma in situ (DCIS) from invasive ductal carcinoma (IDC)³. This distinction has clinical implications for patient prognosis as DCIS has a 96-98% 10-year survival after diagnosis⁴ whereas IDC has a 77% 10-year survival after diagnosis (Cancer Research UK). Because there is no gene signature predictive of invasive progression, clinical management of DCIS is based largely on histopathologic findings, and even focal disruptions in the myoepithelium are prognostic⁵.

We sought to understand how different cell types within the epithelium interact with one another during dissemination. We previously demonstrated that constitutive expression of the transcription factor *Twist1* in primary normal mammary epithelium induced dissemination of both mammary cell types⁶. Moreover, time-lapse confocal imaging of cell type-specific behavior suggested that cell-cell interactions could regulate whether dissemination is successful. However, in our previous work, we were expressing *Twist1* in both luminal and myoepithelial cells. Here, we sought to test the sufficiency of *Twist1* to induce dissemination in distinct mammary subpopulations and developed mouse models that use cell type-specific promoters to drive *Twist1* expression in myoepithelial and luminal lineages (Fig. 6-1). Our findings support the hypothesis that a normal myoepithelium acts as a barrier to luminal cell dissemination.

Results

Myoepithelial-specific *Twist1* expression induces myoepithelial cell dissemination

We first restricted *Twist1* to the myoepithelial compartment by generating mice carrying a reverse tetracycline transactivator (rtTA) expressed under the Keratin 14 promoter and our previously described Tet-responsive *Twist1* allele (Fig. 6-2A, *K14::rtTA;TRE-Twist1*). We isolated mammary organoids and activated *Twist1* expression in vitro with doxycycline. In basal medium without growth factors, *Twist1* activation induced high levels of dissemination in 87% of organoids (Fig. 6-2B,D). Interestingly, the addition of FGF2 to the medium significantly reduced the percentage of disseminating organoids to 49% (Fig. 6-2D), and these organoids usually disseminated less than ten cells each. In addition, we observed no defect in branching (Fig. 6-2E), unlike the near complete inhibition of branching observed using the ubiquitous *CMV::rtTA* driver⁶. Importantly, disseminated cells were always K14⁺, in both basal medium and FGF2-containing medium (Fig. 6-2B',C'). In the latter, branched organoids notably did not possess mislocalized myoepithelial cells and rather appeared to maintain an intact, basally positioned myoepithelium, although we have not yet tested whether these cells are *Twist1*⁺ or *Twist1*⁻. In contrast, we frequently observed myoepithelial ingression into the epithelium with constitutive *Twist1* expression. We conclude that myoepithelial-specific *Twist1* expression induces cell autonomous myoepithelial dissemination and appears regulated by the presence of FGF2.

Luminal cell-specific *Twist1* expression induces rare to no dissemination

We next restricted *Twist1* to the luminal compartment by generating mice carrying a tamoxifen-inducible Cre recombinase expressed under the Keratin 8 promoter, a Cre-inducible rtTA, the Tet-responsive *Twist1* allele, and a fluorescent Cre biosensor (Fig. 6-

3A, *K8::Cre-ER;R26::LSL-rtTA;TRE-Twist1;mT/mG*). We had previously used Adeno-CMV-Cre to generate random activation of *rtTA* in *R26::LSL-rtTA;TRE-Twist1;mT/mG* epithelium and demonstrated that dissemination was autonomous to *rtTA*⁺*Twist1*⁺ cells⁶. In genetic mosaic mixtures of *Twist1*⁻ and *Twist1*⁺ cells, we observed a mix of branching (mostly *Twist1*⁻ cells) and dissemination (only *Twist1*⁺ cells). We next combined this genetic model for inducing *rtTA* and *Twist1* expression with the genetically encoded, luminal-specific *K8::Cre-ER* to activate *rtTA* specifically in luminal, *K8*⁺ cells. We used time-lapse microscopy to directly compare the outcomes of inducing *rtTA* and *Twist1* in a random versus luminal-specific cell population. In organoids with random *Twist1*⁺ cells, we observed a mix of branching and dissemination (Fig. 6-3B), and we confirmed by immunofluorescence that disseminated cells could be luminal (Fig. 6-3C, *K8*⁺, red arrows). In contrast, in organoids with luminal *Twist1*⁺ cells, we observed branching and, strikingly, almost no dissemination (Fig. 6-3D). By immunofluorescence, we validated that many cells within the epithelium were *Twist1*⁺ (Fig. 6-3E).

We next isolated organoids from *K8::Cre-ER;R26::LSL-rtTA;TRE-Twist1;mT/mG* mice and divided epithelium from the same mouse into two groups to induce *rtTA* expression either with Adeno-Cre or tamoxifen. Thus, tissue from the same mouse served as an internal control for dissemination capacity. We induced *Twist1* with doxycycline and quantified branching and dissemination on day 7. With Adeno-Cre and random *rtTA* activation, 87% of organoids disseminated (Fig. 6-3F). In contrast, with tamoxifen and luminal-specific *rtTA* activation, only 8% of organoids disseminated (Fig. 6-3F). Importantly, random *Twist1* activation could result in *K8*⁺ cell dissemination (Fig. 6-3C), demonstrating that luminal cells have the intrinsic potential to disseminate. Collectively, our data reveal that *Twist1* in both cell types results in both luminal and myoepithelial cell dissemination; *Twist1* in myoepithelial cells results in myoepithelial cell

dissemination; and *Twist1* in luminal cells results in practically no dissemination. We therefore expect that cell extrinsic factors regulate *Twist1*⁺ luminal cell dissemination.

Myoepithelial cells appear to contain protruding *Twist1*⁺ luminal cells

We have observed that basally positioned, *Twist1*-expressing myoepithelial cells in *CMV::rtTA;TRE-Twist1* organoids can wrap around and contain invasive luminal cells (see Chapter 5). In turn, we hypothesized that the presence of a normal myoepithelium in *K8::Cre-ER;R26::LSL-rtTA;TRE-Twist1;mT/mG* organoids may similarly restrict luminal cell dissemination. We used confocal microscopy and the Cre biosensor *mT/mG* to distinguish the interactions between *Twist1*⁺ luminal cells (green) and wild-type myoepithelial cells (most red cells). In real-time, we observed that luminal cells extended subcellular protrusions into the ECM past a continuous myoepithelial layer but remained within the epithelium (Fig. 6-4A-A’). Luminal cells also invaded at gaps in the myoepithelium (Fig. 6-4B, white arrows) but appeared contained by adjacent myoepithelial cells, which ultimately re-established a continuous basal layer (Fig. 6-4B-B’, red arrowheads). We therefore hypothesize that the myoepithelium may represent a physical barrier to *Twist1*-induced luminal cell dissemination.

Myoepithelial cells dynamically cover basal E-cad⁻ luminal cells

We next sought to test whether myoepithelial containment of invasive luminal cells represented a conserved myoepithelial cell behavior. We had previously found that loss of E-cadherin (E-cad), the major classical cadherin in luminal cells, disrupted epithelial architecture and branching morphogenesis but did not induce dissemination⁶. Interestingly, E-cad⁻ cells orthotopically transplanted in vivo remained as disorganized clusters at the injection site and were consistently surrounded by myoepithelial cells⁶. To characterize the dynamic interactions between myoepithelial cells and E-cad⁻ cells, we

introduced a myoepithelial-specific fluorescent reporter (*K14::Actin-GFP*) onto an *E-cad^{fl/fl}* background and labeled all cell membranes with Cell Tracker Red (Fig. 6-5A). We used Adeno-Cre to induce *E-cad* deletion in most cells and then monitored the behavior of myoepithelial cells by time-lapse confocal microscopy. We observed individual (Fig. 6-5B-B') or groups (Fig. 6-5C-C') of rounded *E-cad⁻* cells (red) emerge onto the basal epithelial surface in direct contact with the extracellular matrix (ECM). However, myoepithelial cells (green) rapidly migrated to positions between the *E-cad⁻* cells and the ECM (Fig. 6-5B-C', 36/42 time-lapse movies, 3 biological replicates). Myoepithelial cells (Fig. 6-5B,C-C', white arrowheads) were typically successful in covering *E-cad⁻* luminal cells and restoring them to an interior position within the epithelium. We confirmed by immunofluorescence that rounded cells on the basal surface were luminal (Fig. 6-5D-D', $K8^+$) and lacked *E-cad* (Fig. 6-5E-E') and β -catenin (Fig. 6-5F-F'). In fixed samples, we observed both large groups of *E-cad⁻* cells covered by myoepithelial cells (Fig. 6-5E') and large groups of *E-cad⁻* cells that were directly exposed to the ECM (Fig. 6-5F'). Taken together, our data suggest that there exists a dynamic interplay between *E-cad⁻* cells invading into the ECM and myoepithelial cells migrating to maintain basal coverage.

Discussion

We anticipated that different mammary epithelial cell types and cells at different stages of differentiation would have distinct dissemination potential. We therefore generated mouse models in which we could target *Twist1* expression to specific epithelial subpopulations. We first tested the effect of driving *Twist1* in K14⁺ cells, where K14 is considered a marker of basal progenitors (Fig. 6-1). Consistent with our previous findings with genetic mosaic *Twist1* expression, dissemination was autonomous to K14⁺ cells. However, we observed a striking inhibition of dissemination in the presence of FGF2. We therefore expect that the differentiation state of K14⁺ cells influences their ability to activate *Twist1* or to respond to the *Twist1* signal to disseminate. Our findings also suggest that the phenotypic consequences of *Twist1* activation in K14⁺ cells vary in different growth environments and that FGF2 signaling appears to antagonize dissemination. In future experiments, we will test this hypothesis by modulating activation of growth factor versus *Twist1* pathways. Interestingly, we previously observed that constitutive *Twist1* expression inhibits FGF2-induced branching morphogenesis⁶. In contrast, organoids with K14⁺ cell-specific *Twist1* expression branch efficiently. Taken together, our data suggest that *Twist1*-induced branching inhibition is due to *Twist1*-expressing luminal cells and is independent of *Twist1*-expressing K14⁺ cells.

We next tested the effect of driving *Twist1* in K8⁺ cells, where K8 is considered a marker of luminal progenitors (Fig. 6-1). Surprisingly, while we observe K8⁺ disseminated cells in response to constitutive or genetic mosaic *Twist1* expression, we observed almost no dissemination in response to luminal-specific *Twist1* expression. Interestingly, using cell type-specific fluorescent reporters, we observed that myoepithelial cells appear to dynamically cover and contain invading *Twist1*⁺ luminal cells at the basal tissue surface.

Analogous interactions with E-cad⁻ cells suggested to us that myoepithelial cells display a conserved response to invasive luminal cell behavior. Notably, the integrity of the myoepithelium is used in diagnosis and management of breast cancer patients, and when this layer is compromised, prognosis is poor⁷. As such, myoepithelial cells have been posited to function as suppressors of tumor cell invasion⁸. Consistent with this concept, we hypothesize that complete retention of a normal myoepithelium may explain the lack of dissemination by Twist1⁺ luminal cells when *Twist1* expression is restricted the luminal compartment. However, the functional consequences of gaps in myoepithelial coverage or compromised myoepithelial gene expression remain untested. We now seek to test the molecular basis of myoepithelial barrier function by knocking down myoepithelial-specific genes important for contractility, cell-cell adhesion, and the intermediate filament network. We have already validated shRNAs to knock down smooth muscle actin, smooth muscle myosin, Desmocollin 3, Desmoglein 3, and Keratin 14 and are currently testing the effect of perturbing these genes concurrently with *E-cad* deletion and *Twist1* expression. We expect that perturbation of myoepithelial function will enable E-cad⁻ and Twist1⁺ luminal cell dissemination.

Materials and methods

Mouse strains. The *Twist1-tetO7-luc* (*TRE-Twist1*) transgenic line was previously described⁹. The *K14::Actin-GFP* transgenic line¹⁰ was a kind gift of Elaine Fuchs (The Rockefeller University, New York, NY). *K14::rtTA*¹¹, *K8::Cre-ER*¹², *mT/mG*¹³, *R26::Lox-Stop-Lox-rtTA-IRES-EGFP* (*R26::LSL-rtTA*)¹⁴, and *E-cad*^{fl/fl15} mouse lines were acquired from the Jackson Laboratory. Mouse husbandry and procedures were all conducted under an IACUC-approved animal protocol.

Isolation and 3D culture of primary mammary epithelial organoids. We used a combination of mechanical disruption, collagenase/trypsin digestion, and differential centrifugation to purify fragments of primary mammary epithelial ducts, termed “organoids”, as previously described^{6,16-18}. Organoids were embedded in 3D Matrigel (354230; BD Biosciences) at 2-3 organoids/ μ L and plated as 100 μ L suspensions in 24-well coverslip-bottomed plates (662892; Greiner Bio-One) over a 37°C heating block. Gels were allowed to polymerize for 30 min at 37°C and then cultured in organoid medium: DMEM (D6546; Sigma) with 1% Insulin-Transferrin-Selenium (51500-056; GIBCO) and 1% Penicillin-Streptomycin (P4333; Sigma). Branching morphogenesis was induced with 2.5 nM FGF2 (F0291; Sigma). Branching was scored as organoids with three or more elongated buds. Dissemination was scored as organoids with more than one adjacent single cell clearly separated from the epithelial group. Branching and dissemination were quantified at approximately 7 days in culture.

Cell type-specific *Twist1* activation. For all experiments, *Twist1* expression was induced by supplementing organoid medium with 5 μ g/mL doxycycline (Shanghai RenYoung Pharmaceutical Co., Ltd), and medium was replaced every 48 h. In *K8::Cre-*

ER;R26::LSL-rtTA;TRE-Twist1;mT/mG mice, *rtTA* expression was induced by culturing organoids overnight with 50 nM tamoxifen once embedded in Matrigel. To wash out tamoxifen, samples were rinsed with PBS, incubated in organoid medium for 20 min at 37°C, and then cultured in fresh organoid medium. Genetic mosaic *Twist1* expression was induced in the same tissue by infecting organoids with Adeno-Cre (Vector Biolabs #1045), as previously described⁶, prior to embedding in Matrigel.

***E-cad* deletion.** Prior to embedding in Matrigel, *E-cad^{fl/fl};K14::Actin-GFP* organoids were infected with Adeno-Cre, as previously described⁶, to yield recombination in a high percentage of cells.

Confocal microscopy. Confocal imaging was performed on a spinning-disk confocal microscope (Solamere Technology Group) with an XR/MEGA-10 S30 camera (Stanford Photonics, Inc.), as previously described^{19,20}. An LD C-Apochromat 40X/1.1 W Korr objective lens (Carl Zeiss) was used for high magnification single and time-lapse image acquisition, with water and oil used as the imaging mediums, respectively. Acquisition of both fixed and time-lapse images was performed using a combination of μ Manager²¹ and Piper (Stanford Photonics, Inc.). Imaris (Bitplane) was used to analyze time-lapse movies, place scale bars, and export individual TIFFs. Adobe Photoshop CS5 was used as needed to adjust levels for each channel on entire images to maximize image clarity.

Differential interference contrast (DIC) microscopy. Time-lapse imaging of mammary organoids was conducted using an LD Plan-Neofluar 20X/0.4 Korr Ph2 objective lens and a Cell Observer system with an AxioObserver Z1 and an AxioCam MRM camera (Carl Zeiss). Images were acquired at 20-min intervals for 5-7 days. Temperature was maintained at 37°C and CO₂ at 5%. AxioVision (Carl Zeiss) was used to analyze time-

lapse movies, place scale bars, and export individual TIFFs. Adobe Photoshop CS5 was used to adjust levels on entire images to maximize image clarity.

Cell Tracker Red labeling. One 50 μ g vial of Cell Tracker Red was resuspended in 73 μ l sterile DMSO to make a 1 mM stock. The vial was warmed for several minutes at 37°C to dissolve the solution. Cell Tracker was added to organoid medium at 1 μ M. Samples were stained overnight at 37°C. The next day, the Cell Tracker-containing medium was removed, and wells were rinsed with basal organoid medium three times for 20 min at 37°C. After the last wash, fresh medium with 2.5 nM FGF2 was added back.

Immunofluorescence. Organoids grown in Matrigel were fixed in 4% paraformaldehyde for 10 min, rinsed three times in PBS for 10 min, embedded in Optimal Cutting Temperature compound (OCT), and frozen at -80°C. OCT blocks were sectioned at 50- μ m thickness by cryostat at -20°C. Sections were placed on Superfrost Plus Gold microscope slides (15-188-48; Fisherbrand) and stored at -80°C. For antibody staining, samples were thawed at room temperature, rinsed twice in PBS for 10 min to remove OCT, permeabilized with 0.5% Triton X-100 for 1 h, and rinsed twice in PBS for 10 min. Samples were blocked for 1–3 h with 10% FBS/1% BSA, incubated with primary antibodies overnight at 4°C in 1% FBS/1% BSA, and rinsed three times in 1% FBS/1% BSA for 15 min. Incubation with secondary antibodies was conducted in 1% FBS/1% BSA overnight at 4°C. Slides were rinsed three times in PBS for 10 min, mounted with Fluoromount (F4680; Sigma-Aldrich), and sealed with coverslips. F-Actin was stained with Alexa Fluor Phalloidin (1:100) (Invitrogen), and nuclei were stained with DAPI (1:1,000) (D3571; Invitrogen). Primary antibodies used were rat anti-cytokeratin-8 (1:100; TROMA-I; Developmental Studies Hybrid-oma Bank), rabbit anti-cytokeratin-14

(1:500; PRB-155P; Covance), mouse anti-Twist1 (1:50; sc-81417; Santa Cruz Biotechnology Inc.), rat anti-E-cadherin (1:250) (13-1900; Invitrogen), and rabbit anti- β -catenin (1:1,000) (C2206; Sigma-Aldrich). Secondary antibodies used were all Alexa Fluor-conjugated antibodies (1:200; Invitrogen).

References

1. Sahai, E. Illuminating the metastatic process. *Nat Rev Cancer* **7**, 737–749 (2007).
2. Gudjonsson, T., Adriance, M. C., Sternlicht, M. D., Petersen, O. W. & Bissell, M. J. Myoepithelial cells: their origin and function in breast morphogenesis and neoplasia. *J Mammary Gland Biol Neoplasia* **10**, 261–272 (2005).
3. Polyak, K. Molecular markers for the diagnosis and management of ductal carcinoma in situ. *J. Natl. Cancer Inst. Monographs* **2010**, 210–213 (2010).
4. Allegra, C. J. *et al.* National Institutes of Health State-of-the-Science Conference statement: Diagnosis and Management of Ductal Carcinoma In Situ September 22-24, 2009. in *J. Natl. Cancer Inst.* **102**, 161–169 (2010).
5. Man, Y.-G. *et al.* Cell clusters overlying focally disrupted mammary myoepithelial cell layers and adjacent cells within the same duct display different immunohistochemical and genetic features: implications for tumor progression and invasion. *Breast Cancer Res.* **5**, R231–41 (2003).
6. Shamir, E. R. *et al.* Twist1-induced dissemination preserves epithelial identity and requires E-cadherin. *J. Cell Biol.* **204**, 839–856 (2014).
7. Man, Y.-G. & Sang, Q.-X. A. The significance of focal myoepithelial cell layer disruptions in human breast tumor invasion: a paradigm shift from the ‘protease-centered’ hypothesis. *Exp. Cell Res.* **301**, 103–118 (2004).
8. Polyak, K. & Hu, M. Do myoepithelial cells hold the key for breast tumor progression? *J Mammary Gland Biol Neoplasia* **10**, 231–247 (2005).
9. Tran, P. T. *et al.* Twist1 Suppresses Senescence Programs and Thereby Accelerates and Maintains Mutant Kras-Induced Lung Tumorigenesis. *PLoS Genet* **8**, e1002650 (2012).
10. Vaezi, A., Bauer, C., Vasioukhin, V. & Fuchs, E. Actin cable dynamics and Rho/Rock orchestrate a polarized cytoskeletal architecture in the early steps of assembling a stratified epithelium. *Dev. Cell* **3**, 367–381 (2002).
11. Nguyen, H., Rendl, M. & Fuchs, E. Tcf3 Governs Stem Cell Features and Represses Cell Fate Determination in Skin. *Cell* **127**, 171–183 (2006).
12. Van Keymeulen, A. *et al.* Distinct stem cells contribute to mammary gland development and maintenance. *Nature* **479**, 189–193 (2011).
13. Muzumdar, M. D., Tasic, B., Miyamichi, K., Li, L. & Luo, L. A global double-fluorescent Cre reporter mouse. *genesis* **45**, 593–605 (2007).
14. Belteki, G. *et al.* Conditional and inducible transgene expression in mice through the combinatorial use of Cre-mediated recombination and tetracycline induction. *Nucleic Acids Res.* **33**, e51 (2005).
15. Boussadia, O., Kutsch, S., Hierholzer, A., Delmas, V. & Kemler, R. E-cadherin is a survival factor for the lactating mouse mammary gland. *Mech. Dev.* **115**, 53–62 (2002).
16. Ewald, A. J., Brenot, A., Duong, M., Chan, B. S. & Werb, Z. Collective epithelial migration and cell rearrangements drive mammary branching morphogenesis. *Dev. Cell* **14**, 570–581 (2008).
17. Ewald, A. J. *et al.* Mammary collective cell migration involves transient loss of epithelial features and individual cell migration within the epithelium. *J. Cell. Sci.* **125**, 2638–2654 (2012).
18. Nguyen-Ngoc, K.-V. *et al.* ECM microenvironment regulates collective migration and local dissemination in normal and malignant mammary epithelium. *Proc Natl Acad Sci USA* **109**, E2595–604 (2012).
19. Ewald, A. J., Werb, Z. & Egeblad, M. Dynamic, Long-Term In Vivo Imaging of

- Tumor-Stroma Interactions in Mouse Models of Breast Cancer Using Spinning-Disk Confocal Microscopy. *Cold Spring Harbor Protocols* **2011**, pdb.top97–pdb.top97 (2011).
20. Ewald, A. J. Practical Considerations for Long-Term Time-Lapse Imaging of Epithelial Morphogenesis in Three-Dimensional Organotypic Cultures. *Cold Spring Harbor Protocols* **2013**, pdb.top072884–pdb.top072884 (2013).
 21. Edelstein, A. A., Amodaj, N. N., Hoover, K. K., Vale, R. R. & Stuurman, N. N. Computer control of microscopes using μ Manager. *Audio, Transactions of the IRE Professional Group on* **Chapter 14**, Unit14–Unit20 (2010).

Figure 6-1

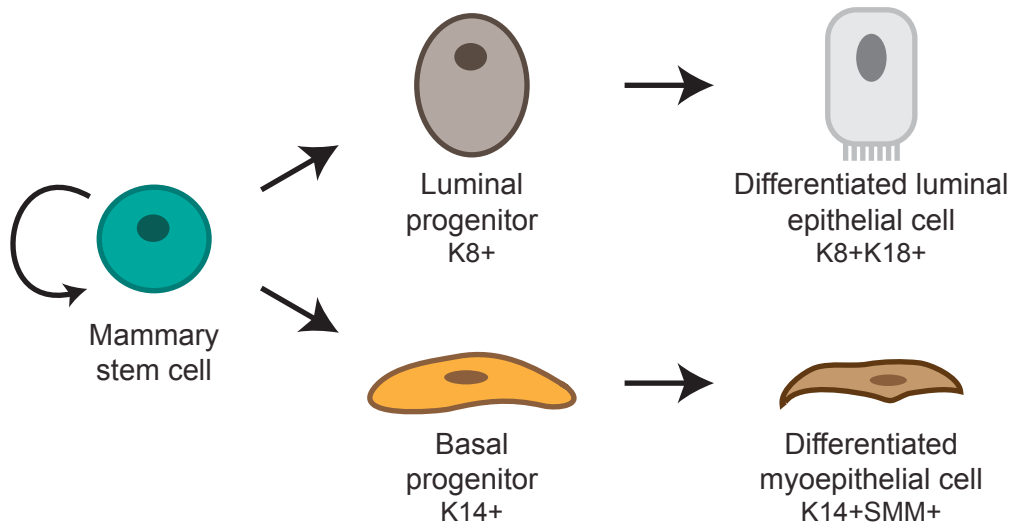


Figure 6-1. Distinct mammary epithelial lineages express cell type-specific markers. Mammary epithelium is composed of two major lineages, luminal and basal/myoepithelial. Specific cytokeratin expression distinguishes the two lineages and the differentiation state of luminal cells while expression of contractility proteins distinguishes basal progenitors from differentiated myoepithelial cells. K8, cytokeratin 8; K18, cytokeratin 18; K14, cytokeratin 14; SMM, smooth muscle myosin.

Figure 6-2. Myoepithelial-specific *Twist1* expression induces cell autonomous dissemination that is regulated by FGF2. (A) We isolated organoids from *K14::rtTA;TRE-Twist1* mice and induced *Twist1* expression with doxycycline. (B-C) Organoids robustly disseminated in basal medium (B) but branched and disseminated few cells in FGF2-containing medium (C). Disseminated cells were K14⁺ (B',C'). (D) With doxycycline, dissemination occurred in 87% of organoids in basal medium (****P=3x10⁻⁶, Student's *t* test, 2-tailed, equal variance) and 49% of organoids in FGF2-containing medium (****P=6x10⁻⁶, Student's *t* test, 2-tailed, equal variance). Addition of FGF2 significantly inhibited dissemination (****P=0.0001, Student's *t* test, 2-tailed, equal variance). n, total # of organoids; r, # of biological replicates. Error bars indicate SD. (E) In FGF2-containing medium, organoids branched at equal rates with and without *Twist1* induction (P=0.5, Student's *t* test, 2-tailed, equal variance).

Figure 6-2

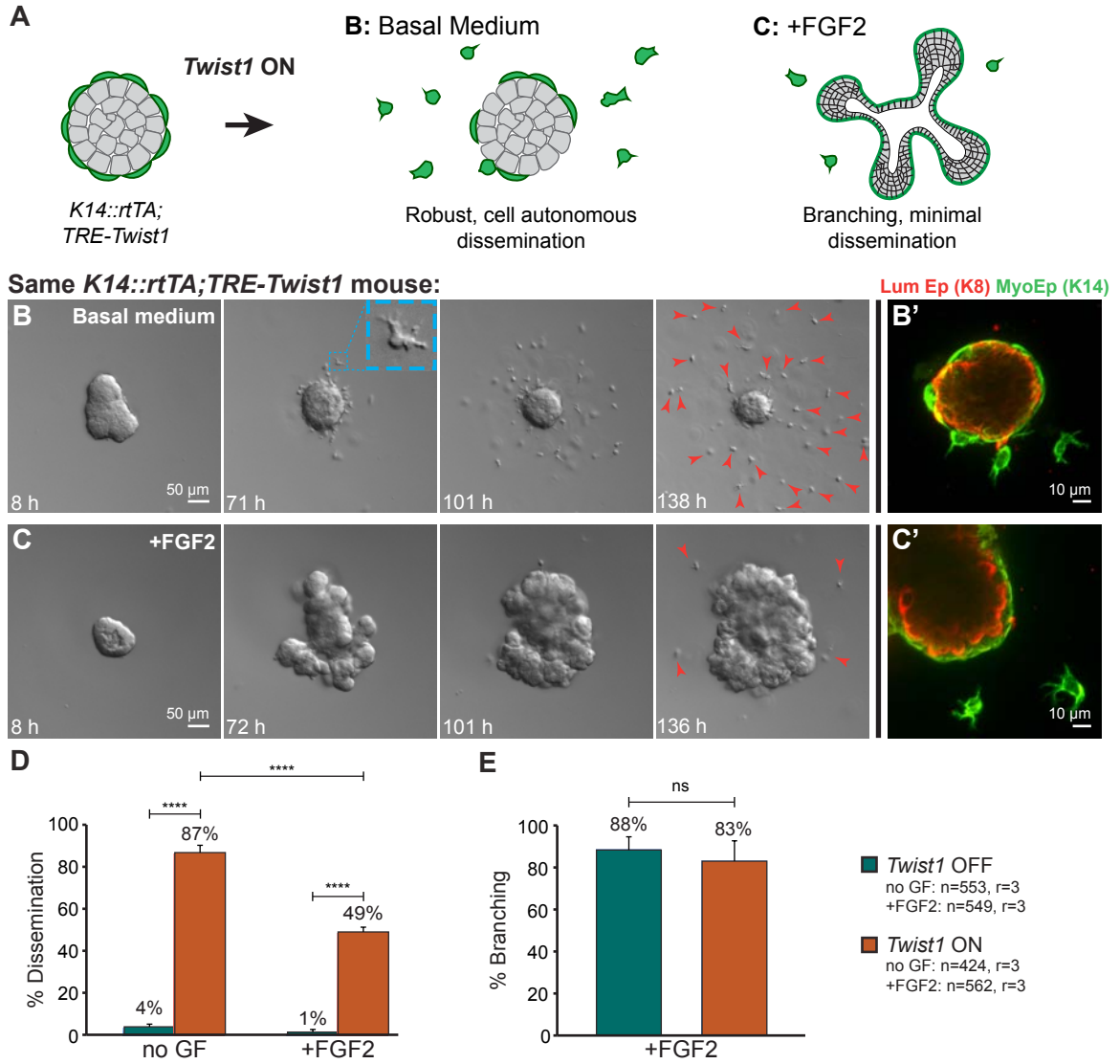
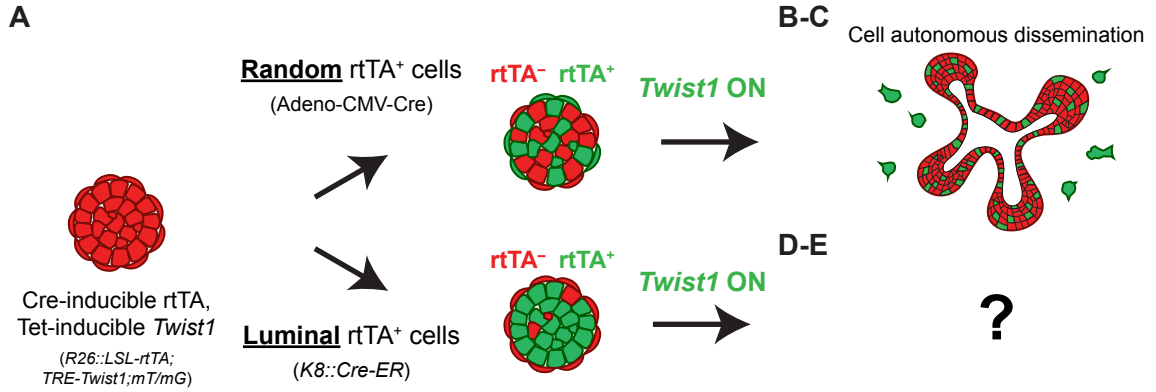


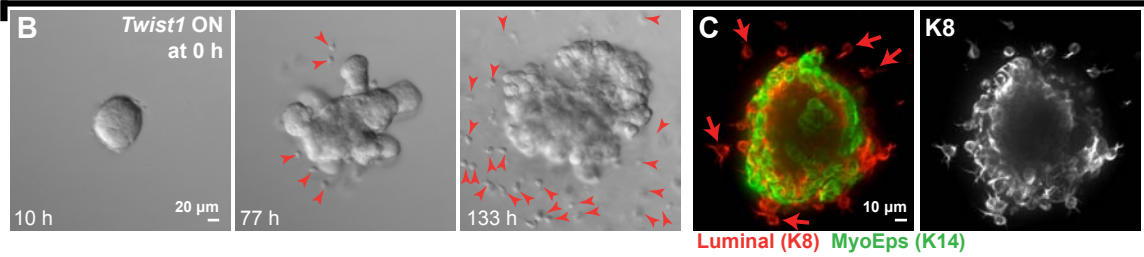
Figure 6-3. Luminal-specific *Twist1* expression induces rare to no dissemination.

(A) We induced random and luminal-specific *rtTA* expression in *R26::LSL-rtTA;TRE-Twist1;mT/mG* organoids using an adenovirus encoding Cre recombinase (Adeno-Cre) and a genetically encoded, tamoxifen-inducible *K8::Cre-ER*, respectively. (B-C) Random *Twist1* expression induced a mix of branching and dissemination (B), where disseminated cells could be luminal (C, $K8^+$). (D-E) Luminal-specific *Twist1* expression induced rare to no dissemination (D), despite many $Twist1^+$ cells within the epithelium (E). (F) Organoids isolated from *K8::Cre-ER;R26::LSL-rtTA;TRE-Twist1;mT/mG* mice were divided into Adeno-Cre and tamoxifen treatment groups. Dissemination was observed in 87% of Adeno-Cre-treated organoids and in 8% of tamoxifen-treated organoids across 3 biological replicates (**** $P=3 \times 10^{-5}$, Student's *t* test, 2-tailed, equal variance). n, total # of organoids.

Figure 6-3



Random *Twist1*⁺ cells



Luminal *Twist1*⁺ cells

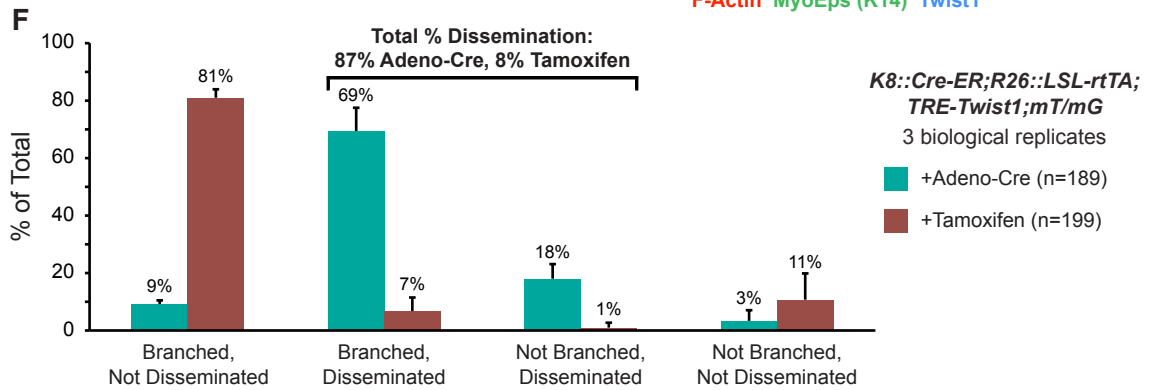
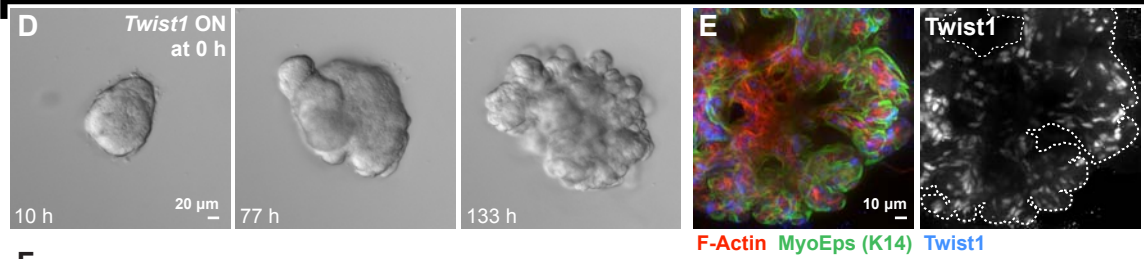


Figure 6-4

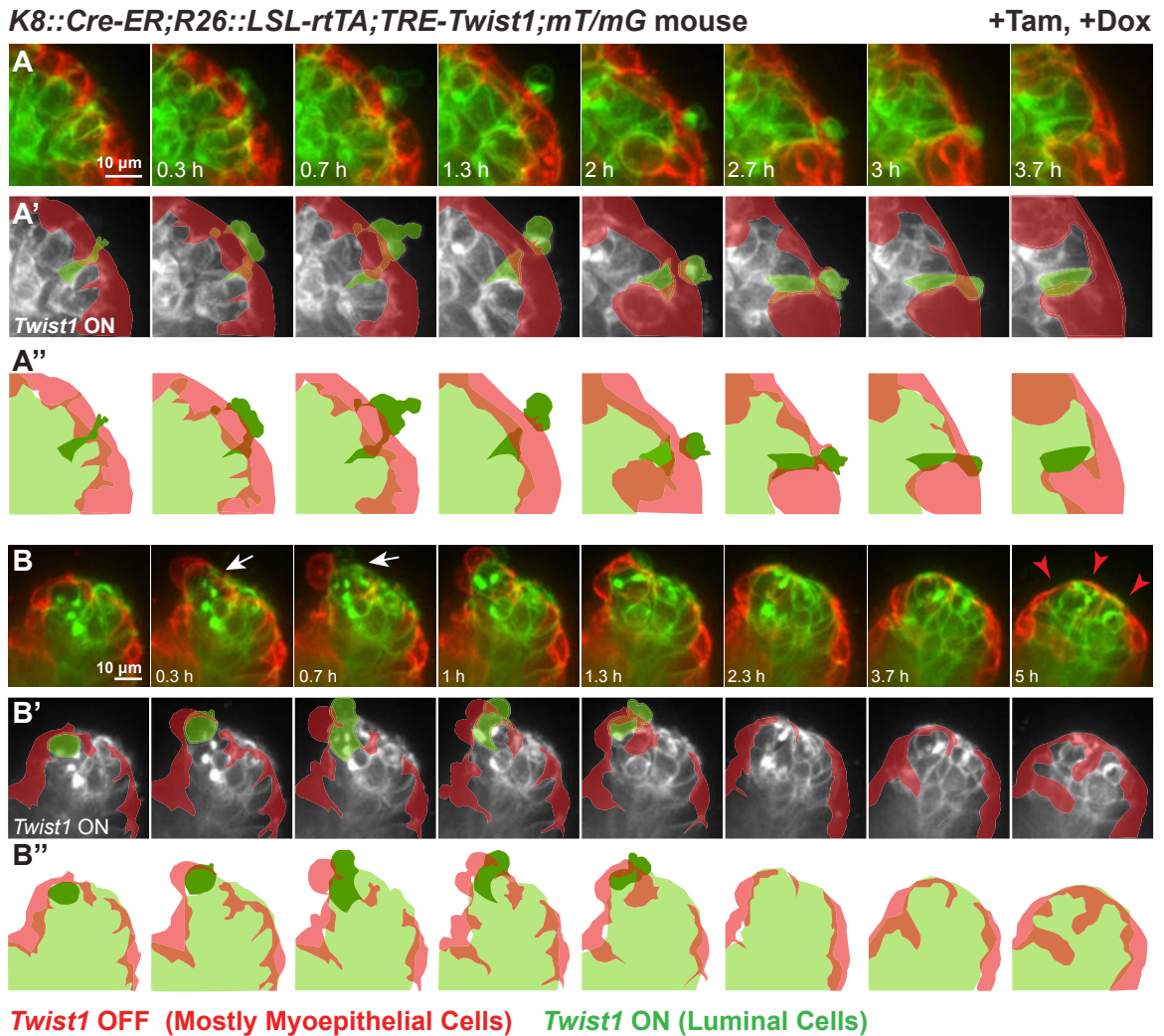


Figure 6-4. The myoepithelium appears to contain protruding *Twist1*+ luminal cells. (A-B) Organoids were isolated from *K8::Cre-ER;R26::LSL-rtTA;TRE-Twist1;mT/mG* mice, treated with tamoxifen to induce *rtTA* expression in *K8*⁺ cells, and cultured in doxycycline to induce *Twist1* in the luminal compartment. *Twist1*⁺ luminal cells (green) protruded past a complete myoepithelium (red) (A-A'') and invaded at gaps in the myoepithelium (B-B'') but did not disseminate. Myoepithelial cells appeared to migrate over and contain invasive luminal cells (B-B'').

Figure 6-5

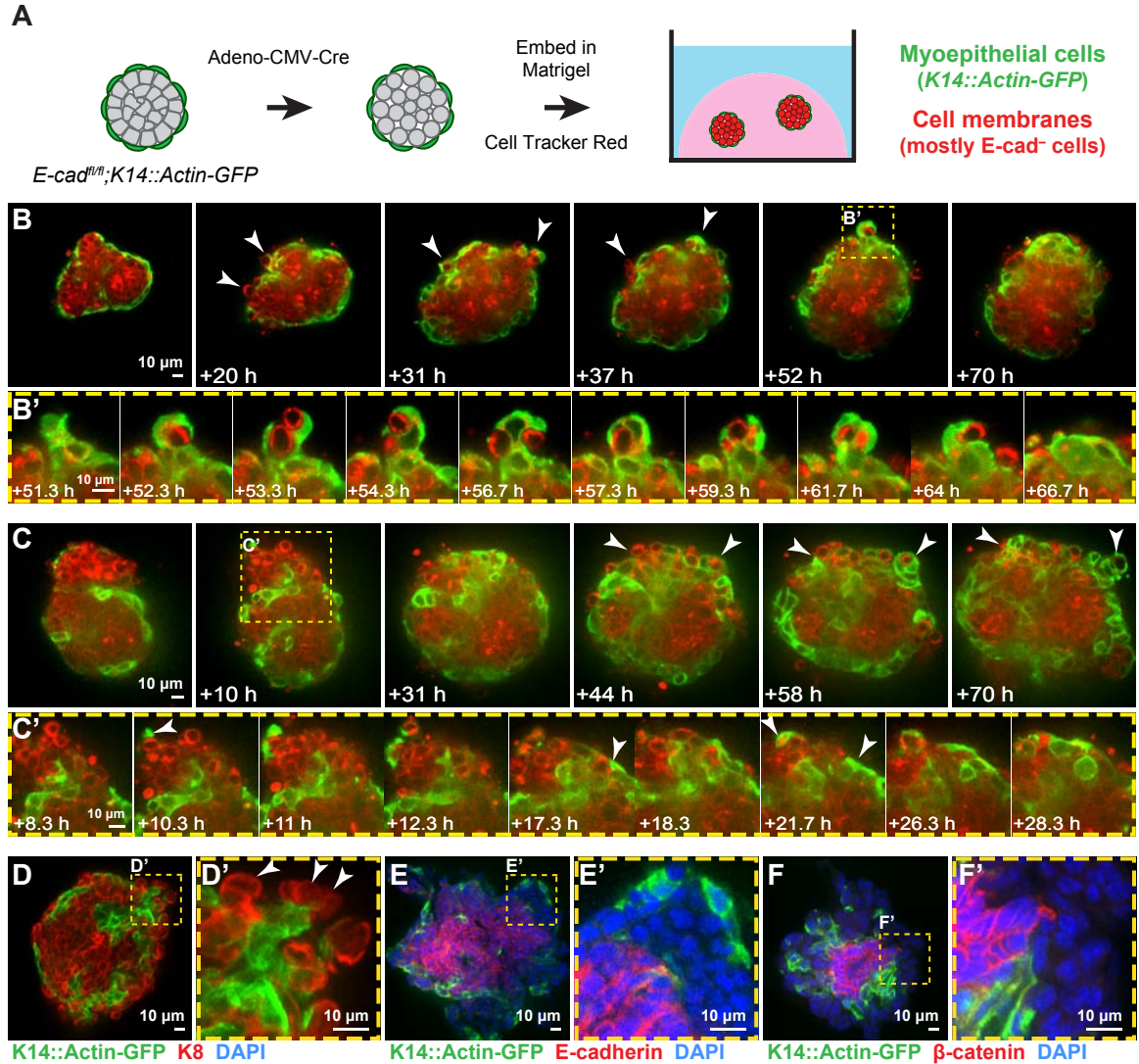


Figure 6-5. Myoepithelial cells appear to restrain *E-cad⁻* cell dissemination. (A) We isolated organoids from *E-cad^{fl/fl};K14::Actin-GFP* mice, induced *E-cad* deletion by Adeno-Cre, and labeled all cells with Cell Tracker Red. (B-C) Individual (B-B') or groups (C-C') of red *E-cad⁻* cells emerged onto the basal tissue surface, in direct contact with the ECM, only to be covered by migrating myoepithelial cells (white arrowheads). (D-F) Rounded cells at or near the basal surface were K8⁺ (D-D', white arrowheads), *E-cad⁻* (E-E'), and β -catenin⁻ (F-F').

CHAPTER 7

Conclusion:

Rethinking the concept of an “epithelial” cell

Epithelium is one of the fundamental tissues of the body that lines all cavities and body surfaces¹. Epithelial tissues consist of one or more layers of polarized, tightly connected cells¹. This anatomical or morphological definition has largely guided our conceptualization of what epithelial cells are capable of doing. During development, epithelial cells in multiple organs undergo branching morphogenesis to generate a network of polarized ducts. While branching itself is recognized to involve collective cell migration², the resulting epithelial ducts are largely considered quiescent at homeostasis. Therefore, our traditional notion of “epithelial” is that of a stationary cell stabilized by many cell-cell junctions with its neighbors³. In contrast, metastasis of cancer cells that arise in epithelial tissues begins with their dissemination into the surrounding extracellular matrix (ECM). This process requires at least two conceptual shifts: a break in connections to cell neighbors and significant movement to escape and travel to distant organs^{4,5}. The cellular events that must be accomplished in metastasis are thus contrary to our notion of what constitute “epithelial” cell behaviors. As such, one posited model for dissemination is that epithelial cells fundamentally change their identity and undergo an epithelial to mesenchymal transition (EMT) to migrate away from a tissue as a single cell⁶.

The concept of an EMT derives from normal developmental contexts, such as neural crest formation, and its application in cancer arose first from morphological definitions of epithelium and mesenchyme⁶⁻⁸. Classic experiments by Elizabeth Hay demonstrated that epithelia suspended within collagen gels lost polarity and migrated into the matrix as single cells that strongly resembled mesenchymal cells^{7,9}. These morphological observations formed the basis for a “loss of the epithelial phenotype”, which expanded to include loss of epithelial-specific gene expression⁶.

Importantly, there is no gene expression or protein signature that exclusively defines epithelial cells or even a master gene or single gene not also expressed in other tissue types³. Nevertheless, adhesion proteins and the cell-cell junctions they form are shared features across epithelial organs and may serve as a useful starting point¹⁰. More junctions are present at homeostasis, in resting, simple epithelial ducts; fewer junctions are present in regions of active branching (a stratified terminal end bud) and during remodeling (e.g., lactation) and disease (cancer)^{11,12} (Fig. 7-1). Therefore, it is reasonable to infer that the types and total levels of adhesion proteins may regulate normal and disease states. In turn, the molecular definition of EMT has largely focused on repression of the cell adhesion gene *E-cadherin* (E-cad) as the molecular effector and oft-used surrogate marker^{13,14}.

In principle, EMT is a broad transcriptional program that can be induced by a set of transcription factors, such as Snail, Slug, and Twist1, which play essential roles in embryogenesis but are not expressed in adult tissues¹⁵. High expression of these transcription factors has been correlated with invasion and metastasis in multiple epithelial cancers¹⁶⁻²², and the concept that metastasis occurs by EMT has increasingly become dogma^{6,7,9,13,15,23}. However, there exists little functional evidence for EMT's role in cancer metastasis^{6,24}. Human tumors typically contain thousands of coexisting mutations^{25,26}, which collectively obscure the contribution of individual genetic events to discrete steps in metastasis. Specifically, the presence of additional mutations in cancer cell lines and the shortage of in vitro models that recapitulate tissue-level behavior have made it difficult to distinguish the individual sufficiency of E-cad loss or EMT activator expression for dissemination. Moreover, neither E-cad nor the EMT transcription factors represent "druggable" molecular targets, creating a barrier to development of targeted, anti-metastasis cancer therapies. We therefore have a need for assays that model

metastatic cell behaviors and enable rapid identification of compounds that specifically antagonize these behaviors.

These challenges led us to simplify our question of study: how could cells disseminate from a normal epithelial tissue? With this approach, we sought to define the minimum molecular events sufficient for dissemination of normal cells out of an epithelium. I developed genetic techniques to contrast deletion of *E-cad* with expression of *Twist1* in primary mouse mammary epithelium²⁷. I tested the acute consequences of these single gene manipulations in our organoid assay, in which fragments of mammary ducts, called “organoids”, are explanted into a basement membrane-rich, 3D ECM^{11,28,29}.

We first induced Cre-lox-based *E-cad* deletion in isolated mammary organoids. While *E-cad*⁺ epithelium formed a simple, polarized bi-layer, *E-cad*⁻ epithelium was disorganized and multi-layered. Basal *E-cad*⁻ cells initiated single-file migration columns into the ECM that were frequently located beyond basement membrane, a hallmark of benign to malignant progression. Nevertheless, most *E-cad*⁻ cells remained connected to each other by desmosomes. Thus, a model for dissemination driven solely by *E-cad* loss is incomplete.

We next used a tetracycline-inducible system to ubiquitously express *Twist1* in isolated mammary organoids. Remarkably, acute *Twist1* expression induced robust dissemination, and disseminated cells proliferated to form secondary epithelial sites within the ECM. A major paradigm in EMT is that dissemination requires a fundamental change in cell fate. In turn, we performed RNA-seq to test whether *Twist1* induced a loss of epithelial-specific gene expression. Among 77 genes thought to define epithelial identity, only one changed significantly downstream of *Twist1*. Moreover, no canonical

EMT genes, including *E-cad*, *N-cad*, and *Vimentin*, were differentially expressed. Instead, *Twist1* regulated genes that collectively reprogram the extracellular space and cell-ECM interactions.

E-cad loss is a central component of the molecular model of EMT¹⁴. Surprisingly, we observed E-cad, β -catenin, and α E-catenin protein at the membranes of cells at every stage of dissemination: protrusion, detachment, and migration. This unexpected localization suggested that E-cad might contribute to *Twist1*-induced cell behaviors. Accordingly, we used lentiviral shRNA to test the effect of complete E-cad loss. Remarkably, *E-cad* knockdown significantly blocked single cell dissemination and promoted more cohesive migration. We therefore speculate that adhesion proteins such as E-cadherin play novel, yet unrecognized roles that may critically regulate whether cells disseminate individually or invade collectively. Importantly, our data are consistent with the finding that E-cad is present in most primary breast tumors and in distant metastases³⁰. Taken together, my data demonstrate that epithelial cells can disseminate while retaining their epithelial character and do not require a molecular transition to mesenchymal fate²⁷.

We next sought to understand how dissemination is regulated at the cell and tissue level. We used imaging analysis and cell type-specific *Twist1* activation to describe the cellular events involved in how a single cell leaves a tissue and to further define which cells disseminate and in what context. We observed that both detachment from the epithelium and migration in the ECM involve protrusive activity at the cell front and squeezing and contraction of the cell body at the rear. By transmission electron microscopy, cells appear to clear matrix around protrusions at the leading edge, suggesting that migrating *Twist1*⁺ cells may digest their way forward, directionally away

from the main epithelium. Notably, Twist1⁺ cells retain an amoeboid morphology throughout this process, lending further support that epithelial cells can disseminate without a cellular transition to a mesenchymal morphology.

More broadly, our data lead us to rethink our concept of “epithelial”: can an “epithelial” cell be migratory? While epithelial tissues have traditionally been thought of as static, branching morphogenesis is fundamentally a cell migration event, driven by a migratory “epithelium”, or a collective group. In the mammary gland, ultrastructural analysis and confocal imaging of stratification and bud elongation have revealed that cells within these groups lack apico-basal polarity, have reduced cell-cell junctions, are individually motile, and can appear elongated and even protrusive¹². The presence of such features in normal epithelial cells during normal developmental processes suggests that the scope of our morphological definition of epithelial cells should be expanded. Moreover, if we accept motility as a normal epithelial cell behavior, then epithelial dissemination no longer appears an extreme conceptual leap. It appears more readily achievable to modulate a conserved epithelial migratory program than to change differentiation state or switch back and forth in cell fate in EMT-MET cycles. In turn, dissemination might be explained by a transition in the substrate for migration: in a normal migratory *epithelium*, the substrate is adjacent cells; in a disseminating migratory *epithelial cell*, the substrate is the surrounding ECM (Fig. 7-2). Consistent with this concept, our RNA-seq analysis of Twist1-induced transcriptional changes reveals that the majority of differentially expressed genes reside in the extracellular compartment. Thus, dissemination may primarily involve a change in the type of adhesion proteins on the cell surface and the composition of the immediate extracellular environment.

We now envision our Twist1-induced dissemination assay as a platform to define the molecular and cellular basis of metastatic cell behaviors and to identify inhibitors of dissemination that could ultimately provide a basis for anti-metastatic therapies. Currently, most cancer drugs target the unlimited replicative potential of cancer cells, but they rarely try to specifically block the cell behaviors driving invasion and dissemination. Few of these drugs have proven clinical benefit in metastatic breast cancer patients³¹. *Twist1* is overexpressed in multiple invasive human cancers but, as a transcription factor, is itself inaccessible to small molecule inhibition. Our novel Twist1-regulated gene set now offers the potential to identify and target essential, druggable Twist1 effectors to antagonize cancer cell dissemination.

References

1. Alberts, B. *et al.* *Molecular Biology of the Cell*. (Garland Science, 2007).
2. Friedl, P. & Gilmour, D. Collective cell migration in morphogenesis, regeneration and cancer. *Nat. Rev. Mol. Cell Biol.* **10**, 445–457 (2009).
3. Davies, J. A. & Garrod, D. R. Molecular aspects of the epithelial phenotype. *Bioessays* **19**, 699–704 (1997).
4. Nguyen, D. X., Bos, P. D. & Massagué, J. Metastasis: from dissemination to organ-specific colonization. *Nat Rev Cancer* **9**, 274–284 (2009).
5. Nelson, W. J. Remodeling epithelial cell organization: transitions between front-rear and apical-basal polarity. *Cold Spring Harbor Perspectives in Biology* **1**, a000513 (2009).
6. Thiery, J. P. Epithelial–mesenchymal transitions in tumour progression. *Nat Rev Cancer* **2**, 442–454 (2002).
7. Greenburg, G. & Hay, E. D. Epithelia suspended in collagen gels can lose polarity and express characteristics of migrating mesenchymal cells. *J. Cell Biol.* **95**, 333–339 (1982).
8. Hay, E. D. An overview of epithelio-mesenchymal transformation. *Acta Anat (Basel)* **154**, 8–20 (1995).
9. Hay, E. D. & Zuk, A. Transformations between epithelium and mesenchyme: normal, pathological, and experimentally induced. *Am. J. Kidney Dis.* **26**, 678–690 (1995).
10. Gumbiner, B. M. Cell adhesion: the molecular basis of tissue architecture and morphogenesis. *Cell* **84**, 345–357 (1996).
11. Ewald, A. J., Brenot, A., Duong, M., Chan, B. S. & Werb, Z. Collective epithelial migration and cell rearrangements drive mammary branching morphogenesis. *Dev. Cell* **14**, 570–581 (2008).
12. Ewald, A. J. *et al.* Mammary collective cell migration involves transient loss of epithelial features and individual cell migration within the epithelium. *J. Cell. Sci.* **125**, 2638–2654 (2012).
13. Yang, J. & Weinberg, R. A. Epithelial-Mesenchymal Transition: At the Crossroads of Development and Tumor Metastasis. *Dev. Cell* **14**, 818–829 (2008).
14. Peinado, H., Olmeda, D. & Cano, A. Snail, Zeb and bHLH factors in tumour progression: an alliance against the epithelial phenotype? *Nat Rev Cancer* **7**, 415–428 (2007).
15. Thiery, J. P., Acloque, H., Huang, R. Y. J. & Nieto, M. A. Epithelial-Mesenchymal Transitions in Development and Disease. *Cell* **139**, 871–890 (2009).
16. Blanco, M. J. *et al.* Correlation of Snail expression with histological grade and lymph node status in breast carcinomas. *Oncogene* **21**, 3241–3246 (2002).
17. Yang, J. *et al.* Twist, a Master Regulator of Morphogenesis, Plays an Essential Role in Tumor Metastasis. *Cell* **117**, 927–939 (2004).
18. Martin, T. A., Goyal, A., Watkins, G. & Jiang, W. G. Expression of the Transcription Factors Snail, Slug, and Twist and Their Clinical Significance in Human Breast Cancer. *Ann Surg Oncol* **12**, 488–496 (2005).
19. Mironchik, Y. *et al.* Twist overexpression induces in vivo angiogenesis and correlates with chromosomal instability in breast cancer. *Cancer Research* **65**, 10801–10809 (2005).
20. Kwok, W. K. Up-Regulation of TWIST in Prostate Cancer and Its Implication as a Therapeutic Target. *Cancer Research* **65**, 5153–5162 (2005).
21. Yuen, H. F. *et al.* Upregulation of Twist in oesophageal squamous cell carcinoma

- is associated with neoplastic transformation and distant metastasis. *Journal of Clinical Pathology* **60**, 510–514 (2006).
22. Lee, T. K. *et al.* Twist Overexpression Correlates with Hepatocellular Carcinoma Metastasis through Induction of Epithelial-Mesenchymal Transition. *Clinical Cancer Research* **12**, 5369–5376 (2006).
 23. Polyak, K. & Weinberg, R. A. Transitions between epithelial and mesenchymal states: acquisition of malignant and stem cell traits. *Nat Rev Cancer* **9**, 265–273 (2009).
 24. Tarin, D. The Fallacy of Epithelial Mesenchymal Transition in Neoplasia. *Cancer Research* **65**, 5996–6001 (2005).
 25. Wood, L. D. *et al.* The genomic landscapes of human breast and colorectal cancers. *Science* **318**, 1108–1113 (2007).
 26. Stephens, P. J. *et al.* Complex landscapes of somatic rearrangement in human breast cancer genomes. *Nature* **462**, 1005–1010 (2009).
 27. Shamir, E. R. *et al.* Twist1-induced dissemination preserves epithelial identity and requires E-cadherin. *J. Cell Biol.* **204**, 839–856 (2014).
 28. Simian, M. *et al.* The interplay of matrix metalloproteinases, morphogens and growth factors is necessary for branching of mammary epithelial cells. *Development* **128**, 3117–3131 (2001).
 29. Fata, J. E. *et al.* The MAPKERK-1,2 pathway integrates distinct and antagonistic signals from TGF α and FGF7 in morphogenesis of mouse mammary epithelium. *Developmental Biology* **306**, 193–207 (2007).
 30. Kowalski, P. J., Rubin, M. A. & Kleer, C. G. E-cadherin expression in primary carcinomas of the breast and its distant metastases. *Breast Cancer Res.* **5**, R217–22 (2003).
 31. Carey, L. A. Through a glass darkly: advances in understanding breast cancer biology, 2000-2010. *Clin. Breast Cancer* **10**, 188–195 (2010).

Figure 7-1

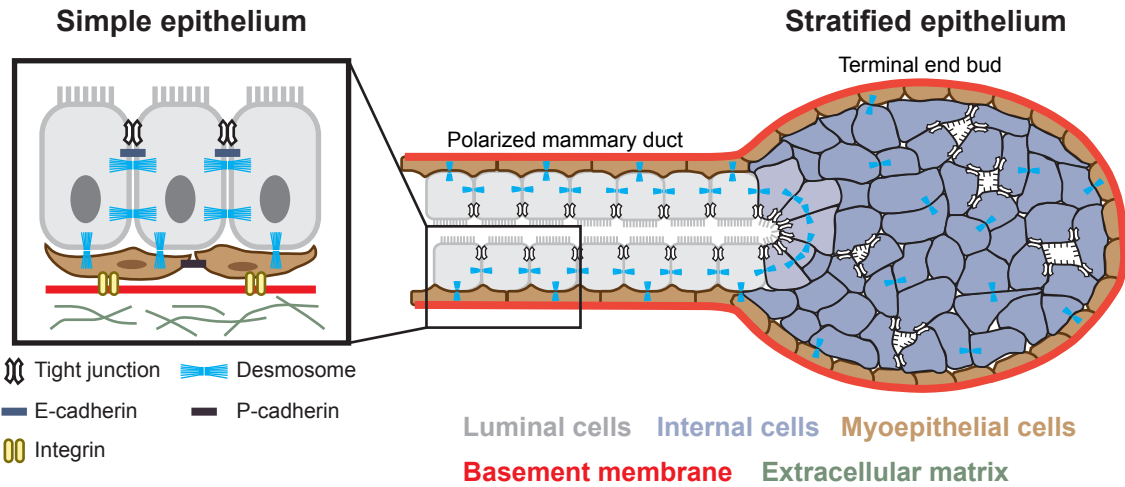


Figure 7-1. Normal transitions in adhesion during epithelial branching morphogenesis. Mammary epithelium initiates branching morphogenesis postnatally. Tube elongation is accomplished by a stratified terminal end bud, which contains many internal luminal cells that lack apico-basal polarity and display reduced numbers of intercellular junctions. The epithelium finally polarizes to a bilayered, simple ductal architecture consisting of an inner layer of luminal cells and a basal layer of myoepithelial cells. Epithelial cells in the ducts are connected by many cell-cell junctions. Schematic adapted from original by Robert Huebner, with permission.

Figure 7-2

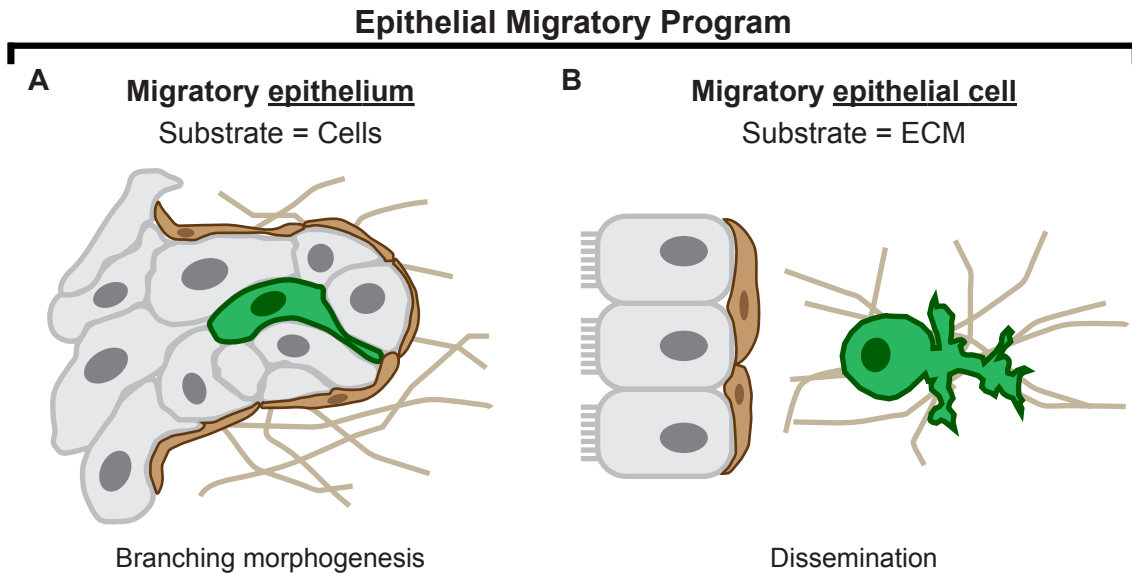


Figure 7-2. Is there are conserved epithelial migratory program? Dissemination might be explained by a switch in the substrate of migration from adjacent cells to ECM. (A) Epithelial cells collectively migrate as an elongating bud during mammary branching morphogenesis. Within the multilayer, an individual epithelial cell (green) can appear elongated and protrusive. (B) During Twist1-induced dissemination, a single epithelial cell (green) migrates through the ECM with amoeboid morphology and extensive protrusions at the leading front.

APPENDIX A

A collagen I ECM induces dissemination of
E-cadherin⁻ luminal cells

Results

A collagen I microenvironment *in vitro* induces a transition from collective invasion to dissemination in E-cad⁻ cells

Our results in basement membrane-rich microenvironments *in vitro* and *in vivo* demonstrated that *E-cadherin* deletion alone was insufficient to induce cell dissemination¹. We next sought to test whether a stromal ECM microenvironment could cooperate with reduced luminal cell-cell adhesion to induce dissemination. We embedded normal and *E-cad^{fl/fl}* genetic mosaic epithelium into 3D gels of collagen I (Fig. A-1A). In contrast to Matrigel, collagen I induced protrusive and disseminative behavior in normal mammary epithelium (Fig. A-1B), as we have shown previously². However, normal organoids only disseminate myoepithelial cells, and disseminated cells most commonly reintegrate into the epithelium². In contrast, *E-cad^{fl/fl}* genetic mosaic fragments in collagen I exhibited robust and sustained dissemination of cells, particularly of amoeboid morphology (Fig. A-1C-C'). The *mT/mG* reporter revealed a majority of these cells to be green, Cre⁺. Immunofluorescence staining for both myoepithelial (Fig. A-1D, SMA⁺) and luminal (Fig. A-1E, K8⁺) cell markers confirmed that both mammary cell types disseminated, but disseminating luminal cells were always Cre⁺, or E-cad⁻. We conclude that loss of E-cad is sufficient for robust dissemination into a collagen I-rich ECM.

A stromal ECM encountered by mammary epithelium early post-transplantation *in vivo* induces robust E-cad⁻ cell dissemination

Our observations in collagen I 3D gels led us to hypothesize that E-cad⁻ cells might disseminate *in vivo* if they experienced direct contact with the abundant collagen I in the stromal compartment of the mammary fat pad. Previously, we transplanted *E-cad^{fl/fl}* organoids into the mammary fat pad using Matrigel as a carrier. The Matrigel functions

as a survival factor during transplantation and ensures that epithelial cells remain within a differentiating ECM while branching morphogenesis is initiated. To test whether E-cad⁻ cells could disseminate into a stromal matrix in vivo, we instead directly transplanted Adeno-Cre-transduced *E-cad^{fl/fl};mT/mG* organoids into the mammary fat pad using DMEM as a carrier. As a control, we transplanted Adeno-Cre-transduced *E-cad^{+/+};mT/mG* organoids in DMEM into the contralateral glands of the same mice (Fig. A-1F). Under these conditions, epithelial cells immediately encounter a collagen I-rich stromal microenvironment, prior to cell-derived basement membrane secretion. We harvested transplanted glands after one week to assess the acute response of E-cad⁺ and E-cad⁻ cells to the stromal matrix.

Outgrowths from *E-cad^{+/+};mT/mG* organoids displayed collective protrusive migration into the surrounding ECM (Fig. A-1G), analogous to the migratory pattern observed in normal organoids cultured in 3D collagen I gels². We rarely observed dissemination of amoeboid cells around the transplanted *E-cad^{+/+};mT/mG* organoids (14% of 44 independent sites, n=9 mice). In contrast, outgrowths from *E-cad^{fl/fl};mT/mG* organoids displayed high levels of amoeboid cell dissemination (Fig. A-1H, 91% of 74 independent sites, n=11 mice). Within these genetic mosaic transplants, the E-cad⁺ (red) cells were protrusive, but essentially non-disseminative. The green, disseminated cells were E-cad⁻, K8⁺, and SMA⁻ by immunofluorescence, consistent with a luminal lineage (Fig. A-2A-C). Furthermore, disseminated cells were observed beyond a basement membrane (Laminin 332⁺) that had completely formed around the main epithelium (Fig. A-2D). While we cannot track the specific fate of disseminated E-cad⁻ cells in real-time in vivo, we hypothesize from our data that some of these cells give rise to the exclusively E-cad⁻ cell clusters that we observe at the injection site at 6 weeks post-transplantation¹. Taken together, our data demonstrate that a collagen I-rich stromal microenvironment is

sufficient to induce a transition from collective epithelial invasion to individual dissemination in E-cad⁻ cells.

Discussion

Our recent work demonstrated that the phenotypic consequences of specific genetic changes depend strongly on the composition of the ECM microenvironment². Previously, we found that in basement membrane-rich microenvironments in vitro and in vivo, loss of E-cad induces collective invasion of luminal cells but rarely results in dissemination¹. Here, we demonstrate that a collagen I-rich microenvironment promotes single cell dissemination of E-cad⁻ cells. Importantly, the microenvironment surrounding human breast tumors becomes progressively enriched in collagen I^{3,4}. Our data suggest that the collagen I-rich tumor microenvironment may be critical to the initiation and maintenance of invasive and metastatic cell behaviors. We therefore speculate that therapeutic strategies targeting a cell's molecular interpretation of the ECM microenvironment could be effective in limiting invasion and metastasis.

References

1. Shamir, E. R. *et al.* Twist1-induced dissemination preserves epithelial identity and requires E-cadherin. *J. Cell Biol.* **204**, 839–856 (2014).
2. Nguyen-Ngoc, K.-V. *et al.* ECM microenvironment regulates collective migration and local dissemination in normal and malignant mammary epithelium. *Proc Natl Acad Sci USA* **109**, E2595–604 (2012).
3. Conklin, M. W. *et al.* Aligned collagen is a prognostic signature for survival in human breast carcinoma. *The American Journal of Pathology* **178**, 1221–1232 (2011).
4. Egeblad, M., Rasch, M. G. & Weaver, V. M. Dynamic interplay between the collagen scaffold and tumor evolution. *Current Opinion in Cell Biology* **22**, 697–706 (2010).

Figure A-1. A collagen I-rich ECM induces E-cad⁻ cell dissemination in 3D culture and in vivo. (A) *E-cad^{+/+};mT/mG* and *E-cad^{fl/fl};mT/mG* organoids were isolated, and recombination was induced with Adeno-Cre. Organoids were cultured with FGF2 within 3D collagen I gels, and invasion and dissemination were monitored by time-lapse microscopy. (B) E-cad⁺ organoids exhibited collective protrusive migration. (C) E-cad⁻ organoids robustly disseminated both elongated and rounded cells (C'). White arrowheads indicate rounded cells emerging on the basal tissue surface. (D,E) Both myoepithelial (D, SMA⁺) and luminal epithelial (E, K8⁺) cells disseminated from genetic mosaic *E-cad^{fl/fl};mT/mG* organoids cultured in collagen I. Disseminated luminal cells had an amoeboid morphology and were always Cre⁺ (green). (F) Adeno-Cre-transduced *mT/mG* organoids (E-cad⁺) and *E-cad^{fl/fl};mT/mG* organoids were transplanted into contralateral cleared mammary fat pads, and glands were harvested after 1 week in vivo. (G) Genetic mosaic *E-cad^{+/+}* outgrowths were protrusive but were rarely surrounded by disseminated amoeboid cells. (H) Genetic mosaic *E-cad^{fl/fl}* outgrowths consisted of a protrusive, mostly red (Cre⁻, E-cad⁺) epithelial core surrounded by many green (Cre⁺, E-cad⁻), amoeboid cells.

Figure A-1

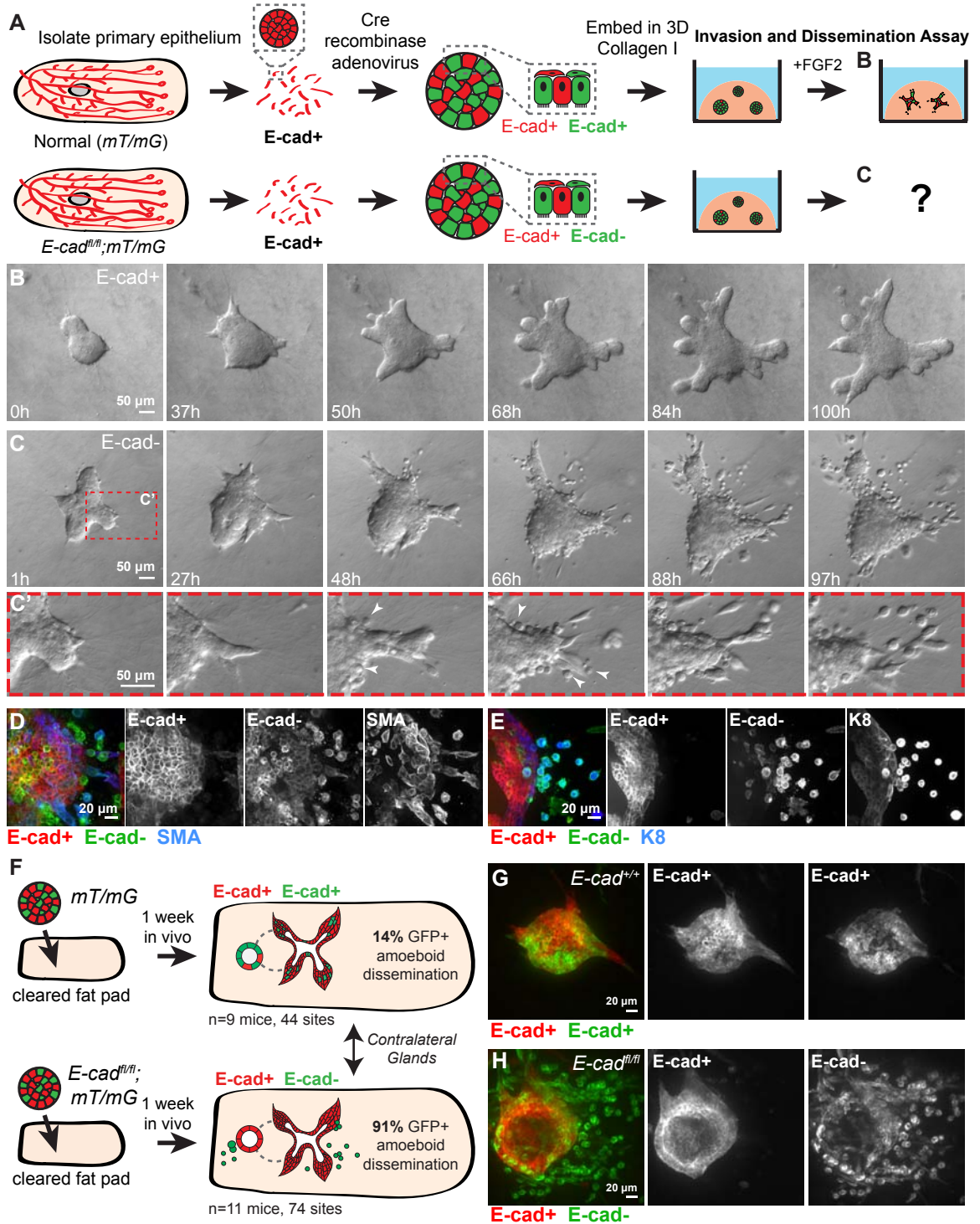


Figure A-2

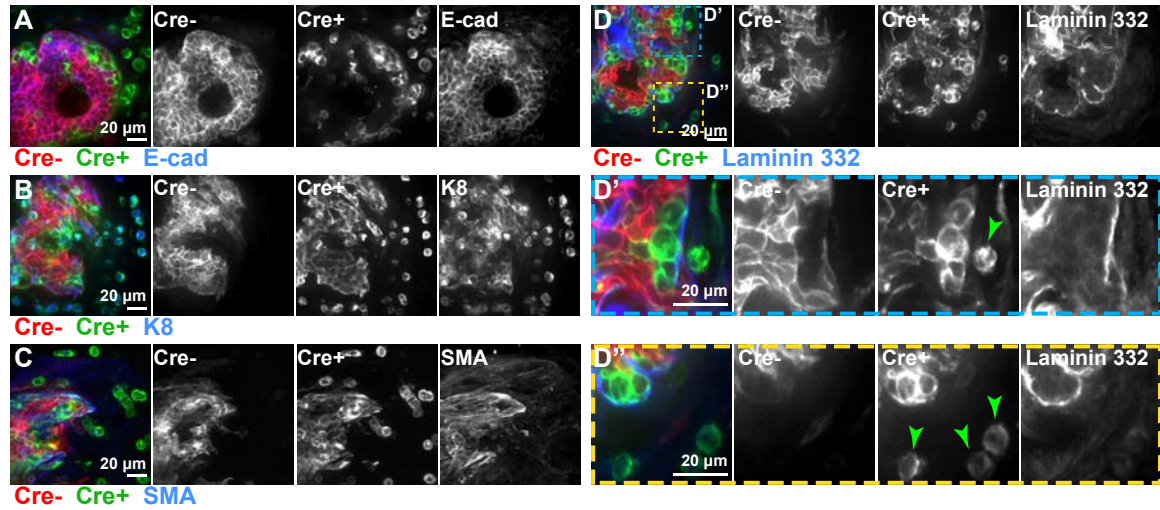


Figure A-2. A stromal ECM induces E-cad⁻ cell dissemination in vivo. Adeno-Cre-transduced *E-cad^{fl/m};mT/mG* organoids were transplanted into cleared mammary fat pads, and glands were harvested after 1 week. (A-D) Outgrowths displayed robust GFP⁺, amoeboid cell dissemination. Disseminated cells were E-cad⁻ (A), K8⁺ (B), and SMA⁻ (C), consistent with a luminal lineage, and they were frequently located beyond a basement membrane (D, Laminin 332⁺). Green arrowheads in D'-D'' indicate GFP⁺, amoeboid cells located in the fat pad, past a complete basement membrane.

Curriculum Vitae

Elijah R. Shamir

855 N. Wolfe St., Rangos 480-26
Baltimore, MD 21205

703-732-9029
eshamir1@jhmi.edu

EDUCATION

Johns Hopkins University School of Medicine, Medical Scientist Training Program, 2016
Biochemistry, Cellular & Molecular Biology (BCMB) Program, GPA: 4.0

University of Virginia, School of Engineering & Applied Science, 2008
B.S., Biomedical Engineering, with Highest Distinction; Global Public Health Minor
GPA: 3.99, Dean's List (Fall 2004 – Fall 2006)

Thomas Jefferson High School for Science & Technology, 2004
Advanced Studies Diploma; Governor's Seal of Academic Excellence; GPA: 4.16

RESEARCH EXPERIENCE

2010- Ewald Lab, Departments of Cell Biology & Oncology, Johns Hopkins University School of Medicine (PhD Thesis Lab)

UNDERGRADUATE RESEARCH

2007 Hang Lab for Chemical Biology & Microbial Pathogenesis, Rockefeller University
2006-8 Hoffman Lab, Division of Infectious Diseases & International Health, University of Virginia
2006 "HIV/AIDS Vulnerability among Migrants in Thailand and Challenges to Health Care Delivery", research protocol written by ERS, approved by University of Virginia IRB-SBS
2005 Sant'Angelo Lab, Department of Immunology, Memorial Sloan-Kettering Cancer Center

HONORS & AWARDS

2014 **Safeway Breast Cancer Research Retreat** – best poster
2014 **Martin and Carol Macht Award – Young Investigators' Day Award**, awarded by Johns Hopkins School of Medicine to graduate students based on their research
2013 American Society for Cell Biology Travel Award
2013 **Nature Cell Biology Poster Award** – best poster, Cell Contact and Adhesion GRC
2013 **SKCCC Oncology Fellow Research Day** – 1st Place in basic science research
2012 BCMB Retreat Poster Presentation Award – 1st Place, best poster
2012 **Isaac Morris and Lucille Elizabeth Hay Graduate Fellowship**
2012 **SKCCC Oncology Fellow Research Day** – 1st Place in basic science research
2012 Lewis Travel Award – awarded by JHU Dept of Cell Biology
2011 **BCMB Retreat Oral Presentation Award** – 1st Runner-Up, best student research talk
2011 **Kelly Award** – awarded by the JH Institute for Basic Biomedical Sciences to the top first year graduate students in the Johns Hopkins School of Medicine
2008 **UVA School of Engineering & Applied Science (UVA SEAS) Outstanding Student Award** – awarded to the top three graduating students in SEAS
2008 **Edgar F. Shannon Award** – recognition by UVA's Z Society as the best graduating student in UVA SEAS

- 2008 **UVA Undergraduate Research and Design Symposium Award** – 2nd Place Winner
- 2007 **Raven Society Scholar from SEAS** – scholarship support to one student per school at UVA, granted by the Raven Society (UVA’s oldest and most prestigious honor society)
- 2007 Robert W. and Eileen M. Honse Scholarship (UVA SEAS)
- 2006 **Barry Goldwater Scholar in Mathematics, Science, & Engineering** – selected as a college sophomore
- 2006 Margaret Elinor George Scholarship (UVA SEAS)
- 2006 **Pfizer-Center for Global Health Research Award in Infectious Disease**
- 2006 Raven Society member, UVA’s oldest honor society
- 2006 Tau Beta Pi member, National Engineering Honor Society
- 2006 **UVA Center for Global Health Scholar Award**
- 2006 **UVA Raven Society Fellowship** – funding awarded to 4-5 student research projects per year
- 2005 SEAS Class of 1986 Scholarship
- 2005 Virginia Future Leaders VCTA Scholarship
- 2004 Bani Taneja Memorial Scholarship
- 2004 Best Buy Scholarship
- 2004 **EF Global Citizen Award** – awarded to 10-12 high school students dedicated to promoting global awareness; essay selected from a pool of nationwide applications
- 2004 Jack E. Aalseth Scholarship
- 2004 National Society of Professional Engineers Auxiliary Scholarship
- 2004 Rodman Scholar in UVA SEAS – honors program for top 5% of each engineering school class
- 2004 Virginia Future Leaders VCTA Scholarship

PUBLICATIONS

RESEARCH PAPERS

- Shamir, E. R.**, Pappalardo, E., Jorgens, D. M., Coutinho, K., Tsai, W.-T., Aziz, K., Auer, M., Tran, P. T., Bader, J. S., & Ewald, A. J. Twist1-induced dissemination preserves epithelial identity and requires E-cadherin. *J. Cell Biol.* **204**, 839–856 (2014).
- Nguyen-Ngoc, K.-V., Cheung, K. J., Brenot, A., **Shamir, E. R.**, Gray, R. S., Hines, W. C., Yaswen, P., Werb, Z., & Ewald, A. J. ECM microenvironment regulates collective migration and local dissemination in normal and malignant mammary epithelium. *Proc. Natl. Acad. Sci. U.S.A.* **109**, E2595–604 (2012).
- Shamir, E. R.**, Warthan, M., Brown, S. P., Nataro, J. P., Guerrant, R. L., & Hoffman, P. S. Nitazoxanide inhibits biofilm production and hemagglutination by enteroaggregative *Escherichia coli* strains by blocking assembly of AafA fimbriae. *Antimicrob. Agents Chemother.* **54**, 1526–1533 (2010).
- Charron, G., Zhang, M. M., Yount, J. S., Wilson, J., Raghavan, A. S., **Shamir, E.**, & Hang, H. C. Robust fluorescent detection of protein fatty-acylation with chemical reporters. *J. Am. Chem. Soc.* **131**, 4967–4975 (2009).

CHAPTERS/REVIEWS

- Shamir, E. R.**, & Ewald, A. J. Adhesion in mammary development: novel roles for E-cadherin in individual and collective cell migration. *Curr Top Dev Biol.* [invited review, manuscript in preparation]
- Shamir, E. R.**, & Ewald, A. J. 3D Organotypic Culture: Experimental Models of Mammalian

Biology and Disease. *Nat. Rev. Mol. Cell Biol.* [invited review, in press]
Nguyen-Ngoc, K.-V., **Shamir, E. R.**, Huebner, R. J., Beck, J. N., Cheung, K. J., & Ewald, A. J. “3D Culture Assays of Murine Mammary Branching Morphogenesis and Epithelial Invasion.” *Methods Mol. Biol.* **1189** (2014).

TALKS

Gordon Research Conference – Cell Polarity Signaling: Invited Speaker, “Molecular and cellular regulators of Twist1-induced epithelial dissemination”, Bentley University, Waltham, MA (6/2014)
Experimental Biology: Invited Speaker, “Twist1 induces dissemination by activating an epithelial motility program that requires E-cadherin”, San Diego Convention Center, San Diego, CA (4/2014)
Gordon Research Conference – Mammary Gland Biology: Speaker (selected from abstracts), “Regulation of mammary epithelial dissemination”, Il Ciocco Resort, Italy (6/2012)
Biochemistry, Cellular & Molecular Biology Annual Program Retreat: Speaker, “The role of intercellular adhesion in limiting mammary epithelial dissemination” (1st Runner-Up, best student research talk), Sheppard Pratt Conference Center, Baltimore, MD (10/2011)
UVA Undergraduate Research & Design Symposium: Speaker, “Treating infection by Enterococcal *E. coli*, an emerging diarrheal pathogen” (2nd Place Award), University of Virginia, Charlottesville, VA (4/2008)
The Role of Religion in Battered Women's Safety Planning: Panelist, Sponsored by The Shelter for Help in Emergency, Charlottesville, VA (10/2007)
Raven Fellowship Symposium: Speaker, University of Virginia, Charlottesville, VA (2/2007)
Center for Global Health Symposium: Celebrating Global Health -- Pathways to the Future: Invited Speaker, “Assessing health, vulnerability, and care for migrants in Thailand living with HIV/AIDS”, University of Virginia, Charlottesville, VA (9/2006)

POSTER PRESENTATIONS

Annual Safeway Breast Cancer Research Retreat: “Molecular and cellular regulation of epithelial dissemination” (best poster), Mt. Washington Conference Center, Baltimore, MD (5/2014)
Oncology Fellows Research Day: “Molecular and cellular regulation of epithelial dissemination”, Sidney Kimmel Comprehensive Cancer Center, Baltimore, MD (5/2014)
American Society for Cell Biology Annual Meeting: “Twist1-induced dissemination preserves epithelial identity and requires E-cadherin”, Morial Convention Center, New Orleans, LA (12/2013)
American Association for Cancer Research Special Conference – Frontiers in Basic Cancer Research: “Building a novel molecular model for Twist1-induced epithelial dissemination”, Gaylord National Resort and Convention Center, National Harbor, MD (9/2013)
Gordon Research Conference – Cell Contact and Adhesion: “Distinct roles for E-cadherin and Twist1 in epithelial invasion and dissemination” (Nature Cell Biology Poster Award), Il Ciocco Resort, Italy (6/2013)
Annual Safeway Breast Cancer Research Retreat: “Distinct roles for E-cadherin and Twist1 in epithelial invasion and dissemination”, Mt. Washington Conference Center, Baltimore, MD (5/2013)
Oncology Fellows Research Day: “Distinct roles for E-cadherin and Twist1 in epithelial invasion and dissemination” (1st Place in basic research),

- Sidney Kimmel Comprehensive Cancer Center, Baltimore, MD (5/2013)
- American Society for Cell Biology Annual Meeting*: “Molecular requirements for mammary epithelial cell dissemination”, Moscone Center, San Francisco, CA (12/2012)
- Biochemistry, Cellular & Molecular Biology Annual Program Retreat*: “Regulation of mammary epithelial dissemination” (1st Place, best poster), Sheppard Pratt Conference Center, Baltimore, MD (10/2012)
- Annual Safeway Breast Cancer Research Retreat*: “Regulation of mammary epithelial dissemination”, Mt. Washington Conference Center, Baltimore, MD (5/2012)
- Oncology Fellows Research Day*: “Regulation of mammary epithelial dissemination” (1st Place in basic research), Sidney Kimmel Comprehensive Cancer Center, Baltimore, MD (5/2012)
- Annual Safeway Breast Cancer Research Retreat*: “The role of cadherins and ECM composition in modulating mammary epithelial dissemination”, Mt. Washington Conference Center, Baltimore, MD (5/2011)
- Oncology Fellows Research Day*: “The role of cadherins and ECM composition in modulating mammary epithelial dissemination”, Sidney Kimmel Comprehensive Cancer Center, Baltimore, MD (5/2011)

PATENTS

- Ewald, A.J., **Shamir, E.R.**, & Tran, P.T. “Platform to Study TWIST-1 Mediated Cancer Metastasis”, Invention Disclosure, JHU Ref. C11782 (2011)

LEADERSHIP ACTIVITIES & CAREER MENTORING

- 2013- Women's Careers in Academic Medicine Research Group (JHUSOM), committee member
- 2013 Emerging Women’s Leadership Program (JHUSOM), student participant (by selection) in program for female instructors and assistant professors
- 2013 “Girl Rising” Screening Steering Committee (JHU), member
- 2012- Association of Women Student MD-PhDs (JHUSOM), co-founder and leader
- 2012- Health Professions Committee, JHU Office of Pre-Professional Programs & Advising, interviewer
- 2012- MD-PhD Student Advisory Board (JHUSOM), member
- 2007 Global Public Health Week – Migrant Health & Wellbeing: A Global Challenge (UVA), chief organizer
- 2006 Human Trafficking in Thailand and the United States: Next Steps in Activism and Advocacy (Chulalongkorn University, College of Public Health; Bangkok, Thailand), workshop organizer
- 2006 1st Annual Global Public Health Society Research Symposium (UVA), symposium organizer
- 2006 Center for Global Health Course Selection Committee (UVA), member
- 2005-7 Center for Global Health Student Advisory Board (UVA), member

PROFESSIONAL ASSOCIATIONS

- 2013- American Association for Cancer Research, Associate member
- 2013- American Association for the Advancement of Science, sponsored membership through AAAS/Science Program for Excellence in Science
- 2012- American Society for Cell Biology, student member

Figure 1-5

